Wilfrid Laurier University

Scholars Commons @ Laurier

2018

Synthesis, Properties, and Solid-State Structures of a Series of 6,13-Dicyanoheteropentacene Analogues: Towards New Liquid Crystalline Materials

L Hiscock
hisc2250@mylaurier.ca

Kenneth E. Maly
Wilfrid Laurier University

Louise N. Dawe
Wilfrid Laurier University

Recommended Citation

Synthesis, Properties, and Solid-State Structures of a Series of 6,13-Dicyanoheteropentacene Analogues: Towards New Liquid Crystalline Materials

L. K. Hiscock

Honours Bachelor of Science in Chemistry,
Memorial University of Newfoundland, 2013

THESIS

Submitted to the Department of Chemistry and Biochemistry

Faculty of Science

in partial fulfilment of the requirements for

Master of Science in Chemistry

Wilfrid Laurier University

Waterloo, Ontario, Canada, 2018

Abstract

The focus of this thesis is the synthesis of novel heterocyclic pentacene analogs and the investigation of their self-organization for the development of new materials for organic electronics. The thesis consists of two interrelated projects: the first being development of an improved synthesis of a series of liquid crystalline dicyanotetraoxapentacenes (DCTOPs) while the second entails the exploratory synthesis of several novel dicyanoheteropentacene analogues and a preliminary investigation of their photophysical properties and solid-state structures. Both of these projects centre around the use of nucleophilic aromatic substitution reactions on tetrafluoroterephthalonitrile.

Soluble, tetrakis(bis(alkoxy)phenyl)-substituted DCTOPs were originally synthesised *via* a short synthesis complicated by a tedious purification required in the last step. Despite this, derivatives bearing long alkyl chains were prepared which displayed liquid crystalline properties in addition to aggregation-induced emission. Building upon this success, but with the goal of achieving DCTOPs in an efficient synthetic manner for this thesis, changes were made which eliminated the troublesome fourfold Suzuki coupling by changing the order of reactions, which in turn required a protection-deprotection sequence. Purification in the new synthesis was greatly simplified and the target tetraaryl-DCTOPs were accessed in good overall yields and purities. The synthesis and solid state structures of these DCTOPs are discussed in Chapter 2.

Building on the methods developed in Chapter 2, several novel pentacene analogues containing combinations of nitrogen, oxygen, and sulfur atoms installed within the pentacene core were also synthesised. These compounds were prepared in good yields, and preliminary photophysical studies show that all the compounds displayed luminescence in solution and the solid

state. It was also shown that replacement of O with N leads to a red shift in absorption and emission spectra. The X-ray crystal structures show that several of these compounds exhibit π−stacking in the solid state, which is an important design element for applications in organic electronics. The synthesis, photophysical properties, and solid-state organization of these novel 6,13-dicyanoheteropentacene analogues are discussed in Chapter 3.
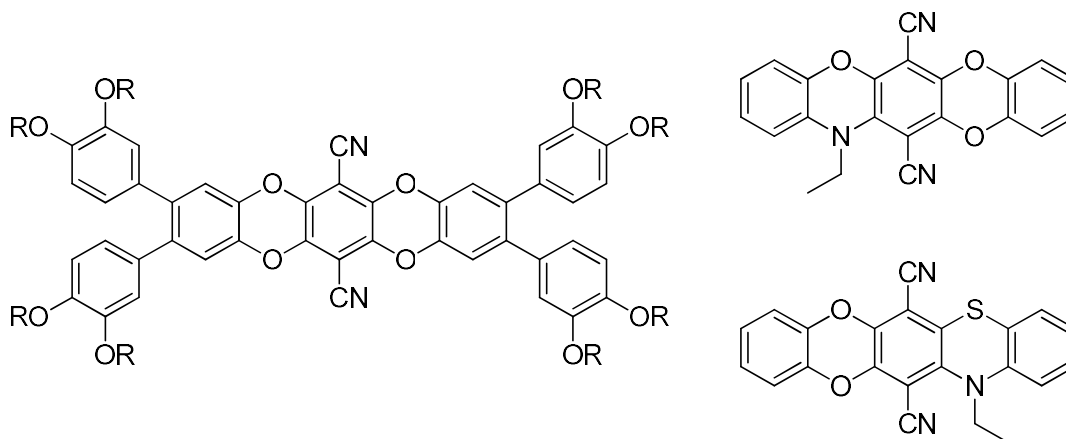
Acknowledgements

I would like to thank my supervisors Drs. Ken Maly and Louise Dawe, without whom none of this would be possible. I am forever grateful for the support and kindness you've both shown to me, and the lab environment you choose to foster. Working with the two of you brings immeasurable meaning and happiness to my life, and I thank you for being our Lab-Dad and Lab-Mom. Additional thanks to LD for solving and refining all crystal structures.

Thanks to all past and present Maly and Dawe group members especially Zachary Schroeder, a highly talented and exceptionally motivated chemist. Special thanks to Brooke Raycraft (Honours 2014) for beginning the DCTOP project and completing the original synthesis.

I would like to thank my parents, Colin and Trudy Hiscock, for all their love and support through many difficult times; thank you for never giving up on me. I'm eternally grateful for the blissful childhood you gave me, and I love you both with all my heart. I would like to thank my sister for being an excellent (and younger) role model.

Finally, I would like to thank my boyfriend, Matthew Tuckett, who has been with me during good times and bad. You are such a large part of my life, and I can't imagine this past year without you.

Table of Contents

List of Figures

List of Tables

List of Schemes

Abbreviations

^{13}C	carbon-13 nucleus
^{19}F	fluorine-19 nucleus
^{1}H	proton nucleus
2-AP	2-aminophenol
Å	Ångstrom (10^{-10} m)
ADOTP	**a**za**dio**xa**t**hia**p**entacene
AIE	aggregation-induced emission
aq.	aqueous
ASAP-MS	atmospheric solids analysis probe mass spectrometry
ATOP	**a**za**tri**o**xa**p**entacene
AU	arbitrary units
(Bpin)$_2$	bis(pinacolato)diboron

Col$_h$	columnar hexagonal
d	doublet
DADOP	**d**ia**z**a**di**o**x**a**p**entacene
DADTP	**d**ia**z**a**di**thia**p**entacene
DBU	1,8-diazabicyclo[5.4.0]undec-7-ene
DCTAP	**d**i**c**yano**t**etra**a**za**p**entacene
DCTOP	**d**i**c**yano**t**etra**o**xa**p**entacene
dd	doublet of doublets
dfppe	1,2-bis[bis(pentafluorophenyl)phosphino]ethane
DME	dimethoxyethane
DMF	dimethylformamide
DMSO	dimethyl sulfoxide
dppf	1,1′-ferrocenediyl-bis(diphenylphosphine)
DSSC	dye-sensitised solar cell
eq	equivalents
ESI-MS	electrospray ionisation-mass spectrometry
Et$_3$N	triethylamine
eV	electron-volt

g	gram
HOMO	highest occupied molecular orbital
HRMS	high resolution mass spectrometry
Hz	hertz
J	coupling constant
KO*t*Bu	potassium *tert*-butoxide
LAH	lithium aluminium hydride
LC	liquid crystalline
LCD	liquid crystal display
LUMO	lowest unoccupied molecular orbital
M	molar (mol/L)
m	multiplet
MBBA	*N*-(4-methoxybenzylidene)-4-butylaniline
MEK	methyl ethyl ketone
MHz	megahertz
mL	millilitre
mmHg	millimetres mercury
MO	molecular orbital

mol	mole
MOM	methoxymethyl
MOMCl	chloromethyl methyl ether
mp	melting point
NBS	*N*-bromosuccinimide
*n*BuLi	*n*-butyllithium
NDI	naphthalene diimide
NMR	nuclear magnetic resonance
NR	no reaction
OE	organic electronics
OFET	organic field-effect transistor
OLED	organic light-emitting diode
PAH	polycyclic aromatic hydrocarbon
PG	protecting group
phen	1,10-phenanthroline
pK_a	logarithmic acid dissociation constant
POM	polarised optical microscopy
ppm	parts per million

p-TsOH	*para*-toluenesulfonic acid
pyr	pyridine
q	quartet
R*f*	retention factor
RIR	restricted intramolecular rotation
RMSD	root mean squared deviation
rt	room temperature
S_N2	nucleophilic bimolecular substitution
S_NAr	nucleophilic aromatic substitution reaction
SPhos	2-dicyclohexylphosphino-2',6'-dimethoxybiphenyl
t	triplet
TAOP	**t**ri**a**za**o**xa**p**entacene
TBAB	tetra-*n*-butylammonium bromide
TBAF	tetra-*n*-butylammonium fluoride
TCNQ	tetracyanoquinodimethane
TCTP	tetrachloroterephthalonitrile
TFTP	tetrafluoroterephthalonitrile
THF	tetrahydrofuran

TIPS	triisopropylsilyl
TLC	thin-layer chromatography
TPDO	triphenodioxazine
UV	ultraviolet
UV-vis	ultraviolet-visible spectroscopy
XRD	X-ray diffraction
δ	chemical shift
ε	molar absorptivity constant
λ_{em}	wavelength (nm) of maximum fluorescence emission
λ_{ex}	wavelength (nm) of fluorescence excitation
λ_{max}	wavelength (nm) of maximum absorption
μL	microlitre

Chapter I - Introduction

1.1   Polycyclic Aromatic Hydrocarbons (PAHs) and Acenes

Polycyclic aromatic hydrocarbons (PAHs) are well-known materials with interesting electronic and photophysical properties. They contain two (or more) fused benzene rings in various configurations without substituents nor the presence of heteroatoms within the skeleton (Figure 1-1).[1]

Naphthalene   Pyrene   Dibenz[a,c]anthracene   Chrysene
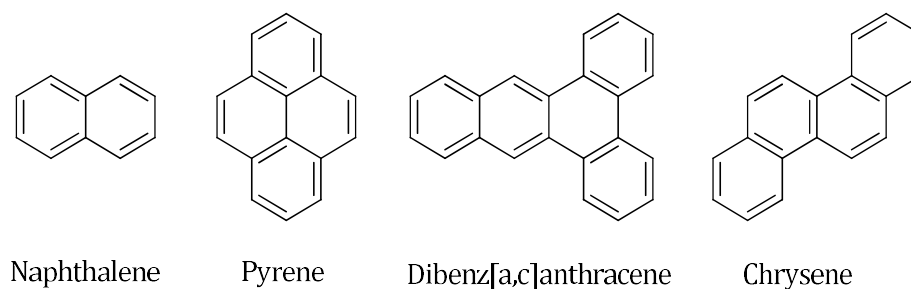
Figure 1-1: Representative PAHs.

The interesting properties of PAHs, such as organic semiconductor characteristics or fluorescence, are caused by the interaction of electrons or photons with the molecular orbitals of the molecules. As is well-known, the gap between the highest occupied molecular orbital (HOMO) and the lowest unoccupied molecular orbital (LUMO) can be lowered with increasing conjugation.[2] For example, the HOMO-LUMO gap energy decreases along the series benzene > naphthalene > anthracene > tetracene > pentacene, translating into the practical consideration of stability and reactivity in that pentacene is rather easily oxidised

by molecular oxygen and degraded by visible light whereas benzene is not. Another obvious difference is that of colouration – benzene is without colour while the more conjugated pentacene is purple-black. As the HOMO-LUMO gap is decreased with increasing conjugation, a redshift in the UV-vis absorption maxima is also observed.

One theory of this behaviour is described by Clar's rule, formulated in 1972, which attempts to rationalise the relative stabilities (and other properties) of PAHs by how many aromatic sextets are present in the molecule.[3] This is shown more clearly when observing the structural formulas for the anthracene (**1.1**), phenanthrene (**1.2**), and triphenylene (**1.3**) series. (Figure 1-2). Anthracene contains one sextet (shown as delocalised benzene rings), phenanthrene two, and triphenylene contains three sextets making it the most stable of the series.

1.1   1.2   1.3
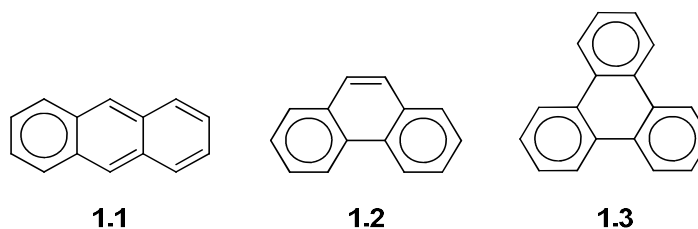
Figure 1-2: Structures of anthracene (1.1), phenanthrene (1.2), and triphenylene (1.3)

with aromatic sextets drawn as delocalised rings.

Clar's rule also has ramifications for acenes; in fact, anthracene (**1.1**, Figure 1-2) is the second member in the family of acenes (naphthalene being the smallest). A *bona fide* acene is composed of "linearly fused benzene rings"[4], and as such consist of a core of carbon atoms,

although other substituents may be appended. The structures of the first five acenes in the series (naphthalene **1.4** to hexacene **1.7**) are shown in Figure 1-3.
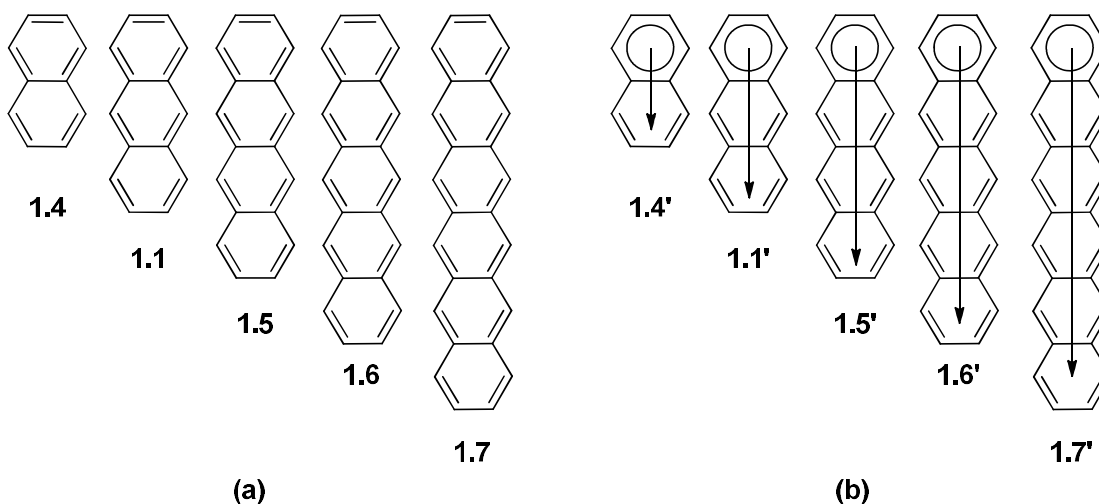
Figure 1-3: (a) Kekulé structures of the first five members of the acene series, and (b) Clar formulae for the same.

Shown in Figure 1-3(b) are the Clar formula for the same set of acenes; as the length of conjugation increases, the number of aromatic sextets does not. In other words, as the energy difference between the HOMO and LUMO becomes smaller, the aromatic stabilisation of the acene does not significantly increase, as no new sextets are added. This helps explain in a qualitative manner why naphthalene is colourless and stable, while pentacene is purple-black and degrades photochemically as well as *via* intermolecular cycloadditions.[5]

Thus, we are introduced to the balancing act between the requisite electronic properties, obtained usually by extended conjugation or introducing substituents, and the stability of these molecules. The stability of acenes can be improved in several ways:[6] firstly,

3

kinetic stability can be imparted by the introduction of bulky substituents such as John Anthony's use of the triisopropylsilylethynyl (TIPS-ethynyl) group to make an air and light stable pentacene (*vide infra*).[7]

A second method of altering the stability of acenes is through the incorporation of heteroatoms. These derivatives are no longer acenes, as they no longer contain only carbon atoms within the core, however, they can be considered acene analogues. Apart from an imine-type nitrogen, other heteroatoms such as sulfur, oxygen, and sp^3-hybridised nitrogen may induce a change in the electronics of the acene which is dependent on the substitution pattern. Dithiapentacene derivative **1.8** (Figure 1-4) was synthesised by Chi *et al.* and adopts a quinoidal structure; nonetheless, the compound is highly stable and was investigated as a promising organic semiconductor.[8]
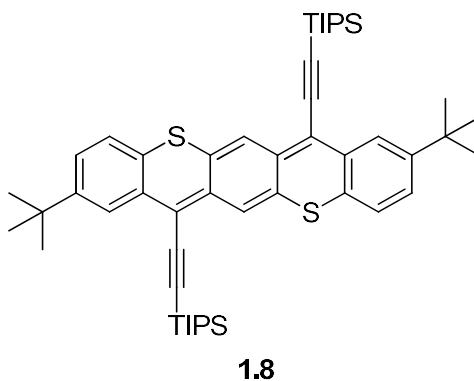
Figure 1-4: Quinoidal dithiapentacene analogue 1.8 investigated

by Chi et al.[8] as an organic semiconductor.

In motifs such as in **1.8**, the quinoidal core is cross-conjugated with the terminal phenyl rings of the acene analogue. This leads to two separate aromatic sextets contributing

to the stability of the compound. A similar motif is observed for the triphenodioxazine (TPDO) dyes which also incorporate imine-type nitrogens in *para*-positions around the central ring (Figure 1-5).
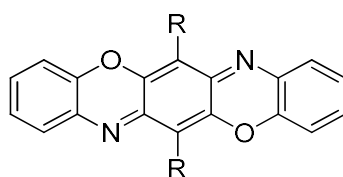
Figure 1-5: Typical triphenodioxazine (TPDO) dye, R is often a halide (Cl, Br).

These dyes exhibit excellent colourfastness (*i.e.* photostability) but suffer from extremely poor solubility.[9]

A different substitution pattern less well known in the literature than the TPDOs, yet structurally similar, is shown in Figure 1-6. Due to the substituents on nitrogen, compounds of this type cannot form the quinoidal congener, and are therefore stable reduced forms of TPDOs (*e.g.* dihydrotriphenodioxazine **1.10**), as indicated by the presence of three aromatic sextets.
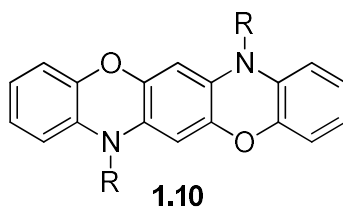
Figure 1-6: Core of a generic dihydrotriphenodioxazine.

Much work has been accomplished in improving the synthesis and properties of acenes and acene analogues in the literature, although there remain systems still to be fully explored.[10,11]

1.2   A Brief Introduction to Organic Electronics

Utilization of organic components, such as liquid crystals or organic light-emitting diodes (OLEDS, *vide infra*), in many ways led to the ability to produce small, high-resolution electronic displays, rather than the previously used cathode-ray tube or plasma technologies. The use of organic molecules provides benefits such as tunability *via* manipulation of functional groups, controlled alteration of the solid-state structure, and solution processability.[12,13]

Taking into account the current progress within the field, manufacturing devices with foldable displays is imminently possible using organic materials.[14] In a rather recent development, the use of OLED technology has placed curved, high resolution displays on the consumer market.[15]

Further developments in this broad field, however, rests upon the "molecular toolkit" available to the materials chemist. Ever more interesting devices with increasingly useful applications will be fabricated using molecules which have not yet been discovered, and for which properties have not been determined. The synthesis and characterisation of novel compounds possessing interesting characteristics is therefore a worthwhile pursuit.

1.3   Molecular Design and Solid-State Importance in Organic Electronics

Organic electronics (OE) fall into several broad categories, including solar cells/energy storage, organic field-effect transistors (OFETs), organic light-emitting diodes (OLEDs), and others. Additionally, it should be borne in mind that OE as a field is very broad, and the molecular design of the material will necessarily depend on the desired property and end application. For example, the desired characteristics of a compound intended for a dye-sensitised solar cell (DSSC) are quite different from those of a liquid crystal intended for display applications. Nonetheless there are some basic considerations common to all, such as the requirement for control of the HOMO-LUMO gap energy, which leads to the general observation that most organic electronics contain conjugated aromatic units (benzene, pyridine, PAHs, *etc*).

Indeed, several "gold standards" of OE materials are compounds like rubrene (**1.11**, Figure 1-7) or pentacene (**1.6**, Figure 1-9).[16] Rubrene contains a tetracene core, shown in red, as well as four appended phenyl rings for a total of eight aromatic ring units (although it should be noted that the four phenyl substituents are not in the plane of the tetracene core, and therefore not fully conjugated therewith). Rubrene displays high hole mobilities (how fast an electron moves through a semiconducting material when exposed to an electric field) of up to 20 $cm^2V^{-1}s^{-1}$ in OFET devices and good stability when compared to many other tetracenes.[17]

1.11
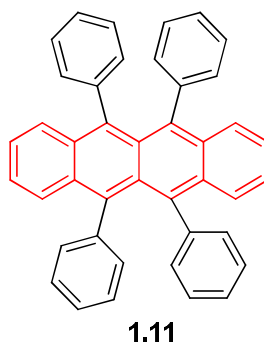
Figure 1-7: Rubrene (1.11), a well-known organic semiconductor.

Both rubrene and pentacene contain an "acene" unit which is a common motif in the design of organic electronics. As discussed previously, the HOMO-LUMO gap in an acene is low, brought about by a lowering of the LUMO and raising of the HOMO energy level (Figure 1-8, used with permission)[18]; this can allow the transport of charge, and the material may act as a semiconductor.[19]
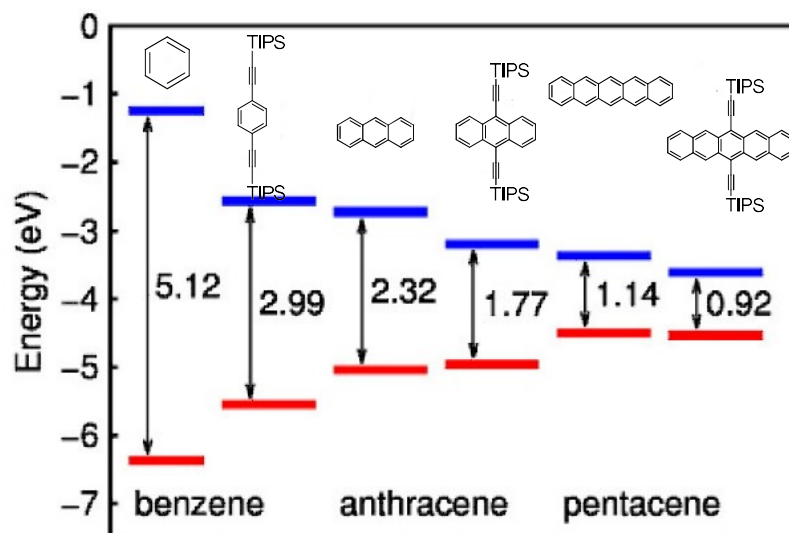
Figure 1-8: Relative HOMO-LUMO energies (eV) of benzene,

anthracene, pentacene, and respective TIPS(ethynyl)-analogues;

figure used with permission.[18]

Despite the inherent ability to transport charge due to a HOMO-LUMO gap of appropriate energy, pentacene itself requires specific processing conditions to form a material with large charge transport properties, such as a microcrystalline thin film.[20] Moreover, the way the individual molecules interact within the crystal lattice can have a large impact on the electronic capabilities of the bulk material. To transport charge as an organic semiconductor, efficient overlap of the MOs of neighbouring molecules is required. Since pentacene crystallises in various *polymorphs* (different crystal structures for the same chemical structure) there can be variability in the charge mobility measurements made on

different samples.[5] Understanding and being able to describe the different arrangements of molecules becomes necessary.

Supramolecularly, aromatic surfaces (such as acenes) tend to interact with one another in several different ways, such as π-π stacking, where molecules align face-to-face with a major interaction between the respective aromatic π-electron clouds. Alternatively, an edge-to-face or C–H···π-interaction can predominate, forming a pattern called "herringbone". This dichotomy is illustrated nicely in the differences between the solid-state structures of pentacene (**1.6**) and 6,13-bis(triisopropylsilylethynyl)pentacene (TIPS-pentacene, **1.12**) shown in Figure 1-9. While pentacene packs in a herringbone fashion in the solid state, TIPS-pentacene adopts a face-to-face interaction of the pentacene cores, which are also closer to one another (3.47 Å *vs.* 6.27 Å for pentacene).[21] This solid-state arrangement of the molecules in TIPS-pentacene leads to an overall improvement in properties (solubility, stability, solid-state packing) over the parent compound.
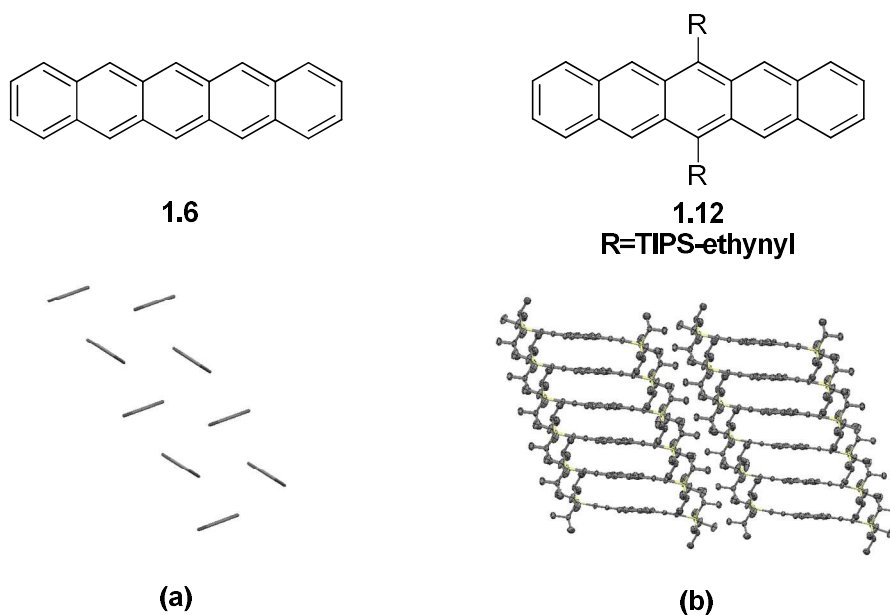
Figure 1-9: (a) Pentacene (1.6) and its herringbone crystal packing structure,

and (b) TIPS-pentacene (1.12) and its crystal packing structure

(H-atoms omitted for clarity in b).

Not only do the TIPS-ethynyl groups allow for improved physical characteristics, but chemical stability is also conferred. Whereas pentacene suffers from photodegradation and oxygen sensitivity, **1.12** is stable (and more soluble) in solution.[22]

Control of solid state packing can also be achieved in heteroaromatic systems. Desiraju *et al.* recognized that herringbone packing decreased with a corresponding increase in π−π overlap in systems such as **1.13** (Figure 1-10) where heteroatoms and substituents reduce the number of H atoms available for C−H···π-interactions.[23] **1.13** packs in a herringbone manner, while compounds **1.14** and **1.15** pack in a π−π stacking rich packing motif termed *β*-packing.
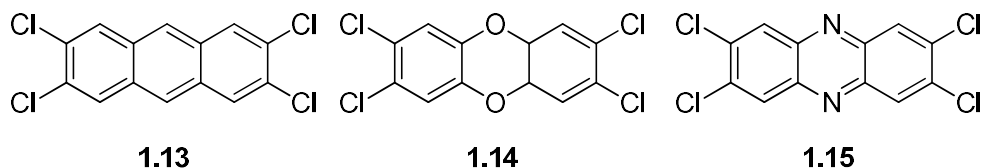
Figure 1-10: Tetrachloroanthracene 1.13 adopts a herringbone packing motif, while dibenzodioxin 1.14 and phenazine 1.15 adopt β-packing motifs.

In addition to conjugation (appropriate HOMO-LUMO levels) and supramolecular organization, targets should be soluble enough to allow for characterisation (structural, photophysical, electrochemical, *etc*.) Since many flat, aromatic compounds tend to form insoluble aggregates, solubilising alkyl groups are often appended to aid in processability. An example is in the case of the soluble quinacridone derivative **1.17** (Figure 1-11) which was synthesised by Mullen *et al*.[24,25] to investigate the H-bonded self-association in solution. This cannot be done using the parent quinacridone (**1.16**) since it is extremely insoluble (due to intermolecular H-bonding), and the normal method of solubilising quinacridones involves substitution of the N atoms.[26] Thus, placement of dodecyloxy (and other) solubilising alkyl chains at the periphery of the compound allowed sufficient solubility to study the compound's behaviour.
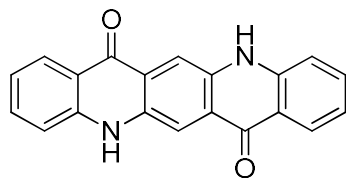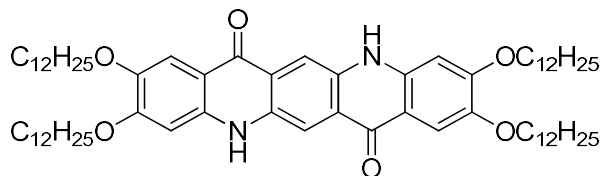
Figure 1-11: Quinacridone (1.16) and Mullen's soluble quinacridone 1.17.

Thus, one can see that controlling supramolecular organization can be very important not only for practical processability of OE but also the end property of the material; understanding and finding methods of controlling this behaviour is integral to progress within the field.

1.4   A Brief Introduction to Liquid Crystals

A liquid crystalline (LC) material is unique in that it contains features of both the solid crystalline and isotropic liquid phases. More specifically, a liquid crystal exhibits, to some degree, both the order of the solid state *and* the disorder of the liquid state. A simpler way of thinking about this phenomenon would be that the material is not so ordered as to prohibit flowing like a liquid, but does order the individual molecules in some specific, reproducible manner.

The first LC phase was discovered in 1888 by examining the melting and freezing behaviour of cholesteryl benzoate (**1.18**).[27] This compound first melts into a cloudy liquid at 145°C and, at 178.5°C, becomes a clear liquid. Over this temperature range, a LC material will

exhibit a phase of matter which is distinct from a solid, liquid, or gas, and is termed the LC

mesophase.[28]

1.18
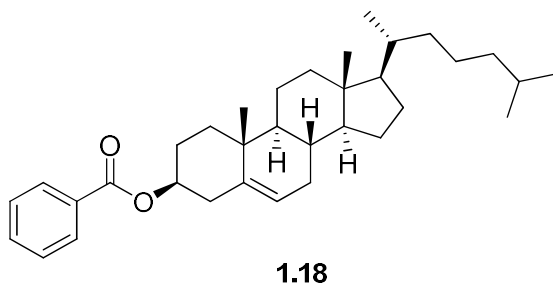
Figure 1-12: Cholesteryl benzoate (1.18), the first liquid crystalline compound

discovered in 1888.

LC phases can be grouped together based on the way the molecules are ordered. Cholesteryl benzoate, for example, exhibits a *nematic* phase, meaning that the molecules orient themselves in a threadlike fashion (more accurately **1.18** exhibits a *chiral nematic* phase due to the asymmetry of the molecule.)[29] Liquid crystals possessing nematic phases have been used in liquid crystal displays (LCDs).[30] Other liquid crystals exhibit *smectic* phases wherein the molecules are ordered in such a way that the layers can slide over one another in a 'soapy' manner (*smecticus* is Latin for soap.)[31] There are fewer applications of smectic LC phases. However, progress has been made in smectic LCDs.[32]

Of particular importance to the discussion at hand are *columnar* mesophases in which the molecules are arranged in columns; compounds exhibiting such a phase are of interest due to the possible charge-transport arising from the columnar arrangement of molecules in the bulk structure leading to semiconductor properties.[12]

LC compounds are often divided into categories based upon structural and mesophase properties. *Discotic* and *calamitic* are two broad categories of compounds which display liquid crystalline properties, and these can be differentiated by their structural features (Figure 1-13). *N*-(4-Methoxybenzylidene)-4-butylaniline (MBBA, **1.19**) is a prototypical example of the calamitic class, distinguished as such by its rod-like structure. Also of note in MBBA is the presence of a butyl chain; many liquid crystals contain the motif of an aromatic/conjugated group with flexible side chains. The combination of planar sp^2-hybridised 'cores' attached to flexible chains such as alkyl or alkoxy groups often provides the correct amounts of order and disorder to form a mesophase.

1.19   **1.20**
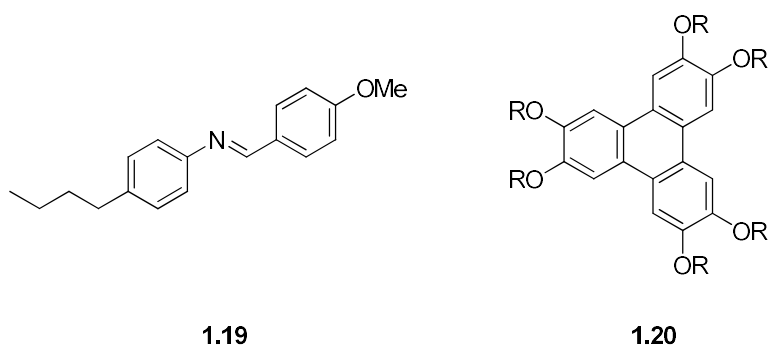
Figure 1-13: MBBA- (1.19) and triphenylene-based (1.20) liquid crystals.

In contrast to MBBA, structure **1.20** is based upon the triphenylene core and forms the quintessential structural motif of the *discotic* liquid crystal class, containing, as the name implies, a disc-like aromatic core. While calamitic liquid crystals often form smectic and nematic mesophases, discotic liquid crystals most often form columnar mesophases. These discotic columnar mesophases are desirable due to the increased intermolecular orbital

overlap between molecules within the columns which has the ability to increase charge carrier mobility, fluorescence intensity, and exciton diffusion length (the distance traveled by an electron or hole, which determines useful thickness of semiconductor layers.)[12,33]

1.5   *Aggregation-Induced Emission (AIE)*

Light can interact with matter in a variety of ways. The colours we see are due to light interacting with matter in such a way that some wavelengths are absorbed, and the colour observed results from the reflection of the remaining (visible) wavelengths. This absorption and reflection of light energy is well understood.

Fluorescence (emission) is another generally well understood mode through which light and matter interact. In this instance, light is absorbed by the substance which then promotes an electron from a lower-lying molecular orbital (MO) to one of higher energy. As the electron relaxes to its original lower-lying MO the light which was absorbed is emitted as light of a different wavelength.

Fluorescence is a sensitive process, and there are many factors which can increase or decrease fluorescence activity such as crystal packing,[34] metal ion coordination,[35,36] nitroarenes,[37] temperature,[38,39] and aggregation.[40,41]

Aggregation-induced emission (AIE) is a phenomenon reported relatively recently in 2001 by the Tang group in which a pentaphenylsilole compound (**1.21**, Figure 1-14) exhibited no fluorescence in solution but in the solid state exhibited bright fluorescence.[42] The derivative was found to have the same fluorescence spectrum as a solution in ethanol-water or as a solid thin film, but not as a solution in ethanol, where the fluorescence

behaviour was severely attenuated. These observations show that emission is significantly increased as a result of aggregation, whether in solution or the solid state.
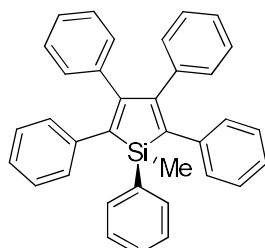
1.21

Figure 1-14: 1-Methyl-1,2,3,4,5-pentaphenylsilole (1.21),

the first demonstrated AIE luminogen.

In the specific case of **1.21**, the AIE effect was ascribed to the inability of the phenyl rings to assume an entirely coplanar conformation in the solution state which would decrease the resonance in the structure, in turn decreasing the fluorescence of the molecule. In the solid and aggregate states, it is theorised that the molecule can assume a more coplanar conformation allowing for increased conjugation between the central silole and appended phenyl rings, increasing the intensity of the fluorescence and causing a red-shift in intensity. Of critical importance, however, is the fact that steric hindrance precludes the possibility of complete co-planarity and as such also precludes the process of quenching *via* excimer (excited-dimer) formation (concentration quenching).

A more general theory of AIE is that found for compounds like tetraphenylethylene (**1.22**, Figure 1-15).[43]
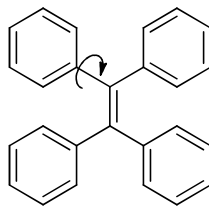
1.22

Figure 1-15: AIE luminogen tetraphenylethylene (1.22) with one

of four rotatable bonds indicated.

In compounds such as **1.22**, aggregation is theorised to inhibit rotation about the ethylene-phenyl bonds, thus limiting non-radiative decay (*i.e.* relaxation wherein no light is emitted). This restricted intramolecular rotation (RIR) process is thought to be responsible for much of AIE's effects in compounds where conformational mobility can be limited by aggregation.

A large number of compounds that display the AIE effect are currently in the literature and more continue to be reported due to the interesting applications made possible by such solid state fluorescence and electronic properties.[44–47]

1.6 Dicyanotetraoxapentacenes as Novel LC Mesogens and AIE Luminogens

In the quest for materials with the optimum properties for organic electronics applications, new structural motifs must necessarily be investigated. By way of rational modification of existing structures, new structures can be investigated which may have interesting or ideal properties for various applications. There are several structures which have been investigated with respect to LC and fluorescence properties, such as the pentacenequinone system shown in Figure 1-16 synthesised in the Maly lab. [48]
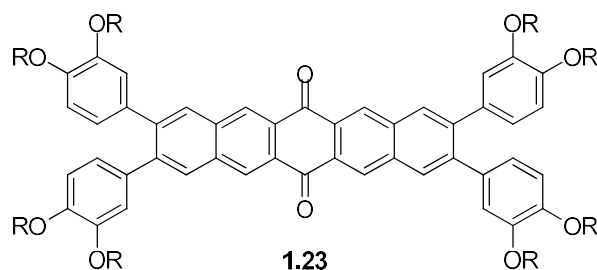
Figure 1-16: Example of a pentacenequinone-based liquid crystalline compound synthesised previously in the Maly lab (R = C₁₀H₂₁).[48]

When the R groups in structure **1.23** are *n*-decyl alkane chains the compound exhibits a columnar hexagonal LC phase from 109-145°C. Of interest within the field of liquid crystalline materials is the relationship between structural features and physical properties such as mesophase range and fluorescence capabilities.

Similar in structure to the pentacenequinone system, compounds **1.24** (R = C_6H_{13} or $C_{10}H_{21}$) were previously synthesised in the Maly lab and exhibited AIE as well as a LC mesophase.[49] The synthesis, however, required a tedious and difficult separation *via*

chromatography to acquire the final product and for that reason was not ideal. As the solid-state interactions for these compounds are of interest and have not previously been explored, a route which provides material in adequate quantities to grow X-ray quality single crystals is also desirable.
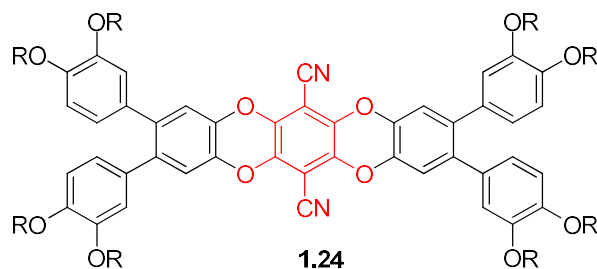
Figure 1-17: Representative substituted dicyanotetraoxapentacene with the central tetraoxaterephthalonitrile moiety highlighted in red.

1.7   Thesis Objectives

The primary goal of this thesis is the development of a practical synthetic route to a series of bis(alkoxy)phenyl-substituted dicyanotetraoxapentacenes as novel liquid crystalline pentacene analogues; this is covered in depth in the following chapter.

A second goal of this project is the expansion of this methodology to access structures wherein heteroatoms other than oxygen (*i.e.* nitrogen, sulfur) are installed within the pentacene core (Figure 1-18); Chapter Three covers these endeavours in detail.
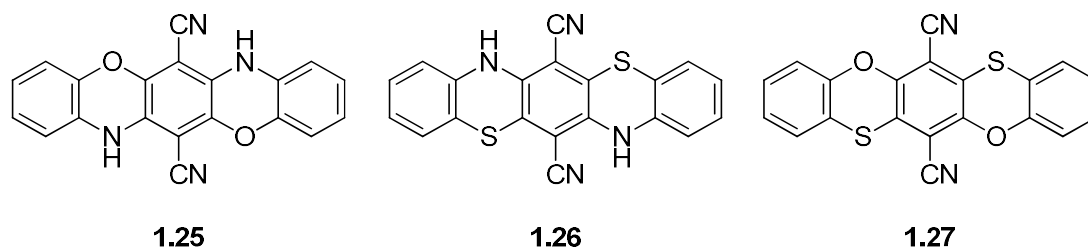
Figure 1-18: Several target dicyanoheteropentacene analogues.

Not only are the above dicyanopentacene analogues (*e.g.* **1.25**) unknown in the literature, but the unsubstituted heteroaromatic cores have been likewise unexplored.

The reactivity of tetrafluoroterephthalonitrile with respect to 1,2-bifunctional aromatic nucleophiles is a major theme in this work (especially Chapter Three). While a limited number of heterocycles have been derived from TFTP, unreported systems (and some previously reported) based on this structural motif may possess surprising reactivity and photophysical properties to be explored. This work adds several new members to the family of TFTP-derived dicyanopentacene analogues, in addition to investigating their photophysical properties and solid-state organisation.

Chapter II - An Improved Synthesis of Soluble, Liquid Crystalline Dicyanotetraoxapentacenes

2.1 Previous Synthesis and Investigation of Physical Properties of DCTOPs

Previous work within the Maly group by former Honours student Ms. Brooke Raycraft[49] showed that it was possible to synthesise the target dicyanotetraoxapentacenes (DCTOPs) **2.1a,b** *via* a fourfold Suzuki coupling between tetrabromide **2.3** and boronate ester derivative **2.2a** or **2.2b**, shown in the retrosynthetic scheme below (Scheme 2-1).
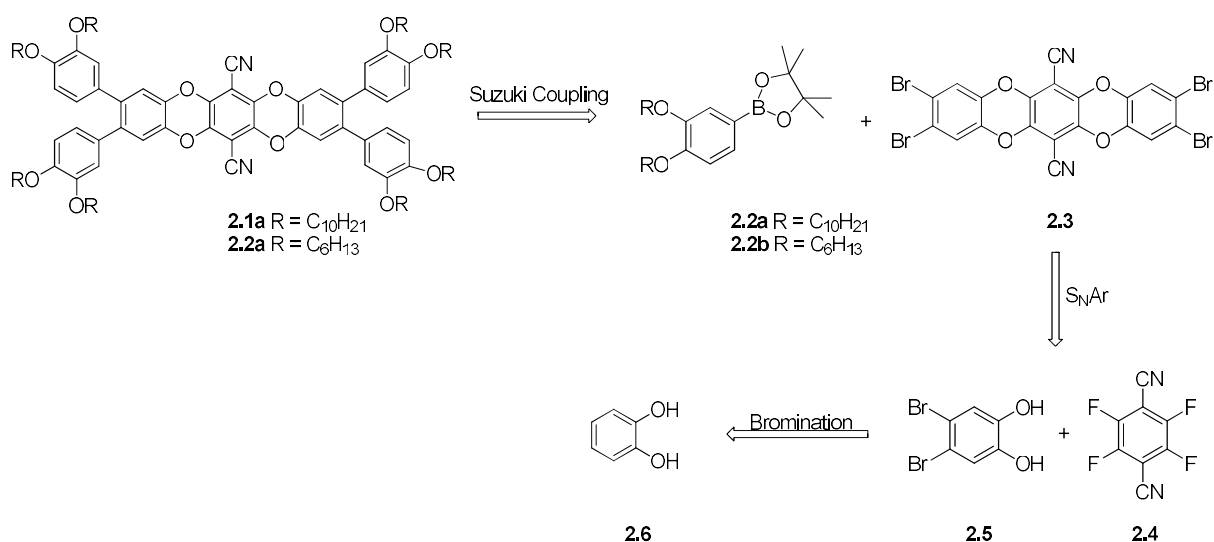
Scheme 2-1: Retrosynthetic analysis for the original synthesis

of LC DCTOPs 2.1a,b (Raycraft, 2014).

Compound **2.3** can retrosynthetically be derived from the nucleophilic aromatic substitution reaction between dibromocatechol and tetrafluoroterephthalonitrile (TFTP

2.4), which is synthesised from the tetrachloro compound[50] or purchased. Finally, compound **2.5** can be accessed by electrophilic bromination of catechol.[51]

Scheme 2-2 shows the resulting forward synthesis pursued by Raycraft and the yields obtained. Bromination of catechol followed by a nucleophilic aromatic substitution (S_NAr) reaction with TFTP (**2.4**) proceeds in good yields and facile preparation. Unfortunately, the following fourfold Suzuki coupling with the respective pinacol boronate ester proceeded in poor yield, and perhaps more importantly, resulted in a mixture of variously substituted products, which made separation and purification difficult. Additionally, long reaction times (2 to 6 days) were required in order to push the reaction fully to the end product.
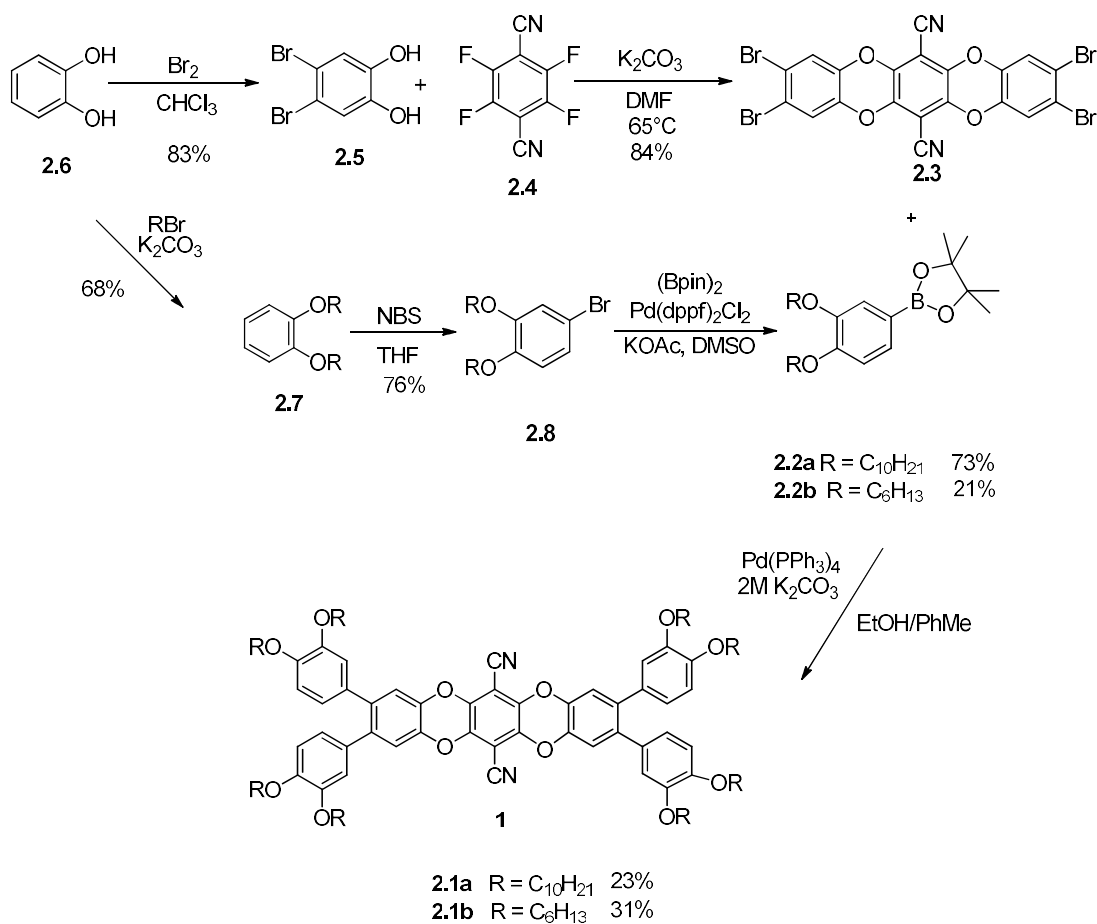
Scheme 2-2: Forward Synthesis for the original synthetic

route to LC DCTOPs (Raycraft, 2014).

It was found during this 2014 work that the target dicyanotetraoxapentacenes **2.1a,b** exhibit a columnar hexagonal liquid crystalline mesophase upon heating up to the clearing point at 162 °C. Preliminary investigation into the fluorescence properties of **2.1a,b** indicated the compounds exhibit aggregation-induced emission; in addition to intensely bright solid-state fluorescence both compounds experience an intensification and redshift

in the emission maximum upon addition of water to THF solutions of **2.1a** or 2.**1b**. A representative photo of this effect is shown in Figure 2-1 as well as the fluorescent solid.
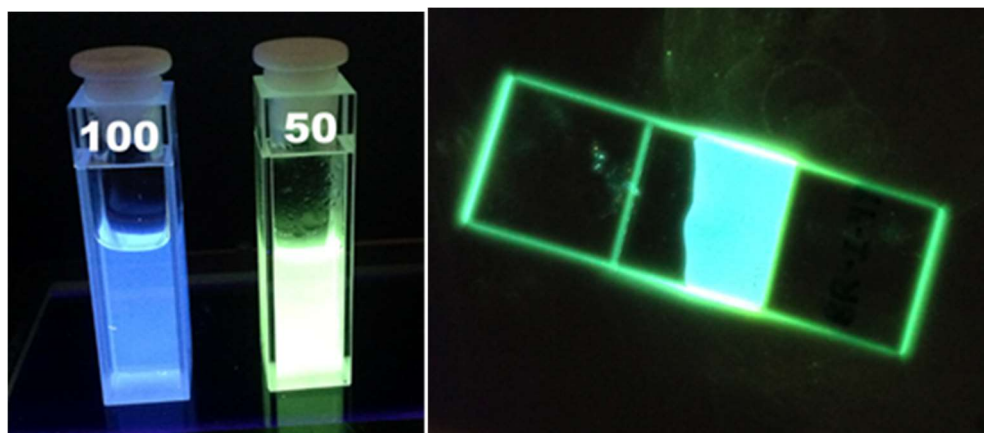
Figure 2-1: Images of compound 2.1a in 100% THF (blue) and 50% THF/water (green) and (b) as a thin film under long wave UV irradiation (365 nm).[49]

Due to the promising nature of these initial investigations it was clear that optimising the synthetic route to derivatives of **2.1** was both necessary and worthwhile.

2.2   *Initial Fourfold Suzuki Optimisation Attempt*

Due to the very low solubility of tetrabromide **2.3**, in addition to the well-known positive effects of microwave heating on Suzuki couplings, microwave chemistry was explored as an alternative to conventional heating. The methoxy-substituted derivative (using the commercially available 3,4-dimethoxyphenyl boronic acid **2.2c**, Scheme 2-3) was used to screen microwave heating conditions (Table 2-1).
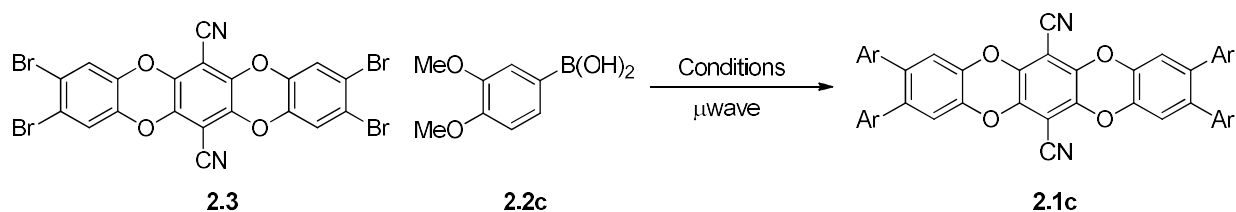
Scheme 2-3: Attempted microwave Suzuki coupling of tetrabromide 2.3a

with boronic acid 2.2c.

Table 2-1: Attempted microwave reaction conditions to form DCTOP derivative 2.1c.

Entry	Pd Source	Ligand	Base	Additive	Solvent	Temp. (°C)	Time (min)	Yield (%)
1	Pd(PPh$_3$)$_4$	-	K$_2$CO$_3$	-	EtOH-PhMe-H$_2$O	155	60	35
2	Pd/C	-	K$_2$CO$_3$	-	EtOH-H$_2$O	95	10	mixture
3	Pd(OAc)$_2$	-	K$_2$CO$_3$	TBAB	H$_2$O	100	30	mixture
4	Pd(PPh$_3$)$_4$	-	CsF	-	DME	100	20	0 (homocoupling)
5	Pd(OAc)$_2$	dfppe	KOH	-	1,4-dioxane	120	20	0 (homocoupling)
6	Pd(OAc)$_2$	SPhos	BaCO$_3$	-	n-BuOH-PhMe-H$_2$O	120	20	mixture

					EtOH-			
7	Pd(OAc)$_2$	dfppe	K$_2$CO$_3$	TBAB	PhMe- H$_2$O	150	5	mixture
8	Pd(PhCN)$_2$Cl$_2$	Phen	Cs$_2$CO$_3$	Dibenzo-24- crown-8	EtOH- PhMe- H$_2$O	140	60	mixture
9	Pd(PPh$_3$)$_4$	-	NaOH	-	PhMe- H$_2$O- EtOH	150	30	0 (nitrile hydrolysis)

In keeping with the results of the reaction of the longer alkyl derivatives, under conventional heating conditions the product was obtained in a low 35% yield *via* microwave heating (Table 2-1, Entry 1). Attempts were then made to improve this yield by again changing the palladium catalyst source, solvent, time, *etc*. However, like previously, the main product (TLC, ^{1}H NMR) appeared to be homocoupled boronate likely formed due to unreactivity or insolubility of the aryl bromide; in other cases where an inseparable mixture was obtained, the products (all yellow) likely consisted of variously arylated products. In the case of Entry 9, it is hypothesised that nitrile hydrolysis may have occurred, since an insoluble and unidentifiable product was obtained from a reaction mixture which smelled strongly of ammonia.

Despite the poor results, Suzuki coupling to form the hexyloxyphenyl- and decyloxyphenyl-substituted dicyanotetraoxapentacenes were conducted in a microwave reactor under the otherwise original conditions. Unfortunately, yields were still less than

impressive (14% and 30% respectively) and purification was possible but was of comparable tediousness to the reaction *via* conventional heating.

Considering these results, as well as rather extensive screening of reaction conditions such as palladium(0) sources, base, solvent, time, and temperature, it appears that this coupling is not amenable to microwave heating enhancements.

2.3   Revised Retrosynthetic Analysis

With respect to the initial synthetic route, one outstanding feature is the expediency of the preparation in that very few steps (three linear) are required to arrive at the target compound. Thus, despite the low yield and difficult separation of the final Suzuki coupling reaction, any improved synthetic route would necessarily compete with an extremely short synthesis of a large polycyclic substituted heteropentacene.

As shown in the retrosynthesis below, the target compound could be envisaged as coming from the S_NAr reaction between terphenyl diol **2.9** and TFTP (**2.4**), and the terphenyl moiety being derived from the Suzuki coupling between the protected dibromocatechol and the appropriate phenylboronate species (Scheme 2-4). Essentially this amounts to a reversal in the order of reaction of the S_NAr and Suzuki reactions.
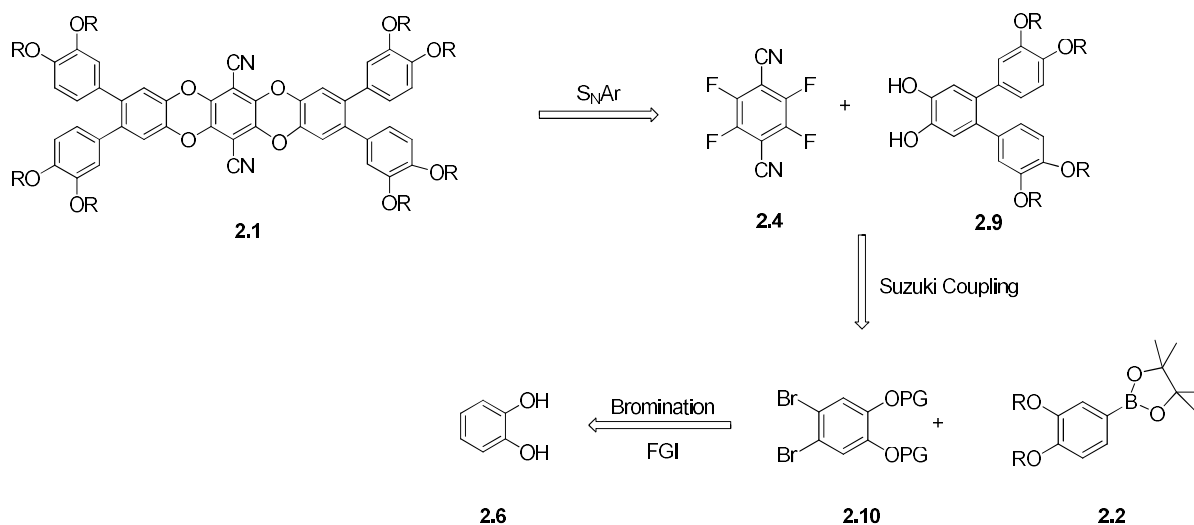
Scheme 2-4: Revised retrosynthesis of dicyanotetraoxapentacene 2.1 (PG = protective group).

2.4 Revised Synthesis of DCTOPs 2.1

As can be seen in Scheme 2-4, a protected dibromocatechol (**2.10**) is required for the Suzuki coupling to prepare diol **2.9**. Because Suzuki couplings are carried out in basic media, and catechols are relatively acidic under such conditions ($pK_a \approx 10$), coupling reactions of this type are rarely carried out on phenols and catechols. Phenoxide is much more electron donating than phenol, and this increased electron density *para* to the aryl bromides can strongly deactivate the coupling partner.[52] In fact, due to difficulties with the original synthesis, Raycraft attempted the direct Suzuki coupling between dibromocatechol **2.5** and boronate **2.2a** and showed that this route did not furnish the desired terphenyl diol in appreciable quantities. Indeed, the diol ($R = C_{10}H_{21}$) was obtained as a brown solid from the attempted coupling (Raycraft, Honours Thesis, 2014) albeit in a 4% yield from dibromocatechol.

Necessarily, a protection, Suzuki coupling, and deprotection sequence was developed. As with any protective group (PG) chemistry it is essential that both the protection and deprotection steps proceed in high yield and ease of purification to maintain practical synthetic efficiency.

The first protecting group briefly investigated was the acetonide with attempted installation *via* *p*-TsOH-catalysed condensation of dibromocatechol with acetone, which furnished the starting material as beautiful crystals. Acetylation of the phenolic OH groups was then explored as an easily installed PG, and diacetylated dibromocatechol **2.11** was obtained in a low (46%) yield (Scheme 2-5). The easily attached acetyl moieties were just as easily hydrolysed under the basic aqueous Suzuki reaction conditions providing a mixture of products, mainly deacetylated dibromocatechol **2.5**.
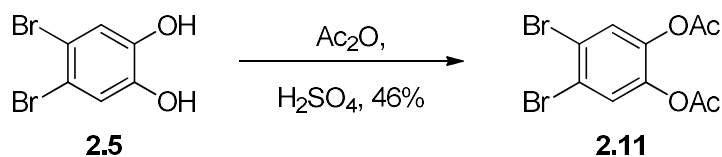
Scheme 2-5: Protection of dibromocatechol as the bis(acetate) (2.11).

Thus, the methoxymethyl (MOM) protective group was then chosen as a base-stable alternative. Wishing to avoid the highly toxic and carcinogenic chloromethyl methyl ether (MOMCl) the more common protection route of deprotonation of the alcohol with NaH followed by treatment of the resulting anion with MOMCl was discarded in favour of a more obscure method of MOM introduction; this method involves use of phosphorous pentoxide

P$_2$O$_5$ in a dimethoxymethane/chloroform solution (Scheme 2-6).[53,54] The reaction gratifyingly proceeded in an excellent 95% yield to give the bis(MOM)-protected catechol **2.12**.
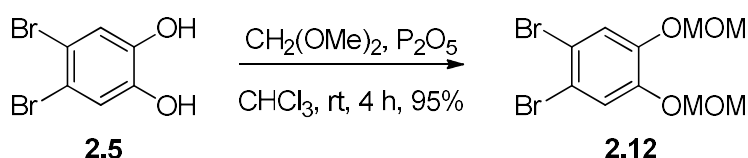
Scheme 2-6: Protection of dibromocatechol 2.5 as the methoxymethyl ether (OMOM).

This product was unexpectedly unstable, converting over several weeks at room temperature from a white, crystalline solid to a black, sticky substance. The author is unaware of similar behaviour by other MOM-protected alcohols or catechols. Laschat *et al*.[54] describe the preparation of 4-bromo-1,2-bis(methoxymethoxy)benzene and do not mention any instability in that very similar compound. Nonetheless, if kept at −20 °C, **2.12** remains as white crystals for several months (>8) without noticeable decomposition.

With protected catechol in hand, subsequent Suzuki coupling with commercially available 3,4-dimethoxyphenylboronic acid required attempting the reaction under several conditions in order to acquire the desired product in satisfactory yield. (*N.B.* This methoxy derivative would not yield a liquid crystalline product, rather it serves as a model compound using a commercial boronic acid.) Initial attempts involved using, again, a procedure published by the Laschat group to make similar terphenyl compounds from aryl 1,2-dibromides.[54] Unfortunately, these reaction conditions (Pd(PPh$_3$)$_4$, K$_2$CO$_3$, NaF, DME-H$_2$O,

reflux) yielded a small amount of material with a low overall mass balance. Using slightly different conditions (Pd(PPh$_3$)$_4$, Na$_2$CO$_3$, DME-H$_2$O, reflux) gave the product (**2.13**) in 70% yield (Scheme 2-7). An additional benefit is that no column was necessary to isolate the pure product provided the organic extracts were filtered through a short pad of Celite® before concentration (to remove palladium residue) or, alternatively, decolourised with activated charcoal during recrystallisation from hot methanol.
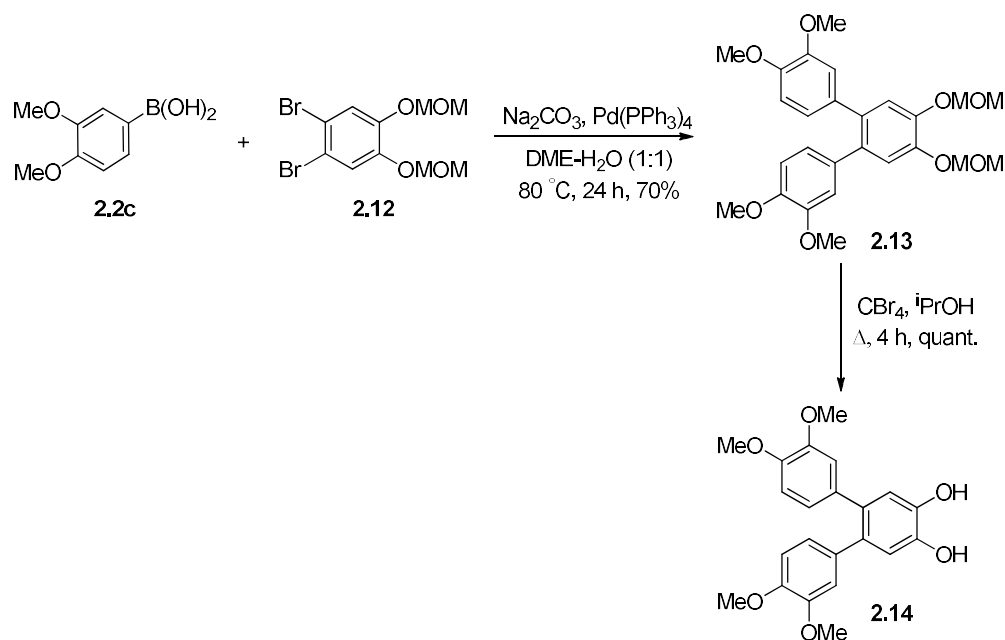
Scheme 2-7: Synthesis of terphenyl diol 2.9c via a two-fold Suzuki coupling, deprotection sequence.

Deprotection of the bis(methoxymethoxy)terphenyl compound **2.13** was initially effected using 38% aqueous hydrobromic acid in acetonitrile. However, this method was deemed unsatisfactory due to the disappointing deprotection yield (~70-80%) as well as

product impurity likely caused by instability of the catechol derivative towards such highly acidic conditions and possible demethylation of the aryl methyl ethers. A more favourable deprotection strategy was then employed utilising a catalytic amount of CBr$_4$ (10 mol% per methoxymethyl ether) in 2-propanol, presumably forming small amounts of anhydrous HBr which catalyse the deprotection in quantitative yield and excellent purity (Scheme 2-7).[55]

Finally, reaction of tetra(methoxy)terphenyl diol **2.14** with TFTP (Scheme 2-8), initially carried out using potassium carbonate in DMF gave the tetraphenyl-dicyanotetraoxapentacene **2.1c** in 82% yield.
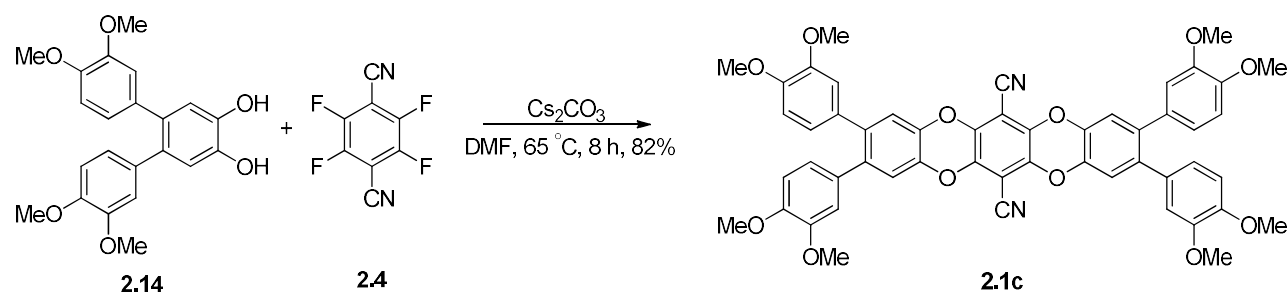
Scheme 2-8: S$_N$Ar reaction of diol 2.14 with TFTP to afford DCTOP 1c.

Methoxy-substituted dicyanotetraoxapentacene **2.1c** was obtained as a bright yellow solid exhibiting brilliant fluorescence under UV irradiation (365 nm), much like the C$_6$- and C$_{10}$-substituted congeners obtained previously within the group by Raycraft. Indeed, solutions of **2.1c**, especially in more polar solvents, fluoresce even in sunlight and the solid is green fluorescent under a UV lamp.

As mentioned previously, however, the normal motif in liquid crystal design is that of *long*, *flexible* side chains of which the methyl ethers in **2.1c** certainly are not. Therefore, the octamethoxy-substituted derivative would not be expected to exhibit a LC mesophase and, indeed, the melting point was too high to be determined (>260°C).

Crystals of **2.1c** were grown from chloroform-*iso*propanol utilizing the slow vapor diffusion method and were of quality suitable for X-ray diffraction. The obtained crystal structure indicates several important structural features (Figure 2-2).
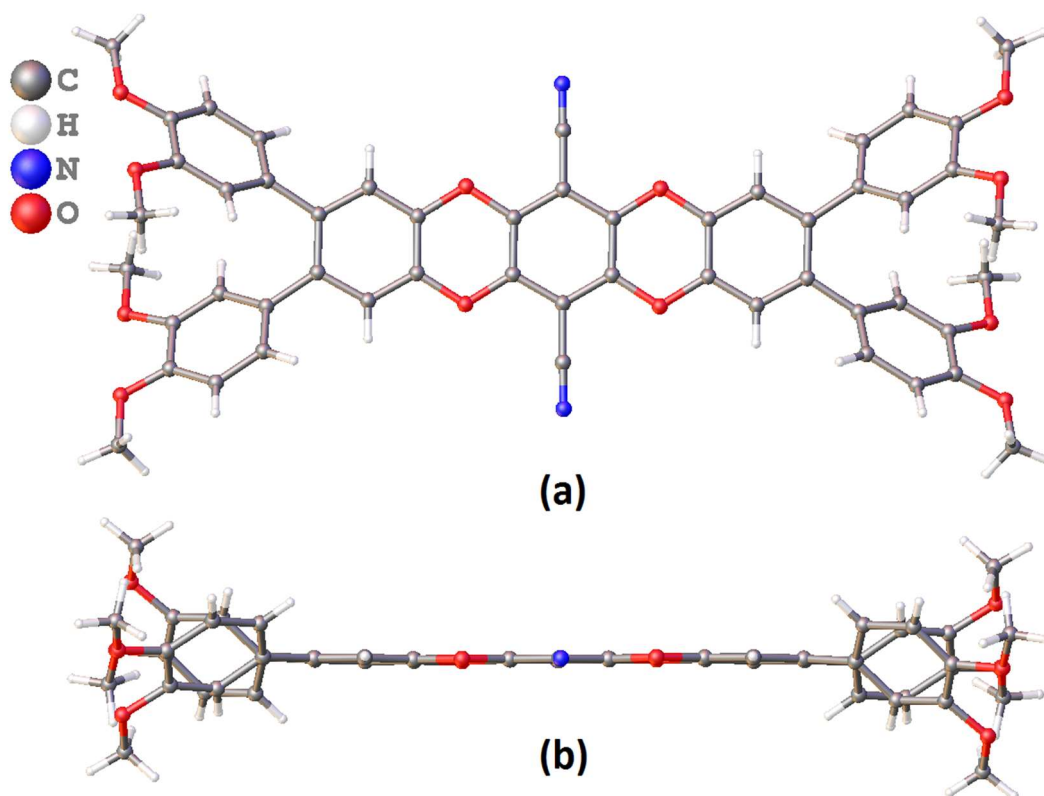
Figure 2-2: Crystal structure of 2.1c showing (a) the top-down view of the core and (b) the side-on view of the planar DCTOP molecule.

The compound crystallised in a triclinic space group (P-1) with two crystallographically non-identical molecules per unit cell. The dicyanotetraoxapentacene core was shown to be highly planar, possessing a root mean squared deviation (RMSD) from planarity of 0.014-0.037 Å (Figure 2-2b). This is similar to what is known from reported structures of other tetraoxapentacenes.[56,57] Bond lengths in the core range from 1.360(8)-1.410(8) Å and suggest significant electron delocalization (Appendix A.) Moreover, the C–O–C bond angles are an average 115.1 °, closer to that expected for a sp^2-hybridised carbon than sp^3-hybridised oxygen. The phenyl substituents are twisted out of the plane of the core (Figure 2-2a), with dihedral angles between phenyl ring and that of the core ranging from 38.23(14) to 57.02(17) °.

Because the peripheral phenyl rings are not co-planar with the tetraoxapentacene cores, molecules of **2.1a** do not engage in effective π-stacking interactions in the crystal structure. Rather, the two molecules in the asymmetric units have cores that are offset by 13.48(10) Å, with a centroid-to-centroid distance of 6.4509(4) Å (Figure 2-3).
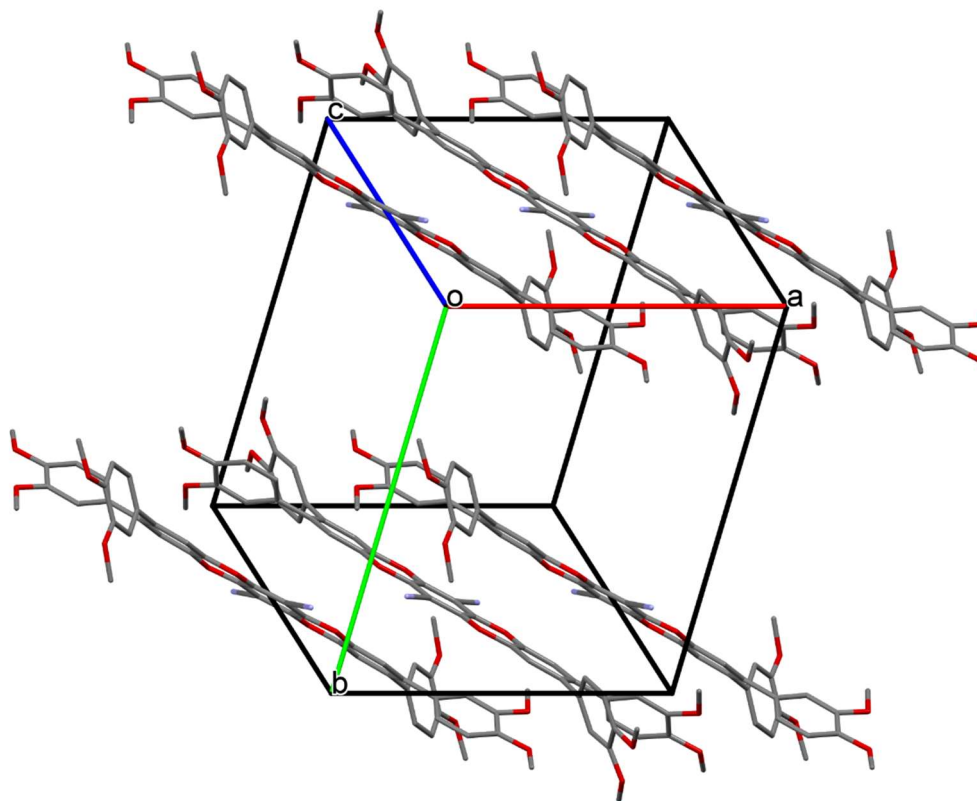
Figure 2-3: Crystal packing in DCTOP 2.1c.

Unfortunately, there are no published dicyanotetraoxapentacene crystal structures with which to compare, other than a dimerized derivative exhibiting bent DCTOP cores.[58] This is unsurprising considering the parent compound's marked insolubility in nearly every organic solvent and tendency to "powder out" of solution rather than crystallise. Additionally, many of the DCTOP derivatives in the literature consist of polymers, which rarely crystallise. We therefore sought to obtain single crystals of the parent, unsubstituted DCTOP in order to provide a basis for comparison with **2.1c.**

A range of crystallisation methods and solvents were attempted, and small, thin crystals were successfully grown from mesitylene *via* slow evaporation (1-2 months) and subjected to X-ray analysis.

DCTOP crystallised in an orthorhombic space group (Pbca) with three symmetry-related molecules per unit cell. Unsurprisingly, this compound exhibits bond lengths and angles in agreement with that of the tetra-aryl derivative; a similarly low RMSD from planarity of 0.039 Å was also observed.

The packing of this compound has not been described previously in the literature and was of primary interest in obtaining crystallographic data. Unlike pentacene, which packs in a herringbone pattern (Chapter 1) and therefore exhibits few effective π-π interactions, DCTOP does show limited co-facial overlap (Figure 2-4).
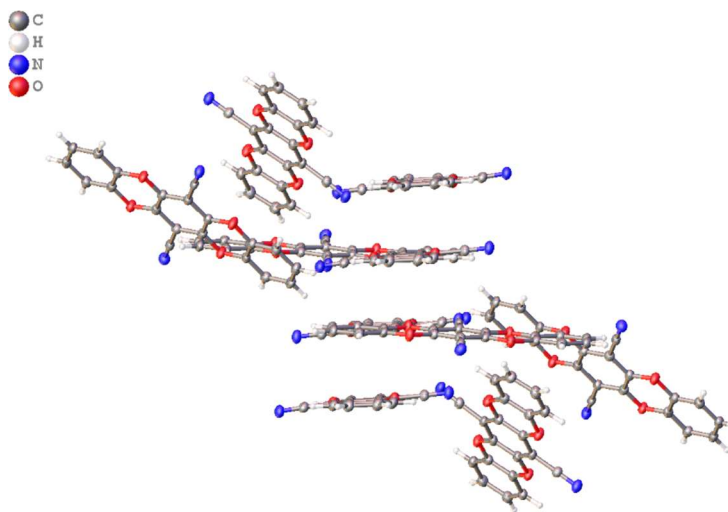
Figure 2-4: Crystal packing of parent, unsubstituted DCTOP.

Each molecule has two molecules above and below the plane of the aromatic system (Figure 2-5). The molecules which are packed parallel but rotated ≈90 ° in plane (parallel-perpendicular) are at a distance of 3.28 Å (plane to plane centroid) with a plane-normal-to-plane-normal angle of 6.5 °. The molecules which pack in a parallel fashion have plane-to-plane centroid distances of 3.29 Å while the angle between the plane normals was found to be 0 ° (indicating a high degree of co-planarity). In each case the interaction geometries are well within those required for face-to-face π-π stacking interactions between the aromatic rings, and no C−H···π-interactions were observed.[59,60]
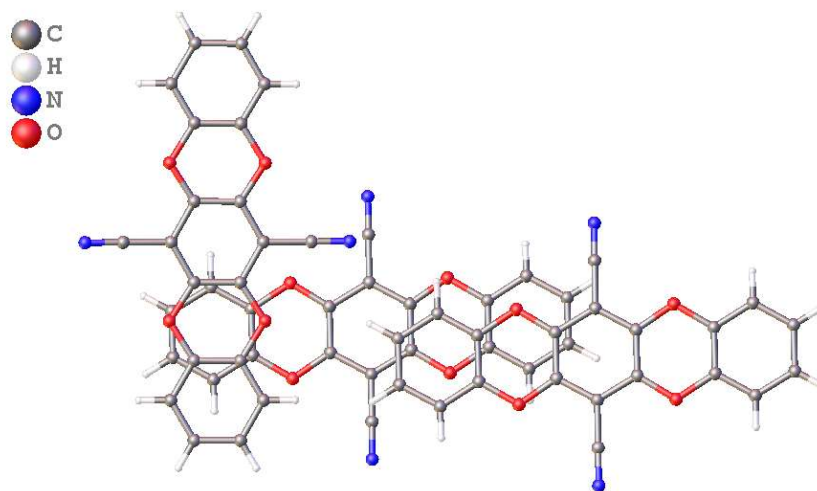
Figure 2-5: Crystal structure of parent DCTOP, showing

parallel and parallel-perpendicular π−π stacking.

Comparing the parent and tetraarylated derivative **2.1c** structures leads to the observation that parallel-perpendicular packing of the cores is eliminated in preference to a lengthened π–π stacking distance (6.45 Å *vs.* 3.29 Å) in the substituted derivative.

2.5   *Synthesis of C6 and C10-Substituted DCTOP Derivatives*

With the new synthetic route tested, the corresponding boronic acids **2.2a,b** were synthesised from the corresponding aryl bromides **2.8a,b**[61,62] *via* a slightly modified published procedure,[63] substituting triisopropyl borate for trimethyl borate (Scheme 2-9), in moderate to good yields (60-80%). It is worth noting that during the lithium-halogen exchange reaction precipitation of the aryllithium and/or the starting material is possible, preventing further stirring. This is an issue for both the hexyloxy- and decyloxy-substituted compounds but is of more importance for the C_{10} derivative. Control of the cooling temperature during this reaction is imperative, as precipitation during the exchange is deleterious for the yield.
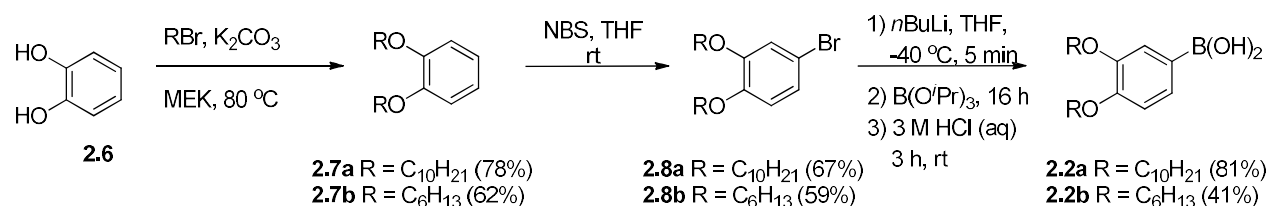
Scheme 2-9: Synthesis of boronic acids 2.2a,b via literature procedures.[63]

Reacting 3 equivalents of the appropriate boronic acid with previously prepared **2.12** led to the desired terphenyl derivatives in good yields (70-79%, Scheme 2-10).
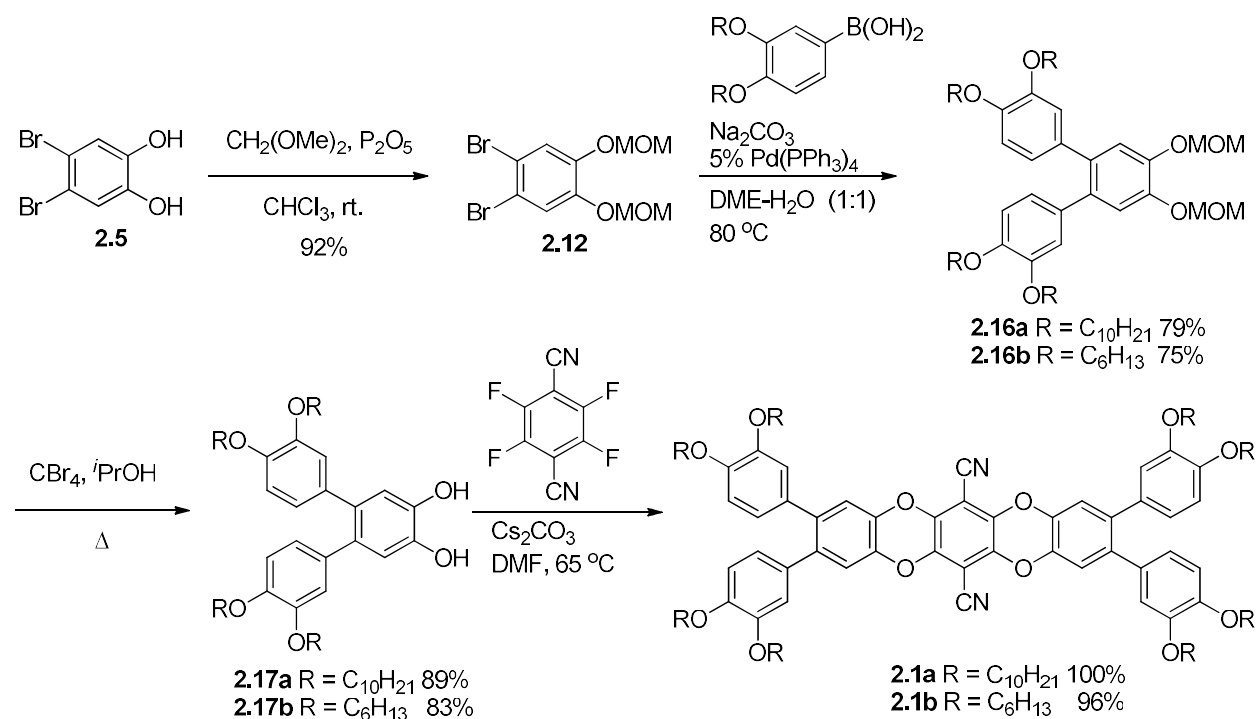
Scheme 2-10: Synthesis of substituted DCTOPs 2.1a,b via new route.

Deprotection proceeded in good yield (83-89%) to give the requisite terphenyl diol. Finally, reaction with TFTP gave the final C₆- and C₁₀-DCTOPs in excellent yields (96-100%) and, perhaps more importantly, in good purity with ease of purification. This new, more convenient route to substituted DCTOPs, while slightly longer (two extra steps) is therefore more satisfactory.

2.6   Preparation of Less Symmetric Soluble Dicyanotetraoxapentacenes

Less symmetric DCTOPs can now be synthesised *via* this modified synthetic route; previously, it would not have been possible to synthesise dissymmetric derivatives, since no control could be exerted on the fourfold Suzuki coupling.

Thus, reaction of terphenyl diol **2.14**, previously synthesised *via* Suzuki coupling, was then reacted with TFTP to form difluoride **2.18** in 89% yield (Scheme 2-11).
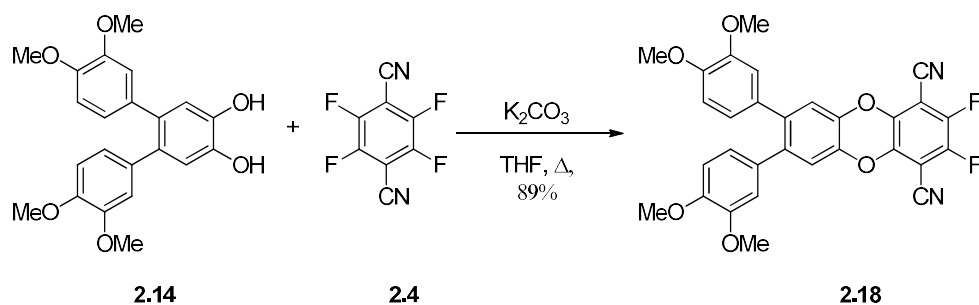
Scheme 2-11: S$_N$Ar between terphenyl diol 19 and TFTP to afford difluoride 2.18.

With difluoride **2.18** in hand, substitution to form dissymmetric DCTOP **2.19** proceeded in 79% yield (Scheme 2-12). Somewhat surprisingly, this compound displayed excellent solubility in organic solvents (*e.g.* chloroform, THF); it had been expected that this derivative may prove rather insoluble due to the large, unsubstituted, planar aromatic surface.
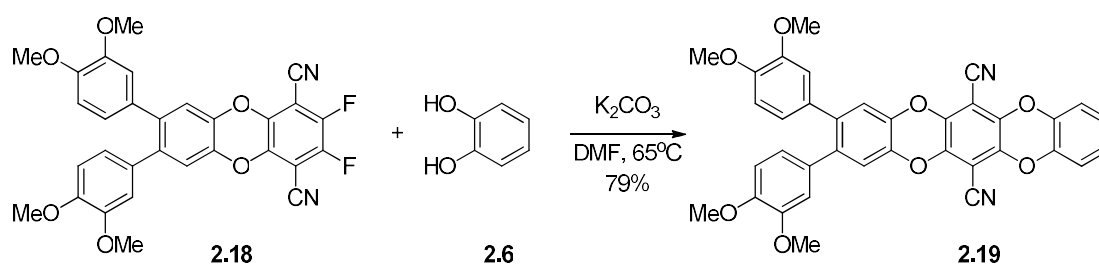
Scheme 2-12: Synthesis of first asymmetrically substituted dicyanotetraoxapentacene 2.19.

UV-visible measurements for **2.19** showed a λ_{max} at 427 nm in THF (10^{-5} M), nearly identical to that of the parent unsubstituted DCTOP (430 nm, CHCl$_3$); fluorescence spectroscopy (Figure 2-6, 10^{-6} M in THF) showed a λ_{em} at 497 nm (excitation at 420 nm), also comparable to C$_6$-DCTOP **2.1b** ($\lambda_{em} \approx 500$ nm, 10^{-6} M in THF, excitation at 325 nm).
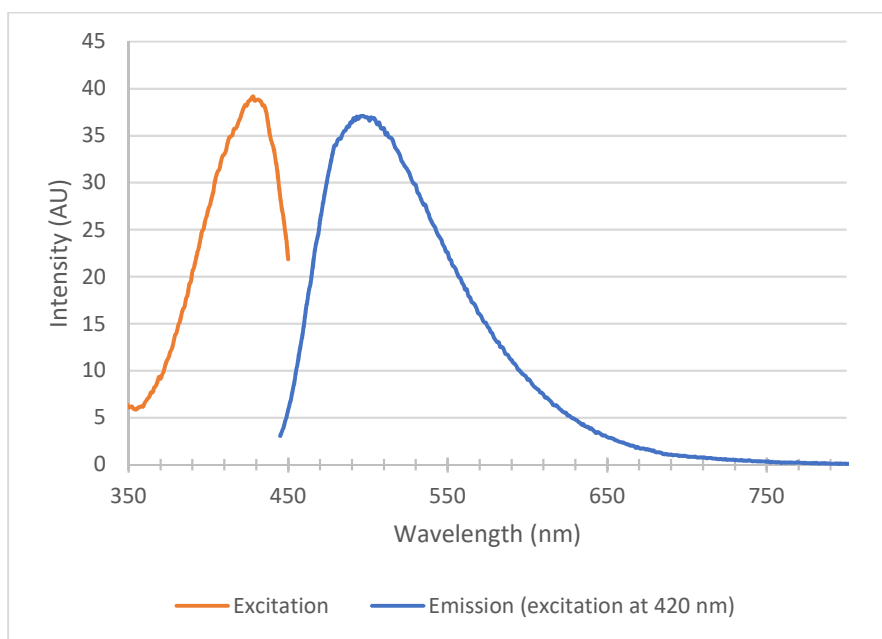
Figure 2-6: Excitation-emission spectra for dissymmetric DCTOP 2.24

(excitation at 420 nm, 10^{-6} M, CHCl$_3$).

Although not explored, it may be of interest to investigate the fluorescence activity of this derivative relative to that of the tetra-aryl derivatives (**2.1a-c**) to see if the lack of substituents at one end of the molecule has any bearing on the AIE behaviour.

2.7   Summary and Future Work

A new route to tetraphenyl-substituted dicyanotetraoxapentacenes **2.1a,b** has been developed, and methoxy-substituted DCTOP **2.1c** was synthesised for the first time. This methodology affords the desired products in good overall yields (52-65% from catechol) and with ease of purification, especially in the pentacene-forming step: each of the final pentacene derivatives (**2.1a-c**) can be obtained from the final reaction without the need for column chromatography.

Crystal structures were obtained for the parent DCTOP and methoxy-substituted derivative **2.1c**. Both compounds displayed highly planar cores while differing highly in their packing arrangements.

Using the synthetic methodology, dissymmetric DCTOPs such as **2.19** have been synthesised. Future work in this area could involve the synthesis of dissymmetric LC derivatives of **2.19**.

Chapter III – Other Dicyanoheteropentacene Analogues

3.1   Introduction

Introduction of heteroatoms into the framework of pentacenes can dramatically modulate their properties, and this is a fruitful area of interest.[13,64–67] Several well-known examples include the work of Prof. Uwe Bunz (U. Heidelberg) who has published extensively on the chemistry of N-heteroacenes; the structures of several of these compounds are shown in Figure 3-1.[64,68–70]
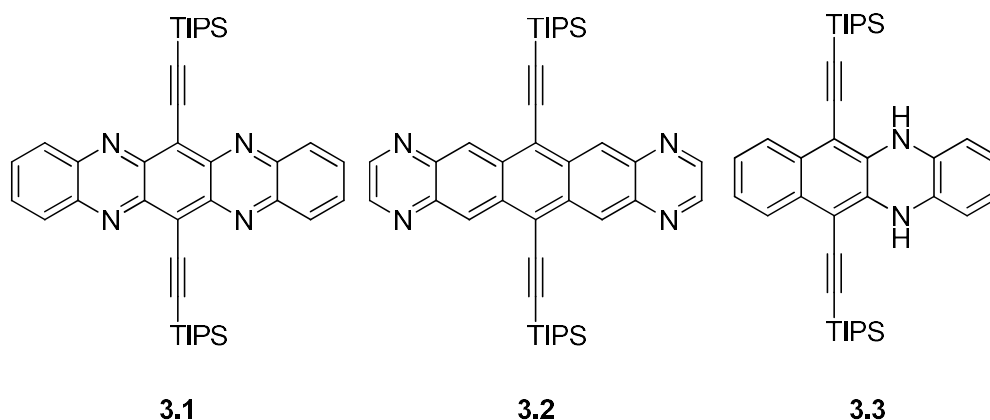
Figure 3-1: A selection of Bunz' N-heteroacenes[64]

Bunz found that the identity and location of the nitrogen atom within the aromatic core can affect the properties of the final material.[64] A comparison of the difference in electron mobilities found for **3.1** and **3.2** (3.3 vs. 4×10^{-4} cm^2/Vs, respectively) led to examination of the solid state structures where it was found that **3.2** crystallised in a herringbone fashion thus leading to attenuated mobility; **3.1** packed in a manner analogous

to TIPS-pentacene with efficient face-to-face π–π stacking of the cores, leading to an improved charge mobility. The crystal packing of other N-heteroacenes have also been compared to their acene analogues as well as the dihydro derivatives.[71]

Dihydroheteroacene derivatives such as **3.3** (Figure 3-1) possess formally sp^3 hybridized heteroatoms and as such cannot truly be considered acenes but rather, as acene analogues. In the case of the dihydrophenazine moiety of **3.3** and similar compounds, conversion to the acene is achievable by treatment with an oxidising agent such as MnO_2.

Examples of acenes incorporating both oxygen and nitrogen in the core are also known in the literature (Figure 3-2). Due to the limitations on the number of bonds oxygen can make, these compounds often adopt a quinoidal core structure, as in TIPS-triphenodioxazine **3.4**. Two additional properties of note include a 2D-brick layer packing structure, akin to TIPS-pentacene, as well as improved n-type performance in organic field-effect transistor (OFET) devices.[72] Compound **3.5,** also shown in Figure 3-2, was prepared by Zhu *et al.* in 2008 and exhibited n-type characteristics in OFET devices.[73]
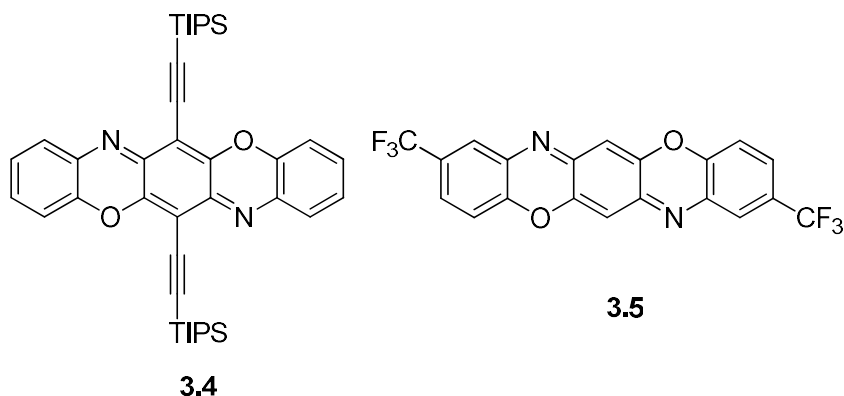
Figure 3-2: Typical structures of triphenodioxazines which have been used as OFET components.

In addition to organic electronics applications, triphenodioxazines have also been used as dyes; although the orange parent compound has no use as a colorant due to insolubility, Pigment Violet 23 (**3.6**, Figure 3-3) was discovered in 1952 and has been used in colouring inks and plastics.[74] A more modern application of the dye properties of these compounds is in the field of dye-sensitized solar cells (DSSCs), where triphenodioxazines such as **3.7** (Figure 3-3) have been used as the active dye component.[9] Importantly, **3.7** was designed to be *soluble* such that solution processing of any end material would be viable, as well as dissymmetric, to provide a push-pull effect and tune the optical properties. The push-pull effect was obtained by the positioning of electron-withdrawing and electron-donating groups on opposing sides of the core.
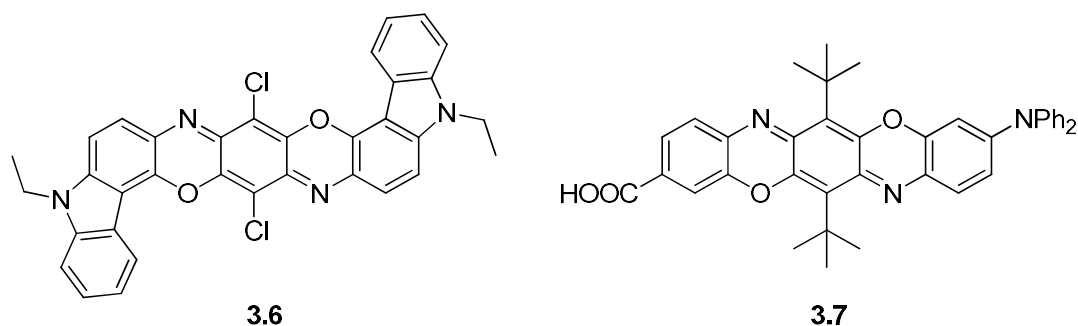
Figure 3-3: Examples of triphenodioxazine-based dyes.

In addition to compounds incorporating nitrogen and oxygen, of particular current interest in organic electronics are aromatic sulfur-containing moieties (*e.g.* thiophene, phenothiazine).[75–77] This interest in sulfur containing compounds can be traced partially to the redox chemistry of sulfur containing compounds, which can open them up to various applications. Compound **3.8b** (Figure 3-4, X = S) was shown to form stable radical cation salts electrochemically, as well as charge-transfer complexes with TCNQ, and was tested as a hole-injection material for organic light-emitting diode (OLED) applications.[78]

3.8a, X = O
3.8b, X = S
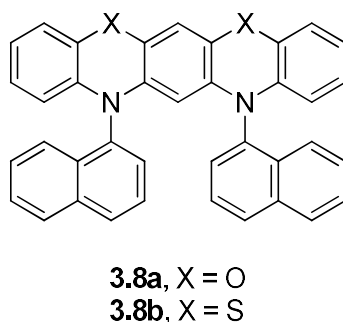
Figure 3-4: Heteroacene analogues incorporating O,N (8a) or S,N (8b).

It can be seen, then, from the previous examples that incorporation of heteroatoms in acenes and acene analogues can alter the solid-state characteristics such as crystal packing and charge transport capabilities. Pursuing novel heteroaromatic compounds allows for an investigation of their properties.

3.2   Synthetic Approach

Surprisingly, there are no pentacene analogues in the literature derived from tetrafluoroterephthalonitrile and nucleophiles other than 1,2-dihydroxyarenes, which leads to previously-discussed DCTOP compounds (Chapter 2). As shown below (Scheme 3-1) there are several derivatives imaginable from varying the heteroatoms of the nucleophilic/electrophilic partner.
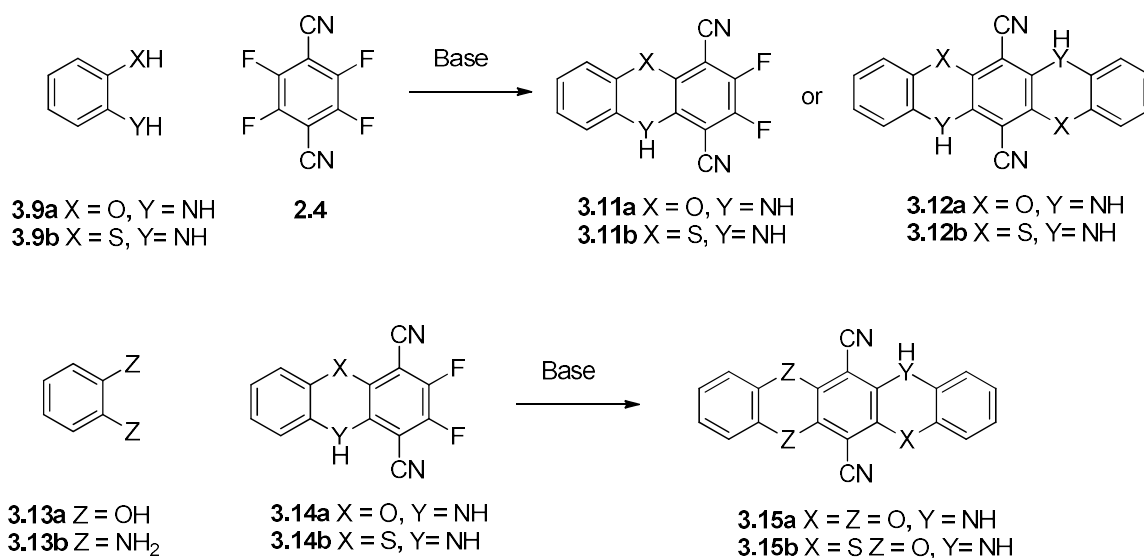
Scheme 3-1: Possible synthetic route to TFTP-derived

dicyanoheteropentacene analogues.

Analogues in which one or more oxygen atoms of the parent DCTOP compound are replaced with other heteroatoms such as nitrogen or sulfur could lead to compounds with drastically different properties. Although there are literature reports for the preparation of the dibenzodioxin (**3.16**),[79,80] dihydrophenazine (**3.17**),[79] thianthrene (**3.18**),[79] and dioxatetracene (**3.19**)[79] (Figure 3-5) there are virtually no reports of the pentacenes which could be formed from these difluoroanthracene analogues other than the tetraoxa congener.

3.16   3.17   3.18   3.19
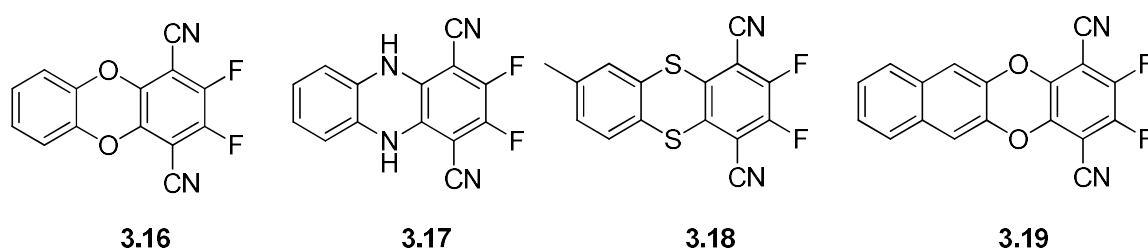
Figure 3-5: Previously reported reaction products of TFTP

and 1,2-bifunctional nucleophiles.

3.3   Attempted Reactions between 2-Aminophenol and TFTP

As a starting point, the reaction between tetrafluoroterephthalonitrile (TFTP, **2.4**) and commercially available 2-aminophenol (2-AP, **3.20**) was investigated under basic and neutral conditions (Scheme 3-2).
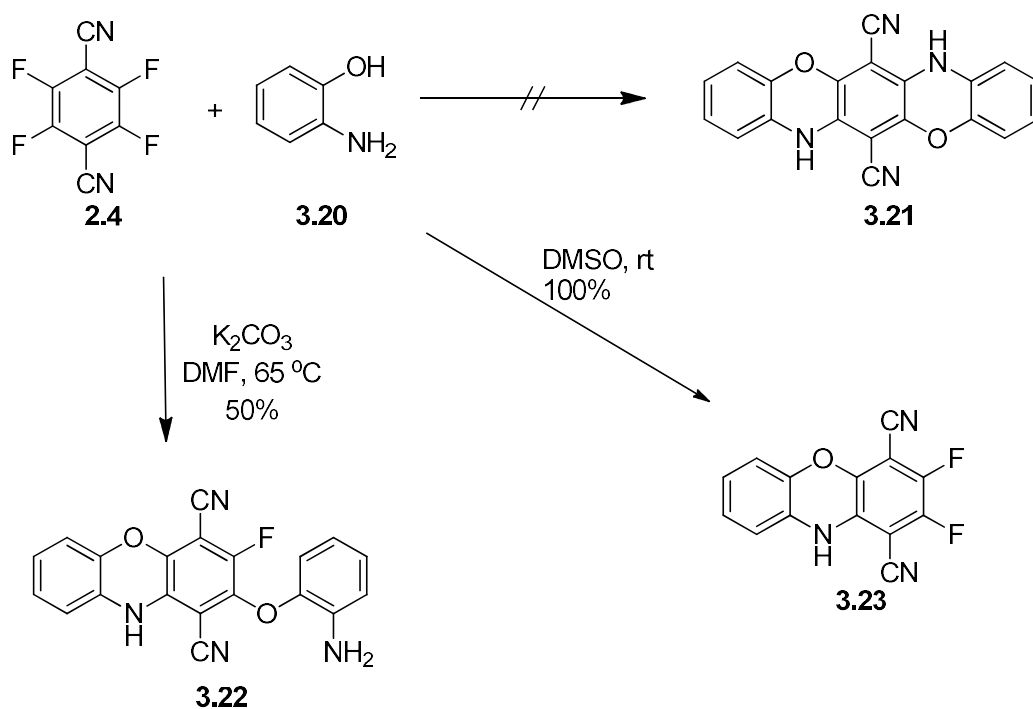
Scheme 3-2: Attempted synthesis of diazadioxapentacene analogue 3.21,

and actual products, phenoxazines 3.22 and 3.23.

In the first set of conditions attempted, TFTP was combined with 2-AP (**3.20**) in DMF with potassium carbonate as the base and heated to 65 °C under N_2. Under these conditions the mixture turned dark purple in colour and a brick-red microcrystalline solid was obtained upon workup (pouring into H_2O) in 50% yield based on TFTP, however, ^{1}H NMR indicated a mixture of products, inseparable by TLC. To learn the identity of the constituents, single

crystals were grown from a DMF solution of the mixture, and the compound was identified as phenoxazine **3.22** *via* X-ray crystallography (Figure 3-6).
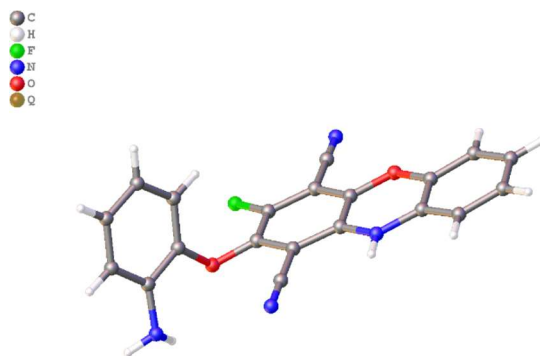
Figure 3-6: Crystal structure of substituted phenoxazine 3.22.

Repeating the reaction in the absence of base stirring at room temperature in DMSO, a vividly bright orange precipitate formed (quantitative yield) and was likewise characterised. Markedly different in colour (orange) and practically insoluble in most organic solvents at room temperature at concentrations greater than 10^{-3} M, this derivative was shown to be the mono-cyclised product **3.23** by single crystal X-ray diffraction (Figure 3-7).
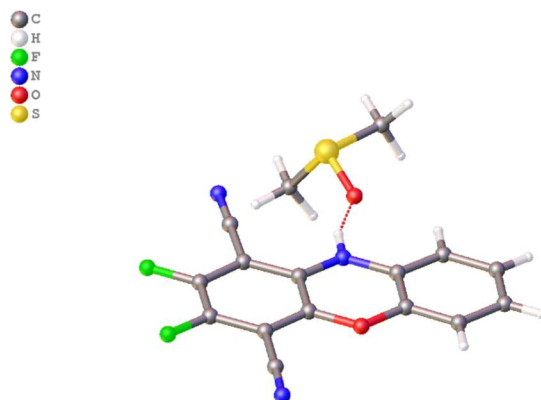
Figure 3-7: Crystal structure of phenoxazine 3.23; DMSO (solvent) is also shown; dashed red line represents hydrogen bonding.

The crystal structure of **3.23** shows near complete planarity of the phenoxazine ring, possessing a root mean square deviation of 0.013 Å from planarity. Interestingly, but perhaps not surprisingly, the molecules adopt an alternating arrangement within slipped stacks, with a plane to plane centroid distance of 3.34 Å and a plane to plane shift of 1.32 Å between successive molecules (Figure 3-8).
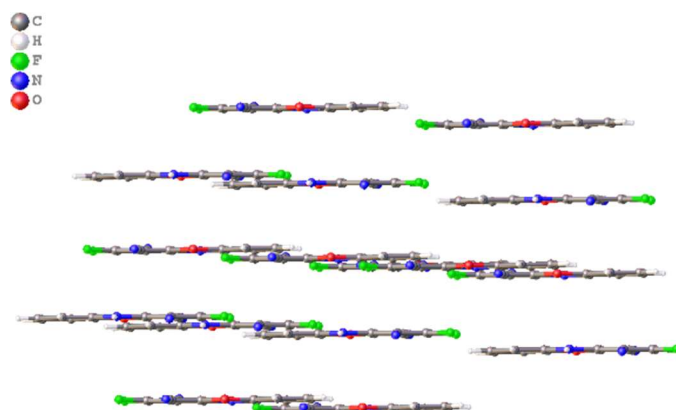
(a)
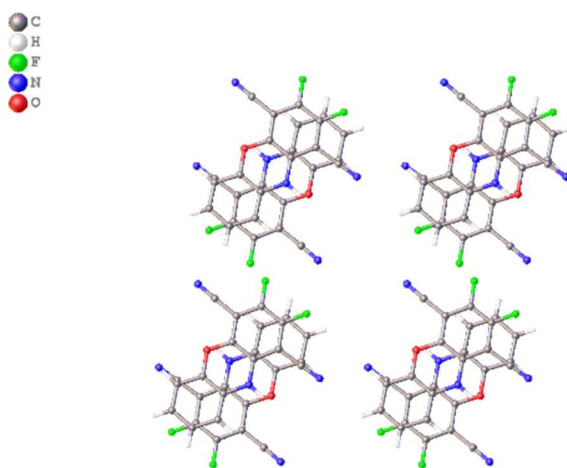
(b)

Figure 3-8: Crystal packing of phenoxazine 3.23 from (a) side view and (b) top-down view.

This alternating arrangement could be due to dipole cancellation and/or π–π interactions of the more electron-deficient (dicyanodifluoro) aromatic ring with the more electron rich terminal benzene ring. The N-H bond does not appear to hydrogen bond

strongly to another phenoxazine but does form H-bonds to the co-crystallised solvent (DMSO). A similar motif is observed in phenoxazines, although in some cases this appears to be due to sterics of the *N*-substituent or H-bonding interactions.[81,82]

As mentioned previously, **3.22** forms a dark purple anion in the presence of a base such as hydroxide or carbonate. The same is true for the orange compound **3.23**. Addition of acid (HCl) to the purple anion reforms the original orange material with concomitant precipitation. As shown below (Figure 3-9) deprotonation of the phenoxazine N-H leads to a resonance-stabilised anion, the resulting charge of which can be delocalized onto the *para* fluoro-substituted carbon (contributor **3.24**), thus stabilised *via* the inductive effect, and further delocalized into the nitrile *ortho* to the phenoxazine N-H (contributor **3.25**). Both effects in tandem could lead to the increased acidity of the N-H bond.
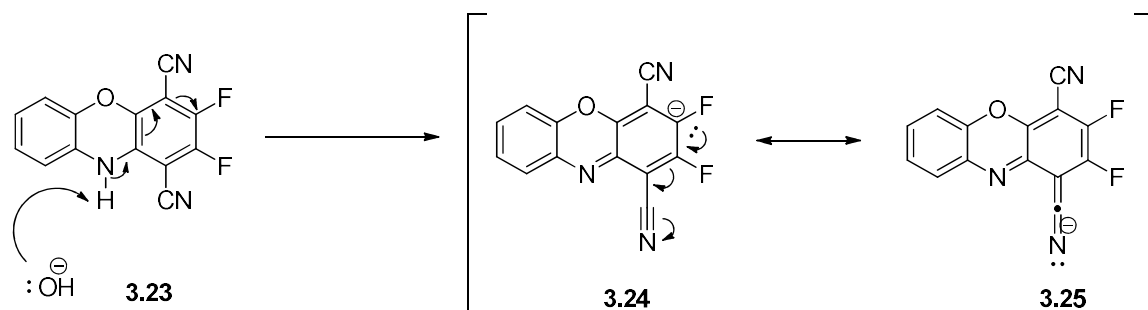
Figure 3-9: Deprotonation and resultant resonance contributors of phenoxazine 23.

It then follows from this discussion that the reaction may stall after three substitutions (one cyclisation) due to the high negative charge density on the carbon of the

54

last remaining C-F bond. This is unsurprising when one considers the trend that nucleophilic aromatic substitution reactions on electron-rich aromatic rings proceeds extremely slowly or not at all. The fluorine atom *meta* to the phenoxazine nitrogen is evidently not as deactivated, as the charge has no way to delocalize to that carbon atom, and substitution proceeds at that position to give **3.22** (and other unidentified products).

Although it was unexpected to proceed for reasons stated above, several attempts were made to force the cyclisation of the mixture containing trisubstituted **3.22** to the desired product. Conditions attempted included using KO^{t}Bu or NaH in excess as the base, however this was unsuccessful, providing an insoluble and unidentifiable brown amorphous material. The reaction was again attempted in DMF in the absence of base, using heat alone to force the cyclization, however starting material was recovered. Attempting to heat 2-AP and TFTP (0.5 eq) led to only difluorophenoxazine **3.23** as the product.

Although this was disappointing, the surprising nature of the unexpected phenoxazine **3.23**, and its relative ease of preparation, made up for the misfortune. While the crystalline solid displayed a bright orange colour (Figure 3-10) the deprotonated material possessed deep violet coloration. We chose to briefly explore both the acidity of the compound as well as its spectral properties.

Figure 3-10: Phenoxazine 3.22 as an orange crystalline solid (left) and

in the purple deprotonated form in iso-propanol/DBU (right).

It was found through some experimentation that several organic bases such as DBU were able to deprotonate phenoxazine **3.23** and generate the purple anion. Also of note was that a 1.0 M solution of TBAF in THF was also capable of producing the same purple colour of the anion when dripped into a saturated THF solution of the compound. This can possibly be explained by the high basicity of fluoride in anhydrous solution; Christe showed that anhydrous fluoride could abstract a proton from acetonitrile, as well as participate in S_N2 reactions with dichloromethane and chloroform.[83] This behaviour is, in retrospect, unsurprising, however it did lead to an interesting observation with a related compound (*vide infra*).

UV-visible spectra for both phenoxazine **3.23** and the anion thereof were obtained in THF (Figure 3-11). The deprotonated form was obtained by adding an excess of DBU, which has a negligible absorption spectrum.

Figure 3-11: UV-visible spectra of phenoxazine 3.23 in THF (1.0 x 10⁻⁴M, solid line) and 3.23 with excess DBU in THF (1.0 x 10⁻⁴ M, dotted line).

The growth of a broad, red-shifted peak is apparent, as well as several peaks which are blue-shifted relative to the N-H phenoxazine. This red-shift could be indicative of an increase in conjugation, which fits with the proposed resonance contributors.

It is known from the literature that phenoxazines can be difficult to alkylate, although procedures are known involving strong bases (KOH, KO*t*Bu) in polar aprotic solvents (DMF, DMSO).[84–86] Interestingly, Gilman noted that "Phenoxazine, similar to carbazole, is not acidic enough to condense with ethyl iodide in a refluxing acetone solution of potassium hydroxide,

Figure 3-11: UV-visible spectra of phenoxazine 3.23 in THF (1.0 x 10^{-4}M, solid line) and 3.23 with excess DBU in THF (1.0 x 10^{-4} M, dotted line).

The growth of a broad, red-shifted peak is apparent, as well as several peaks which are blue-shifted relative to the N-H phenoxazine. This red-shift could be indicative of an increase in conjugation, which fits with the proposed resonance contributors.

It is known from the literature that phenoxazines can be difficult to alkylate, although procedures are known involving strong bases (KOH, KO*t*Bu) in polar aprotic solvents (DMF, DMSO).[84–86] Interestingly, Gilman noted that "Phenoxazine, similar to carbazole, is not acidic enough to condense with ethyl iodide in a refluxing acetone solution of potassium hydroxide,

as do nitrocarbazoles."[87] In the case of **3.23**, it does not appear that lack of an acidic N-H bond is the issue, as weak bases such as piperidine (pK_a = 11.22, 0.1 M MeOH/CCl$_4$)[88] are capable of, presumably, deprotonating and forming the putative purple-coloured anion.

Methylation of **3.23** was attempted utilizing either dimethyl sulphate or methyl iodide as the methylating agent, under either neutral or basic conditions (Me$_2$SO$_4$-DMSO-H$_2$O or MeI-KOH-DMSO) and using a stronger base than hydroxide (KO^{t}Bu). In each instance no evidence of alkylation was observed (absence of methyl signal *via* ^{1}H NMR).

Attempted acetylation using acetyl chloride in toluene/triethylamine likewise failed, in all instances with unreacted starting material being recovered. This pattern of non-nucleophilicity led us to the realization that the troublesomely acidic N-H bond formed during the reaction would need to be avoided entirely.

3.4 *Synthesis and Properties of p-Dicyanodiazadioxapentacenes (p-DADOPs)*

Turning our attention back to the failed attempted synthesis of heteropentacene derivatives, since the S$_N$Ar reaction itself did not seem to be the problem, rather the deactivating effect of the amide anion, use of a 2-aminophenol derivative bearing an appropriate *N*-substituent appeared viable. An alkyl group would allow the nitrogen to retain nucleophilicity as opposed to an amide or carbamate nitrogen, where nucleophilicity is attenuated. Due to synthetic feasibility 2-(ethylamino)phenol was chosen as the reactive

partner. 2-Aminophenol was first acetylated using acetic anhydride in ethyl acetate and the resulting amide (**3.26**) reduced using lithium aluminum hydride (LAH) in THF to furnish 2-(*N*-ethylamino)phenol (**3.27**) in a two-step sequence (Scheme 3-3).
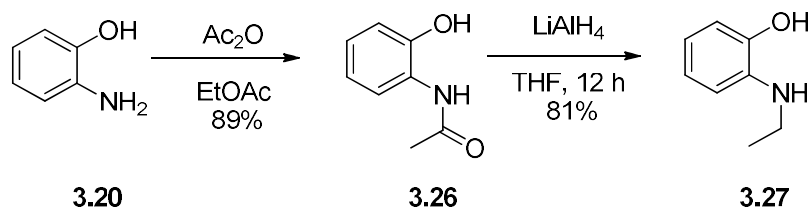
Scheme 3-3: Synthesis of 2-(ethylamino)phenol (3.27).

Rather than protect the acidic phenol, an excess of LAH was used (2.0 eq) to deprotonate the alcohol fully. Care should be taken when adding the reagent, since the deprotonation proceeds rapidly, whereas the reduction does not.

Compound **3.27**, although forming white needles from chloroform, was found to be unstable, decomposing in light at room temperature. NMR samples in CDCl$_3$ were initially colorless but would discolor within minutes in sunlight and turn dark green within an hour. The compound appears stable for several months if stored as a pure, crystalline solid at −20 °C, in the dark. No new signals appear in the ^{1}H or ^{13}C NMR, however significant line broadening is apparent in both spectra.

Reacting two equivalents of 2-(ethylamino)phenol with TFTP led to the fully cyclised diazadioxadicyanopentacene (DADOP) **3.28** (Scheme 3-4) in 100% yield. It was found through some experimentation that a higher temperature relative to the DCTOP derivative (100 °C *vs.* 65 °C respectively) was optimal. This is rationalised by the amine being a neutral nucleophile under the reaction conditions, while the alcohols of catechol were deprotonated and therefore more nucleophilic.
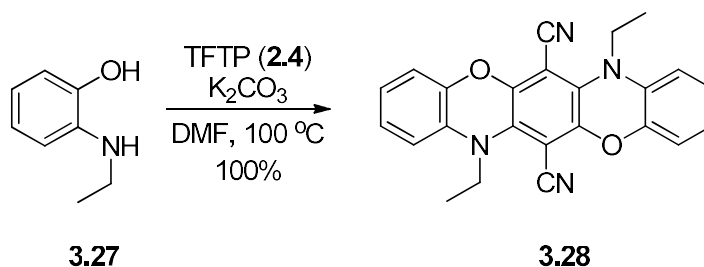
Scheme 3-4: Synthesis of para-diazadioxapentacene (p-DADOP) derivative 3.28.

This compound, as opposed to the parent dicyanotetraoxapentacene (DCTOP) and phenoxazine derivative **3.23**, displays enhanced solubility in chloroform. In addition to the marked increase in solubility, compound **3.28,** shown in Figure 3-12 as a deep red, crystalline solid, shows bright orange fluorescence in both the solid and solution states. In contrast, phenoxazine **3.23** exhibits only weak fluorescence in solution (DMF) and no activity as a crystalline solid. Although the compound formed beautiful crystals from chloroform-methanol, they were incredibly tiny (so much so that they possess a "sparkle",

see Figure 3-12). Growing X-ray quality single crystals from a variety of solvents and solvent mixtures has not yielded results to date, with any crystalline material forming as microcrystals.

Figure 3-12: Diethyl-p-DADOP 3.28 as a bright red, microcrystalline solid.

Sublimation of this compound was therefore attempted to obtain a diffraction quality single crystal. The technique was successful inasmuch as sublimation occurred at 185 °C / 0.5 mmHg, but the formed crystals were of lower quality. When attempting to acquire a melting point by using the polarised optical microscope the compound was sufficiently volatile at 300 °C to sublime and condense on the cover of the heating stage, indicating some measure of thermal stability, however, no melting was observed.

Since the structural features (*e.g.* planarity) of, and interactions between, the cores were of main interest, synthesis and crystallisation of a differently soluble derivative was

attempted. To this end, the *N*-decyl-substituted analogue was chosen as a "model" with hopefully more attainable crystallization conditions.

Slightly different conditions were employed to install the decyl group since the anhydride of decanoic acid is prohibitively expensive (and not at all atom economical!). Thus, alkanoylation of 2-aminophenol proceeded with decanoyl chloride in THF-pyridine giving the amide (**3.29**) in 80% yield after recrystallisation from methanol-water (Scheme 3-5, modified from a literature procedure for the analogous hexadecylamidophenol.)[89] Reduction with LAH in THF proceeded in 80% yield to give the decylaminophenol (**3.30**). This compound, like 2-(ethylamino)phenol (**3.27**) previously prepared, was an unstable compound which decomposed over several weeks at −20 °C and suffered line broadening in the NMR spectra. This was then reacted with 0.5 equivalents of TFTP under the standard conditions to furnish the C$_{10}$-DADOP analogue **3.31** in 84% yield.
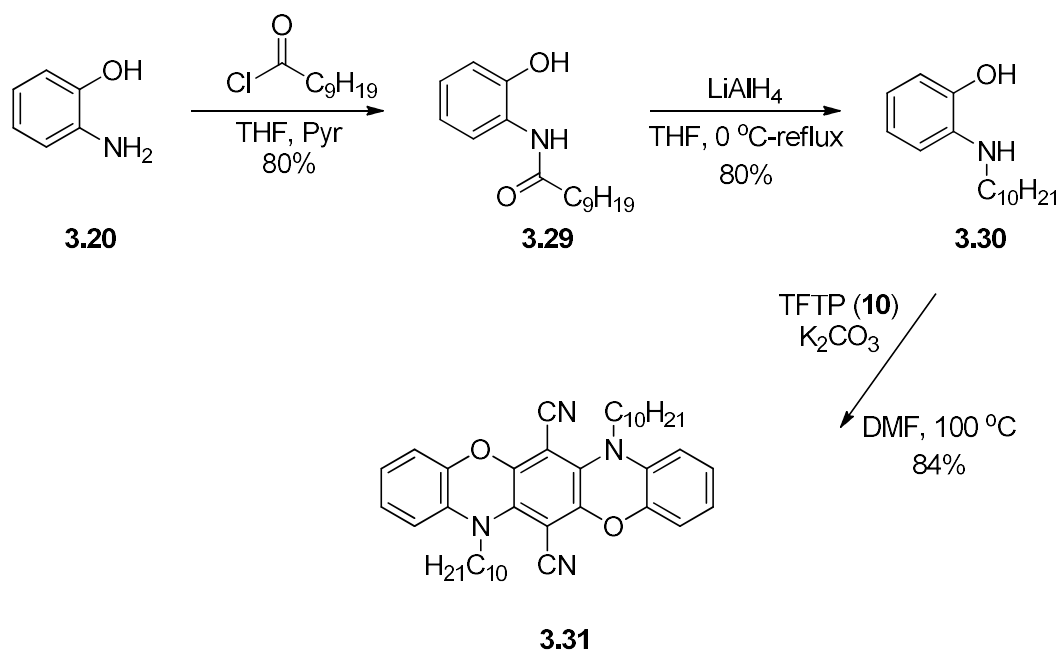
Scheme 3-5: Synthesis of N,N'-didecyl-p-DADOP 3.31.

Crystals of **3.31** shown in Figure 3-13 were grown from slow diffusion of acetonitrile into a saturated chlorobenzene solution and were of suitable size and quality for X-ray diffraction.
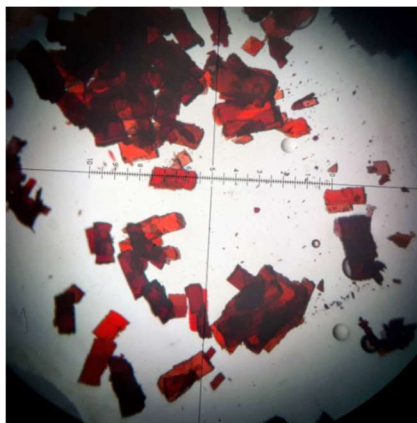
Figure 3-13: Red crystals of C₁₀-p-DADOP 31 viewed under

an optical microscope.

Compound **3.31** crystallised in a triclinic space group (P-1) with one molecule per unit cell (the asymmetric unit contained one-half of the full molecule). The diazadioxapentacene core exhibited a root mean squared deviation from planarity of 0.099 Å, indicating a surprising degree of planarity considering the four formally sp^3 hybridised heteroatoms in the core (Figure 3-14).
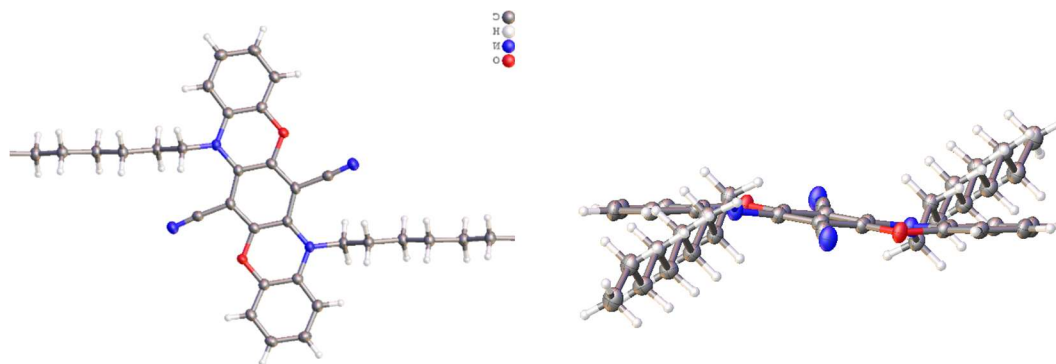
Figure 3-14: Top-down view of DADOP core in 3.31 (left), and

side view (right).

The C−O−C bond angle around each oxygen is 117.8 °, slightly larger than in the DCTOP series (average 115 °), while the C−N−C bond angle is 118.1 °; both angles are larger than expected for sp³ hybridised oxygen or nitrogen, however, they fit within angles normally seen for phenoxazines (*N*-ethylphenoxazine ∠C−O−C = 117.4 °, ∠C−N−C = 118.9 °). The bond lengths in the core vary from 1.3708(19) to 1.413(2) Å, indicating electron delocalisation.

The crystal packing of **3.31** indicates an interesting arrangement of the molecules within the crystalline state (Figure 3-15). The cores of the DADOP molecules pack in a half-staircase arrangement, where the ends of the core alternate over an alkyl chain or another DADOP core. A π−π stacking interaction occurs between the terminal pentacene benzene ring and the central dicyanobenzene ring of another molecule. Additionally, the alkyl chains are remarkably ordered as well, interdigitating between the aromatic cores.
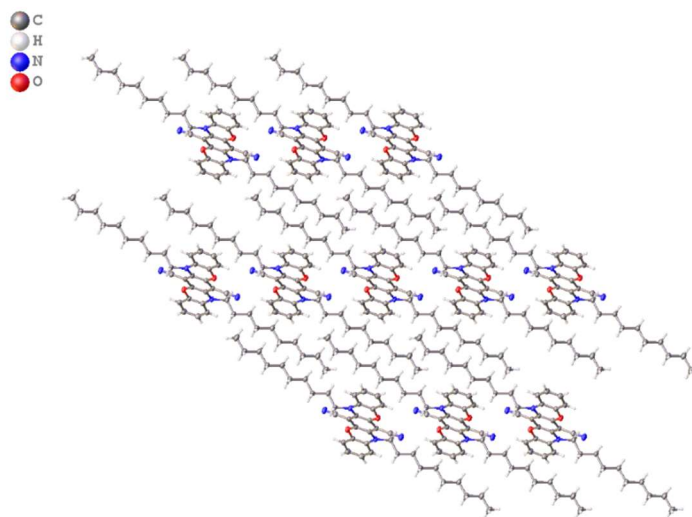
(a)
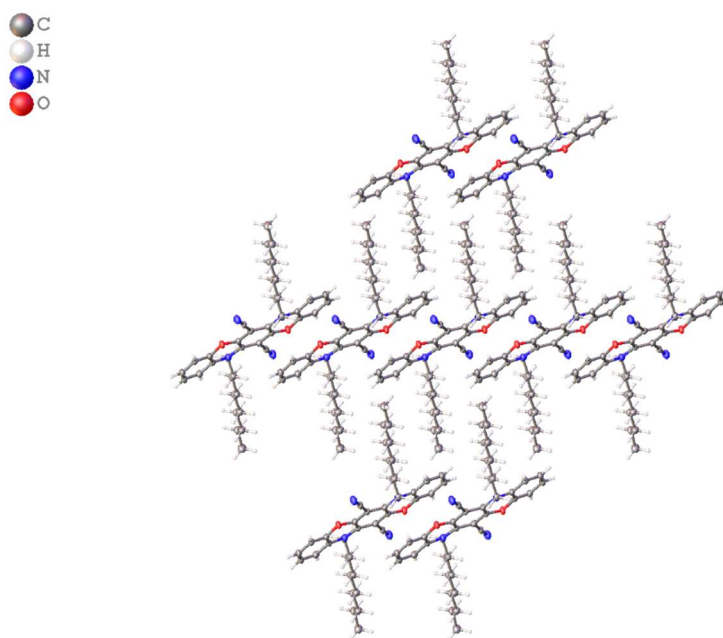
(b)

Figure 3-15: Crystal packing of p-DADOP 3.31 looking along the (a) [100] direction or (b) [101] direction.

It should also be noted that this crystal data also gives definitive proof of the substitution pattern of TFTP when reacting with a nucleophile such as 2-(ethylamino)phenol; it had been presumed that the substitution would proceed in a *para*-fashion with respect to like atoms, due to the obtained crystal structure of trisubstituted phenoxazine **3.22**, however, that product was obtained as a mixture. DADOP **3.31** shows that even with a bulkier ethyl substituent (*cf.* NH$_2$) the substitution proceeds in good yield in a *para*-substitution pattern.

3.5   Synthesis and Properties of N-ethyl-dicyanodifluorophenoxazine 3.32

In addition to forming the full pentacene analogue, it was also of interest to expand our chemical library. As previously mentioned, some tricyclic products of TFTP-substitution are known in the literature[79], however, they have been poorly characterised and have not been used for preparing pentacene derivatives. Moreover, there are no phenoxazine derivatives in the literature derived from TFTP.

In this vein, reacting 2-(ethylamino)phenol (**3.27**) with TFTP in the absence of base with DMSO as the solvent gave *N*-ethylphenoxazine difluoride **3.32** in 80% yield (Scheme 3-6).
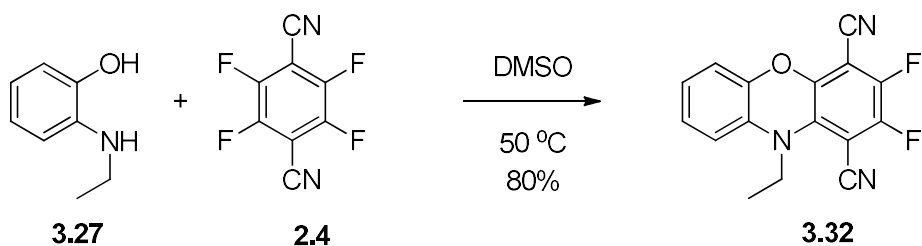
Scheme 3-6: Synthesis of N-ethylphenoxazine 3.32.

Much like the H-substituted phenoxazine **3.23**, derivative **3.32** also displayed a very similar orange colour. However, the solubility of the compound in everyday organic solvents (*e.g.* chloroform, ethyl acetate) had greatly improved, such that NMR data was collected in CDCl$_3$.

In contrast to the N-H derivative, the *N*-ethyl phenoxazine (**3.32**) exhibits no colour change upon exposure to bases nor fluoride ion. The absence of colour change upon treatment with base is expected, since compound **3.32** no longer has the acidic N-H group. Surprisingly, however, an effect *was* noticed with respect to the fluorescence behaviour of **3.32** in the presence of anhydrous, ethereal fluoride, and no such effect was seen with Cl⁻ or Br⁻ anions. Figure 3-16 shows the fluorescence spectra of **3.32** (1.0 x 10⁻⁴ M in THF, excitation at 450 nm) with no fluoride present (low intensity) and upon titration of 5 µL of TBAF (0.025 M in THF, 0.5 eq F⁻) up to 3.5 equivalents of fluoride (high intensity).
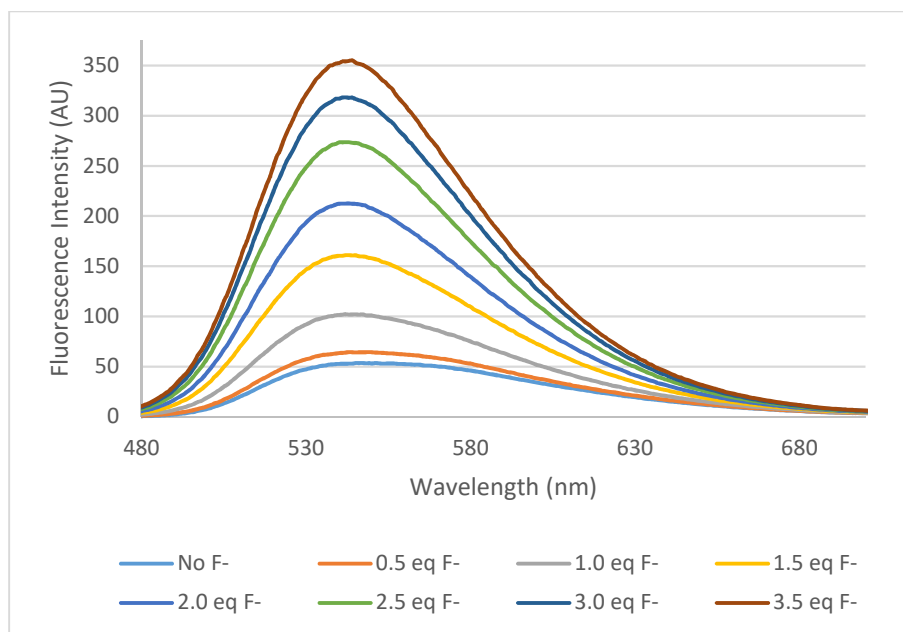
*Figure 3-16: Fluorescence titration of phenoxazine 3.32 (1.0x10^{-4} M)
with TBAF (5 µL portions, 0.025 M, 0.5 eq).*

This behaviour is not unknown in the literature, although there are several different mechanisms by which fluoride can interact with π-systems. Firstly, if fluoride is acting as a nucleophile, the increase in intensity could be attributed to the formation of a Meisenheimer complex, which is the 1:1 adduct of a nucleophile with an electron-deficient aromatic system. Fluoride was shown to bind to electron-deficient hexafluorobenzene (in the gas phase) in a Meinsenheimer-type complex.[90] Increases in fluorescence intensity have been noted for the formation of Meisenheimer complexes.[91] Were this the case, however, it would be expected that more than one molar equivalent of fluoride would cause a saturation effect, which is obviously not observed, although this does not, necessarily, rule out the possibility.

A second explanation involves an anion-π interaction, whereby the electron-rich fluoride anion can donate electron density into the electron-deficient aromatic ring. Guha, *et al.* reported the synthesis of a linked naphthalene diimide (NDI) dimer which led to a fluoride to NDI electron transfer event, along with changes to the UV-vis and fluorescence spectra.[92] In the case of anion-π interactions, which are generally weak, the lack of ceiling effect up to 3.5 equivalents is unsurprising, as these interactions are often observed in the literature with 0-50 equivalents of anion being used.[93]

Not enough information is known at present about the system to make a determination of how the fluorescence intensity is increasing. Studies towards this end are ongoing.

Phenoxazine **3.32** formed orange needles from acetonitrile, from which a crystal of suitable quality was subjected to X-ray diffraction. The compound crystallised in a monoclinic space group (P2$_1$/n) with four molecules per unit cell; the *N*-ethyl group crystallised in two conformations, both of which are modeled (Figure 3-17).
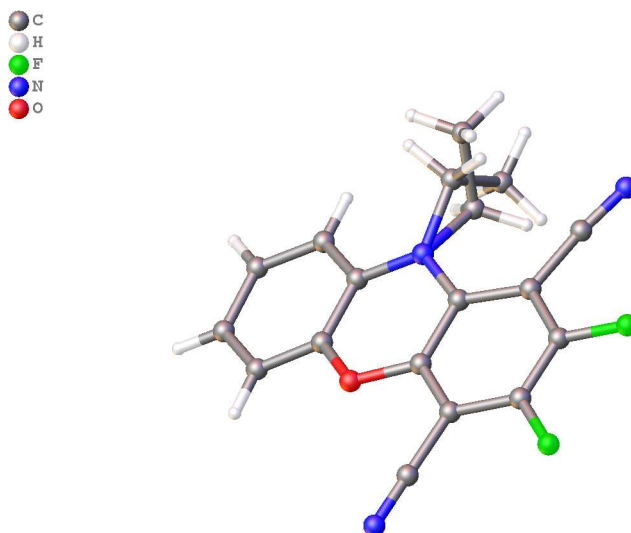
Figure 3-17: Crystal structure of N-ethylphenoxazine 3.32.

A root mean squared deviation from planarity of 0.099 Å (*cf.* RMSD = 0.013 Å for **3.32**) was observed, which is consistent with other *N*-substituted phenoxazines.[81,82] Furthermore, C−N−C and C−O−C bond angles in the core were found to be 119.2 and 117.7 ° respectively, consistent with the N-H analogue, as well as C_{10}-*p*-DADOP **3.31**.

The packing motif of **3.32** was also consistent with that of the N-H analogue: alternation within stacks occurred such that electron-deficient and electron-rich rings overlapped in a parallel co-facial arrangement. However, unlike the crystal structure of **3.23,** no solvent molecules were included in the lattice and the larger RMSD from planarity also had an interesting ramification for the solid-state packing (Figure 3-18a) where the stacks of molecules alternated in bending direction up the individual columns. Due to steric effects, the molecules also alternate such that ethyl groups are not directly above one another within

stacks (Figure 3-18b) This behaviour is akin to that of phenoxazine **3-23**, wherein the hydrogen-bonded DMSO fulfills the bulky group role.
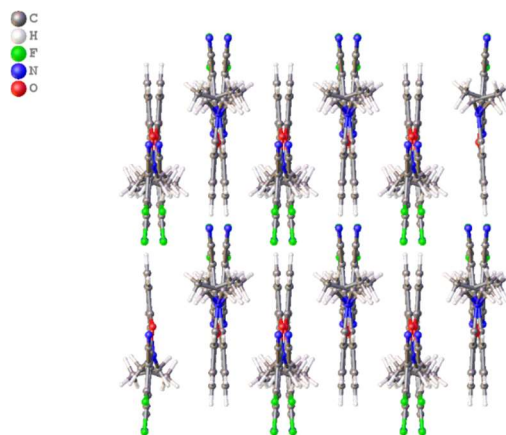
(a)
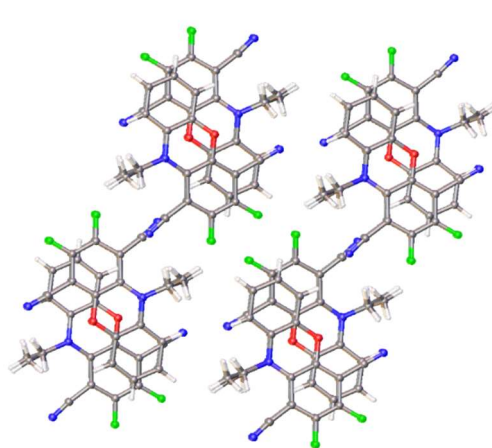
(b)

Figure 3-18: Crystal packing in N-ethylphenoxazine 3.32, showing the (a) alternation in bending within columns, and (b) alternation along the long and short axes of 3.32.

The cores overlap in a π-π stacking arrangement, with a plane to plane centroid distance of 3.61-3.67 Å and a plane to plane shift of 1.38-1.57 Å between consecutive rings. The plane normal to plane normal angle was 1.36(5) °, indicating a highly parallel contact between the rings.

The crystal structure of **3.32** was also compared to the parent *N*-ethylphenoxazine, the crystal structure of which has been published in the literature.[82] This compound, in contrast to the dicyanodifluoro analogue, exhibits no π-π interactions, and packs in an almost pure herringbone motif (Figure 3-19). Although the plane to plane centroid distance is similar (3.61 Å) to dicyanodifluorophenoxazine **3.32** (3.34 Å), the planes are offset by almost double that in **3.32** (plane to plane shift = 3.45 *vs.* 1.32 Å in **3.32**) such that the actual degree of overlap is low.
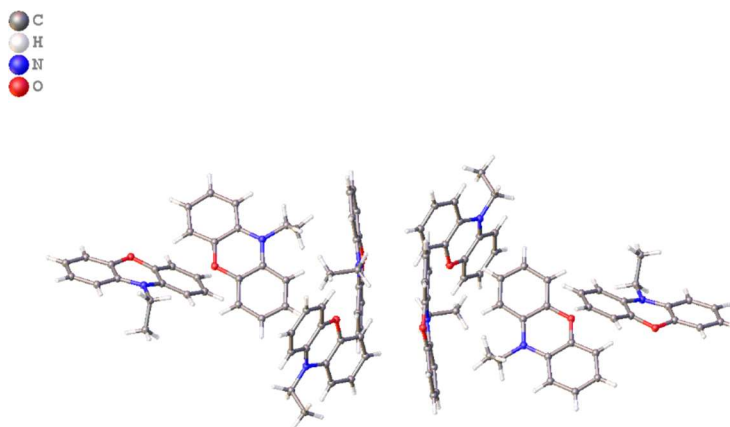
Figure 3-19: Crystal structure of otherwise unsubstituted N-ethylphenoxazine from the literature.

It is perhaps unsurprising that a compound with less C–H bonds shows fewer C–H···π interactions. However, the complete lack of any such interactions for compound **3.32** is interesting and could be indicative of high orbital overlap.

This new difluorophenoxazine could be used as a useful building block to more complex structures incorporating the phenoxazine core.

3.6   Attempted Synthesis of Parent N-H p-DADOP 3.21

Although the synthesis of both *N*-ethyl and *N*-decyl *p*-DADOP proceeded well, we were still interested in obtaining the parent, unsubstituted compound **3.21** (Figure 3-20).

This compound is interesting for several reasons; firstly, its packing in the solid state would be of interest as compared with the *N*-alkyl substituted derivatives. Synthesis of this compound would allow a comparison with quinacridones (Chapter 1), which have been studied in the solid state.[25,26] Secondly, it should be possible to oxidise the dihydro analog **3.21** to the quinoidal triphenodioxazine **3.33**.
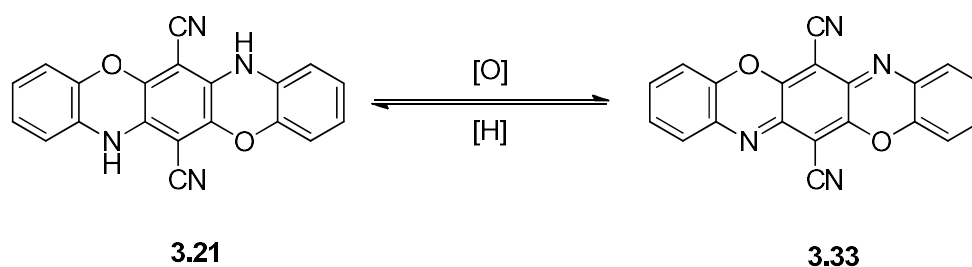
Figure 3-20: Conversion between dihydrotriphenodioxazines (3.21)

and triphenodioxazines (3.33).

There have been only three reports of dicyanotriphenodioxazines such as **3.33** in the literature, none in English, and all from the 1970s.[94] Considering the interesting chemistry of the alkylated reduced analogue (*i.e.* **3.28**), access to **3.33** would be exciting (although the product would be expected to be quite insoluble).

Removing the *N*-alkyl groups was briefly considered but discarded; one published literature procedure from 1979 for the demethylation of phenoxazines employs very harsh

conditions (pyridinium bromide at 200 °C) and only seems to work for certain phenoxazines, leading to black tarry products in others.[95]

Use of *N*-(2-hydroxyphenyl)acetamide **3.26**, precursor to the DADOP derivatives, was also considered. This was not attempted, since amides are much less nucleophilic than their amine counterparts and would thus constitute a much larger change to the reaction conditions (*i.e.* chance of failure). Moreover, cleavage of acetamides is usually carried out under basic conditions and could lead to undesired degradation.

We envisioned a protection-deprotection sequence wherein the target compound could be easily formed during the S$_N$Ar reaction and deprotected under mild conditions. For this purpose, the benzyl protecting group was chosen, which is cleaved under mild reducing conditions preventing oxidation of the target dihydro compound **3.21** (retrosynthetic analysis shown in Scheme 3-7).
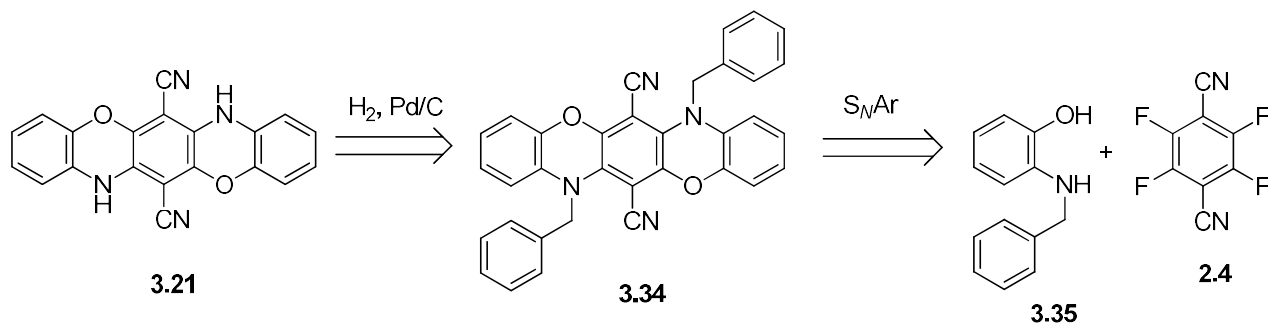
Scheme 3-7: Retrosynthetic analysis for N-H p-DADOP 3.21.

Fortunately 2-(benzylamino)phenol **3.35** is a known compound, and was synthesised in a two step sequence (Scheme 3-8).[96] First, freshly distilled benzaldehyde **3.36** was condensed with 2-aminophenol in THF with $MgSO_4$ driving the reaction forward by adsorbing water as it forms. The crude imine **3.37** (quantitative yield) was then reduced with sodium borohydride in methanol at 0 °C to give the product (**3.35**) as an unstable green oil which solidified upon storage at −20 °C.
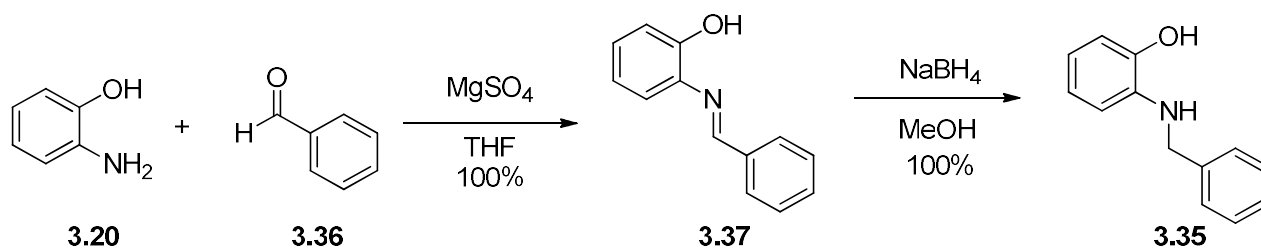
Scheme 3-8: Synthesis of 2-(N-benzylamino)phenol 3.35.[96]

Reaction of **3.35** with 0.5 equivalents of TFTP did not, however, provide the desired product (Scheme 3-9). Rather, several products were formed during the reaction (TLC) and upon workup and purification *via* column chromatography (SiO_2) a brick-red product was obtained as an inseparable mixture.
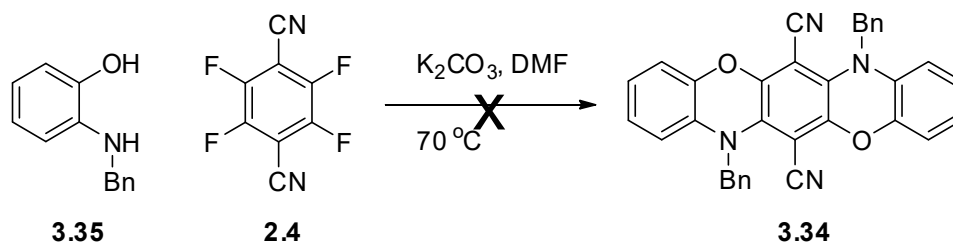
Scheme 3-9: Failed attempted reaction of 2-(N-benzylamino)phenol 3.35 with TFTP to form N-Bn-p-DADOP 3.34.

^{1}H NMR of the mixture in CDCl$_3$ shows that, although the aromatic region is quite complicated (Figure 3-21), there are three clear benzyl methylene singlets at 5.17, 5.01, and 4.88 ppm in relative intensities of 1:2:1. If this were the desired product **3.34**, it would be expected to see only one signal due to symmetry.
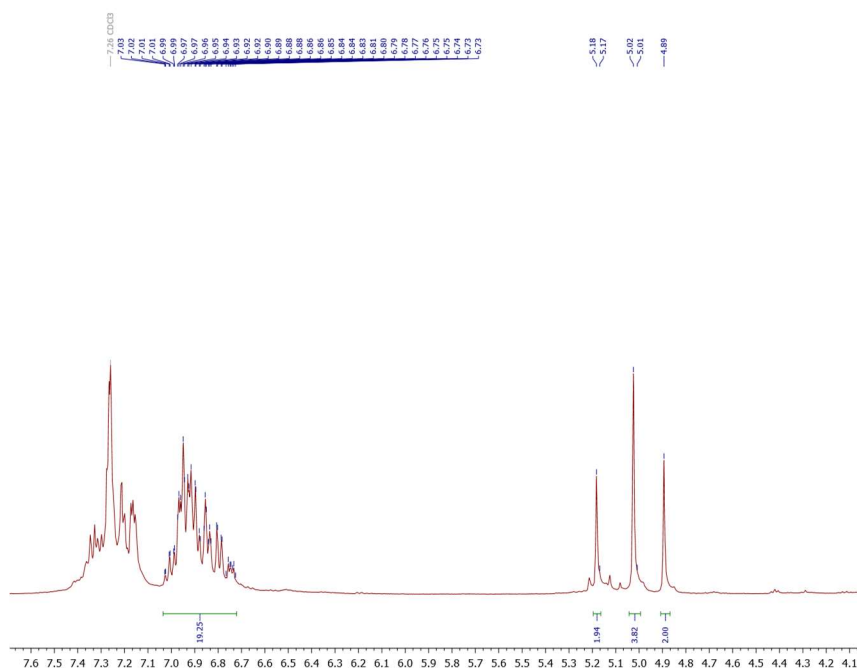
Figure 3-21: ^{1}H NMR of reaction mixture from attempt to form N,N'-dibenzyl-p-DADOP 3.34

When the reaction was carried out with 1:1 stoichiometry it was possible to form the *N*-benzyl phenoxazine **3.38** (Scheme 3-10), which required tedious chromatography for isolation.
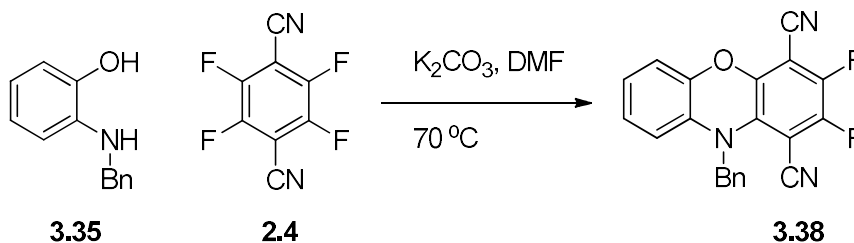
Scheme 3-10: Synthesis of N-benzylphenoxazine 3.38.

The structure of this compound was confirmed conclusively *via* X-ray crystallography; single crystals were obtained *via* evaporation of an ethyl acetate/hexane solution. Compound **3.38** crystallised in a monoclinic space group (P2$_1$/c) with four molecules per unit cell. The core is much more bent relative to N-H analogue **3.23** (Figure 3-22a) displaying a RMSD from planarity of 0.161 Å (*cf.* 0.013 Å for **3.23**).
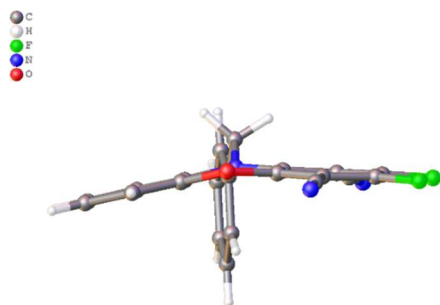
(a)
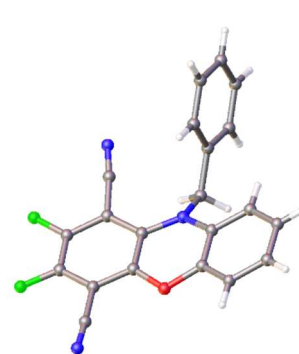
(b)

Figure 3-22: (a) Crystal structure of 3.38 showing bending within the phenoxazine core, and (b) looking down on the plane of the aromatic system.

The packing of the molecules in the crystalline state followed that of the N-H derivative, with each molecule alternating within π-stacks (Figure 3-23). The terminal phenoxazine rings are separated from those above and below by a plane-to-plane centroid distance of 3.591(2)-3.696(2) Å, and a plane normal-to-plane normal angle of 4.69(8) °, indicating some degree of π–π stacking.
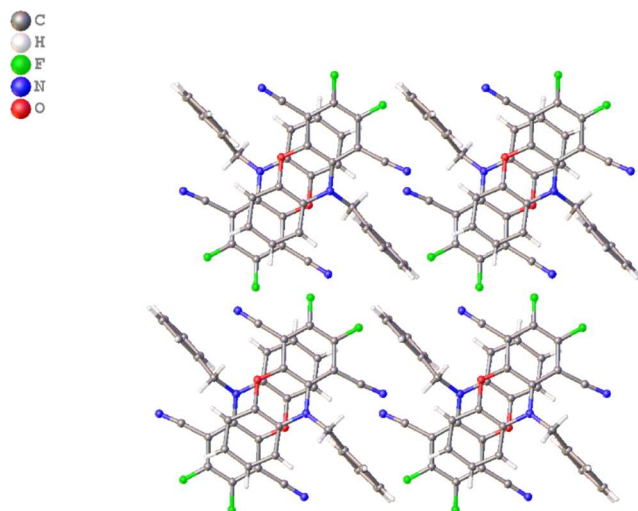
Figure 3-23: Crystal structure of 38 showing alternation within π-stacks.

Due to the poor reactivity (and stability) of the 2-(benzylamino)phenol precursor towards TFTP, access to the parent N-H DADOP **3.21** seems not viable by way of this synthetic route. Thus, attention was then diverted to exploring the other possible congeners in the series.

3.7   Other Possible O,N Isomers and Acronyms

At this point it is worth discussing the possible nitrogen-oxygen isomers which could be the target of future studies (Figure 3-24).
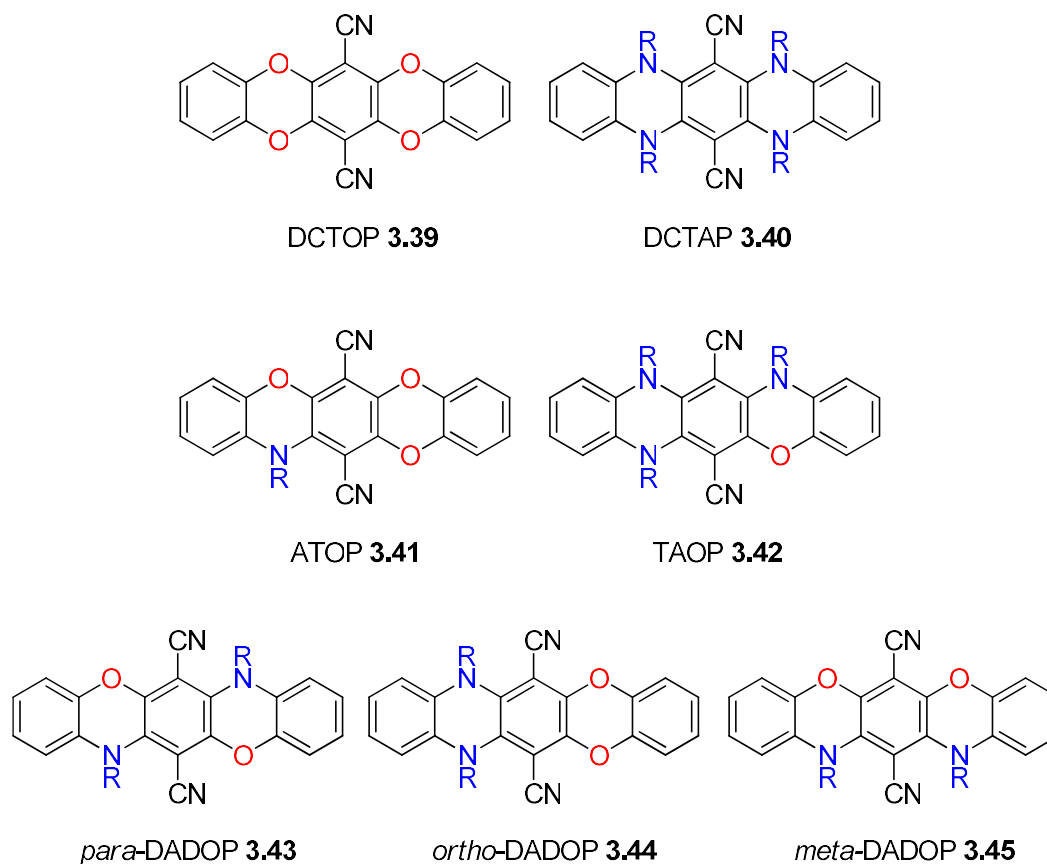
Figure 3-24: Possible dicyanoheteropentacene congeners.

The all-oxygen **di**cyano**t**etra**o**xa**p**entacene (DCTOP) **3.39** should be familiar from Chapter 2 and derives from the reaction of catechol with TFTP. The analogous all-nitrogen **di**cyano**t**etra**a**za**p**entacene (DCTAP) **3.40** could be considered a derivative of *o*-phenylenediamine *via* this methodology, as well as containing a dihydrophenazine core in the product.

The next two congeners are the 3:1 isomers, dicyano**a**za**t**ri**o**xa**p**entacene (ATOP) **3.41** and dicyano**t**ri**a**za**o**xa**p**entacene (TAOP) **3.42**. These compounds are retrosynthetically

different from DCTOP and DCTAP in that they could be obtained *via* preparation of the respective *o*-difluoride **3.16** or **3.49** from a symmetric nucleophile followed by reaction with the second, non-symmetric nucleophilic subunit (Scheme 3-11).
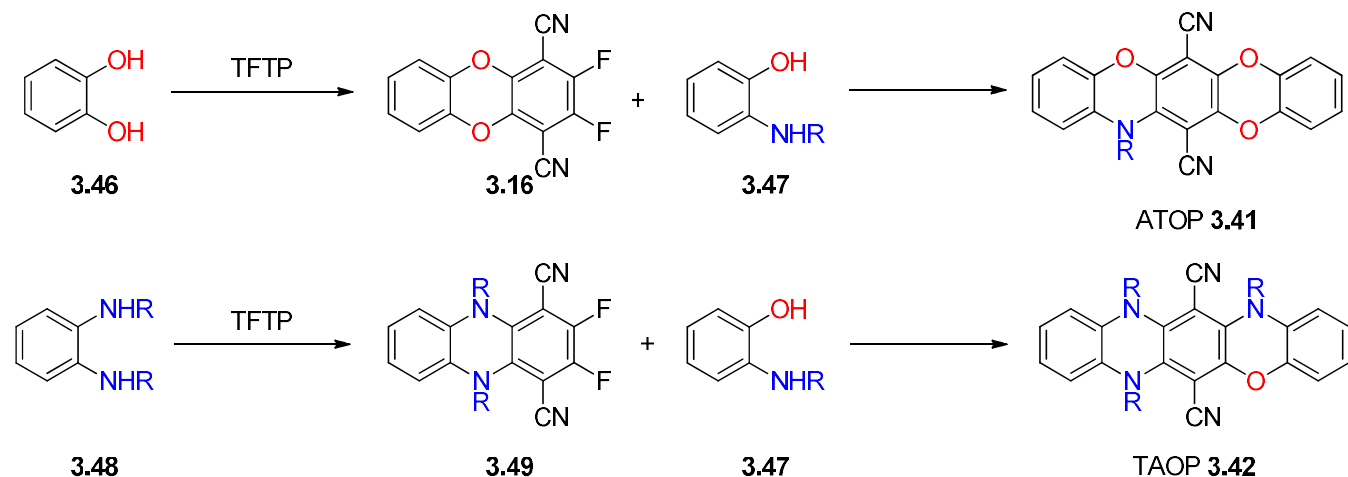
Scheme 3-11: Possible synthetic pathways to ATOP (3.41) and TAOP (3.42) derivatives.

Of the final three isomers, we shall concern ourselves mainly with dicyano-*para*-**di**a**z**a**dio**xa**p**entacene (*para*-DADOP) **3.43** and dicyano-*ortho*-**di**a**z**a**dio**xa**p**entacene (*ortho*-DADOP) **3.44**. In these cases, the *ortho*, *meta*, and *para* descriptors are taken to refer to the relative positions of like atoms (N and O). Due to the reactivity of the compounds, dicyano-*meta*-**di**a**z**a**dio**xa**p**entacene (*ortho*-DADOP) **3.45** is not obviously accessible *via* the currently utilised S$_N$Ar methodology as the substitution pattern is presumed to occur in the *para* fashion.

Using the proposed names, *N,N'*-diethyl-*para*-DADOP (**3.28**) was the first of the dicyanoazaoxapentacenes synthesised in this manner.

3.8   Synthesis of Dicyanoazatrioxapentacenes (ATOPs)

The unsubstituted azatrioxapentacene core (**3.50**, Figure 3-25) barely appears in the literature save in several Chinese language patents, where there are no experimental details.[97] As such, this motif is a virtually unexplored system. Additionally, aromatic molecules of lower molecular symmetry, such as **3.50**, can show improved photostability and fast intersystem crossing relative to more symmetric analogues.[98]

3.50
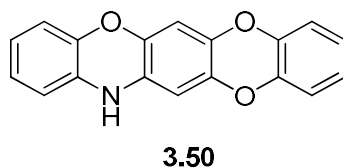
Figure 3-25: Unsubstituted ATOP core (3.50), virtually unexplored in the literature.

Since difluoride **3.16** is a known compound,[80] the route to *N*-ethyl-ATOP **3.51** became quite convenient (Scheme 3-12). Indeed, reaction of 2-(ethylamino)phenol with **3.16** furnished the monoazatrioxa derivative, ATOP **3.51**, in 66% yield as a vibrant orange solid. This compound, like the DCTOPs and DADOPs, again displayed bright fluorescence in the

solution and solid states, as well as enhanced solubility over its tetraoxa congener (DCTOP **3.39**).
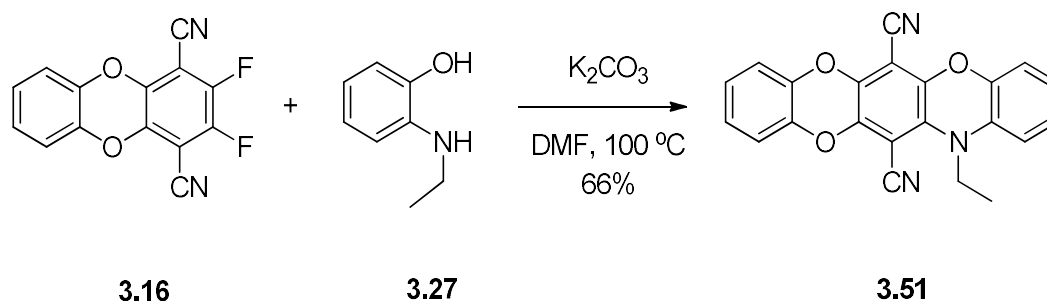
Scheme 3-12: Synthesis of N-ethyl-ATOP 3.31.

Similar to *N,N'*-diethyl-DADOP **3.28**, this compound also formed miniscule crystals when recrystallised from toluene-methanol. Attempts to grow X-ray quality single crystals are ongoing.

It may be remembered from Chapter 2 that difluorides such as **2.18** (Scheme 3-13), generated from reaction between TFTP and a terphenyl catechol, are intermediates in the synthesis of the tetraphenyl-DCTOPs. Taking the tetramethoxy difluoride **2.18** and reacting it with 2-(ethylamino)phenol in DMF at 100 °C the presence of K_2CO_3 gave this unsymmetrical diarylated derivative **3.53** in 87% yield (Scheme 3-13).
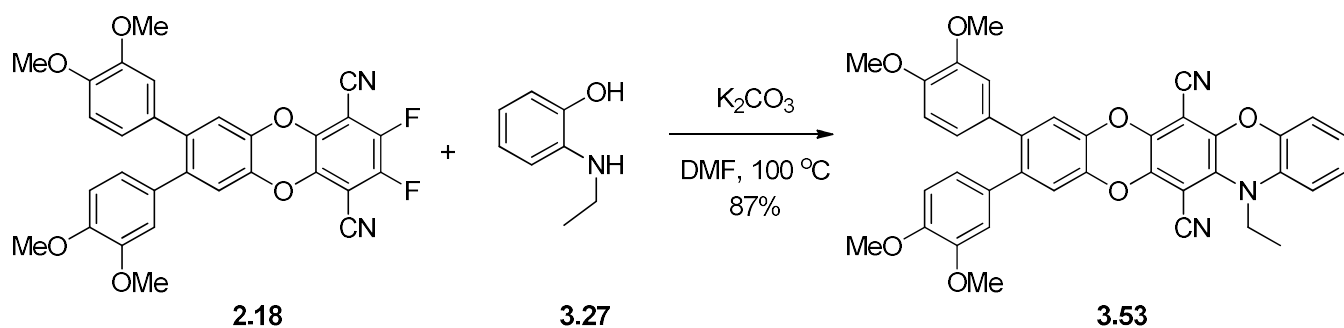
Scheme 3-13: Synthesis of syn-diarylated ATOP 3.53.

The properties of **3.53** are very similar to that of the parent ATOP with respect to UV-visible maximum absorption and emission in fluorescence spectroscopy, indicating little change introduced by the appended aryl groups (λ_{em} = 556 nm, 10^{-6} M, CHCl$_3$, excitation at 475 nm).

UV-vis measurements of the three compounds in chloroform (Figure 3-26) indicates a red shift of the λ_{max} upon introduction of nitrogen atoms. The parent DCTOP (**3.39**) exhibits maximum absorption at 430 nm, the *N*-ethyl-azatrioxa (ATOP, **3.41**) derivative at 467 nm, and *N,N'*-diethyl-DADOP **3.28** at 495 nm, indicating a shift of +37 nm upon addition of one nitrogen atom, and +65 nm upon addition of two nitrogen atoms (in the *para* positions). Additionally, the absorption broadens slightly along the same trend.

86
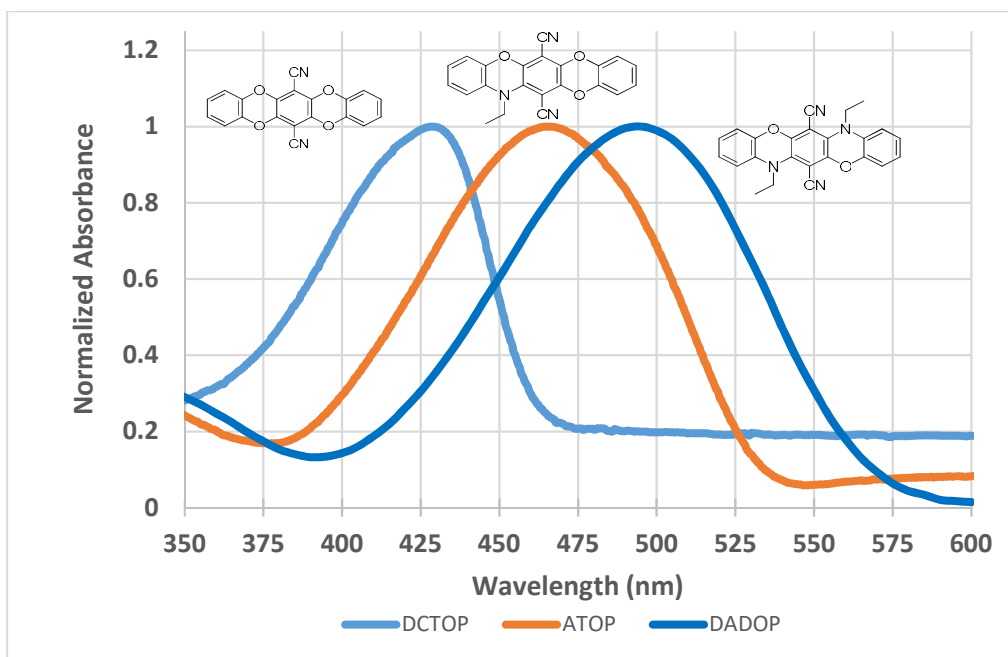
Figure 3-26: Normalized UV-visible absorption spectrum of

DCTOP (3.39), ATOP (3.41), and p-DADOP (3.28) in CHCl$_3$.

The DADOP derivatives (**3.28** and **3.31**) demonstrated an apparent solvatochromism, as solutions in various solvents would appear slightly different colours (shades of red-orange). Initial investigation into this behaviour (UV-visible spectroscopy) indicated that solvatochromism, while present, had a small (≈3-15 nm) effect on the λ$_{max}$ (Figure 3-27).
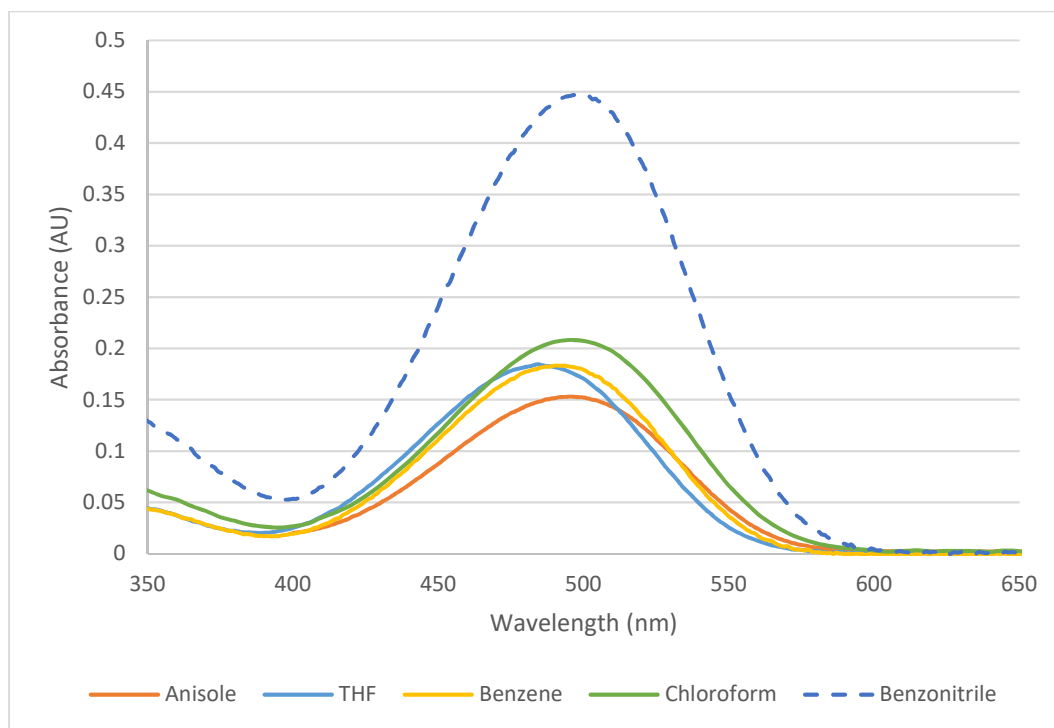
Figure 3-27: UV-visible spectra of 3.31 in several solvents (2x10^{-5} M).

However, far more apparent was the pronounced hyperchromic shift (increase in molar absorptivity) when benzonitrile was used as the solvent. Other solvents used were non-aromatic THF and chloroform, aromatic benzene, and electron-rich aromatic anisole. In each of the other cases a similar absorbance was observed, with the molar absorptivity constant (ε) ranging from 7500 L·mol^{-1}·cm^{-1} in anisole to 10350 L·mol^{-1}·cm^{-1} in chloroform. In benzonitrile, ε experiences a modest, but perceptible, boost to 22 300 L·mol^{-1}·cm^{-1}.

More experimentation is required before the cause of this behaviour can be attributed fully, but a preliminary theory could be simple aggregation in benzonitrile solution.

88

Fluorescence spectra of the two new pentacene derivatives were also compared to that of the parent DCTOP (Figure 3-28).
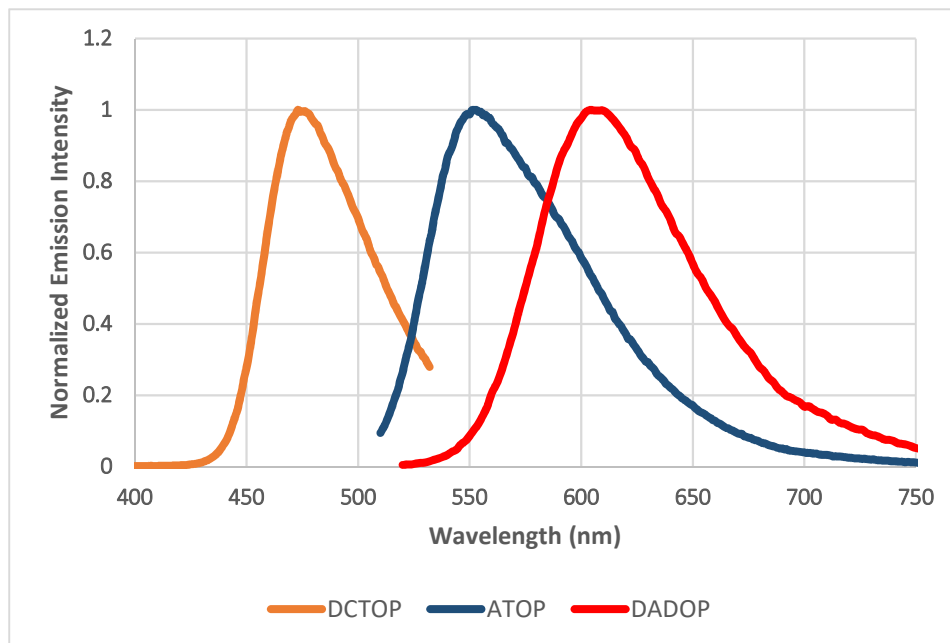
Figure 3-28: Fluorescence spectra of DCTOP 3.39, ATOP 3.41, and DADOP 3.28 (CHCl$_3$, 10^{-6} M, excitation at λ_{max}).

All three compounds are fluorescent in solution, and the emission maxima are red-shifted with increasing nitrogen content. This is in agreement with the UV-visible absorption spectra, wherein λ_{max} also experiences a red-shift with increasing N-atoms in the core.

3.9 Attempted Synthesis of Analogues Derived from o-Phenylenediamine

3.9.1 Introduction

There are many examples of N-heteroacenes within the literature incorporating pyrazine or dihydropyrazine rings. Most of these compounds are produced *via* condensation type reactions between an aryl 1,2-diamine and a 1,2-dione such as in Bunz' syntheses of azaacenes (Scheme 3-14), wherein the two reagents are reacted in a melt.[70]
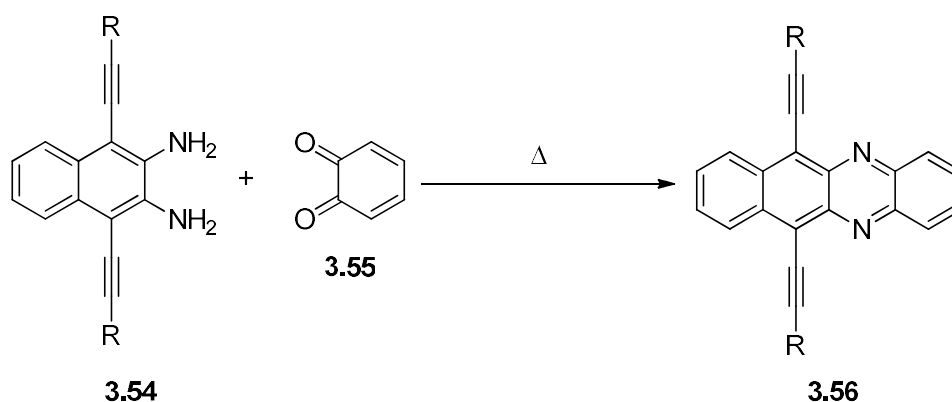
Scheme 3-14: Bunz' synthesis of N-heteroacene 3.56.

While condensation methods are the most common method, nucleophilic aromatic substitution has also been used to synthesise phenazines and other N-heteroacene analogues, such as Bunz' synthesis of the N-heteroacene derivative **3.59** (Scheme 3-15) *via* nucleophilic displacement of fluoride followed by oxidation with MnO_2.[68]
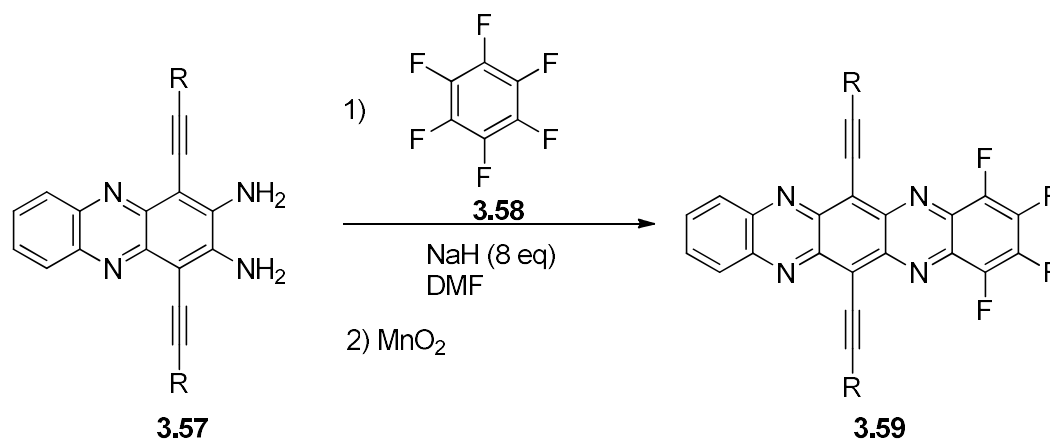
Scheme 3-15: Bunz' synthesis of N-heteroacene 3.59 via S$_N$Ar with hexafluorobenzene.[68]

Additionally, one group has published the synthesis of compound **3.17** derived from TFTP and *o*-phenylenediamine (Scheme 3-16), however no characterization for the derivative was given. In this instance the authors claim to use ultrasound sonication in room temperature DMF with base (K$_2$CO$_3$ or Et$_3$N) to effect the reaction.[79] There have been no reports of alkylated aryl-1,2-diamines reacting with TFTP.
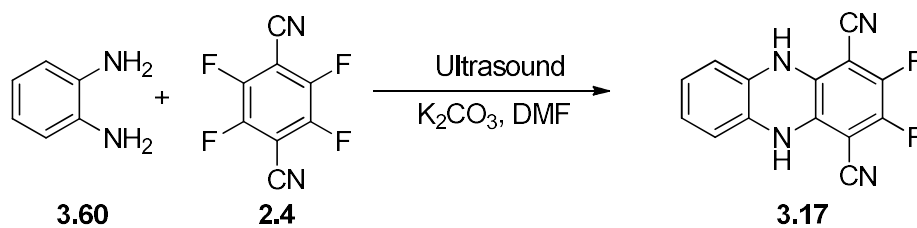
Scheme 3-16: Wang's synthesis of TFTP-derived dihydrophenazine 3.17 via S$_N$Ar reaction.[79]

Therefore, there is both precedent for the type of chemistry we are interested in carrying out as well as interest in N-heteroacene derivatives.

3.9.2 Attempted Synthesis of TFTP-Derived N-Heteroacenes

As in the investigation of the *o*-DADOP derivatives, TFTP was reacted with two equivalents of *o*-phenylenediamine under standard conditions (K$_2$CO$_3$, DMF, 65 °C). However, in this case an unidentifiable mixture of dark black products resulted.

Repeating the reaction in the absence of base provided a dark brown product which formed brilliant red solutions in organic solvents such as DMF. ^{1}H NMR of the product in DMSO-d$_6$ indicated a symmetrical molecule containing an aromatic multiplet (characteristic of the monocyclised products) at 6.60-6.52 ppm, as well as a singlet at 8.54 ppm in a relative integration of 2:1 respectively. ^{19}F NMR indicates the presence of a single peak located at -150.92 ppm which does not correspond to the shift of TFTP in DMSO (-131.07 ppm). ^{13}C NMR was highly indicative of dihydrophenazine **3.17** (Scheme 3-16) being the product due to the characteristic splitting patterns observed for the dicyanodifluorophenyl ring. High-resolution mass spectrometry data, however, was not conclusive for structure **3.17** returning with an *m/z* of 279.0680 amu rather than the expected 268.0561 amu. Single crystals could be grown (acetonitrile) but were of too poor quality to diffract. Due to the lack of characterization in the previous report of this compound,[79] we cannot be certain of its identity, although NMR data points to **3.17**.

Despite the evident challenges working with *o*-phenylenediamine as a nucleophile itself, we decided to apply the strategy of using an alkylated amine as nucleophile in hopes this would provide a desired pentacene analogue.

The requisite 1,2-diamine could be obtained *via* acetylation of *o*-phenylenediamine in ethyl acetate with acetic anhydride (Scheme 3-17) followed by reduction of bis(acetamide) **3.61** to give the known 1,2-diamine **3.62** as a green crystalline solid, as per literature procedure.[99]
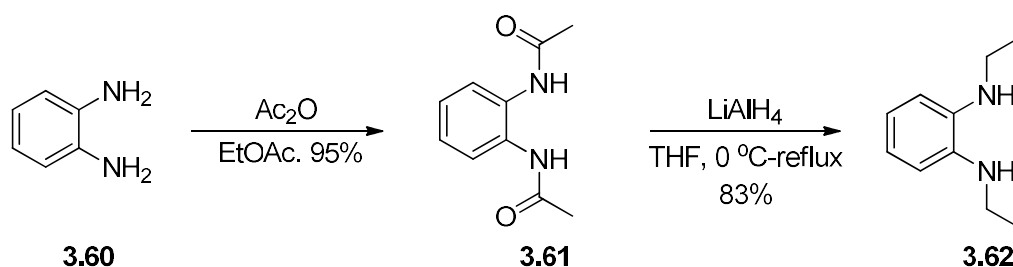
Scheme 3-17: Synthesis of o-phenylenediamine-derived nucleophile 3.62.[99]

Interestingly, it was found that this crude green solid had a ^{1}H NMR spectrum, which, while otherwise satisfactory, suffered an integration slightly too high for the methylene protons relative the methyl protons (5:6, respectively). Column chromatography on alumina, as per literature procedure, yielded a green product of no increased purity by ^{1}H NMR. Additionally, the product spot would turn red during the time it would take to run TLC analysis (SiO$_2$ or Al$_2$O$_3$), and the compound decomposed to a dark red substance over 5-7 days at −20 °C.

93

Kugelrohr vacuum distillation of the green solid was thus attempted and yielded a clear, colorless oil (110-120 °C/0.5 mmHg) which formed white crystals upon cooling at atmospheric pressure. These crystals were more stable, yet still gave rise to unsatisfactory amounts of decomposition after several days, and methylene to methyl integration (6:6) had not improved. It should be noted that ^{13}C NMR, as well as ^{1}H NMR shifts and *J*-couplings, agree otherwise perfectly with the literature characterisation.

Now with the nucleophile (**3.62**) in hand, we first reacted it with 0.5 equivalents of TFTP in DMF using K$_2$CO$_3$ as the base at 100 °C (Scheme 3-18). Unfortunately, this protocol, which worked well for alkylated N-nucleophiles derived from 2-aminophenol to give *p*-DADOPs, gave rise to a dark, intractable mixture of fluorescent products. Column chromatography was not viable, as the material exhibited limited solubility, and TLC indicated a bulk of material that would not move from the baseline regardless of the solvent. Attempts to crystallise the material were met with failure, as was trituration.
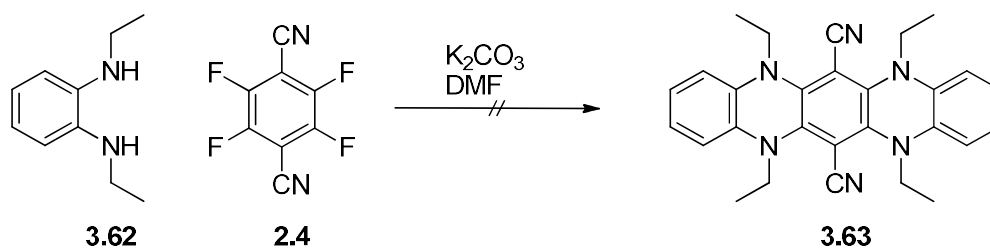
Scheme 3-18: Attempted synthesis of DCTAP 3.63.

Considering the failure of the previous reaction, it was desirable to limit the number of possible products and maximise the likelihood of isolating one of them; we choose to react bis(amine) **3.62** with dibenzodioxin difluoride **3.16** (Scheme 3-19). This electrophile can react twice, compared to four times for TFTP, and therefore fewer by-products are to be expected.
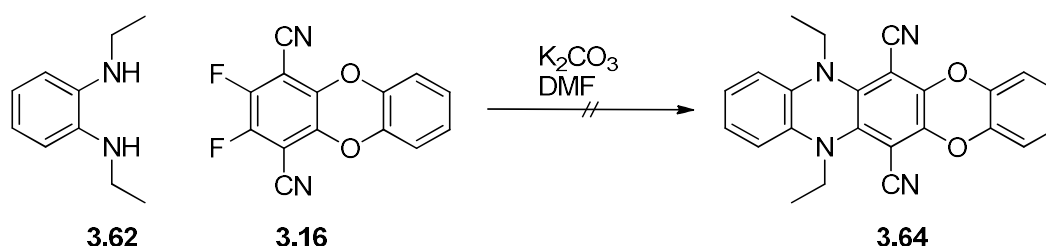
Scheme 3-19: Attempted synthesis of o-DADOP 3.64.

Surprisingly, the reaction went nearly as poorly as for the tetraaza congener, although in this case a solid product could be isolated. The solid displays vexing (in)solubilities, however, it was soluble enough in acetone-d_6 for a ^{1}H NMR, which indicated the presence of aromatic peaks, and the absence of aliphatic ones. Whatever the identity of the product, it appears there were no alkyl chains present. Attempts to find appropriate column chromatography or recrystallisation conditions have likewise failed.

It should be mentioned that in both preceding reactions, some of the produced material exhibited bright blue-green fluorescence, possibly indicating that at least some of the target pentacene (or another interesting compound) was formed.

95

Since any products formed in the preceding reaction were difficult to isolate and characterise, we again resorted to use of a long-chain homolog of our nucleophilic amine. Thus *N,N'*-didecyl-1,2-benzenediamine **3.66** was synthesised *via* acylation with decanoyl chloride followed by reduction of bis(amide) **3.65** to give alkylated diamine **3.66** in 88% yield over two steps (Scheme 3-20).
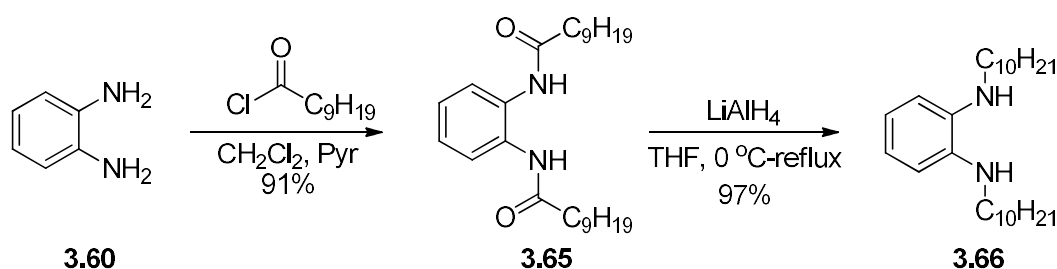
Scheme 3-20: Synthesis of N,N'-didecyl-o-phenylenediamine 3.66.

This material, while dark purple in colour, did not appear to degrade as quickly at −20 °C, as the appearance and NMR spectra of the compound did not change. Nonetheless, decomposition behaviour on SiO_2 was similar to the *N*-ethyl derivative when conducting TLC analysis.

Reaction of bis(decylamine) **3.66** with 0.5 equivalents of TFTP (K_2CO_3/DMF/100 °C) again led to an intractable oil, as in the case of the bis(ethylamine). Dibenzodioxin difluoride **3.16** was then chosen as the next reactive partner and reaction with one equivalent of **3.66** yielded a dark oil from which again no pure product could be isolated (Scheme 3-21).
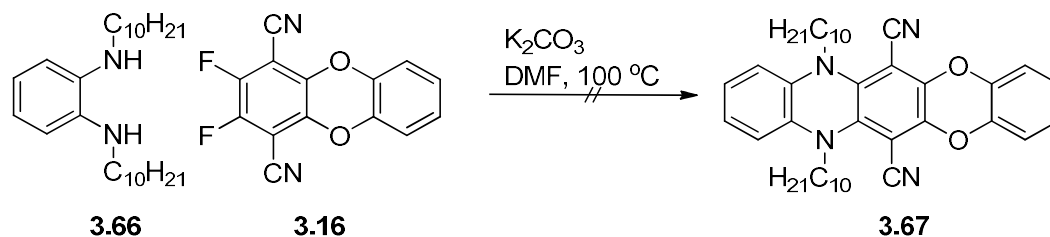
Scheme 3-21: Attempted synthesis of C$_{10}$-ortho-DADOP 3.67.

Reacting **3.66** with 1 equivalent of difluoride **2.18** in DMF at 100 °C in the presence of potassium carbonate likewise yielded an oil of poor purity and unknown composition (Scheme 22). Trituration of the oil with toluene produced a yellow precipitate, insoluble in chloroform, unlike yellow **2.18**. Despite the lack of solubility in chloroform, no other aromatic peaks nor alkyl protons were present other than those matching for difluoride **2.18**.
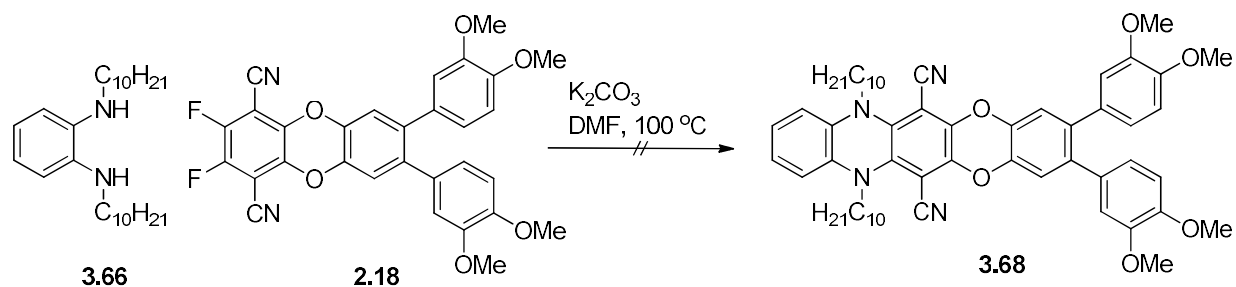
Scheme 3-22: Attempted synthesis of diarylated o-DADOP derivative 68.

Thus far none of the *o*-phenylenediamine-derived nucleophiles had worked to form any identifiable products; in fact, the most promising reaction had been that of *o*-phenylenediamine and TFTP, in DMF in the absence of base, giving previously reported *N,N*-dihydrophenazine **3.17**, without the use of ultrasound.[79] Since that compound decomposed in the presence of bases (*e.g.* K$_2$CO$_3$), it was thought that accessing the *N,N*-diethyl analogue (**3.69**) could prove useful as a building block towards other derivatives.
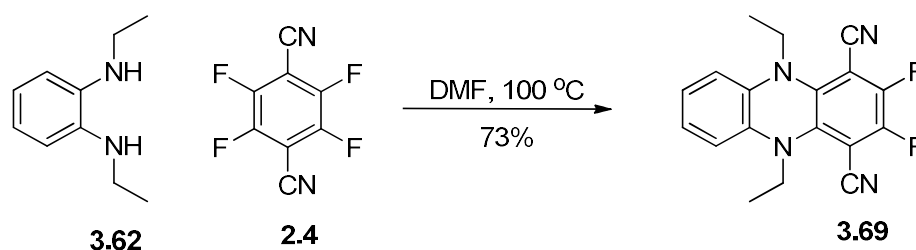
Scheme 3-23: Synthesis of N,N-diethyl-dihydrophenazine 3.69.

Therefore, two equivalents of **3.62** were reacted with TFTP in DMF at 100 °C (Scheme 3-23). Somewhat surprisingly, upon addition of water to the cooled reaction mixture, a reddish product precipitated. ^{1}H NMR of the compound indicated two aromatic multiplets (6.77 and 6.65 ppm) in relative integrations of 2:2, as well as two alkyl proton signals at 3.13 ppm (q) and 1.32 ppm (t) in relative integrations of 4:6 respectively, which fit the expected ^{1}H spectrum of compound **3.69**. The presence of one type of fluorine was evidenced by the singlet at −128.14 ppm in the ^{19}F NMR spectrum and confirmed by the [13]C–[19]F *J*-coupling

observed in the ^{13}C NMR spectrum (note that in this case no *J*-coupling constants could be extracted due to overlap and poor resolution of the less intense quaternary peaks).

While not a targeted pentacene derivative, *N*,N'-dialkylated dihydrophenazine **3.69** could be used in future work as a building block (much the same as dibenzodioxin **3.16**) to access *o*-diaza heteropentacene analogue frameworks.

3.9.3 Discussion

The synthesis of several pentacene analogues was attempted *via* reactions between nucleophiles derived from *o*-phenylenediamine and TFTP as the electrophile. Synthesis of the nucleophiles was accomplished by modified literature procedures.[99] The stability of the 1,2-bis(ethylamino)benzene compound (**3.62**) was found to be less than ideal, decomposing over several days at −20 °C.

Attempts to form pentacene analogues with TFTP or derivatives (**3.16** or **2.18**) and nucleophiles **3.62** and **3.66** formed intractable mixtures of products, the one exception to that being the synthesis of *N*,*N*-diethyl-dihydrophenazine **3.69**. As previously stated, this compound could serve as a building block for some of the desired derivatives, such as *o*-DADOP **3-64** (Scheme 3-24).
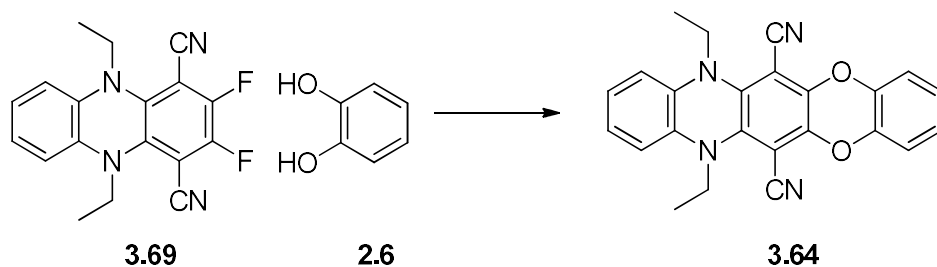
Scheme 3-24: Future proposed synthesis of diethyl-o-DADOP 3.64.

Future work in this area should focus upon the use of accessible building blocks such as **3.69** to synthesise the unknown derivatives. Comparison of the properties of these derivatives, once synthesised, will be instructive in gaining an understanding of the properties of these new heterocyclic compounds.

3.10   Attempted Use of 2-(Ethylamino)thiophenol as Nucleophile

3.10.1   Introduction

Aromatic   sulfur-containing   heterocycles,   such   as   oligothiophene,[100] phenothiazine,[101–103] and thienoacenes (thiophene-acenes)[104] have been investigated as materials for organic electronics. The presence of sulfur within a compound can have a dramatic effect on the properties and potential applications of the material,[105] and methods have been developed specifically to incorporate sulfur into aromatic systems as fused thiophene units.[106] The ability to oxidise the sulfur to a sulfoxide or sulfone can lead to significant structural and electronic alterations.[107]

Acene analogues which incorporate a six-membered sulfur-containing ring (as in phenothiazine) have been known in the literature for many years. For example, compound **3.70** was initially published in 1957 by Farrington *et al. via* a (now-common) sulfur insertion reaction utilising elemental sulfur (Figure 3-29);[108] an extension of that methodology allowed access to heteroheptacene analogue **3.71** by Andreani *et al.* in 1991.[109]

3.70   **3.71**
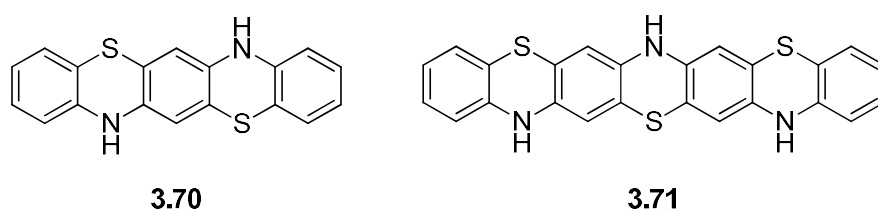
Figure 3-29: Examples of S,N-heteroacene analogues from the literature.[108,109]

Derivatives of a different substitution pattern, such as **3.72** (Figure 3-30), were synthesised by Müllen *et al.* in 1994.[110] **3.72** exists with one phenothiazine subunit in a planar conformation, never before observed crystallographically (phenothiazine itself exists with both terminal rings bent towards one another).

3.72, R = C(CH$_3$)$_2$(CH$_2$)$_3$CH$_3$
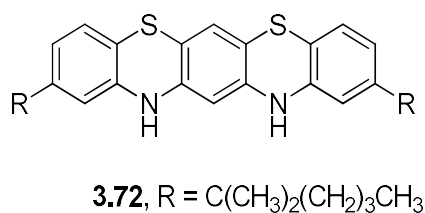
Figure 3-30: Müllen's S,N-heteroacene 3.72.[110]

There are few reactions of sulfur nucleophiles reacting with TFTP in the literature. Wang *et al*. report the synthesis of compound **3.18** (Scheme 3-25), but fail to report any characterisation data for the compound.[79] There are no reactions in the literature giving the analogous TFTP-derived phenothiazine or phenoxathiine, nor any pentacene analogues.
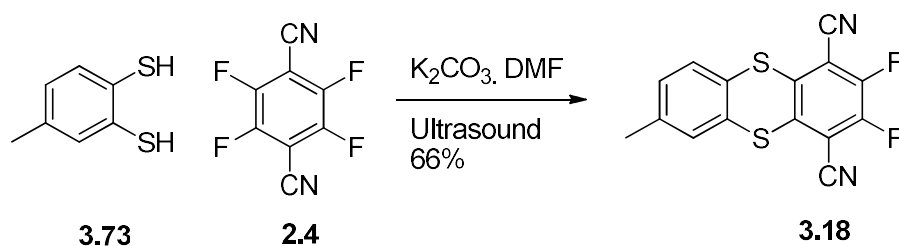
Scheme 3-25: Wang's preparation of dibenzodithiin 3.18.

Voskuhl *et al*. report the synthesis of a tetrathioether obtained via reaction of thiophenols (**3.74**) with tetrachloroterephthalonitrile **3.75** (Scheme 3-26).[111] These derivatives displayed intense fluorescence in solution and solid states due to aggregation-induced emission behaviour.
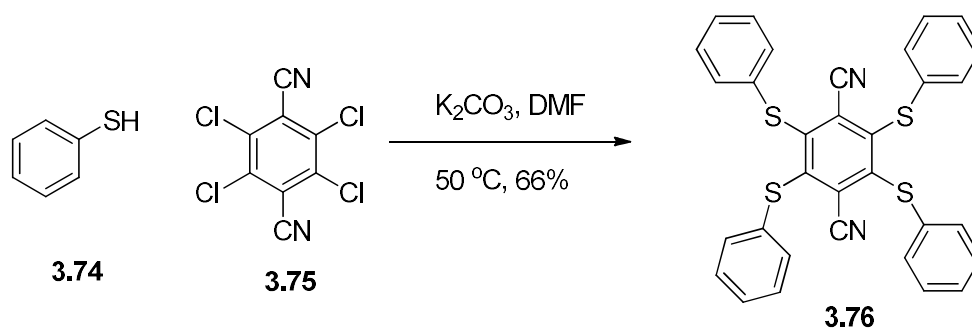
Scheme 3-26: Voskuhl's reaction of TCTP with aryl thiols to form aryl thioether luminogens.

Based on the literature precedent for reactions of aryl thiols and amines with TFTP or TCTP, it was expected that formation of sulfur-nitrogen dicyanopentacene analogues should be eminently accessible.

3.10.2   Synthesis of p-Diazadithiapentacene (DADTP)

Direct analogues to *N,N*-diethyl-DADOP (**3.28**) could be accessed through reaction of TFTP with 2-(ethylamino)thiophenol (**3.77**, Scheme 3-27) to furnish *p*-diazadithiapentacenes (*p*-DADTPs, **3.78**).
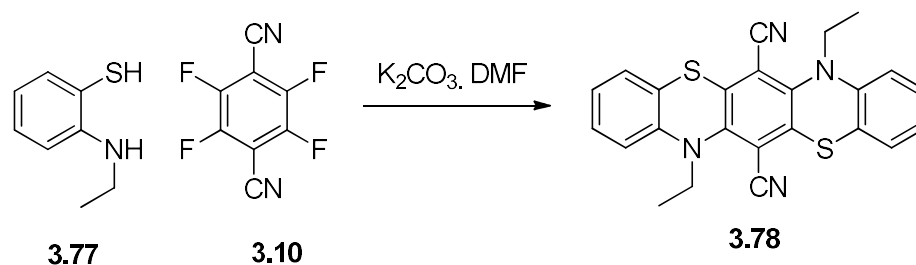
Scheme 3-27: Route to diazadithiapentacene (DADTP, 3.78).

While 2-(ethylamino)thiophenol **3.77** is a known compound, it is not commercially available. Furthermore, there are few published syntheses of the compound, and fewer in English. Nonetheless, a procedure was found wherein the authors produced the desired thiophenol from diborane reduction of 2-methylbenzothiazole (**3.78**) followed by protonolysis (Scheme 3-28).[112]
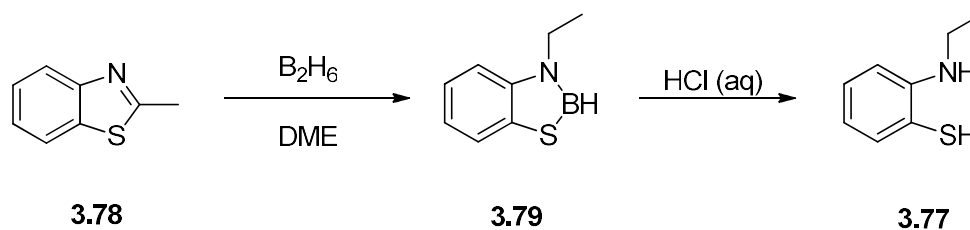
Scheme 3-28: Literature synthesis of 2-(N-ethylamino)thiophenol (3.77)

via diborane reduction of 2-methylbenzothiazole (3.78).[112]

Unfortunately, the original authors did not give experimental details nor characterisation; nonetheless, the procedure was attempted first with borane-

tetrahydrofuran complex, but reaction did not occur (TLC). Since the procedure required diborane, a difficult to handle gas, a different route to access the desired nucleophile was sought.

An analogous route to the *N*-methyl derivative was published by Hünig (of Hünig's base fame) in 1972, and involves the use of lithium aluminum hydride to reduce benzothiazole.[113] Thus, adapting the aforementioned procedure, reduction of 2-methylbenzothiazole (**3.78**) proceeded with LAH in THF to yield 2-(ethylamino)thiophenol (**3.77**) in 65% yield as a clear liquid after distillation (Scheme 3-29). This compound discoloured to yellow upon standing in air, presumably *via* oxidation to the disulfide.

3.78   **3.77**
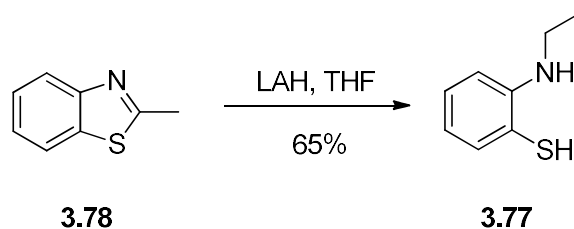
Scheme 3-29: Successful synthesis of 2-(N-ethylamino)thiophenol (3.77) via

a modified literature procedure.[113]

Initially aminothiophenol **3.77** was reacted with 0.5 equivalents of TFTP in DMF (Scheme 3-30); this reaction yielded an orange-red solid which was brightly fluorescent, composed of at least two components (TLC). Column chromatography (30% CH_2Cl_2/hexanes) yielded mixtures of two products, one mixture appearing less pure by [1]H

NMR spectroscopy than the other. The contents of the purer fractions of slightly lower R_f ($\approx$0.4, 50% CH_2Cl_2/hexanes) could be suitably recrystallised from THF to give a pure product, albeit in an exceedingly low isolated yield (8%). ^1H and ^{13}C NMR data, as well as lack of a ^{19}F NMR signal appear to indicate the desired diazadithiapentacene (DADTP) analogue **3.80**.
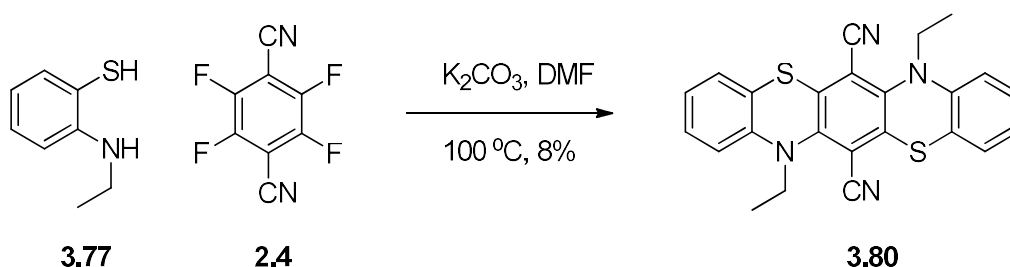
Scheme 3-30: Synthesis of diazadithiapentacene 3.80.

It should be noted that the low yield is partially due to the large amount of material which could not yet be purified and was thus left as a mixture. Further experimentation and yield optimisation could indeed lead to a more efficient synthesis. Nonetheless, the final pentacene was obtained in two steps from 2-methylbenzothiazole. The identity of the second component has not been determined, although there are several possibilities, such as regioisomer formation (*e.g.* **3.81**) or sulfur oxidation (*e.g.* **3.82**) (Figure 3-31).
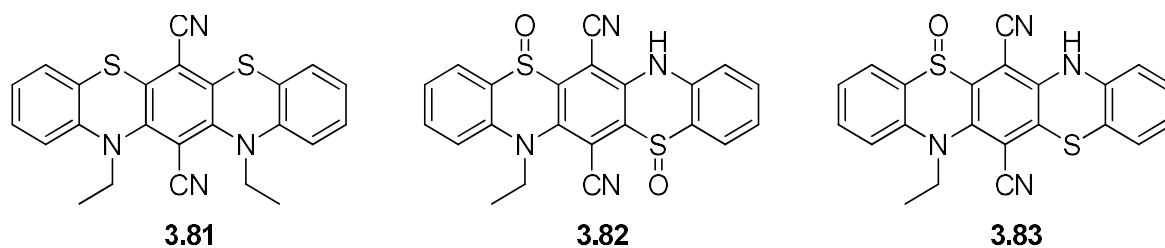
Figure 3-31: Possible by-products of reaction in Scheme 3-30.

Compound **3.80** is bright orange in colour and fluoresces brightly in the solid and solution states, like all other dicyanopentacene derivatives produced thus far. UV-visible spectroscopy (Figure 3-32) indicates a λ_{max} of 497 nm (10^{-5} M, $CHCl_3$) which is within error of the λ_{max} for *p*-DADOP **3.28** (495 nm, 10^{-5} M, $CHCl_3$). Interestingly, while dilute (10^{-5} M) solutions of **3.80** and **3.28** are of similar colour, the crystalline solids are very different (orange *vs.* red).
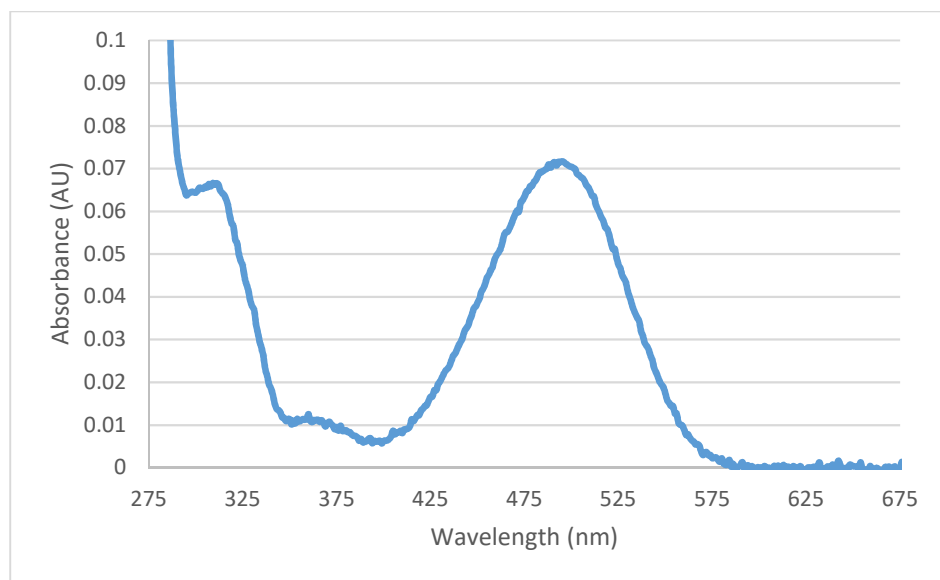
Figure 3-32: UV-Visible spectrum of compound 3.80 (10^{-5} M, CHCl$_3$); λ_{max} = 497 nm.
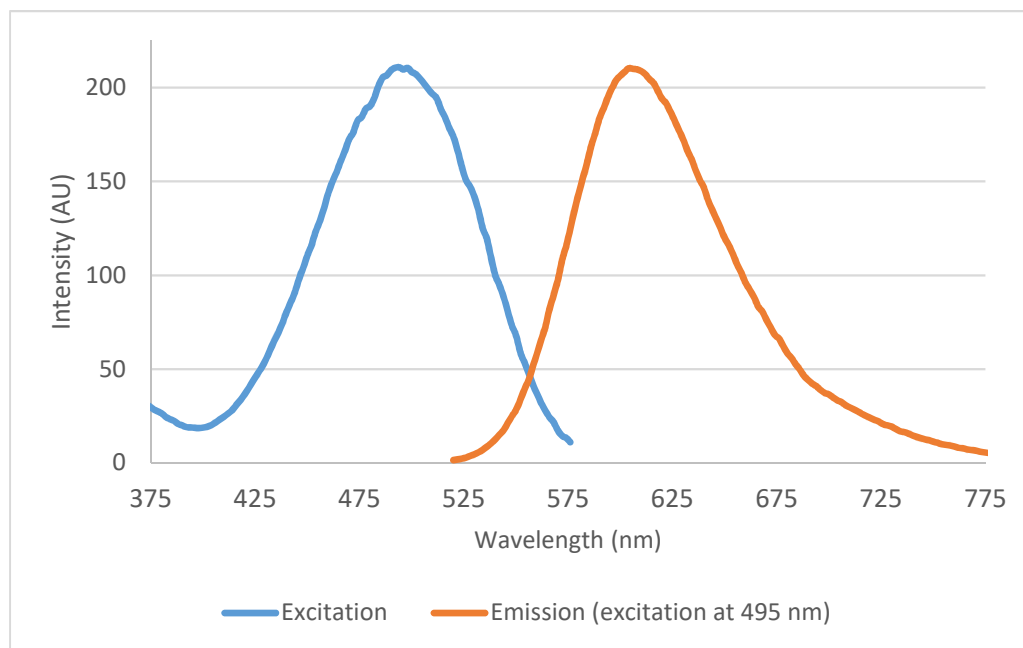
Figure 3-33: Excitation-emission spectra of compound 3.80

(10^{-5} M, CHCl$_3$, excitation at 495 nm).

Fluorescence measurements in $CHCl_3$ (10^{-5} M) indicated a λ_{em} of 610 nm (excitation at 495 nm, Figure 3-33. Like the absorption spectra, *p*-DADTP **3.80** exhibits similar fluorescence behaviour as *p*-DADOP **3.28** (λ_{em} = 612 nm, 10^{-6} M, $CHCl_3$).

Crystallisation experiments to grow X-ray quality single crystals are currently underway. Sublimation of the compound will also be attempted.

3.10.3   *Synthesis   of   Nitrogen-Oxygen-Sulfur   Analogues   – Azadioxathiapentacene (ADOTP)*

Considering the low yield for the initial synthesis of *p*-DADTP **3.80** and the possibility for yield loss due to regioisomer formation, synthesis of the nitrogen-oxygen-sulfur containing derivative **3.84** was proposed (Scheme 3-31). This route has the advantage of not requiring a regioselective second addition of a nucleophile and is doubly advantageous since we have previously synthesised and utilised difluoride **3.16** in the synthesis of the ATOP derivatives.
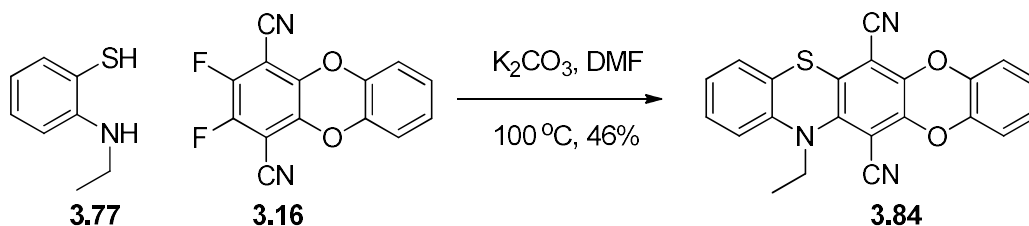
Scheme 3-31: Synthesis of azathiadioxapentacene (ADOTP, 3.84).

Reaction of nucleophile **3.77** with difluoride **3.16** (K_2CO_3, DMF, 100 °C) resulted in a dark red mixture, which upon work-up (pouring into water), formed a bright orange precipitate. Recrystallisation from ethyl acetate provided long, orange needles in 46% yield. ^{1}H and ^{13}C NMR data accords with the identity of the compound as being desired product **3.84**, and no other major component could be isolated from the filtrate. A melting point taken of the recrystallised material showed a narrow range of 243-244 °C.

This compound is also brightly orange fluorescent in the solid and solution states (Figure 3-34). UV-visible measurements (10^{-5} M, CHCl$_3$) indicate a λ_{max} of 467 nm which is virtually identical to ATOP **3.51** (λ_{max} = 467 nm, 10^{-5} M, CHCl$_3$).
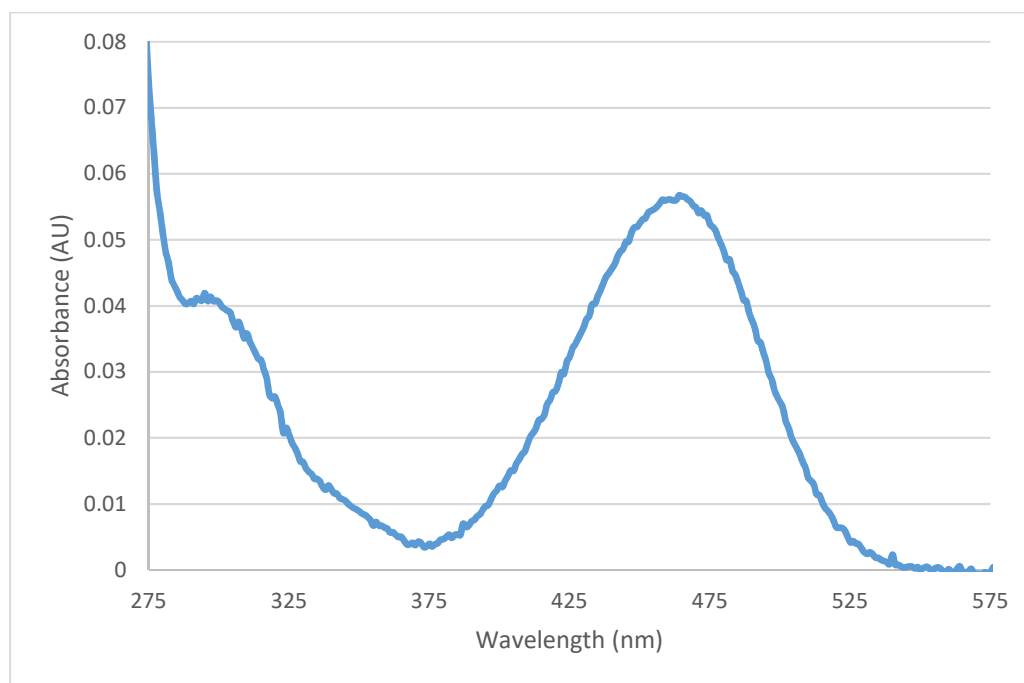
Figure 3-34: UV-visible spectrum of compound 3.84 (10^{-5} M, CHCl$_3$); λ_{max} = 467 nm.

Emission spectra of **3.84** indicated a λ_{em} at 576 nm (10^{-5} M, CHCl$_3$, excitation at 467 nm). This is redshifted with respect to ATOP **3.51** (λ_{em} = 557 nm, 10^{-6} M, CHCl$_3$, excitation at 468 nm) by approximately 19 nm.
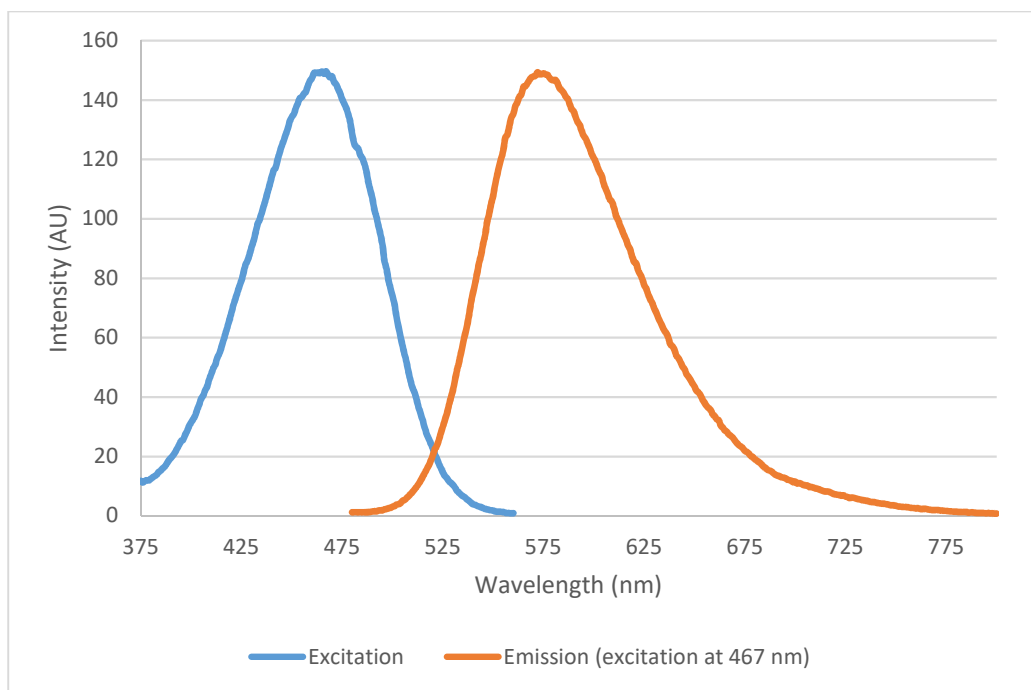
Figure 3-35: Excitation emission spectra of compound 3.84

(10^{-5} M, CHCl$_3$, excitation at 467 nm).

3.10.4 Conclusions and Future Work – Sulfur Derivatives

2-(Ethylamino)thiophenol **3.77** was synthesised *via* lithium aluminum hydride reduction of 2-methylbenzothiazole and was applied to the formation of several heteropentacene derivatives. Diazadithiapentacene **3.80** was synthesised in a low 5.2% overall yield, while azadioxathiapentacene **3.84** was synthesised in a higher 30% overall yield from 2-methylbenzothiazole. The low yield in the former case stems in part from difficulty in separating out the pure compound from a mixture of by-products.

Future work in this area will focus on: (1) improvements to the synthesis of the DADTP **3-80** to increase the yield and ease of purification; (2) synthesis of phenothiazine **3.85**, to be used as a further building block; and (3) the triazathiapentacene **3.86**, a potentially interesting derivative (Figure 3-36).
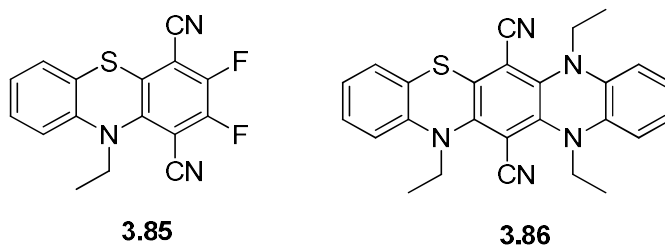
Figure 3-36: Future N,S heterocycle targets.

Chapter IV- Conclusions and Future Work

This thesis focused on the synthesis of novel heterocyclic pentacene analogues _via_ nucleophilic substitution reactions with tetrafluoroterephthalonitrile (TFTP).

Improvements were made to the original synthesis[49] of substituted tetraoxadicyanopentacene (DCTOP) derivatives. The major shortcoming of the original synthesis, a low-yielding fourfold Suzuki coupling involving a tedious purification, was overcome by switching the S$_N$Ar reaction and Suzuki in the reaction sequence. Via this new synthetic route, substituted DCTOPs were prepared in good yields and with facile purification.

The alkoxy-substituted tetraphenyl substituted DCTOPs were identical to the material previously prepared via the original synthetic route. Columnar LC mesophases were observed for both compounds, as had been observed by Raycraft.

The corresponding methoxy-substituted derivative, which had not been previously synthesized, was crystallised and the solid-state structure investigated by single crystal X-ray diffraction, indicating a planar core with coplanar molecules separated by a distance greater than that allowed for efficient π−π interactions. The (highly insoluble) unsubstituted parent DCTOP was also crystallised, and the crystal structure indicates several different π−π interactions.

This new synthetic route to substituted DCTOPs also provided the opportunity to synthesize a dissymmetric DCTOP, which was not found to differ from the unsubstituted parent DCTOP in photophysical measurements, however, this compound proved to be much more soluble than DCTOP.

Based on the synthesis of DCTOP derivatives, methodology for the synthesis of other novel 6,13-dicyanoheteropentacene analogues from TFTP via nucleophilic aromatic substitution chemistry was developed. Several synthetic roadblocks were encountered, and some were successfully navigated while others remain a challenge.

The para-diazadioxapentacenes (*p*-DADOPs) were synthesized in good yields and displayed solution and solid-state luminescence. The structure (and substitution pattern) of *N,N'*-didecyl-p-DADOP was confirmed by single crystal XRD, which also indicated a planar DADOP core as well as close π–π contacts between the cores.

N-Ethyl-azatrioxapentacene (ATOP) was synthesized in good yield, however, this compound did not form crystals suitable for XRD analysis. UV-visible and emission spectra indicate a red-shift relative to DCTOP, and a blue-shift relative to *p*-DADOP. As expected from the behaviour of syn-diarylated DCTOP, the analogous ATOP derivative displayed photophysical properties like those of the parent ATOP compound, indicating a very small effect from the appended phenyl rings.

The sequential substitution of N for O atoms within the core led to a redshift in the absorbance and emission maxima. Analogues containing an S for O substitution displayed photophysical properties similar to that of the O,N congeners. Future work in this area will focus on obtaining crystal structure data for all of these derivatives.

Derivatives which were not accessible under the conditions attempted included the tetraazapentacene (DCTAP) and o-diazadioxapentacene (*o*-DADOP); future work will attempt to access these derivatives via alternate synthetic routes.

In conclusion, significant synthetic and purification challenges were overcome to yield a series of novel 6,13-dicyanoheteropentacene analogues in good yields via nucleophilic aromatic substitution on tetrafluoroterephthalonitrile. Based on the interesting photophysical properties and solid-state organisation, these materials show promise for applications in organic electronics. Furthermore, we have demonstrated that the synthetic approach can be used to access a variety of heterocyclic pentacene analogues that are not readily accessible using other methods.

Chapter V - Experimental

5.1 *General*

5.1.1 NMR Spectroscopy

^{1}H and ^{13}C spectra were recorded on a Varian 300 MHz Unity Inova NMR Spectrometer or an Agilent Technologies 400 MHz Spectrometer, as indicated, using deuterated solvents purchased from CIL Int. Chemical or Millipore-Sigma; shifts are reported (δ-scale) using the residual solvent peak as reference. In the case of ^{19}F NMR no reference was used. For some compounds, such as 2,3-difluoro-10H-phenoxazine-1,4-dicarbonitrile (**3.23**), 5,10-diethyl-2,3-difluoro-5,10-dihydrophenazine-1,4-dicarbonitrile (**3.69**) and 2-(*N*-decylamino)phenol (**3.30**) not all C atoms appeared in the ^{13}C NMR spectra and/or C−F *J*-couplings could not be determined due to low signal-to-noise for the quaternary carbons, and, in the case of the fluorinated derivatives, the intensities are additionally lowered by C−F coupling itself; in these cases the peaks are listed singly.

5.1.2 High-Resolution Mass Spectrometry

High resolution mass spectra were recorded at the Centre Régional de Spectrométrie de Masse à l'Université de Montréal using an Agilent LC-MSD TOF spectrometer in the ionisation mode indicated.

5.1.3 Ultraviolet-visible (UV-Vis) and Fluorescence Spectroscopy

UV-Vis spectra were obtained on a Varian Carey 50 Bio UV-visible spectrophotometer. Fluorescence measurements were obtained on an Agilent Technologies Carey Eclipse fluorescence spectrophotometer. For both techniques, quartz cuvettes ($\ell = 1.0$ cm) were used.

5.1.4 X-ray Diffraction

Crystals of **2.1c**, **3.22**, **3.23**, **3.31, 3.32, 3.38,** and **3.39**, were selected and collected on a Bruker APEX-II CCD diffractometer with MoKα radiation, or on a Nonius CCD diffractometer with CuKα radiation. Using Olex2,[114] the structures were solved with the ShelXT[115] structure solution program using intrinsic phasing and refined with the ShelXL[116] refinement package using least squares minimisation. For all structures, hydrogen atoms bonded to oxygen or nitrogen atoms were introduced in difference map positions and refined isotropically with distance restraints and default standard uncertainties (ShelXL: SADI and DFIX), while all other hydrogen atoms were introduced in calculated positions and refined on a riding model. All other atoms were refined anisotropically. Any exceptions and/or additions to this method of refinement are noted on the first page of the X-ray crystallographic reports, which are included in Appendix A. Full data collection conditions, and tables of displacement and geometric parameters, can also be found in these reports.

5.1.5 Infrared Spectroscopy

Infrared spectra were obtained, neat, on a Bruker Alpha Platinum attenuated total reflectance infrared (ATR-IR) spectrophotometer with a diamond crystal. Peaks are reported in wavenumbers (cm^{-1}; br = broad, w =weak, vw = very weak, s =strong).

5.1.6 Chemicals and Solvents

All reagents and starting materials were purchased from Millipore-Sigma and used as received with the noted exceptions of 2-aminophenol which was recrystallised from EtOH under N$_2$, and catechol, which was recrystallised from toluene. *n*-BuLi (THF solution) was titrated against *N*-benzylbenzamide in THF at −40 °C prior to use.[117] Anhydrous and oxygen-free solvents were dispensed from a custom-built solvent purification system which used purification columns packed with activated alumina and supported copper catalyst (Glasscontour, Irvine, CA) and maintained under argon. Melting points were determined on a Mel-Temp® Electrothermal melting point apparatus and are uncorrected. The following compounds were prepared according to literature procedures: dibromocatechol (**2.5**),[51] 3,4-bis(decyloxy)phenylboronic acid (**2.2a**) and 3,4-bis(hexyloxy)phenylboronic acid (**2.2b**),[63] tetrafluoroterephthalonitrile (**2.4**),[50] 3,4-bis(decyloxy)benzene (**2.7a**) and 3,4-bis(hexyloxy)benzene (**2.7b**),[61] 4-bromo-1,2-bis(decyloxy)benzene (**2.8a**) and 4-bromo-1,2-bis(hexyloxy)benzene (**2.8b**),[62] 2-(*N*-acetamido)phenol (**3.26**),[118] *N,N'*-(1,2-phenylene)diacetamide (**3.61**),[99] *N^1,N^2*-diethyl-1,2-benzenediamine (**3.62**).[99]

5.2 Synthesis
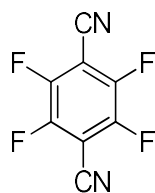
2,3,5,6-Tetrafluoroterephthalonitrile (2.4): To a 250 mL three-neck round bottomed flask, under N_2 and equipped with a condenser, was added tetrachloroterephthalonitrile (20.0 g, 75.2 mmol, 1.0 eq), potassium fluoride (21.9 g, 376 mmol, 5.0 eq), TBAB (0.60 g, 1.9 mmol, 2 mol%), and DMF (125 mL). The reaction mixture was stirred and heated to 110-120 °C. After 24 h the mixture was cooled to room temperature, H_2O (1000 mL) was added, and the solid collected *via* suction filtration, washing with H_2O. The crude material thus obtained was recrystallized from acetone, yielding TFTP (**2.4**) as a straw yellow crystalline solid (12.5 g, 83%). mp = 194-195 °C; ^{19}F NMR (375.9 MHz, CDCl[3]) δ: -133.38. Analytical data agrees with literature values published by Dolbier, *et al.*[50]
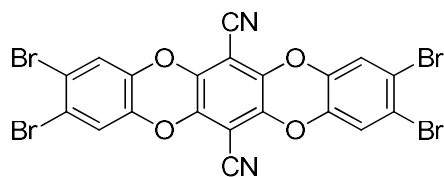
2,3,9,10-Tetrabromo-5,7,12,14-tetraoxa-6,13-dicyanopentacene (2.3): To a two-neck round bottomed flask, under nitrogen gas, were added anhydrous DMF (120 mL), 4,5-dibromocatechol (4.49 g, 40.8 mmol), tetrafluoroterephthalonitrile (3.71 g, 18.5 mmol), and potassium carbonate (16.9 g, 122.4 mmol). The mixture was stirred at 65 °C for 24 hours. After cooling to room temperature, the yellow precipitate was collected by vacuum filtration. The solid was then stirred in water (200 mL) for 30 minutes followed by acetone (200 mL) for an additional 30 minutes to remove any remaining starting materials. The product was then collected by suction filtration to yield compound **2.3** as a luminous yellow solid (6.02 g, 84%). ^{1}H and ^{13}C NMR spectra could not be recorded due to low solubility. mp > 260 °C; HRMS (ASAP) Calc. for $C_{20}H_4N_2O_4Br_4$ M^+: 651.6905 Found: 651.6914.

119
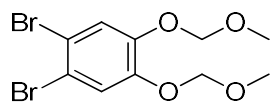
1,2-dibromo-4,5-bis(methoxymethoxy)benzene (2.12): To a 500 mL single-neck round bottomed flask was added dibromocatechol (5.00 g, 18.7 mmol, 1 eq), dimethoxymethane (165 mL, 1.87 mol, 100 eq), and chloroform (200 mL). To this stirred solution was added phosphorous pentoxide (30.0 g, 2.11 mol, 11.3 eq), in portions, over 3-5 min, with mild heat evolution observed. The flask was equipped with a drying tube and the mixture was stirred 18 h. After this time the solution was decanted, and the residue washed with chloroform. The organic solution was washed with saturated $NaHCO_3$ (2 x 25 mL) followed by 1 M HCl (1 x 25 mL), dried over $MgSO_4$, and the solvent removed *in vacuo* to give a colorless oil which solidified upon standing to give a greasy, white solid (6.14 g, 92%). mp = 59-60 °C; ^1H NMR (400 MHz, $CDCl_3$) δ: 7.40 (s, 2H), 5.19 (s, 4H), 3.50 (s, 6H); ^{13}C NMR (100 MHz, $CDCl_3$) δ: 147.22, 121.26, 116.78, 95.75, 56.56; HRMS (ESI+) Calc. for $C_{10}H_{12}O_4Br_2NH_4$ $[M+NH_4]^+$: 371.9441 Found: 371.9434.
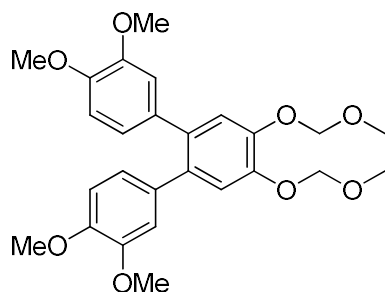
3,3'',4,4''-tetramethoxy-4',5'-bis(methoxymethoxy)-1,1':2',1''-terphenyl (2.13): To a 250 mL 3-neck round bottom flask was added **2.12** (2.40 g, 6.74 mmol, 1 eq), dimethoxyphenylboronic acid (3.68 g, 20.2 mmol, 3 eq), Na_2CO_3 (17.90 g, 169 mmol, 25 eq), dimethoxyethane (70 mL), and H_2O (90 mL). This was thoroughly sparged with N_2 before $Pd(PPh_3)_4$ (80 mg, 0.034 mmol, 1 mol%) was added and the reaction mixture further degassed for 5 min. This was heated to reflux for 24 h after which time the reaction was cooled, concentrated *in vacuo*, and the residue extracted with EtOAc, the combined organic layers were dried over $MgSO_4$, and evaporated via rotary evaporation to give an oily residue.

Addition of MeOH to this residue precipitated the product which was then collected via suction filtration to give the title compound as a powdery white solid (2.22 g, 70%). mp = 109-110 °C; ^{1}H NMR (400 MHz, CDCl$_3$) δ: 7.23 (s, 2H), 6.77 (d, J = 1 Hz, 4H), 6.57-6.56 (m, 2H), 5.29 (s, 4H), 3.85 (s, 6H), 3.58 (s, 6H), 3.55 (s, 6H); ^{13}C NMR (100 MHz, CDCl$_3$) δ: 148.37, 147.85, 146.52, 134.77, 134.13, 121.98, 119.03, 113.82, 111.01, 95.85, 56.45, 56.04, 55.83; HRMS (ESI+) Calc. for C$_{26}$H$_{30}$O$_8$NH$_4$ [M+NH$_4$]$^+$: 488.2276 Found: 488.2279.
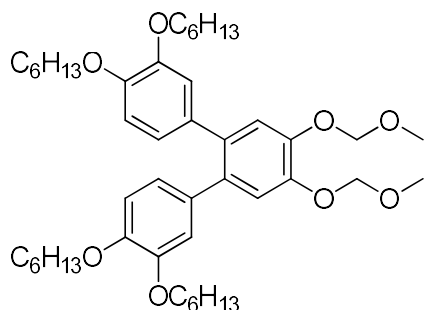
3,3'',4,4''-tetrakis(hexyloxy)-4',5'-bis(methoxymethoxy)-1,1':2',1''-terphenyl (2.16b): To a 100 mL 2-neck round-bottom flask, equipped with a condenser under N$_2$, was added **2.12** (737 mg, 2.07 mmol, 1 eq), 3,4-bis(hexyloxy)phenylboronic acid (2.00 g, 6.21 mol, 3 eq), sodium carbonate (5.44 g, 52.0 mmol, 25 eq) and previously degassed dimethoxyethane (20 mL) and H$_2$O (20 mL). This was further sparged with N$_2$ for 10 min before Pd(PPh$_3$)$_4$ (48 mg, 0.041 mmol, 2 mol%) was added and the reaction mixture heated to reflux. After 16 h the reaction mixture was cooled, brine (30 ml) was added and the aqueous layer extracted with diethyl ether (3 x 25 mL), washed with H$_2$O (1 x 20 mL), dried over MgSO$_4$, and concentrated *via* rotary evaporation to afford a brown oil. This oil was subjected to column chromatography (SiO$_2$, 10% EtOAc/Hexanes) to afford the product as a light yellow oil (1.160 g, 75%). R$_f$: 0.5 (50% EtOAc/Hexanes); ^{1}H NMR (300 MHz, CDCl$_3$) δ: 7.20 (s, 2H), 6.77-6.70 (m, 4H), 6.55 (d, J = 2 Hz), 5.28 (s, 4H), 3.94 (t, J = 7 Hz, 4H), 3.66 (t, J = 7 Hz, 4H), 3.55 (s, 6H), 1.83-1.74 (m, 4H), 1.68-1.61 (m, 4H), 1.48-1.26 (m, 24H), 0.92-0.83 (m, 12H); ^{13}C NMR (75 MHz, CDCl$_3$) δ :148.44, 147.89, 146.32, 134.84, 134.18, 122.02, 118.95, 116.21, 113.45, 95.78, 69.38, 69.19, 56.42, 31.78, 31.70, 29.44, 29.19, 25.86, 25.81, 22.78, 14.17; HRMS (ESI+) Calc. for C$_{46}$H$_{70}$O$_8$ [M+NH$_4$]$^+$: 768.5409 Found: 768.5428.
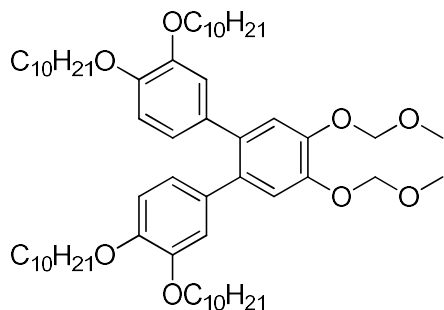
3,3'',4,4''-tetrakis(decyloxy)-4',5'-bis(methoxymethoxy)-1,1':2',1''-terphenyl (2.16a):

To a 100 mL 2-neck round-bottom flask, equipped with a condenser under N_2, was added **2.12** (546 mg, 1.53 mmol, 1 eq), 3,4-bis(decyloxy)phenylboronic acid (2.00 g, 4.60 mmol, 3 eq), sodium carbonate (4.02 g, 38.4 mmol, 25 eq) and previously degassed dimethoxyethane (20 mL) and H_2O (20 mL). This was further sparged with N_2 for 10 min before $Pd(PPh_3)_4$ (40 mg, 0.0306 mmol, 2 mol%) was added and the reaction mixture heated to reflux. After 18 h the reaction mixture was cooled, brine (30 ml) was added and the aqueous layer extracted with diethyl ether (3 x 30 mL), washed with H_2O (1 x 20 mL), dried over $MgSO_4$, and concentrated *via* rotary evaporation to afford a brownish oil. Methanol (~10 mL) was then added and the mixture cooled to effect precipitation of the product which was then collected *via* suction filtration to afford the title compound as an off-white crystalline solid (1.186 g, 79%). mp = 40-42 °C; ^{1}H NMR (400 MHz, CDCl3) δ: 7.20 (s, 2H), 6.76-6.70 (m, 4H), 6.55 (d, *J* = 2 Hz, 2H), 5.28 (s, 4H) 3.95-3.92 (t, *J* = 7 Hz, 4H), 3.67-3.64 (t, *J* = 7 Hz, 4H), 3.54 (s, 6H), 1.82-1.75 (m, 4H), 1.67-1.60 (m, 4H), 1.48-1.40 (m, 4H), 1.36-1.27 (m, 52 H), 0.90-0.85 (m, 12 H); ^{13}C NMR (75 MHz, CDCl3) δ: 148.45, 147.91, 146.33, 134.85, 134.19, 122.03, 118.94, 116.25, 113.48, 95.79, 69.42, 69.22, 56.44, 32.10, 29.88, 29.81, 29.80, 29.77, 29.65, 29.60, 29.56, 29.52, 29.26, 26.22, 22.86, 14.28; HRMS (ESI+) Calc. for $C_{62}H_{102}O_8NH_4$ $[M+NH_4]^+$: 992.7913 Found: 992.7947.
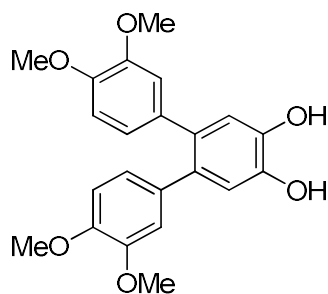
3,3'',4,4''-tetramethoxy-[1,1':2',1''-terphenyl]-4',5'-diol (2.14): To a 100 mL round bottom flask was added **2.13** (911 mg, 1.94 mmol, 1 eq), isopropanol (40 mL), and carbon tetrabromide (128 mg, 0.387 mmol, 0.2 eq). The flask was equipped with a condenser and heating mantle, and the reaction mixture was refluxed for 1 h then stirred at rt for a further 10 h. H_2O (25 mL) was then added and the volume reduced *via* rotary evaporation. The aqueous residue was extracted with EtOAc (3 x 30 mL) and the combined organic layers washed with brine (10 mL), dried over $MgSO_4$, and concentrated *in vacuo* to give the product as a white, powdery solid (830 mg, 99%). mp = 190-192 °C; ^{1}H NMR (400 MHz, CDCl$_3$) δ: 6.91 (s, 2H), 6.75-6.67 (m, 4H), 6.56 (d, J = 2 Hz, 2H), 5.63 (s, 2H), 3.84 (s, 6H), 3.58 (s, 6H); ^{13}C NMR (100 MHz, CDCl$_3$) δ: 148.24, 147.58, 142.88, 134.23, 133.28, 122.02, 117.36, 113.79, 111.04, 56.04, 55.82; HRMS (ESI+) Calc. for $C_{22}H_{22}O_6NH_4$ [M+NH$_4$]: 400.1755 Found: 400.1741.
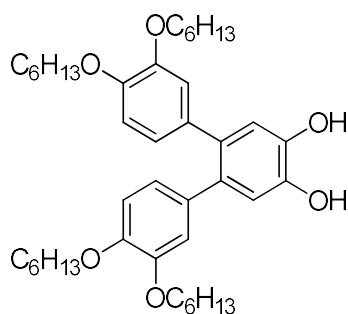
3,3'',4,4''-tetrakis(hexyloxy)-[1,1':2',1''-terphenyl]-4',5'-diol (2.17b): To a 50 mL round bottom flask was added **2.16b** (384 mg, 0.511 mmol, 1 eq), isopropanol (30 mL), and carbon tetrabromide (34 mg, 0.102 mmol, 0.2 eq). The flask was equipped with a condenser and heating mantle, and the reaction mixture was refluxed for 24 h. The mixture was then diluted

with brine and extracted CHCl$_3$ (4 x 15 mL) and the combined organic layers washed with H$_2$O (10 mL), dried over MgSO$_4$, filtered, and concentrated *in vacuo* to give a light brown oil. The crude product was purified by flash column chromatography (SiO$_2$, 1% MeOH/CH$_2$Cl$_2$) to yield the diol as a brown oil (294 mg, 83%). R$_f$ (CH$_2$Cl$_2$) = 0.25; ^{1}H NMR (300 MHz, CDCl$_3$) δ: 6.80 (s, 2H), 6.72 (d, *J* = 8 Hz, 2H), 6.61 (dd, *J* = 8, 2 Hz, 2H), 6.53 (d, *J* = 2 Hz, 2H), 5.57 (s, 2H), 3.95-3.91 (t, *J* = 7 Hz, 4H), 3.68-3.64 (t, *J* = 7 Hz, 4H), 1.83-1.74 (m, 4H), 1.68-1.60 (m, 4H), 1.50-1.28 (m, 24H), 0.92-0.87 (m, 12H); ^{13}C NMR (75 MHz, CDCl$_3$) δ: 148.30, 147.49, 142.73, 134.43, 133.26, 122.11, 117.29, 116.01, 113.52, 69.55, 69.20, 31.78, 31.70, 29.42, 29.17, 25.85, 22.77, 14.18; HRMS (ESI+) Calc. for C$_{42}$H$_{62}$O$_6$NH$_4$ [M+NH$_4$]$^+$: 680.4885 Found: 680.4880.
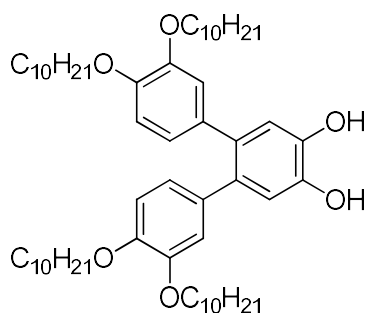
3,3'',4,4''-tetrakis(decyloxy)-[1,1':2',1''-terphenyl]-4',5'-diol (2.17a): To a 50 mL round bottom flask was added **2.16a** (300 mg, 0.308 mmol, 1 eq), isopropanol (20 mL), and carbon tetrabromide (11 mg, 0.031 mmol, 0.1 eq). The flask was equipped with a condenser and heating mantle, and the reaction mixture was refluxed for 2 h then stirred at rt for a further 10 h. H$_2$O (20 mL) was then added and the volume reduced *via* rotary evaporation. The aqueous residue was extracted with CHCl$_3$ (2 x 10 mL) and the combined organic layers washed with H$_2$O (10 mL), dried over Na$_2$SO$_4$, and concentrated *in vacuo* to give a light brown oil. Methanol was added, and the mixture cooled to effect crystallisation of the product, collected as a white, powdery solid (244 mg, 89%). mp = 56-58 °C; ^{1}H NMR (400 MHz, CDCl$_3$) δ: 6.82 (s, 2H), 6.71 (d, *J* = 8 Hz, 2H), 6.62 (dd, *J* = 8, 2 Hz, 2H), 6.53 (d, *J* = 2 Hz, 2H), 5.49 (s, 2H), 3.92 (t, *J* = 7 Hz, 4H), 3.66 (t, *J* = 7 Hz, 4H), 1.83-1.74 (m, 4H), 1.68-1.58 (m, 4H), 1.47-1.27 (m, 56H), 0.88 (m, 12H); ^{13}C NMR (100 MHz, CDCl$_3$) δ: 148.34, 147.54, 142.71, 134.43,

133.30, 122.11, 117.30, 116.09, 113.58, 69.58, 69.24, 32.10, 29.87, 29.81, 29.65, 29.57, 29.25, 26.21, 22.86, 14.28; HRMS (ESI+) Calc for $C_{58}H_{94}O_6NH_4$ [M+NH_4]^+: 904.7389 Found: 904.7391.
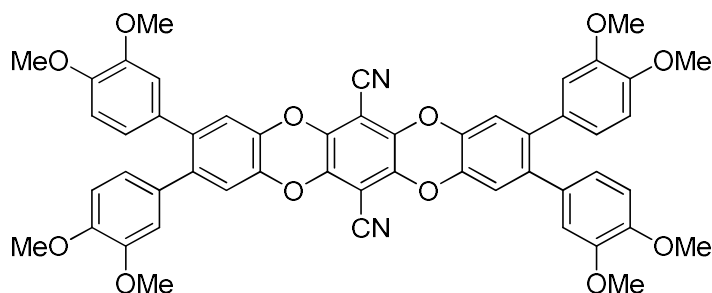
2,3,9,10-tetrakis(3,4-dimethoxyphenyl)benzo[5,6][1,4]dioxino[2,3-b]dibenzo-[b,e][1,4]dioxine-6,13-dicarbonitrile (2.1c): To a 10 mL 2-neck round bottom flask was added terphenyl diol **2.14** (636 mg, 1.66 mmol, 2.0 eq), tetrafluoroterephthalonitrile (166 mg, 0.832 mmol, 1.0 eq), and K_2CO_3 (2.29 g, 16.6 mmol, 10 eq). The flask was placed under an atmosphere of N_2 and dry DMF (10 mL) was added forming a yellow suspension which was then heated to 65 °C. After 14 h the reaction was cooled and diluted with 10 volumes of H_2O and the aqueous mixture extracted with $CHCl_3$ (4 x 20 mL), washed with 5% aqueous LiCl (2 x 15 mL), dried over Na_2SO_4, and the solvent removed *in vacuo*. The yellow residue was recrystallized from 1:1 *i*PrOH/CHCl_3 to give the product as a bright yellow solid (603 mg, 82%). mp = >260 °C; ^1H NMR (400 MHz, CDCl_3) δ: 7.10 (s, 4H), 6.78-6.70 (m, 8H), 6.56 (s, 4H), 3.86 (s, 12H), 3.63 (s, 12H); ^13C NMR (100 MHz, CDCl_3) δ: 148.61, 148.42, 139.44, 138.53, 138.14, 132.30, 121.93, 118.60, 113.19, 111.06, 109.44, 94.75, 56.04, 55.90; HRMS (ESI+) Calc. for $C_{52}H_{40}N_2O_{12}NH_4$ [M+NH_4]^+: 902.2920 Found: 902.2922.
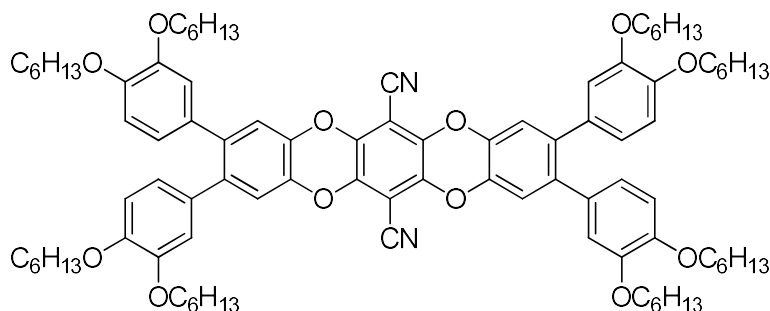
2,3,9,10-tetrakis(3,4-bis(hexyloxy)phenyl)benzo[5,6][1,4]dioxino[2,3-b]dibenzo[b,e][1,4]-dioxine-6,13-dicarbonitrile (2.1b): To a 5 ml 2-neck round bottom flask was added terphenyl diol **6b** (230 mg, 0.331 mmol, 2 eq), tetrafluoroterephthalonitrile (33 mg, 0.165 mmol, 1 eq), K_2CO_3 (182 mg, 1.32 mmol, 8 eq), and DMF (5 mL). This was heated to 65 °C under N_2 for 3 h after which time H_2O (40 mL) was added and the mixture extracted with $CHCl_3$ (4 x 15 mL), washed with 1 M HCl (1 x 10 mL), aqueous 5% LiCl (1 x 10 mL), dried over Na_2SO_4, and concentrated *in vacuo*. The residue was triturated with cold MeOH and the product collected *via* suction filtration as a yellow, powdery solid (230 mg, 96%). ^{1}H NMR (300 MHz, $CDCl_3$) δ: 7.07 (s, 4H), 6.76-6.64 (m, 8H), 6.56 (d, J = 2 Hz, 4H), 3.95 (t, J = 7 Hz, 8H), 3.71 (t, J = 7 Hz, 8H), 1.84-1.75 (m, 8H), 1.70-1.63 (m, 8H), 1.49-1.32 (m, 48H), 0.93-0.88 (m, 24H); ^{13}C NMR (75 MHz, $CDCl_3$) δ: 148.66, 148.47, 139.43, 138.40, 138.21, 132.36, 121.96, 118.57, 115.53, 113.33, 109.51, 94.69, 69.30, 69.27, 31.78, 31.70, 29.41, 29.22, 25.86, 25.82, 22.79, 22.77, 14.18; HRMS (ESI+) Calc. for $C_{92}H_{120}N_2O_{12}NH_4$ $[M+NH_4]^+$: 1462.9180 Found: 1462.9192.
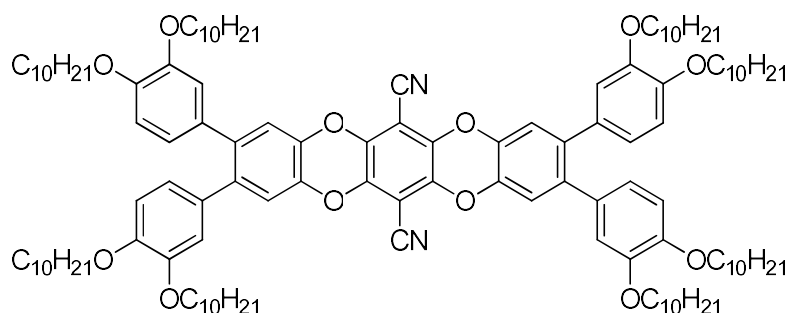
2,3,9,10-tetrakis(3,4-bis(decyloxy)phenyl)benzo[5,6][1,4]dioxino[2,3-b]dibenzo[b,e][1,4]-dioxine-6,13-dicarbonitrile (2.1a): To a 5 ml 2-neck round bottom flask was added terphenyl diol **6c** (130 mg, 0.147 mmol, 2 eq), tetrafluoroterephthalonitrile (15 mg, 0.073 mmol, 1 eq), K_2CO_3 (81 mg, 0.588 mmol, 8 eq), and DMF (5 mL). This was heated to 65 °C under N_2 for 3 h after which time H_2O (10 mL) was added to effect precipitation of a yellow solid. The suspension was cooled and filtered, and the solids washed first with H_2O then methanol to afford the title compound as a bright yellow, powdery solid (137 mg, 100%). ^1H NMR (300 MHz, $CDCl_3$) δ: 7.07 (s, 4H), 6.76-6.64 (m, 8H), 6.56 (s, 4H), 3.94 (t, J = 7 Hz, 8H), 3.70 (t, J = 7 Hz, 8H), 1.82-1.77 (m, 8H), 1.69-1.64 (m, 8H), 1.40-1.28 (br m, 112H), 0.88 (m, 24H); ^{13}C NMR (75 MHz, $CDCl_3$) δ: 148.66, 148.48, 139.44, 138.41, 138.22, 132.37, 121.95, 118.56, 115.58, 113.37, 109.51, 94.69, 69.31, 32.10, 29.87, 29.81, 29.79, 29.76, 29.64, 29.59, 29.57, 29.52, 29.47, 29.29, 26.21, 22.86, 14.28; HRMS (TOF-ASAP+) Calc. for $C_{142}H_{184}N_2O_{12}$ [M+]: 1893.3849 Found: 1893.3793.
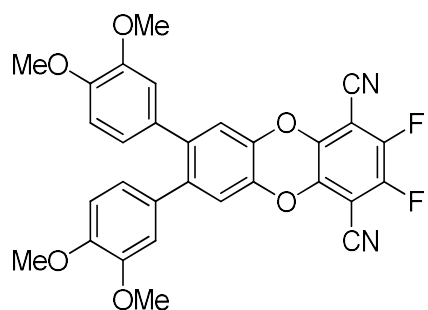
7,8-bis(3,4-dimethoxyphenyl)-2,3-difluorodibenzo[b,e][1,4]dioxine-1,4-dicarbonitrile (2.18): To a 2-neck 25 mL round-bottomed flask, equipped with a condenser under N_2 was added terphenyl catechol **2.14** (283 mg, 0.740 mmol, 1.0 eq), THF (10 mL),

127

K$_2$CO$_3$ (306 mg, 2.22 mmol, 3.0 eq), and finally tetrafluoroterephthalonitrile (148 mg, 0.740 mmol, 1.0 eq). The mixture was heated to reflux; after 6 h the mixture was cooled, H$_2$O (25 mL) was added, and the mixture extracted with CHCl$_3$ (3 x 15 mL). The organic extract was dried over Na$_2$SO$_4$, filtered, and concentrated *via* rotary evaporation to give the product as a bright yellow solid (355 mg, 89%). mp = 218-219 °C; ^{1}H NMR (400 MHz, CDCl$_3$) δ: 7.13 (s, 2H), 6.78-6.69 (m, 4H), 6.54 (s, 2H), 3.86 (s, 6H), 3.63 (s, 6H); ^{13}C NMR (100 MHz, CDCl$_3$) δ: 148.47, 148.36, 145.71 (dd, *J* = 262, 16 Hz), 141.04 (t, *J* = 4 Hz), 138.56, 137.75, 131.80, 121.72, 118.48, 112.89, 110.87, 107.66, 96.74 (dd, *J* = 12, 7 Hz), 55.86, 55.72; ^{19}F NMR (375 MHz, CDCl$_3$) δ: -134.55 (s); HRMS (ESI+) Calc. for C$_{30}$H$_{20}$F$_2$N$_2$O$_6$ [M+NH$_4$]$^+$: 560.1628 Found: 560.1616.
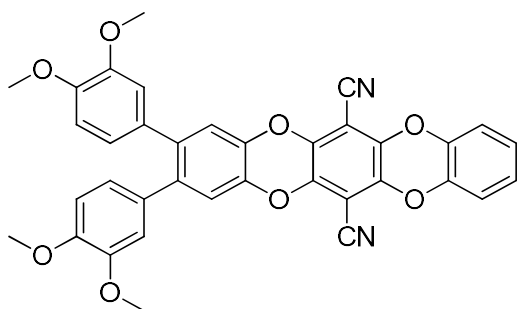
2,3-bis(3,4-dimethoxyphenyl)benzo[5,6][1,4]dioxino[2,3-]dibenzo[b,e][1,4]dioxine-6,13-dicarbonitrile (2.19): To a 25 mL round-bottomed flask was added terphenyl difluorodibenzodioxin **2.18** (0.283 g, 0.522 mmol, 1.0 eq), DMF (5 mL), and K$_2$CO$_3$ (0.290 g, 2.09 mmol, 4.0 eq). The flask was placed under N$_2$ and catechol (0.058 g, 0.52 mmol, 1.0 eq) was added in one portion and the reaction mixture heated to 100 °C for 16 h. After this time the mixture was allowed to cool to rt and subsequently poured into H$_2$O (40 mL). The product was then collected *via* suction filtration, washing with water, then cold MeOH to give a yellow powdery solid (0.252 g, 79%). mp = >260 °C; ^{1}H NMR (400 MHz, CDCl$_3$) δ: 7.09 (s, 2H), 7.07-7.01 (m, 4H), 6.78-6.71 (m, 4H), 6.56 (s, 2H), 3.86 (s, 6H), 3.63 (s, 6H); ^{13}C NMR (100 MHz, CDCl$_3$) δ: 148.44, 148.24, 139.76, 139.39, 139.22, 138.41, 137.96, 132.17, 125.90, 121.78, 118.45, 117.01, 112.99, 110.88, 109.29, 94.53, 55.88, 55.74; HRMS (ESI+) Calc for C$_{36}$H$_{24}$N$_2$O$_8$ [M+Na]$^+$: 635.1425 Found: 635.1420.
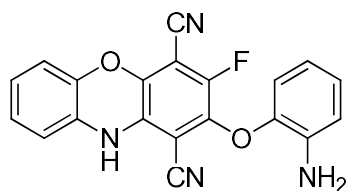
2-(2-aminophenoxy)-3-fluoro-10H-phenoxazine-1,4-dicarbonitrile (3.22): To a 50 mL round-bottomed flask, under N_2, was added tetrafluoroterephthalonitrile (600 mg, 3.00 mmol, 1.0 eq), 2-aminophenol (654 mg, 6.00 mmol, 2.0 eq), dry DMF (20 mL), and finally K_2CO_3 (3.32 g, 24.0 mmol, 8.0 eq). The mixture was heated to 65 °C and quickly became a deep purple colour; this was left to stir 20 h. The reaction mixture was cooled to rt, then H_2O was then added effecting precipitation of a reddish-brown solid, collected *via* suction filtration, and triturated with acetonitrile yielding a mixture of products (400 mg) from which a single crystal (DMF) subjected to X-ray diffraction identified that component as the title compound. IR(ATR) ν_{max} = 3445, 3360, 3279, 2250, 2236, 1626, 1570, 1499, 1466, 1383, 1287, 1196, 1173, 1033, 996, 749, 731 cm^{-1}; HRMS (ESI+) Calc. for $C_{20}H_{11}FN_4O_2$ [M+H]$^+$: 359.0939 Found: 359.0949.
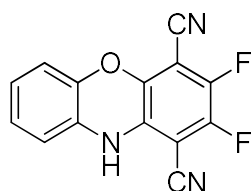
2,3-difluoro-10H-phenoxazine-1,4-dicarbonitrile (3.23): To a 250 mL round-bottomed flask was added 2-aminophenol (1.429 g, 13.1 mmol, 1.0 eq), tetrafluoroterephthalonitrile (2.62 g, 13.1 mmol, 1.0 eq), and DMSO (65 mL). This was equipped with a drying tube (CaSO$_4$) and stirred at rt for 18 h, by which time a bright orange solid had precipitated. H_2O (200 mL) was added to effect full precipitation and the product was collected *via* suction filtration (3.500 g, 100%). This powdery solid could be recrystallised from hot DMF to afford long orange needles. MP > 260 °C. ^{1}H NMR (400 MHz, DMSO-d_6) δ: 9.58 (s, 1H), 6.90 (s, 2H), 6.81 (s, 2H); ^{13}C NMR (100 MHz, acetone-d_6) δ: 147.54, 147.35, 144.66, 144.61, 144.56, 144.22, 144.07, 144.04, 143.88, 142.27 140.78, 140.59, 135.46, 135.42, 135.38, 128.74, 126.74,

124.72, 116.66, 116.27, 110.52, 110.48, 109.52, 109.47, 95.73, 95.48, 89.83, 89.85; ^{19}F NMR (282 MHz, acetone-d_6) δ: −142.3 (d, J = 20 Hz), −148.16 (d, J = 20 Hz); IR (ATR) ν_{max}: 3157 (w), 3113 (w), 3063 (w), 2951, 2898, 2239, 2230, 1470, 1288, 1023, 993, 759 cm^{-1}; HRMS (APCI+) Calc. for $C_{14}H_5N_3OF_2$ [M]$^+$: 269.0401 Found: 269.0391.
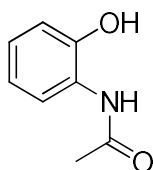
N-(2-hydroxyphenyl)acetamide (3.26): To a 500 mL round bottomed flask was added 2-aminophenol (5.00 g, 45.8 mmol, 1.0 eq), EtOAc (100 mL), followed by acetic anhydride (4.70 mL, 50.4 mmol, 1.1 eq). This was stirred at room temperature for 4 h, diethyl ether (100 mL) was added and the mixture cooled to ~5 °C. The precipitate was collected as a grey powder *via* suction filtration, washing with diethyl ether. The crude product was recrystallized from aqueous ethanol as off-white plates (6.11 g, 89%). mp = 208-209 °C (lit. mp = 209 °C); ^{1}H NMR (400 MHz, DMSO-$d6$) δ: 9.72 (s, 1H), 9.29 (s, 1H), 7.66 (d, J = 8 Hz, 1H), 6.93 (t, J = 8 Hz, 1H), 6.84 (d, J = 8 Hz, 1H), 6.75 (t, J = 8 Hz, 1H), 2.10 (s, 3H); ^{13}C NMR (100 MHz, MeOD) δ: 172.21, 149.73, 127.08, 126.81, 123.96, 120.60, 117.28, 23.43. Analytical data agrees with literature values published by Sivaguru, *et al.*[118]
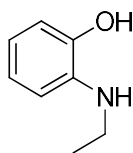
2-(N-ethylamino)phenol (3.27): To a dry, 250 mL three-neck round bottomed flask, equipped with a dried stir bar, condenser, and N$_2$ inlet, was added N-(2-hydroxyphenyl)acetamide **3.26** (1.50 g, 9.92 mmol, 1.0 eq) and THF (75 mL). This was then cooled to 0 °C, and lithium aluminum hydride (1.0 M in THF, 19.8 mL, 2.0 eq) was added dropwise, pausing as appropriate for hydrogen evolution. The ice bath was then replaced

with an oil bath and the reaction mixture heated to reflux. After 12 h, the reaction was cooled to 0 °C and sodium sulfate decahydrate ($Na_2SO_4·10H_2O$) was added in *small* portions, over approximately 25 min, until hydrogen evolution subsided. Aqueous ammonium chloride was then added until neutral, and the emulsion thus obtained filtered through a pad of Celite®, washing the filter cake with diethyl ether. The volatiles were then removed *in vacuo*, the residue partitioned between ether and H_2O, and the aqueous layer extracted with ether (3 x 20 mL). The pooled organic extracts were washed with saturated aqueous $NaHCO_3$ (20 mL), brine (20 mL), dried over $MgSO_4$, filtered, and concentrated *in vacuo*. The residue was recrystallized from chloroform to give the product as white needles (1.10 g, 81%), stored at −20 °C to slow decomposition. ^{1}H NMR (400 MHz, $CDCl_3$) δ: 6.87-6.83 (m, 1H), 6.70-6.60 (m, 3H), 4.12 (br s, 2H), 3.16-3.14 (m, 2H), 1.27 (t, *J* = 7 Hz, 3H); ^{13}C NMR (100 MHz, $CDCl_3$) δ: 143.77, 137.12, 121.63, 117.83, 114.30, 112.72, 38.96, 14.87. Analytical data agrees with literature values published by Neogi, *et al.*[119]
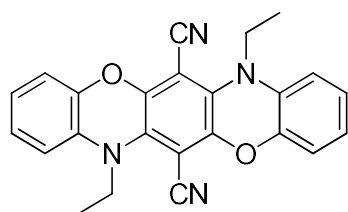
7,14-diethyl-7,14-dihydrobenzo[5,6][1,4]oxazino[2,3-b]phenoxazine-6,13-dicarbonitrile (3.28): To a 25 mL round bottomed flask, under N_2, was added 2-(*N*-ethylamino)phenol **3.27** (120 mg, 0.875 mmol, 2.0 eq), tetrafluoroterephthalonitrile (88 mg, 0.437, 1.0 eq), DMF (5 mL), and finally K_2CO_3 (726 mg, 5.25 mmol, 6.0 eq). This was stirred and heated to 100 °C for 24 h, after which time the mixture was cooled to rt and poured into H_2O (75 mL). After cooling overnight, the precipitate was collected as a red solid which was recrystallized from chloroform-methanol (172 mg, 100%). mp > 260 °C; R_f (50% EtOAc/Hexanes) = 0.33; ^{1}H NMR (400 MHz, $CDCl_3$) δ: 7.03-6.84 (m, 8H), 3.94 (t, *J* = 7 Hz, 4H), 1.28 (t, *J* = 7 Hz, 6H); ^{13}C NMR (100 MHz, $CDCl_3$) δ: 147.87, 147.44, 132.57, 131.46, 125.26, 124.36, 118.85, 116.39, 112.85, 94.89, 48.56, 13.06; HRMS (ESI+) Calc. for $C_{24}H_{18}N_4O_2$ [M+H]$^+$: 395.1503 Found: 395.1505.
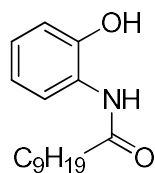
N-(2-hydroxyphenyl)decanamide (3.29): To a 250 mL round bottomed flask was added 2-aminophenol (2.500 g, 22.9 mmol, 1.0 eq), THF (100 mL), pyridine (4.1 mL, 50.4 mmol). This was stirred until dissolution, and decanoyl chloride (4.8 mL, 22.9 mmol, 1.0 eq) was added dropwise causing a precipitate which dissolved by the end of addition. This was left to stir under N_2 overnight (18 h). Volatiles were removed *in vacuo*, and the residue was partitioned between chloroform and water. The aqueous layer was extracted with chloroform (2 x 25 mL) and the pooled organic solvents washed with 1 M HCl (25 mL), H_2O (25 mL), dried over $MgSO_4$, filtered, and concentrated *in vacuo*. The crude solid thus obtained was recrystallized from aqueous methanol to yield *N*-(2-hydroxyphenyl)decanamide as a white fluffy solid (4.39 g, 73%). mp = 67-68 °C (lit. 71 °C)[120]; ^{1}H NMR (400 MHz, $CDCl_3$) δ: 8.96 (s, 1H), 7.92 (s, 1H), 7.14-7.06 (m, 2H), 6.97 (d, *J* = 8 Hz, 1H), 6.84 (t, *J* = 8 Hz, 1H), 2.42 (t, *J* = 8 Hz, 2H), 1.75-1.68 (m, 2H), 1.35-1.24 (m, 14H), 0.87 (t, *J* = 7 Hz, 3H); ^{13}C NMR (100 MHz, $CDCl_3$) δ: 173.72, 148.63, 127.05, 125.62, 122.05, 120.38, 119.70, 37.01, 31.82, 29.38, 29.28, 29.22, 29.12, 25.76, 22.63, 14.08.
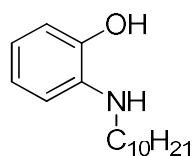
2-(*N*-decylamino)phenol (3.30): To a 250 mL two-neck round-bottomed flask, equipped with a reflux condenser under N_2 and equipped with an addition funnel, was added lithium aluminum hydride (0.915 g, 24.1 mmol, 2.0 eq) and THF (60 mL), and this was cooled to 0 °C. A solution of *N*-(2-hydroxyphenyl)decanamide **3.29** (3.171 g, 12.0 mmol, 1.0 eq) in THF (35 mL) was then placed in the addition funnel and added dropwise to the cold reaction flask over 15 minutes. The ice bath was then removed, and the mixture gradually brought to reflux for 12 h, after which time the mixture was cooled to 0 °C and quenched *via* cautious addition

of $Na_2SO_4 \cdot 10H_2O$ in small portions. The mixture was then brought to neutral pH with saturated NH_4Cl (pH paper), filtered through Celite®, and concentrated *in vacuo.* The residue was dissolved in EtOAc (50 mL), washed with saturated $NaHCO_3$ (20 mL), H_2O (20 mL), and brine (40 ml). The organic layer was dried over Na_2SO_4, filtered, and concentrated *in vacuo* to give the aminophenol as a purple solid, which was used for the following reactions without further purification (2.40 g, 80%). ^{1}H NMR (400 MHz, CDCl$_3$) δ: 6.90-6.84 (m, 1H), 6.72-6.62 (m, 3H), 4.46 (br s, 2H), 3.13-3.10 (m, 2H), 1.68-1.61 (m, 2H), 1.45-1.29 (m, 14H), 0.90 (t, $J =$ 7 Hz, 3H); ^{13}C NMR (100 MHz, CDCl$_3$) δ: 143.73, 137.28, 121.58, 117.67, 114.36, 112.59, 44.53, 31.90, 29.60, 29.58, 29.47, 29.32, 27.20, 22.68, 14.11.
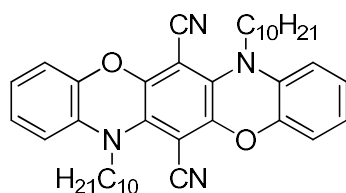
7,14-didecyl-7,14-dihydrobenzo[5,6][1,4]oxazino[2,3-b]phenoxazine-6,13-dicarbonitrile (3.31): To a 50 mL round-bottomed flask was added tetrafluoroterephthalonitrile (225 mg, 1.12 mmol, 1.0 eq), K_2CO_3 (1.24 g, 8.96 mmol, 8.0 eq), and DMF (20 mL). This was placed under N_2 and 2-(*N*-decylamino)phenol **3.30** (560 mg, 2.25 mmol, 2.0 eq) was added in portions. The mixture was heated to 100 °C. After 24 h, the mixture was cooled, poured into H_2O (125 mL), and the red solid collected *via* suction filtration, washing with H_2O. This was then recrystallised from toluene-methanol to yield the product as a red, microcrystalline solid (583 mg, 84%). mp = 145-146 °C; ^{1}H NMR (400 MHz, CDCl$_3$) δ: 7.03-6.99 (m, 2H), 6.94-6.89 (m, 4H), 6.83 (d, $J =$ 8 Hz, 2H), 3.88 (t, $J =$ 8 Hz, 4H), 1.70-1.62 (m, 4H), 1.33-1.21 (m, 28), 0.86 (t, $J =$ 7 Hz, 6H); ^{13}C NMR (100 MHz, CDCl$_3$) δ: 147.79, 147.40, 133.16, 131.83, 125.21, 124.14, 118.64, 116.44, 112.92, 94.73, 53.16, 31.86, 29.47, 29.45, 29.26, 29.19, 27.43, 26.29, 22.66, 14.11.
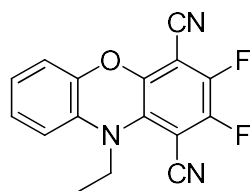
10-ethyl-2,3-difluoro-10H-phenoxazine-1,4-dicarbonitrile (3.32): To a 25 mL pear-shaped flask was added tetrafluoroterephthalonitrile (559 mg, 2.79 mmol, 1.0 eq), followed by DMSO. This was warmed to dissolution (50 °C) and 2-(ethylamino)phenol **3.27** (383 mg, 2.79 mmol, 1.0 eq) was added in portions. This was stirred at room temperature for 24 h, after which time H_2O (60 mL) was added and the solid collected *via* suction filtration, washing with water. The powder thus obtained was recrystallised from acetonitrile to furnish the product as long, orange needles (665 mg, 80%). mp = 223-225 °C; ^{1}H NMR (400 MHz, CDCl$_3$) δ: 7.05 (t, J = 8 Hz, 1H), 6.96 (t, J = 8 Hz, 1H), 6.91-6.89 (m, 1H), 6.85-6.83 (m, 1H), 4.04 (q, J = 7 Hz, 2H), 1.38 (t, J = 7 Hz, 3H); ^{13}C NMR (100 MHz, CDCl$_3$) δ: 147.88 (t, J = 3.3 Hz), 146.44 (dd, J = 255, 14 Hz), 145.51, 143.03 (dd, J = 256, 15 Hz), 135.80 (dd, J = 3, 1 Hz), 131.09, 126.11, 125.08, 117.07, 116.65, 111.20 (d, J = 4 Hz), 108.7 (d, J = 4 Hz), 95.76 (dd, J = 17, 3.0 Hz), 93.57 (d, J = 17 Hz), 46.60, 13.77; ^{19}F NMR (376 MHz, CDCl$_3$) δ: -135.43 (d, J = 21 Hz), -140.55 (d, J = 21 Hz); HRMS (ESI+) Calc. for $C_{16}H_9F_2N_3O$ [M+H]$^+$: 298.0786 Found: 298.0791.
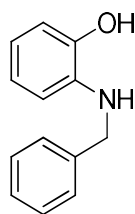
2-(benzylamino)phenol (3.35): To a 250 mL round-bottomed flask was added 2-aminophenol (5.00 g, 45.8 mmol, 1.0 eq), dry THF (50 mL), and MgSO$_4$ (16 g). This was placed under N$_2$, and freshly distilled benzaldehyde (4.6 mL) was added via syringe. After 12 h, the mixture was filtered and concentrated *in vacuo* to give the crude imine (10.7 g) as a yellow-brown solid. The crude imine (45.8 mmol, 1.0 eq) was then placed in a 250 mL round-

bottomed flask with MeOH (200 mL) and this was cooled to 0 °C (ice bath). NaBH$_4$ (2.08 g, 55.0 mmol, 1.2 eq) was added in small portions over 10 min. After the addition was complete the reaction mixture was concentrated *in vacuo* and the residue partitioned between EtOAc and H$_2$O, washing the organic layer with H$_2$O, then brine. The organic layer was dried over MgSO$_4$, filtered, and concentrated to give an unstable green oil which decomposed over several weeks. ^{1}H NMR (400 MHz, CDCl$_3$) δ: 7.45-7.30 (m, 5H), 6.86 (t, *J* = 7 Hz, 1H), 6.78-6.63 (m, 3H), 4.39 (s, 2H). ^{1}H NMR data agrees with that reported by Ohsawa, *et al.*[121]
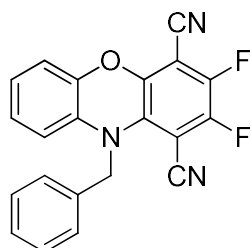
10-benzyl-2,3-difluoro-10H-phenoxazine-1,4-dicarbonitrile (3.38): To a 50 mL round-bottomed flask was added 2-(*N*-benzylamino)phenol **3.35** (750 mg, 3.76 mmol, 1.0 eq), TFTP (753 mg, 3.76 mmol, 1.0 eq), K$_2$CO$_3$ (2.08 g, 15.0 mmol, 4.0 eq) and DMF (20 mL). This was placed under N$_2$ and heated to 70 °C for 24 h. The reaction mixture was cooled to room temperature, poured into H$_2$O and the precipitate collected *via* suction filtration, washing with H$_2$O. The crude solid was subjected to column chromatography (SiO$_2$, 30% EtOAc/hexanes) to afford the product as a yellow solid (300 mg, 22%). ^{1}H NMR (400 MHz, Acetone-*d$_6$*) δ: 7.37-7.26 (m, 5H), 7.00-6.92 (m 4H), 5.30 (s, 2H); ^{13}C NMR (100 MHz, Acetone-*d$_6$*) δ: 147.92 (t, *J* = 3 Hz), 146.35 (dd, *J* = 251, 14 Hz), 145.41, 143.20 (dd, *J* = 251, 15 Hz), 136.4-136.5 (m), 136.03, 131.64, 128.71, 127.78, 127.05, 125,76, 124.84, 118.10, 115.82, 110.81 (d, *J* = 4 Hz), 108.53 (d, *J* = 4 Hz), 55.45; ^{19}F NMR (376 MHz, Acetone-*d$_6$*) δ: -139.14 (d, *J* = 20 Hz), -143.91 (d, *J* = 21 Hz).
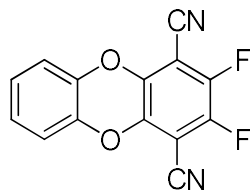
2,3-difluorodibenzo[b,e][1,4]dioxine-1,4-dicarbonitrile (3.16): To a 250 mL single neck round-bottomed flask was added catechol (2.00 g, 18.2 mmol, 1 eq), tetrafluoroterephthalonitrile (3.64 g, 18.2 mmol, 1 eq), and potassium carbonate (7.53 g, 54.5 mmol, 3 eq) followed by dry THF (150 mL). The flask was equipped with a condenser under N_2 and the mixture was heated to reflux with stirring for 2 h, then stirred at rt for 8 h. After this time H_2O (150 mL) was added to effect crystallization of the product and the mixture was cooled to ~5 °C. The yellow suspension was suction filtered, washed three times with H_2O and dried to give the product as a yellow powdery solid which was recrystallised from DME to give the product as very light-yellow plates (3.62 g, 74%). mp = 209-210 °C; ^{1}H NMR (400 MHz, CDCl$_3$) δ: 7.09-7.02 (m, 4H); ^{13}C NMR (75 MHz, CDCl$_3$) δ: 145.73 (dd, J = 261, 16 Hz), 141.46 (t, J = 4 Hz), 139.34, 126.49, 117.13, 107.7 (d, J = 2 Hz), 96.71 (dd, J = 11, 8 Hz); ^{19}F NMR (376 MHz, CDCl$_3$) δ: -134.75. Analytical data agrees with literature values published by Banerjee, *et al.*[80]
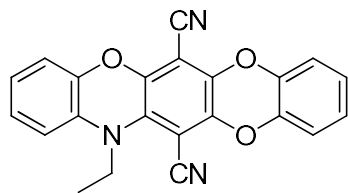
14-ethyl-14H-benzo[5,6][1,4]dioxino[2,3-b]phenoxazine-6,13-dicarbonitrile (3.51): To a 50 mL round-bottomed flask was added difluoride **3.16** (905 mg, 3.35 mmol, 1.0 eq) and DMF (15 mL) under N_2. K_2CO_3 (1.85 g, 13.4 mmol, 4.0 eq) was then added, followed by 2-(ethylamino)phenol **3.27** (459 mg, 3.35 mmol, 1.0 eq). This was heated to 100 °C for 24 h, after which time the orange mixture was cooled, poured into H_2O, and then filtered. The collected precipitate was recrystallised from toluene-methanol to yield the title compound as an orange crystalline solid (851 mg, 70%). mp = 241 °C (dec.); R$_f$ = 0.38 (50%

CHCl₃/hexanes); ^{1}H NMR (400 MHz, CDCl₃) δ: 7.04-6.84 (m, 8H), 3.96 (q, J = 7 Hz, 2H), 1.29 (t, J = 7 Hz, 3H); ^{13}C NMR (100 MHz, CDCl₃) δ: 146.97, 146.74, 140.15, 140.03, 139.68, 137.14, 133.62, 132.05, 125.80, 125.49, 125.46, 124.55, 118.43, 116.96, 116.91, 116.83, 116.37, 112.18, 109.94, 48.21, 13.19; HRMS (ESI+) Calc. for C₂₂H₁₃N₃O₃ [M+H]: 368.1030 Found: 368.1037.
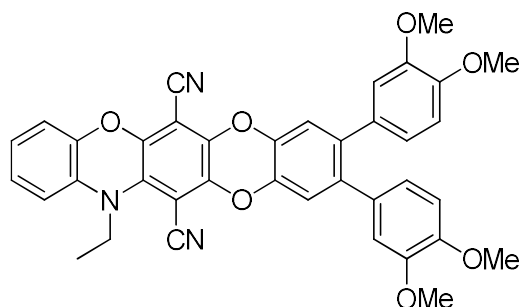
9,10-bis(3,4-dimethoxyphenyl)-14-ethyl-14H-benzo[5,6][1,4]dioxino[2,3-b]phenoxazine-6,13-dicarbonitrile (5.53): To a 25 mL round bottomed flask, under N₂, was added difluoride **2.18** (409 mg, 0.753 mmol, 1.0 eq), followed by DMF (5 mL) and K₂CO₃ (416 mg, 3.01 mmol, 4.0 eq). To this was added 2-(ethylamino)phenol **3.27** (103 mg, 0.753, 1.0 eq) and the mixture was heated to 100 °C for 16 h. The mixture was then cooled to room temperature and H₂O was added, the product being collected *via* suction filtration as an orange powdery solid (420 mg, 87%). mp = 116 °C (dec.); ^{1}H NMR (400 MHz, CDCl₃) δ: 7.09-6.87 (m, 6H), 6.77-6.69 (m, 4H), 6.56 (s, 2H), 4.00 (q, J = 7 Hz, 2H), 3.86 (s, 6H), 3.63 (s, 6H), 1.33 (t, J = 7 Hz, 3H); ^{13}C NMR (100 MHz, CDCl₃) δ: 148.38, 148.12, 147.03, 146.70, 139.58, 138.83, 138.73, 137.56, 137.54, 136.98, 133.76, 132.32, 132.30, 132.02, 125.52, 124.58, 121.76, 118.41, 118.34, 118.31, 116.39, 113.00, 112.26, 110.82, 109.99, 94.14, 94.17, 55.84, 55.70, 48.10, 13.27; HRMS (ESI+) Calc. for C₃₈H₂₉N₃O₇ [M+H]⁺: 640.2078 Found: 640.2080.
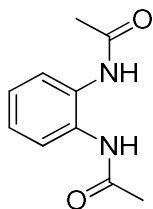
N,N'-(1,2-phenylene)diacetamide (3.61): To a 100 mL round-bottomed flask was added freshly recrystallised *o*-phenylenediamine (2.500 g, 23.1 mmol, 1.0 eq) followed by EtOAc (50 mL) and this was stirred to dissolution. Acetic anhydride (4.8 mL, 50.8 mmol, 2.2 eq) was added all at once, causing concomitant warming of the reaction mixture (40-45 °C). This was allowed to stir at room temperature for 4 h, after which time diethyl ether was added to effect precipitation, and the product collected *via* suction filtration, washing with ether. The solids were recrystallised from aqueous ethanol to give the product as a white, crystalline solid (4.22 g, 95%). mp = 187-189 °C; ^{1}H NMR (400 MHz, DMSO-d_6) δ: 9.31 (s, 2H), 7.54 (s, 2H), 7.11 (s, 2H), 2.07 (s, 6H); ^{13}C NMR (100 MHz, MeOD) δ: 170.79, 130.60, 125.55, 125.14, 22.01. Analytical data agrees with literature values published by Alder, *et al.*[99]
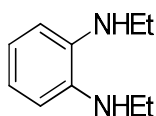
N^1,N^2-diethyl-1,2-benzenediamine (3.62): To a dry 250 mL round bottomed flask, equipped with a condenser, was added *N,N'*-(1,2-phenylene)diacetamide **3.61** (2.50 g, 13.0 mmol, 1.0 eq) and dry THF (40 mL), and this was cooled to 0 °C. LiAlH$_4$ (32.5 mL, 1.0 M in THF, 2.5 eq) was added dropwise to the cooled solution under N$_2$. After addition was complete, the light-yellow solution was heated to reflux for 16 h. The mixture was then cooled, and excess hydride was quenched by cautious addition of Na$_2$SO$_4$·10H$_2$O in small portions until hydrogen evolution ceased. The mixture was filtered through a pad of Celite®, washing with EtOAc. The organic layer was washed with H$_2$O, then saturated NaHCO$_3$, and finally with brine. Concentration of this extract gave a green oil which was then purified *via*

bulb-to-bulb vacuum distillation (110-120 °C / 0.5 mmHg) to give the product as an unstable white, crystalline solid upon cooling (1.77 g, 83%) which could be stored at −20 °C for 1-2 weeks. ^{1}H NMR (400 MHz, CDCl3) δ: 6.81-6.79 (m, 2H), 6.70-6.68 (m, 2H), 3.15 (q, J = 7 Hz, 6H), 1.32 (t, J = 7 Hz, 6H); ^{13}C NMR (100 MHz, CDCl3) δ: 137.34, 118.99, 111.36, 38.83, 15.07. Analytical data agrees with literature values published by Alder, *et al.*[99]
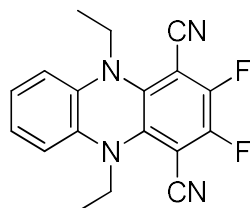
5,10-diethyl-2,3-difluoro-5,10-dihydrophenazine-1,4-dicarbonitrile (3.69): To a 5 mL micro-vial was added tetrafluoroterephthalonitrile (122 mg, 0.609 mmol, 1.0 eq), DMF (3 mL), followed by *N,N'*-diethyl-1,2-benzenediamine **3.62** (200 mg, 1.22 mmol, 2.0 eq), immediately forming a red solution upon addition of the amine. This was heated to 100 °C for 14 h, cooled, and the reaction mixture poured into H_2O (40 mL), filtering to give the product as a red powdery solid. ^{1}H NMR (400 MHz, CDCl3) δ: 6.78-6.76 (m, 2H), 6.66-6.64 (m, 2H), 3.14 (q, J = 7 Hz, 4H), 1.32 (t, J = 7 Hz, 6H); ^{13}C NMR (100 MHz, CDCl3) δ: 148.51, 148.46, 148.42, 148.40, 148.36, 148.32, 148.29, 148.26, 145.84, 145.79, 145.74, 145.64, 145.59, 137.19, 118.96, 111.20, 105.92, 38.79, 15.02; ^{19}F NMR (282 MHz, CDCl3): −128.14.
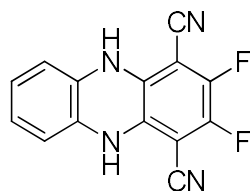
2,3-difluoro-5,10-dihydrophenazine-1,4-dicarbonitrile (3.17): To a 100 mL round-bottomed flask was added tetrafluoroterephthalonitrile (1.049 g, 5.24 mmol, 1.0 eq), DMF (15 mL), and *o*-phenylenediamine (0.567 g, 5.24 mmol, 1.0 eq). The now-red mixture was placed under N_2 and heated to 100 °C for 24 h, after which time it was cooled, poured into

H$_2$O (100 mL) and the solids collected *via* suction filtration. The material thus obtained was recrystallised from DMSO/acetonitrile to give the product as dark brown crystalline solid (922 mg, 66%). ^{1}H NMR (400 MHz, DMSO-d_6) δ: 8.85 (s, 2H), 6.60-6.52 (m, 4H); ^{13}C NMR (100 MHz, DMSO-d_6) δ: 139.70 (dd, J = 243, 16 Hz), 138.34 (t, J = 3 Hz), 129.89, 123.70, 114.73, 111.84 (t, J = 3 Hz), 83.68 (dd, J = 12, 9 Hz); ^{19}F NMR (376 MHz, DMSO-d_6) δ: -150.92. Analytical data for this compound has not been previously reported.[79]
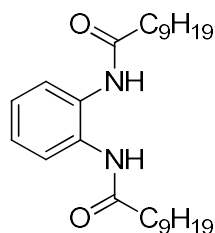
***N,N'*-(1,2-phenylene)bis(decanamide) (3.65):** To a 250 mL round-bottomed flask was added *o*-phenylenediamine (4.00 g, 37.0 mmol, 1.0 eq), CH$_2$Cl$_2$ (150 mL) and pyridine (6.6 mL, 81.4 mmol, 2.2 eq). This was stirred and decanoyl chloride (15.3 mL, 74.0 mmol, 2.0 eq) in CH$_2$Cl$_2$ was added slowly *via* addition funnel. After addition was complete, the flask was equipped with a drying tube and stirred 14 h. The reaction mixture was then washed with 1 M HCl (2 x 20 mL), H$_2$O, dried over Na$_2$SO$_4$ and evaporated to give the product as a white solid. ^{1}H NMR (300 MHz, CDCl$_3$) δ: 8.31 (s, 2H), 7.38-7.33 (m, 2H), 7.20-7.17 (m, 2H), 2.34 (t, J = 8 Hz, 4H), 1.75-1.66 (m, 4H), 1.41-1.30 (m, 24H), 0.95-0.90 (m, 6H); ^{13}C NMR (75 MHz, CDCl$_3$) δ: 172.91, 130.67, 126.09, 125.59, 37.22, 31.92, 29.55, 29.46, 29.37, 29.35, 25.77, 22.71, 14.15; HRMS (ESI+) Calc. for C$_{26}$H$_{44}$N$_2$O$_2$ [M+H]$^+$: 417.3476 Found: 417.3478.
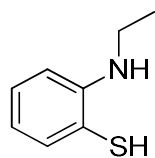
2-(*N*-ethylamino)thiophenol (3.77): To a dry 250 mL three-neck round-bottomed flask equipped with a reflux condenser was added solid lithium aluminum hydride (1.90 g, 50.0

mmol, 0.75 eq), dry THF (75 mL), and this was cooled to 0 °C (ice bath) under N_2. To this stirred suspension was added a solution of 2-methylbenzothiazole **3.78** (10.0 g, 67.0 mmol, 1.0 eq) in dry THF (10 mL), dropwise. After addition was complete, the ice bath was replaced with an oil bath and the mixture heated to reflux for 2.5 h. The yellow mixture was cooled to 0 °C and decomposed (carefully) with wet THF (15 mL THF, 5 mL H_2O). The pH was then brought to ≈2-3 (pH paper) with concentrated HCl (8 mL) and the mixture filtered and concentrated *in vacuo.* The bright yellow oil obtained was subjected to vacuum distillation (60-90 °C/0.5 mmHg), and a second vacuum distillation through a 10 cm Vigreux column (94-95 °C/0.5 mmHg). The clear, colorless liquid (6.67 g, 65%) thus obtained contained a small amount (approx. 5-7%) of 2-methylbenzothiazole (as evidenced in the ^{1}H NMR and ^{13}C NMR spectra) and required distillation prior to each use due to air oxidation and discoloration (bright yellow) forming a yellow precipitate. ^{1}H NMR (400 MHz, $CDCl_3$): 7.38-7.37 (m, 1H), 7.20-7.18 (m, 1H), 6.62-6.59 (m, 2H), 3.20 (q, *J* = 7 Hz, 2H), 1.31 (t, *J* = 7 Hz, 3H). A literature procedure for the *N*-methyl derivative was followed, published by Hunig, *et al.*[113]
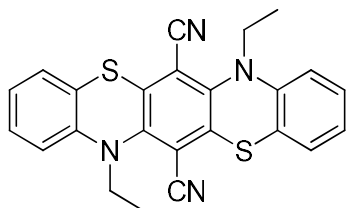
7,14-diethyl-7,14-dihydrobenzo[5,6][1,4]thiazino[2,3-b]phenothiazine-6,13-dicarbonitrile (3.80): To a 25 mL two-neck round-bottomed flask, under N_2, was added TFTP (400 mg, 2.0 mmol, 1.0 eq), K_2CO_3 (1.66 g, 12.0 mmol, 6.0 eq) and dry DMF (10 mL). A solution of 2-(*N*-ethylamino)thiophenol **3.77** (645 mg, 4.2 mmol, 2.1 eq) in DMF (1 mL) was then added dropwise. After addition was complete, the orange mixture was heated to 100 °C, turning dark red in colour. After 1.5 h at temperature, a red-orange, fluorescent (365 nm) solid began to precipitate, and the mixture was left for 4 h at 100 °C. The mixture was cooled, diluted with H_2O (100 mL), and the precipitate collected *via* suction filtration, washing with H_2O, then cold methanol. The solids were subjected to column chromatography (SiO_2, 30%

CH$_2$Cl$_2$/hexanes) from which fractions 13-19 were concentrated *in vacuo* to yield an orange solid; recrystallisation of this material from THF provided the desired product as a bright orange solid (70 mg, 8%). mp > 260 °C; R$_f$ = 0.40 (50% CH$_2$Cl$_2$/hexanes); ^{1}H NMR (400 MHz, C$_6$D$_6$) δ: 6.83-6.80 (m, 4H), 6.63 (t, *J* = 7 Hz, 2H), 6.51 (d, *J* = 8 Hz, 2H), 3.75 (q, *J* = 7 Hz, 4H), 0.88 (t, *J* = 7 Hz, 6H); ^{13}C NMR (100 MHz, CDCl$_3$) δ: 144.19, 143.65, 136.71, 128.40, 127.46, 126.18, 124.75, 120.88, 114.50, 105.97, 49.34, 14.43; HRMS (ESI+) Calc. for C$_{24}$H$_{18}$N$_4$S$_2$ [M+H]$^+$: 427.1046 Found: 427.1047.
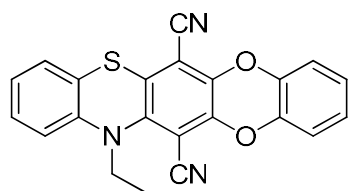
12-ethyl-12H-benzo[5,6][1,4]dioxino[2,3-b]phenothiazine-6,13-dicarbonitrile (3.84): To a 25 mL round-bottomed flask was added dibenzodioxin difluoride **3.16** (401 mg, 1.49 mmol, 1.0 eq), K$_2$CO$_3$ (830 mg, 5.86 mmol, 4.0 eq), and dry DMF (8 mL). This was placed under N$_2$, and a solution of 2-(ethylamino)thiophenol (229 mg, 1.49 mmol, 1.0 eq) in THF (2 mL) was added dropwise. After stirring 5 min at rt, a non-fluorescent yellow solid precipitated, and the reaction mixture was heated to 100 °C with redissolution. After 24 h, the mixture was cooled to room temperature, poured into H$_2$O (75 mL), and the precipitate collected *via* suction filtration, washing with H$_2$O. The crude solid thus obtained could be recrystallised from ethyl acetate to yield the product as orange needles (263 mg, 46%). mp = 243-244 °C; ^{1}H NMR (400 MHz, C$_6$D$_6$) δ: 6.83-6.78 (m, 2H), 6.64 (t, *J* = 8 Hz, 1H), 6.53-6.43 (m, 5H), 3.80 (q, *J* = 7 Hz, 2H), 0.92 (t, *J* = 7 Hz, 3H); ^{13}C NMR (100 MHz, C$_6$D$_6$) δ: 143.34, 143.25, 140.11, 139.86, 139.40, 129.44, 128.01, 127.25, 126.24, 125.24, 125.16, 124.96, 124.57, 120.43, 116.51, 116.47, 112.03, 111.08, 102.92, 97.20, 48.47, 13.94; HRMS (ESI+) Calc. for C$_{22}$H$_{13}$N$_3$O$_2$S [M+H]$^+$: 384.0801 Found: 384.0788.

References

(1) Feng, X.; Pisula, W.; Müllen, K. Large Polycyclic Aromatic Hydrocarbons: Synthesis and Discotic Organization. *Pure Appl. Chem.* **2009**, *81* (12), 2203–2224.

(2) Li, Y.; Jia, Z.; Xiao, S.; Liu, H.; Li, Y. A Method for Controlling the Synthesis of Stable Twisted Two-Dimensional Conjugated Molecules. *Nat. Commun.* **2016**, *7*, 11637.

(3) Clar, E. The Aromatic Sextet. In *Mobile Source Emissions Including Policyclic Organic Species*; Springer Netherlands: Dordrecht, 1983; pp 49–58.

(4) Bettinger, H. F.; Tonshoff, C. The Longest Acenes. *Chem. Rec.* **2015**, *15* (1), 364–369.

(5) Anthony, J. E. The Larger Acenes: Versatile Organic Semiconductors. *Angew. Chem. Int. Ed.* **2008**, *47* (3), 452–483.

(6) Shi, X.; Chi, C. Different Strategies for the Stabilization of Acenes and Acene Analogues. *Chem. Rec.* **2016**, *16* (3), 1690–1700.

(7) Anthony, J. E.; Brooks, J. S.; Eaton, D. L.; Parkin, S. R. Functionalized Pentacene: Improved Electronic Properties from Control of Solid-State Order. *J. Am. Chem. Soc.* **2001**, *123* (38), 9482–9483.

(8) Ye, Q.; Chang, J.; Shi, X.; Dai, G.; Zhang, W.; Huang, K. W.; Chi, C. Stable 7,14-Disubstituted-5,12-Dithiapentacenes with Quinoidal Conjugation. *Org. Lett.* **2014**, *16* (15), 3966–3969.

(9) Nicolas, Y.; Allama, F.; Lepeltier, M.; Massin, J.; Castet, F.; Ducasse, L.; Hirsch, L.; Boubegtiten, Z.; Jonusauskas, G.; Olivier, C.; et al. New Synthetic Routes towards Soluble and Dissymmetric Triphenodioxazine Dyes Designed for Dye-Sensitized Solar Cells. *Chem. - A Eur. J.* **2014**, *20* (13), 3678–3688.

(10) Tönshoff, C.; Bettinger, H. F. Beyond Pentacenes: Synthesis and Properties of Higher Acenes. *Top. Curr. Chem.* **2014**, *349*, 1–30.

(11) Ye, Q.; Chi, C. Recent Highlights and Perspectives on Acene Based Molecules and Materials. *Chem. Mater.* **2014**, *26* (14), 4046–4056.

(12) Sergeyev, S.; Pisula, W.; Geerts, Y. H. Discotic Liquid Crystals: A New Generation of Organic Semiconductors. *Chem. Soc. Rev.* **2007**, *36* (12), 1902–1929.

(13) Anthony, J. E. Functionalized Acenes and Heteroacenes for Organic Electronics. *Chem. Rev.* **2006**, *106* (12), 5028–5048.

(14) Yi, H. T.; Payne, M. M.; Anthony, J. E.; Podzorov, V. Ultra-Flexible Solution-Processed Organic Field-Effect Transistors. *Nat. Commun.* **2012**, *3* (1), 1259.

(15) Samsung OLED TV | CBC News http://www.cbc.ca/news/samsung-oled-tv-1.1706883 (accessed Jun 13, 2018).

(16) Reyes-Martinez, M. A.; Crosby, A. J.; Briseno, A. L. Rubrene Crystal Field-Effect Mobility Modulation via Conducting Channel Wrinkling. *Nat. Commun.* **2015**, *6* (1), 6948.

(17) McGarry, K. A.; Xie, W.; Sutton, C.; Risko, C.; Wu, Y.; Young, V. G.; Brédas, J. L.; Frisbie, C. D.; Douglas, C. J. Rubrene-Based Single-Crystal Organic Semiconductors: Synthesis, Electronic Structure, and Charge-Transport Properties. *Chem. Mater.* **2013**, *25* (11), 2254–2263.

(18) Malloci, G.; Cappellini, G.; Mulas, G.; Mattoni, A. A (Time-Dependent) Density Functional Theory Study of the Optoelectronic Properties of Bis-Triisopropylsilylethynyl-Functionalized Acenes. *Thin Solid Films* **2013**, *543*, 32–34.

(19) Bruzek, M. J.; Anthony, J. E. Synthesis and Optical Properties of Dioxolane-

Functionalized Hexacenes and Heptacenes. *Org. Lett.* **2014**, *16* (13), 3608–3610.

(20) Arkhipov, V. I.; Kolesnikov, V. A.; Rudenko, A. I. Dispersive Transport of Charge Carriers in Polycrystalline Pentacene Layers. *J. Phys. D. Appl. Phys.* **1984**, *17* (6), 021.

(21) Cornil, J.; Calbert, J. P.; Brédas, J. L. Electronic Structure of the Pentacene Single Crystal: Relation to Transport Properties [11]. *J. Am. Chem. Soc.* **2001**, *123* (6), 1250–1251.

(22) Maliakal, A.; Raghavachari, K.; Katz, H.; Chandross, E.; Siegrist, T. Photochemical Stability of Pentacene and a Substituted Pentacene in Solution and in Thin Films. *Chem. Mater.* **2004**, *16* (24), 4980–4986.

(23) Desiraju, G. R.; Gavezzotti, A. Crystal Structures of Polynuclear Aromatic Hydrocarbons. Classification, Rationalization and Prediction from Molecular Structure. *Acta Crystallogr. Sect. B* **1989**, *45* (5), 473–482.

(24) Keller, U.; Müllen, K.; De Feyter, S.; De Schryver, F. C. Hydrogen-Bonding and Phase-Forming Behavior of a Soluble Quinacridone. *Adv. Mater.* **1996**, *8* (6), 490–493.

(25) De Feyter, S.; Gesquière, A.; De Schryver, F. C.; Keller, U.; Müllen, K. Aggregation Properties of Soluble Quinacridones in Two and Three Dimensions. *Chem. Mater.* **2002**, *14* (3), 989–997.

(26) Labana, S. S.; Labana, L. L. Quinacridones. *Chem. Rev.* **1967**, *67*, 1.

(27) Reinitzer, F. Contributions to the Knowledge of Cholesterol. *Liq. Cryst.* **1989**, *5* (1), 7–18.

(28) Chandrasekhar, S. *Liquid Crystals*; Cambridge University Press: Cambridge, 1992.

(29) Itahara, T.; Furukawa, S.; Kubota, K.; Morimoto, M.; Sunose, M. Cholesteryl Benzoate Derivatives: Synthesis, Transition Property and Cholesteric Liquid Crystal Glass. *Liq.*

146

Cryst. **2013**, *40* (5), 589–598.

(30)   Raynes, E. P.; Waters, C. M. Supertwisted Nematic Liquid Crystal Displays. *Angew.*
         Chem. Int. Ed. **1987**, *12* (8), 617–630.

(31)   "Smectic" https://www.merriam-webster.com/dictionary/smectic (accessed Feb 6,
         2018).

(32)   Alkeskjold, T. T.; Scolari, L.; Noordegraaf, D.; Lægsgaard, J.; Weirich, J.; Wei, L.;
         Tartarini, G.; Bassi, P.; Gauza, S.; Wu, S. T.; et al. Integrating Liquid Crystal Based Optical
         Devices in Photonic Crystal Fibers. *Opt. Quantum Electron.* **2007**, *39* (12–13), 1009–
         1019.

(33)   Mikhnenko, O. V; Blom, P. W. M.; Nguyen, T.-Q. Exciton Diffusion in Organic
         Semiconductors. *Energy Environ. Sci.* **2015**, *8* (7), 1867–1888.

(34)   Thomas, R.; Varghese, S.; Kulkarni, G. U. The Influence of Crystal Packing on the Solid
         State Fluorescence Behavior of Alkyloxy Substituted Phenyleneethynylenes. *J. Mater.*
         Chem. **2009**, *19* (25), 4401–4406.

(35)   Nugent, J. W.; Lee, H.; Reibenspies, J. H.; Lee, H. S.; Hancock, R. D. Effects of Anion
         Coordination on the Fluorescence of a Photo-Induced Electron Transfer (PET) Sensor
         Complexed with Metal Ions. *Polyhedron* **2017**, *130*, 47–57.

(36)   Tan, S. S.; Kim, S. J.; Kool, E. T. Differentiating between Fluorescence-Quenching Metal
         Ions with Polyfluorophore Sensors Built on a DNA Backbone. *J. Am. Chem. Soc.* **2011**,
         133 (8), 2664–2671.

(37)   Content, S.; Trogler, W. C.; Sailor, M. J. Detection of Nitrobenzene, DNT, and TNT Vapors
         by Quenching of Porous Silicon Photoluminescence. *Chem. - A Eur. J.* **2000**, *6* (12),

2205–2213.

(38) Penfold, T. J.; Dias, F. B.; Monkman, A. P. The Theory of Thermally Activated Delayed Fluorescence for Organic Light Emitting Diodes. *Chem. Commun.* **2018**, *54* (32), 3926–3935.

(39) Feuillastre, S.; Pauton, M.; Gao, L.; Desmarchelier, A.; Riives, A. J.; Prim, D.; Tondelier, D.; Geffroy, B.; Muller, G.; Clavier, G.; et al. Design and Synthesis of New Circularly Polarized Thermally Activated Delayed Fluorescence Emitters. *J. Am. Chem. Soc.* **2016**, *138* (12), 3990–3993.

(40) Mei, J.; Leung, N. L. C.; Kwok, R. T. K.; Lam, J. W. Y.; Tang, B. Z. Aggregation-Induced Emission: Together We Shine, United We Soar! *Chem. Rev.* **2015**, *115* (21), 11718–11940.

(41) Kwok, R. T. K.; Leung, C. W. T.; Lam, J. W. Y.; Tang, B. Z. Biosensing by Luminogens with Aggregation-Induced Emission Characteristics. *Chem. Soc. Rev.* **2015**, *44* (13), 4228–4238.

(42) Luo, J.; Xie, Z.; Xie, Z.; Lam, J. W. Y.; Cheng, L.; Chen, H.; Qiu, C.; Kwok, H. S.; Zhan, X.; Liu, Y.; et al. Aggregation-Induced Emission of 1-Methyl-1,2,3,4,5-Pentaphenylsilole. *Chem. Commun.* **2001**, *18* (18), 1740–1741.

(43) Gabr, M. T.; Pigge, F. C. Synthesis and Aggregation-Induced Emission Properties of Pyridine and Pyridinium Analogues of Tetraphenylethylene. *RSC Adv.* **2015**, *5* (110), 90226–90234.

(44) Mei, J.; Hong, Y.; Lam, J. W. Y.; Qin, A.; Tang, Y.; Tang, B. Z. Aggregation-Induced Emission: The Whole Is More Brilliant than the Parts. *Adv. Mater.* **2014**, *26* (31), 5429–

5479.

(45) Shyamal, M.; Maity, S.; Maity, A.; Maity, R.; Roy, S.; Misra, A. Aggregation Induced Emission Based "Turn-off" Fluorescent Chemosensor for Selective and Swift Sensing of Mercury (II) Ions in Water. *Sensors Actuators, B Chem.* **2018**, *263*, 347–359.

(46) Chen, X.; Wang, L.; Yang, X.; Tang, L.; Zhou, Y.; Liu, R.; Qu, J. A New Aggregation-Induced Emission Active Fluorescent Probe for Sensitive Detection of Cyanide. *Sensors Actuators, B Chem.* **2017**, *241*, 1043–1049.

(47) Gao, M.; Tang, B. Z. Fluorescent Sensors Based on Aggregation-Induced Emission: Recent Advances and Perspectives. *ACS Sensors* **2017**, *2* (10), 1382–1399.

(48) Paquette, J. A.; Yardley, R. E.; Yu, J. W.-Y.; Eichhorn, S. H.; Maly, K. E. Anthra- and Pentacenequinone Derivatives: Influence of Structure on the Formation of Columnar Liquid Crystal Phases. *New J. Chem.* **2016**, *40* (7), 5985–5988.

(49) Raycraft, B.; Maly, K. E. Synthesis and Self-Assembly of Luminescent Tetraoxadicyanopentacene and Derivatives, Wilfrid Laurier University, 2014.

(50) Dolbier, W. R.; Xie, P.; Zhang, L.; Xu, W.; Chang, Y.; Abboud, K. A. Synthesis of Perfluoro[2.2]Paracyclophane. *J. Org. Chem.* **2008**, *73* (6), 2469–2472.

(51) Fleming, M. J.; McManus, H. A.; Rudolph, A.; Chan, W. H.; Ruiz, J.; Dockendorff, C.; Lautens, M. Concise Enantioselective Total Syntheses of (+)-Homochelidonine, (+)-Chelamidine, (+)-Chelidonine, (+)-Chelamine and (+)-Norchelidonine by a PdII-Catalyzed Ring-Opening Strategy. *Chem. - A Eur. J.* **2008**, *14* (7), 2112–2124.

(52) Schmidt, B.; Riemer, M. Suzuki-Miyaura Coupling of Halophenols and Phenol Boronic Acids: Systematic Investigation of Positional Isomer Effects and Conclusions for the

Synthesis of Phytoalexins from Pyrinae. *J. Org. Chem.* **2014**, *79* (9), 4104–4118.

(53) Fuji, K.; Nakano, S.; Fujita, E. An Improved Method for Methoxymethylation of Alcohols under Mild Acidic Conditions. *Synthesis (Stuttg).* **1975**, *1975* (04), 276–277.

(54) Steinke, N.; Jahr, M.; Lehmann, M.; Baro, A.; Frey, W.; Tussetschläger, S.; Sauer, S.; Laschat, S. Crown Ethers with Lateral Ortho-Terphenyl Units: Effect of Ester Groups and Sodium Salts on the Mesomorphic Properties. *J. Mater. Chem.* **2009**, *19* (5), 645–654.

(55) Shih-Yuan Lee, A.; Hu, Y.-J.; Chu, S.-F. A Simple and Highly Efficient Deprotecting Method for Methoxymethyl and Methoxyethoxymethyl Ethers and Methoxyethoxymethyl Esters. *Tetrahedron* **2001**, *57*, 2121–2126.

(56) Taylor, R. G. D.; Carta, M.; Bezzu, C. G.; Walker, J.; Msayib, K. J.; Kariuki, B. M.; McKeown, N. B. Triptycene-Based Organic Molecules of Intrinsic Microporosity. *Org. Lett.* **2014**, *16* (7), 1848–1851.

(57) Taylor, R. G. D.; Bezzu, C. G.; Carta, M.; Msayib, K. J.; Walker, J.; Short, R.; Kariuki, B. M.; McKeown, N. B. The Synthesis of Organic Molecules of Intrinsic Microporosity Designed to Frustrate Efficient Molecular Packing. *Chem. - A Eur. J.* **2016**, *22* (7), 2466–2472.

(58) Short, R.; Carta, M.; Bezzu, C. G.; Fritsch, D.; Kariuki, B. M.; McKeown, N. B. Hexaphenylbenzene-Based Polymers of Intrinsic Microporosity. *Chem. Commun.* **2011**, *47* (24), 6822.

(59) Martinez, C. R.; Iverson, B. L. Rethinking the Term "Pi-Stacking." *Chem. Sci.* **2012**, *3* (7), 2191–2201.

(60) Hunter, C. A.; Sanders, J. K. M. The Nature of π-π Interactions. *J. Am. Chem. Soc.* **1990**, *112* (14), 5525–5534.

(61) Binnemans, K.; Sleven, J.; De Feyter, S.; De Schryver, F. C.; Donnio, B.; Guillon, D. Structure and Mesomorphic Behavior of Alkoxy-Substituted Bis(Phthalocyaninato)Lanthanide(III) Complexes. *Chem. Mater.* **2003**, *15* (20), 3930–3938.

(62) Wöhrle, T.; Gündemir, R.; Frey, W.; Knecht, F.; Köhn, A.; Laschat, S. Thermotropic MIDA Boronates as a Case Study for the Role of Dipolar Interactions in Liquid Crystalline Self-Assembly. *Chem. - A Eur. J.* **2017**, *23* (17), 4149–4159.

(63) Schultz, A.; Laschat, S.; Saipa, A.; Gießelmann, F.; Nimtz, M.; Schulte, J. L.; Baro, A.; Miehlich, B. Columnar Liquid Crystals with a Central Crown Ether Unit. *Adv. Func. Mater.* **2004**, *14* (2), 163–168.

(64) Bunz, U. H. F. The Larger Linear N-Heteroacenes. *Acc. Chem. Res.* **2015**, *48* (6), 1676–1686.

(65) Vázquez, R. J.; Kim, H.; Kobilka, B. M.; Hale, B. J.; Jeffries-EL, M.; Zimmerman, P.; Goodson, T. Evaluating the Effect of Heteroatoms on the Photophysical Properties of Donor–Acceptor Conjugated Polymers Based on 2,6-Di(Thiophen-2-Yl)Benzo[1,2-b:4,5-B']Difuran: Two-Photon Cross-Section and Ultrafast Time-Resolved Spectroscopy. *J. Phys. Chem. C* **2017**, *121* (27), 14382–14392.

(66) Tasior, M.; Gryko, D. T. Synthesis and Properties of Ladder-Type BN-Heteroacenes and Diazabenzoindoles Built on a Pyrrolopyrrole Scaffold. *J. Org. Chem.* **2016**, *81* (15), 6580–6586.

(67) Qu, H.; Chi, C. Synthetic Chemistry of Acenes and Heteroacenes. *Curr. Org. Chem.* **2010**, *14* (18), 2070–2108.

(68) Engelhart, J. U.; Lindner, B. D.; Tverskoy, O.; Rominger, F.; Bunz, U. H. F. Partially Fluorinated Tetraazaacenes by Nucleophilic Aromatic Substitution. *J. Org. Chem.* **2013**, *78* (21), 10832–10839.

(69) Lami, V.; Leibold, D.; Fassl, P.; Hofstetter, Y. J.; Becker-Koch, D.; Biegger, P.; Paulus, F.; Hopkinson, P. E.; Adams, M.; Bunz, U. H. F.; et al. N -Heteroacenes as a New Class of Non-Fullerene Electron Acceptors for Organic Bulk-Heterojunction Photovoltaic Devices. *Sol. RRL* **2017**, *1* (6), 1700053.

(70) Bunz, U. H. F. N-Heteroacenes. *Chem. - A Eur. J.* **2009**, *15* (28), 6780–6789.

(71) Maly, K. E. Acenes vs N-Heteroacenes: The Effect of N-Substitution on the Structural Features of Crystals of Polycyclic Aromatic Hydrocarbons. *Cryst. Growth Des.* **2011**, *11* (12), 5628–5633.

(72) Nicolas, Y.; Castet, F.; Devynck, M.; Tardy, P.; Hirsch, L.; Labrugère, C.; Allouchi, H.; Toupance, T. TIPS-Triphenodioxazine versus TIPS-Pentacene: Enhanced Electron Mobility for n-Type Organic Field-Effect Transistors. *Org. Electron.* **2012**, *13* (8), 1392–1400.

(73) Di, C. A.; Li, J.; Yu, G.; Xiao, Y.; Guo, Y.; Liu, Y.; Qian, X.; Zhu, D. Trifluoromethyltriphenodioxazine: Air-Stable and High-Performance n-Type Semiconductor. *Org. Lett.* **2008**, *10* (14), 3025–3028.

(74) Girard, P. R. Dioxazine Violet Pigments. In *High Performance Pigments: Second Edition*; Wiley-VCH Verlag GmbH & Co. KGaA: Weinheim, FRG, 2009; pp 195–204.

(75) Xie, Z.; Chen, C.; Xu, S.; Li, J.; Zhang, Y.; Liu, S.; Xu, J.; Chi, Z. White-Light Emission Strategy of a Single Organic Compound with Aggregation-Induced Emission and Delayed Fluorescence Properties. *Angew. Chem. Int. Ed.* **2015**, *54* (24), 7181–7184.

(76) Tang, M. L.; Okamoto, T.; Bao, Z. High-Performance Organic Semiconductors: Asymmetric Linear Acenes Containing Sulphur. *J. Am. Chem. Soc.* **2006**, *128* (50), 16002–16003.

(77) Krompiec, M. P.; Baxter, S. N.; Klimareva, E. L.; Yufit, D. S.; Congrave, D. G.; Britten, T. K.; Perepichka, I. F. 3,4-Phenylenedioxythiophenes (PheDOTs) Functionalized with Electron-Withdrawing Groups and Their Analogs for Organic Electronics. *J. Mater. Chem. C* **2018**, *6* (14), 3743–3756.

(78) Okamoto, T.; Kozaki, M.; Doe, M.; Uchida, M.; Wang, G.; Okada, K. 1,4-Benzoxazino[2,3-b]Phenoxazine and Its Sulfur Analogues: Synthesis, Properties, and Application to Organic Light-Emitting Diodes. *Chem. Mater.* **2005**, *17* (22), 5504–5511.

(79) Wang, L.; Chen, T.; Chen, S. C.; Chen, Q.; He, M. Y. Ultrasound Assisted Nucleophilic Cyclization of Tetrafluoroterephthalonitrile: An Efficient Way to Fluorine-Containing Heterocycles. *J. Heterocycl. Chem.* **2015**, *51* (5), 1536–1540.

(80) Banerjee, S.; Chattopadhyay, A.; Saini, P.; Singh, K. S. Synthesis and Optical Properties of 1,4- and 1,2-Dicyanodibenzodioxins Possessing Donor-π-Acceptor Architecture. *Synlett* **2016**, *27* (5), 799–804.

(81) Lokanath, N. K.; Sridhar, M. A.; Prasad, J. S.; Ramegowda, M.; Eregowda, G. B.; Thimmaiah, K. N. Crystal Structure of 10-(3′-N-Morpholinopropyl)-2-Trifluoro Phenoxazine Hydrochloride, C20H21ClF3N2O2. *Zeitschrift für Krist. - Cryst. Mater.*

1997, *212* (1), 21–22.

(82) Ergun, S.; Elliott, C. F.; Kaur, A. P.; Parkin, S. R.; Odom, S. A. Controlling Oxidation Potentials in Redox Shuttle Candidates for Lithium-Ion Batteries. *J. Phys. Chem. C* **2014**, *118* (27), 14824–14832.

(83) Christe, K. O.; Wilson, W. W. Reaction of the Fluoride Anion with Acetonitrile. Chloroform and Methylene Chloride. *J. Fluor. Chem.* **1990**, *47* (1), 117–120.

(84) Zilinskaite, V.; Gudeika, D.; Grazulevicius, J. V.; Sidaravicius, J. Synthesis and Properties of 1,3-Indandione-Disubstituted Derivatives of Carbazole, Phenothiazine, and Phenoxazine. *Mol. Cryst. Liq. Cryst.* **2014**, *590* (1), 80–89.

(85) Tan, H.; Pan, C.; Wang, G.; Wu, Y.; Zhang, Y.; Zou, Y.; Yu, G.; Zhang, M. Phenoxazine-Based Organic Dyes with Different Chromophores for Dye-Sensitized Solar Cells. *Org. Electron.* **2013**, *14* (11), 2795–2801.

(86) Cheon, Y. J.; Gim, H. J.; Jang, H. R.; Ryu, J. H.; Jeon, R. Synthesis of Heterocycle-Linked Thioureas and Their Inhibitory Activities of NO Production in LPS Activated Macrophages. *Bull. Korean Chem. Soc.* **2010**, *31* (1), 27–30.

(87) Gilman, H.; Moore, L. O. The Preparation of Some 10-Substituted Phenoxazines. *J. Am. Chem. Soc.* **1957**, *79* (13), 3485–3487.

(88) Searles, S.; Tamres, M.; Block, F.; Quarterman, L. A. Hydrogen Bonding and Basicity of Cyclic Imines. *J. Am. Chem. Soc.* **1956**, *78* (19), 4917–4920.

(89) Vandevoorde, S.; Jonsson, K. O.; Fowler, C. J.; Lambert, D. M. Modifications of the Ethanolamine Head in N-Palmitoylethanolamine: Synthesis and Evaluation of New Agents Interfering with the Metabolism of Anandamide. *J. Med. Chem.* **2003**, *46* (8),

1440–1448.

(90) Hiraoka, K.; Mizuse, S.; Yamabe, S. High-Symmetric Structure of the Gas-Phase Cluster Ions X-···C6F6 (X = Cl, Br, and I). *J. Phys. Chem.* **1987**, *91* (20), 5294–5297.

(91) Farnham, S.; Taylor, R. Fluorescence Properties of a Meisenheimer Complex. *J. Org. Chem.* **1974**, *39* (16), 2446–2448.

(92) Guha, S.; Saha, S. Fluoride Ion Sensing by an Anion-π Interaction. *J. Am. Chem. Soc.* **2010**, *132* (50), 17674–17677.

(93) Giese, M.; Albrecht, M.; Rissanen, K. Anion-π Interactions with Fluoroarenes. *Chem. Rev.* **2015**, *115* (16), 8867–8895.

(94) Imahori, S.; Murata, Y.; Okada, I.; Maeda, S. Dioxazine Dyes. JP 52030823, 1977.

(95) Fuhrer, H.; Sutter, P.; Weis, C. D. A New Ring Closure Reaction of 2-Phenoxyphenols and 3-(Phenoxy)Pyridines. Synthesis of Halogenated 10-Methylphenoxazines and 10-Methyl[1,4]Benzoxazino[3,2- b]Pyridines. *J. Heterocycl. Chem.* **1979**, *16* (6), 1121–1134.

(96) Le Hiress, M.; Akagah, B.; Bernadat, G.; Tu, L.; Thuillet, R.; Huertas, A.; Phan, C.; Fadel, E.; Simonneau, G.; Humbert, M.; et al. Design, Synthesis and Biological Activity of New N-(Phenylmethyl)-Benzoxazol-2-Thiones as Macrophage Migration Inhibitory Factor (MIF) Antagonists: Efficacies in Experimental Pulmonary Hypertension. *J. Med. Chem.* **2018**, *61*, 2725–2736.

(97) Li, C.; Xu, K.; Zhang, Z. 1. Organic Electroluminescent Device Containing 1,8-Diazafluoren-9-One Compounds and Its Application. CN 107068887, 2016.

(98) Nijegorodov, N.; Mabbs, R. The Dependence of the Fluorescence Properties, Laser

Properties and Photochemical Stability of Aromatic Compounds on the Molecular Symmetry. *Spectrochim. Acta Part A Mol. Biomol. Spectrosc.* **2000**, *56* (11), 2157–2166.

(99) Alder, R. W.; Hyland, N. P.; Jeffery, J. C.; Riis-Johannessen, T.; Riley, D. J. Poly(1,1-Bis(Dialkylamino)Propan-1,3-Diyl)s; Conformationally-Controlled Oligomers Bearing Electroactive Groups. *Org. Biomol. Chem.* **2009**, *7* (13), 2704–2715.

(100) Zhang, L.; Colella, N. S.; Cherniawski, B. P.; Mannsfeld, S. C. B.; Briseno, A. L. Oligothiophene Semiconductors: Synthesis, Characterization, and Applications for Organic Devices. *ACS Appl. Mater. Interfaces* **2014**, *6* (8), 5327–5343.

(101) Chen, Y.-C.; Kuo, Y.-T.; Liang, C.-J. Numbers of Cyanovinyl Substitutes and Their Effect on Phenothiazine Based Organic Dyes for Dye-Sensitized Solar Cells. *RSC Adv.* **2018**, *8* (18), 9783–9789.

(102) Revoju, S.; Biswas, S.; Eliasson, B.; Sharma, G. D. Asymmetric Triphenylamine–phenothiazine Based Small Molecules with Varying Terminal Acceptors for Solution Processed Bulk-Heterojunction Organic Solar Cells. *Phys. Chem. Chem. Phys.* **2018**, *20* (9), 6390–6400.

(103) Tian, H.; Bora, I.; Jiang, X.; Gabrielsson, E.; Karlsson, K. M.; Hagfeldt, A.; Sun, L. Modifying Organic Phenoxazine Dyes for Efficient Dye-Sensitized Solar Cells. *J. Mater. Chem.* **2011**, *21* (33), 12462–12472.

(104) Takimiya, K.; Shinamura, S.; Osaka, I.; Miyazaki, E. Thienoacene-Based Organic Semiconductors. *Adv. Mater.* **2011**, *23* (38), 4347–4370.

(105) Chen, W.; Zhang, J.; Long, G.; Liu, Y.; Zhang, Q. From Non-Detectable to Decent: Replacement of Oxygen with Sulfur in Naphthalene Diimide Boosts Electron Transport

in Organic Thin-Film Transistors (OTFT). *J. Mater. Chem. C* **2015**, *3* (31), 8219–8224.

(106) Meng, L.; Fujikawa, T.; Kuwayama, M.; Segawa, Y.; Itami, K. Thiophene-Fused π-Systems from Diarylacetylenes and Elemental Sulfur. *J. Am. Chem. Soc.* **2016**, *138* (32), 10351–10355.

(107) Varathan, E.; Subramanian, V. The Role of Sulfur Oxidation in Controlling the Electronic Properties of Sulfur-Containing Host Molecules for Phosphorescent Organic Light-Emitting Diodes. *Phys. Chem. Chem. Phys.* **2017**, *19* (19), 12002–12012.

(108) Farrington, K. J.; Warbuton, W. K. Studies in the Chemistry of Phenothiazine. *Aust. J. Chem.* **1957**, *10*, 502–504.

(109) Andreani, F.; Bizzarri, P. C.; Casa, C. D.; Fiorini, M.; Salatelli, E. Ladder Oligophenothiazines by Direct Thionation of N-Arylanilino Derivatives. *J. Heterocycl. Chem.* **1991**, *28* (2), 295–299.

(110) Kistenmacher, A.; Baumgarten, M.; Enkelmann, V.; Pawlik, J.; Müllen, K. Novel Donor 1,4-Benzothiazino[2,3-b]Phenothiazine. *J. Org. Chem.* **1994**, *59* (10), 2743–2747.

(111) Riebe, S.; Vallet, C.; van der Vight, F.; Gonzalez-Abradelo, D.; Wölper, C.; Strassert, C. A.; Jansen, G.; Knauer, S.; Voskuhl, J. Aromatic Thioethers as Novel Luminophores with Aggregation-Induced Fluorescence and Phosphorescence. *Chem. - A Eur. J.* **2017**, *23* (55), 13660–13668.

(112) Knapp, K. K.; Keller, P. C.; Rund, J. V. Reaction of Diborane with Benzoxazole and Its Sulphur and Selenium Analogues. A Novel Rearrangement to Benzoxazaboroles, Benzothiazaboroles, and Benzoselenazaboroles. *J. Chem. Soc. Chem. Commun.* **1978**, *0* (22), 971.

157

(113) Hünig, S.; Scheutzow, D.; Schlaf, H.; Quast, H. Über Zweistufige Redoxsysteme, VIII1) Synthese Heterocyclisch Tetrasubstituierter Äthylene Und Ihrer Höheren Oxidationsstufen. *Justus Liebigs Ann. Chem.* **1973**, *765* (1), 110–125.

(114) Dolomanov, O. V.; Bourhis, L. J.; Gildea, R. J.; Howard, J. A. K.; Puschmann, H. OLEX2: A Complete Structure Solution, Refinement and Analysis Program. *J. Appl. Crystallogr.* **2009**, *42* (2), 339–341.

(115) Sheldrick, G. M. SHELXT - Integrated Space-Group and Crystal-Structure Determination. *Acta Crystallogr. Sect. A Found. Crystallogr.* **2015**, *71* (1), 3–8.

(116) Sheldrick, G. M. Crystal Structure Refinement with SHELXL. *Acta Crystallogr. Sect. C Struct. Chem.* **2015**, *71* (1), 3–8.

(117) Burchat, A. F.; Chong, J. M.; Nielsen, N. Titration of Alkyllithiums with a Simple Reagent to a Blue Endpoint. *J. Organomet. Chem.* **1997**, *542* (2), 281–283.

(118) Kumarasamy, E.; Raghunathan, R.; Jockusch, S.; Ugrinov, A.; Sivaguru, J. Tailoring Atropisomeric Maleimides for Stereospecific [2 + 2] Photocycloaddition-Photochemical and Photophysical Investigations Leading to Visible-Light Photocatalysis. *J. Am. Chem. Soc.* **2014**, *136* (24), 8729–8737.

(119) Neogi, S.; Naskar, D. One-Pot Reductive Mono-n-Alkylation of Aromatic Nitro Compounds Using Nitriles as Alkylating Reagents. *Synth. Commun.* **2011**, *41* (13), 1901–1915.

(120) Fierz-David, H. E.; Kuster, W. Zur Kenntnis Homologer Reihen Acylierter Azofarbstoffe Aus O- Und p-Acylamino-Phenolen Und 1,7-Acylamino-Naphtholen. *Helv. Chim. Acta* **1939**, *22* (1), 82–112.

(121) Itoh, T.; Nagata, K.; Miyazaki, M.; Ishikawa, H.; Kurihara, A.; Ohsawa, A. A Selective Reductive Amination of Aldehydes by the Use of Hantzsch Dihydropyridines as Reductant. *Tetrahedron* **2004**, *60* (31), 6649–6655.

Appendix A – Crystal Structure Reports

Sample: 2,3,9,10-tetrakis(3,4-dimethoxyphenyl)benzo[5,6][1,4]dioxino[2,3-b]dibenzo-[b,e][1,4]dioxine-6,13-dicarbonitrile (**2-1c**) (Western Univeristy Sample Code n17105)

X-ray Structure Report

for

Prof. Ken Maly

Prepared by

Louise N. Dawe, PhD

Department of Chemistry and Biochemistry

Wilfrid Laurier University

Science Building

75 University Ave. W.

Waterloo, ON, ON

ldawe@wlu.ca

July 31, 2017

Introduction

Data for this structure was collected by Dr. Paul Boyle at Department of Chemistry X-Ray Facility, Western University.

All H-atoms were introduced in calculated positions and refined on a riding model. Non-hydrogen atoms were refined anisotropically with a global rigid bond (SHELX RIGU) restraint.

Crystals diffracted weakly, with four sources for this problem:

1) Crystals were thin needles.

2) The molecular structure contains only light atoms.

3) The selected crystal was a two component twin, with the second domain related to the first by a rotation of 180 degrees around [0 0 1] (in reciprocal space.)

4) Significant disorder was present outside the main fragment, which could not be modeled. It was therefore treated using the SQUEEZE routine in PLATON (note that this was properly implemented, using SHELX2014, and by first refining with the hklf5 file, with an included BASF instruction, and a LIST 8 instruction.)

While this resulted in a high wR2 for all reflections, the model does not exhibit any notable deficiencies.

Experimental

A single crystal of $C_{52}H_{40}N_2O_{12}$ was selected and collected on a Bruker APEX-II CCD diffractometer. The crystal was kept at 110(2) K during data collection. Using Olex2 [1], the structure was solved with the ShelXT [2] structure solution program using Direct Methods and refined with the ShelXL [3] refinement package using Least Squares minimisation.

1. Dolomanov, O.V., Bourhis, L.J., Gildea, R.J, Howard, J.A.K. & Puschmann, H. (2009), J. Appl. Cryst. 42, 339-341.

2. Sheldrick, G.M. (2015). Acta Cryst. A71, 3-8.

3. Sheldrick, G.M. (2015). Acta Cryst. C71, 3-8.

Crystal structure determination

Crystal Data for $C_{52}H_{40}N_2O_{12}$ (M =884.86 g/mol): triclinic, space group P-1 (no. 2), a = 12.9017(7) Å, b = 15.3041(9) Å, c = 16.4600(10) Å, α = 109.606(5)°, β = 105.890(5)°, γ = 106.544(5)°, V = 2678.1(3) Å3, Z = 2, T = 110(2) K, μ(CuKα) = 0.649 mm^{-1}, Dcalc = 1.097 g/cm^3, 16216 reflections measured (6.742° ≤ 2θ ≤ 127.382°), 16216 unique (9682 with I > 2σ(I)), Rsigma = 0.0626) which were used in all calculations. The final R1 was 0.0945 (I > 2σ(I)) and wR2 was 0.2957 (all data).

Table 1 Crystal data and structure refinement

Identification code	LKH-2-6 (Western: n17105)
Empirical formula	$C_{52}H_{40}N_2O_{12}$
Formula weight	884.86
Temperature/K	110(2)
Crystal system	triclinic
Space group	P-1
a/Å	12.9017(7)
b/Å	15.3041(9)
c/Å	16.4600(10)
α/°	109.606(5)
β/°	105.890(5)
γ/°	106.544(5)
Volume/Å^3	2678.1(3)
Z	2
ρ_{calc}g/cm^3	1.097
μ/mm^{-1}	0.649
F(000)	924.0
Crystal size/mm^3	0.474 × 0.077 × 0.062
Radiation	CuKα (λ = 1.54184)
2Θ range for data collection/°	6.742 to 127.382

Index ranges	$-14 \leq h \leq 14, -17 \leq k \leq 17, -19 \leq l \leq 19$

Reflections collected	16216

Independent reflections	16216 [9682 with $I > 2\sigma(I)$, $R_{sigma} = 0.0626$]

Data/restraints/parameters	16216/504/604

Goodness-of-fit on F^2	1.035

Final R indexes [$I>=2\sigma$ (I)]	$R_1 = 0.0945$, $wR_2 = 0.2477$

Final R indexes [all data]	$R_1 = 0.1526$, $wR_2 = 0.2957$

Largest diff. peak/hole / e $Å^{-3}$ 0.41/-0.31

Table 2 Fractional Atomic Coordinates (×10⁴) and Equivalent Isotropic Displacement Parameters (Å²×10³). U$_{eq}$ is defined as 1/3 of of the trace of the orthogonalised U$_{IJ}$ tensor.

Atom	x	y	z	U(eq)
O1	5587(4)	45(3)	3514(2)	40.1(9)
O2	2651(3)	−1057(3)	4587(2)	36.0(9)
O3	10198(5)	3109(3)	1744(3)	57.0(12)
O4	9421(5)	1477(4)	196(3)	70.7(15)
O5	12811(4)	2254(4)	3584(3)	54.7(12)
O6	13943(4)	3976(3)	5081(3)	46.9(10)
N1	2589(5)	−1352(4)	2373(4)	52.2(14)
C1	4151(5)	−484(4)	4081(4)	32.7(12)
C2	5320(5)	46(4)	4276(4)	34.3(12)
C3	6771(5)	581(4)	3739(4)	34.6(12)
C4	7082(5)	627(4)	3015(4)	38.3(13)
C5	8251(5)	1169(4)	3188(4)	36.9(13)
C6	9129(5)	1679(4)	4120(4)	33.7(12)
C7	8777(5)	1621(4)	4843(4)	34.6(12)
C8	7626(5)	1079(4)	4655(4)	33.8(12)
C9	3819(5)	−529(4)	4813(4)	33.8(12)
C10	8521(5)	1233(5)	2375(4)	41.4(13)

C11	9196(5)	2170(5)	2438(4)	42.3(13)
C12	9508(6)	2232(5)	1713(4)	45.1(14)
C13	9067(7)	1334(5)	876(5)	52.4(16)
C14	8400(7)	420(5)	781(5)	63.1(19)
C15	8105(6)	355(5)	1539(4)	51.4(16)
C16	10409(5)	2284(4)	4398(4)	35.2(12)
C17	10999(5)	1944(4)	3841(4)	37.6(13)
C18	12154(6)	2518(5)	4082(4)	43.4(14)
C19	12801(5)	3464(4)	4911(4)	39.3(13)
C20	12230(5)	3780(4)	5473(4)	39.0(13)
C21	11048(5)	3197(4)	5210(4)	36.3(12)
C22	3269(5)	-977(4)	3126(4)	39.5(13)
C23	10712(9)	4016(5)	2614(6)	74(2)
C24	8934(9)	598(6)	-699(5)	81(3)
C25	12193(8)	1287(7)	2756(6)	81(3)
C26	14654(6)	4871(5)	5969(5)	51.6(16)
O7	2076(3)	1413(3)	6560(3)	39.0(9)
O8	1998(3)	678(3)	4691(3)	37.6(9)
O9	8068(5)	3956(4)	10187(3)	69.5(14)
O10	9208(5)	5768(4)	10368(3)	71.6(15)
O11	9336(4)	3694(3)	6650(3)	43.8(10)

O12	8935(3)	3952(3)	5145(3)	40.6(9)
N2	119(5)	1049(4)	7595(4)	55.2(14)
C27	32(5)	354(4)	5900(4)	33.7(12)
C28	1059(5)	719(4)	5766(4)	34.4(12)
C29	3074(5)	1777(4)	6382(4)	34.7(12)
C30	4102(5)	2500(4)	7136(4)	41.7(13)
C31	5132(5)	2914(4)	7007(4)	37.9(13)
C32	5096(5)	2583(4)	6089(4)	36.1(12)
C33	4015(5)	1835(4)	5340(4)	34.7(12)
C34	3029(5)	1438(4)	5477(4)	33.5(12)
C35	1035(5)	371(4)	4866(4)	33.2(12)
C36	70(5)	736(4)	6842(4)	41.3(14)
C37	6219(6)	3701(4)	7880(4)	42.6(14)
C38	6614(6)	3443(5)	8619(4)	48.1(15)
C39	7612(6)	4149(6)	9438(5)	55.7(16)
C40	8216(6)	5115(5)	9526(4)	54.4(16)
C41	7836(6)	5365(5)	8822(4)	49.1(15)
C42	6808(6)	4645(5)	7985(4)	48.1(15)
C43	6103(5)	2951(4)	5840(4)	35.7(12)
C44	7261(5)	3157(4)	6408(4)	35.9(12)
C45	8175(5)	3488(4)	6156(4)	36.3(12)

C46	7966(5)	3618(4)	5326(4)	34.1(12)
C47	6823(5)	3406(4)	4770(4)	38.4(13)
C48	5914(5)	3090(4)	5031(4)	37.0(12)
C49	7506(8)	2952(7)	10068(6)	82(3)
C50	9860(7)	6739(6)	10445(5)	75(2)
C51	9589(6)	3578(7)	7509(5)	62(2)
C52	8707(6)	3973(5)	4253(4)	42.5(14)

Table 3 Anisotropic Displacement Parameters (Å^2×10^3). The Anisotropic displacement factor exponent takes the form: -2π^2[h^{2}a*^{2}U$_{11}$+2hka*b*U$_{12}$+...].

Atom	U$_{11}$	U$_{22}$	U$_{33}$	U$_{23}$	U$_{13}$	U$_{12}$
O1	37(2)	46(2)	22.6(19)	11.0(17)	11.7(17)	3.8(19)
O2	33(2)	40(2)	27.2(19)	13.4(16)	14.0(17)	6.1(18)
O3	71(3)	45(2)	41(2)	16(2)	28(2)	5(2)
O4	101(4)	56(3)	37(3)	13(2)	38(3)	8(3)
O5	47(3)	69(3)	38(2)	12(2)	24(2)	21(2)
O6	33(2)	48(2)	51(3)	20(2)	18.5(19)	7(2)
N1	44(3)	58(3)	30(3)	13(2)	11(2)	2(3)
C1	36(3)	29(3)	23(2)	10(2)	11(2)	6(2)
C2	40(3)	30(3)	25(3)	8(2)	14(2)	8(3)
C3	36(3)	33(3)	28(3)	11(2)	14(2)	6(3)
C4	43(3)	42(3)	24(3)	13(2)	17(2)	8(3)
C5	41(3)	39(3)	29(3)	14(2)	17(2)	13(3)
C6	40(3)	35(3)	28(3)	15(2)	17(2)	14(3)
C7	37(3)	30(3)	33(3)	14(2)	13(2)	10(3)
C8	41(3)	32(3)	29(3)	14(2)	19(2)	10(3)
C9	34(3)	33(3)	30(3)	12(2)	16(2)	7(3)
C10	35(3)	53(3)	31(3)	18(3)	15(3)	11(3)
C11	40(3)	49(3)	36(3)	19(3)	19(3)	13(3)

C12	51(4)	42(3)	40(3)	20(3)	25(3)	10(3)
C13	66(5)	46(3)	40(3)	20(3)	27(3)	10(3)
C14	82(5)	48(4)	33(3)	4(3)	23(3)	12(4)
C15	52(4)	48(3)	37(3)	12(3)	23(3)	1(3)
C16	37(3)	39(3)	31(3)	20(2)	17(2)	10(3)
C17	36(3)	41(3)	30(3)	14(2)	15(2)	10(3)
C18	47(4)	54(3)	41(3)	25(3)	26(3)	24(3)
C19	31(3)	44(3)	43(3)	22(3)	15(3)	12(3)
C20	30(3)	37(3)	40(3)	12(3)	12(2)	9(3)
C21	38(3)	41(3)	32(3)	16(2)	18(2)	16(3)
C22	38(3)	44(3)	31(3)	16(2)	17(2)	8(3)
C23	108(7)	45(4)	55(4)	13(3)	51(5)	8(4)
C24	117(8)	61(5)	46(4)	9(4)	44(5)	22(5)
C25	64(5)	93(6)	49(4)	−4(4)	35(4)	15(5)
C26	38(4)	50(4)	47(4)	13(3)	10(3)	10(3)
O7	30(2)	40(2)	26.4(19)	7.2(16)	9.8(16)	−1.7(18)
O8	31(2)	34.5(19)	28.7(19)	4.8(16)	13.0(16)	−0.4(17)
O9	63(3)	82(3)	42(3)	35(3)	10(2)	6(3)
O10	55(3)	80(3)	30(2)	16(2)	2(2)	−13(3)
O11	30(2)	56(2)	33(2)	15.5(19)	10.0(17)	10(2)
O12	32(2)	46(2)	42(2)	19.9(19)	19.8(18)	9.7(19)

N2	52(3)	55(3)	34(3)	7(2)	21(3)	2(3)
C27	34(3)	25(3)	25(3)	3(2)	9(2)	3(2)
C28	32(3)	30(3)	27(3)	8(2)	9(2)	3(2)
C29	31(3)	31(3)	35(3)	11(2)	15(2)	7(2)
C30	39(3)	42(3)	27(3)	5(2)	11(2)	9(3)
C31	33(3)	35(3)	29(3)	6(2)	9(2)	5(3)
C32	37(3)	31(3)	34(3)	10(2)	15(2)	10(3)
C33	33(3)	28(3)	29(3)	6(2)	12(2)	5(2)
C34	32(3)	28(3)	29(3)	8(2)	11(2)	5(2)
C35	35(3)	27(3)	30(3)	10(2)	15(2)	7(3)
C36	30(3)	39(3)	36(3)	9(3)	13(3)	−1(3)
C37	39(3)	39(3)	35(3)	6(2)	16(3)	9(3)
C38	43(4)	50(3)	36(3)	15(3)	16(3)	5(3)
C39	46(4)	67(4)	36(3)	20(3)	12(3)	7(3)
C40	48(4)	58(4)	30(3)	12(3)	11(3)	0(3)
C41	47(4)	43(3)	35(3)	9(3)	15(3)	1(3)
C42	40(4)	51(3)	37(3)	12(3)	13(3)	10(3)
C43	34(3)	30(3)	35(3)	9(2)	16(2)	7(3)
C44	32(3)	37(3)	31(3)	13(2)	13(2)	9(3)
C45	29(3)	33(3)	36(3)	10(2)	11(2)	7(3)
C46	31(3)	29(3)	35(3)	9(2)	16(2)	6(2)

C47	39(3)	38(3)	36(3)	17(3)	17(3)	12(3)
C48	25(3)	40(3)	32(3)	12(2)	7(2)	5(3)
C49	79(6)	90(6)	60(5)	50(5)	12(4)	12(5)
C50	56(5)	68(4)	36(4)	9(3)	1(3)	−26(4)
C51	34(4)	101(6)	42(4)	36(4)	10(3)	18(4)
C52	42(4)	45(3)	41(3)	19(3)	21(3)	14(3)

Table 4 Bond Lengths.

Atom	Atom	Length/Å	Atom	Atom	Length/Å
O1	C2	1.388(7)	O7	C28	1.376(7)
O1	C3	1.384(7)	O7	C29	1.400(7)
O2	C8[1]	1.397(6)	O8	C34	1.401(7)
O2	C9	1.363(7)	O8	C35	1.342(7)
O3	C12	1.359(7)	O9	C39	1.377(8)
O3	C23	1.428(8)	O9	C49	1.419(9)
O4	C13	1.377(8)	O10	C40	1.388(8)
O4	C24	1.434(8)	O10	C50	1.427(9)
O5	C18	1.381(7)	O11	C45	1.378(7)
O5	C25	1.436(9)	O11	C51	1.444(8)
O6	C19	1.354(7)	O12	C46	1.362(7)
O6	C26	1.435(8)	O12	C52	1.430(7)
N1	C22	1.130(8)	N2	C36	1.145(8)
C1	C2	1.377(8)	C27	C28	1.391(8)
C1	C9	1.401(8)	C27	C35[2]	1.399(8)
C1	C22	1.439(8)	C27	C36	1.442(8)
C2	C9[1]	1.380(8)	C28	C35	1.385(8)
C3	C4	1.374(8)	C29	C30	1.365(8)
C3	C8	1.383(8)	C29	C34	1.382(8)

C4	C5	1.391(9)	C30	C31	1.406(9)
C5	C6	1.410(8)	C31	C32	1.405(8)
C5	C10	1.498(8)	C31	C37	1.502(8)
C6	C7	1.406(8)	C32	C33	1.406(8)
C6	C16	1.493(8)	C32	C43	1.484(8)
C7	C8	1.365(8)	C33	C34	1.360(8)
C10	C11	1.402(9)	C37	C38	1.413(9)
C10	C15	1.389(9)	C37	C42	1.353(9)
C11	C12	1.382(9)	C38	C39	1.387(9)
C12	C13	1.402(9)	C39	C40	1.397(10)
C13	C14	1.347(10)	C40	C41	1.350(9)
C14	C15	1.427(10)	C41	C42	1.422(9)
C16	C17	1.405(8)	C43	C44	1.404(8)
C16	C21	1.381(8)	C43	C48	1.385(8)
C17	C18	1.359(9)	C44	C45	1.374(8)
C18	C19	1.420(9)	C45	C46	1.411(8)
C19	C20	1.381(8)	C46	C47	1.382(8)
C20	C21	1.384(9)	C47	C48	1.374(8)

[1]1-X,-Y,1-Z; [2]-X,-Y,1-Z

Table 5 Bond Angles.

Atom	Atom	Atom	Angle/°	Atom	Atom	Atom	Angle/°
C3	O1	C2	115.2(4)	C28	O7	C29	114.8(4)
C9	O2	C8[1]	115.4(4)	C35	O8	C34	115.5(4)
C12	O3	C23	117.4(5)	C39	O9	C49	116.6(6)
C13	O4	C24	116.3(6)	C40	O10	C50	115.7(5)
C18	O5	C25	115.4(5)	C45	O11	C51	116.1(5)
C19	O6	C26	117.0(5)	C46	O12	C52	115.9(4)
C2	C1	C9	120.1(5)	C28	C27	C35[2]	120.9(5)
C2	C1	C22	119.9(5)	C28	C27	C36	119.4(5)
C9	C1	C22	120.0(5)	C35[2]	C27	C36	119.7(5)
C1	C2	O1	116.9(5)	O7	C28	C27	117.2(5)
C1	C2	C9[1]	121.0(5)	O7	C28	C35	122.6(5)
C9[1]	C2	O1	122.1(5)	C35	C28	C27	120.2(5)
C4	C3	O1	117.7(5)	C30	C29	O7	117.8(5)
C4	C3	C8	119.9(5)	C30	C29	C34	120.4(5)
C8	C3	O1	122.4(5)	C34	C29	O7	121.8(5)
C3	C4	C5	121.0(5)	C29	C30	C31	120.8(5)
C4	C5	C6	119.5(5)	C30	C31	C37	116.8(5)
C4	C5	C10	118.4(5)	C32	C31	C30	119.4(5)
C6	C5	C10	122.1(5)	C32	C31	C37	123.8(5)

C5	C6	C16	124.7(5)	C31	C32	C33	117.3(5)
C7	C6	C5	117.9(5)	C31	C32	C43	125.7(5)
C7	C6	C16	117.4(5)	C33	C32	C43	117.0(5)
C8	C7	C6	121.5(5)	C34	C33	C32	122.5(5)
C3	C8	O2[1]	121.9(5)	C29	C34	O8	121.9(5)
C7	C8	O2[1]	118.0(5)	C33	C34	O8	118.6(5)
C7	C8	C3	120.1(5)	C33	C34	C29	119.5(5)
O2	C9	C1	118.0(5)	O8	C35	C27[2]	118.0(5)
O2	C9	C2[1]	123.1(5)	O8	C35	C28	123.1(5)
C2[1]	C9	C1	119.0(5)	C28	C35	C27[2]	118.9(5)
C11	C10	C5	121.2(5)	N2	C36	C27	178.9(7)
C15	C10	C5	120.2(6)	C38	C37	C31	118.2(6)
C15	C10	C11	118.6(6)	C42	C37	C31	122.3(6)
C12	C11	C10	121.7(6)	C42	C37	C38	119.5(6)
O3	C12	C11	124.7(6)	C39	C38	C37	120.0(6)
O3	C12	C13	117.1(5)	O9	C39	C38	123.8(7)
C11	C12	C13	118.3(6)	O9	C39	C40	116.7(6)
O4	C13	C12	113.8(6)	C38	C39	C40	119.5(6)
C14	C13	O4	124.3(6)	O10	C40	C39	115.4(6)
C14	C13	C12	121.8(6)	C41	C40	O10	124.0(6)
C13	C14	C15	119.8(6)	C41	C40	C39	120.6(6)

C10	C15	C14	119.7(6)	C40	C41	C42	120.0(6)
C17	C16	C6	121.2(5)	C37	C42	C41	120.4(6)
C21	C16	C6	120.7(5)	C44	C43	C32	121.2(5)
C21	C16	C17	118.1(5)	C48	C43	C32	120.2(5)
C18	C17	C16	120.7(5)	C48	C43	C44	118.6(5)
O5	C18	C19	113.9(6)	C45	C44	C43	120.0(5)
C17	C18	O5	125.1(6)	O11	C45	C46	114.4(5)
C17	C18	C19	120.9(5)	C44	C45	O11	124.8(5)
O6	C19	C18	116.0(5)	C44	C45	C46	120.8(5)
O6	C19	C20	125.7(5)	O12	C46	C45	116.0(5)
C20	C19	C18	118.3(5)	O12	C46	C47	125.3(5)
C19	C20	C21	120.2(5)	C47	C46	C45	118.7(5)
C16	C21	C20	121.8(5)	C48	C47	C46	120.4(5)
N1	C22	C1	178.8(7)	C47	C48	C43	121.6(5)

[1]1-X,-Y,1-Z; [2]-X,-Y,1-Z

Table 6 Hydrogen Atom Coordinates (Å×10⁴) and Isotropic Displacement Parameters (Å²×10³).

Atom	x	y	z	U(eq)
H4	6502.96	291.06	2400	46
H7	9340.58	1959.02	5464.13	42
H11	9439.64	2765.16	2981.18	51
H14	8133.31	−165.8	222.49	76
H15	7635.39	−272.76	1474.07	62
H17	10594.95	1319.6	3303.19	45
H20	12642.12	4385.66	6030.06	47
H21	10672.69	3427.14	5590.07	44
H23A	11131.13	4587.34	2533.7	111
H23B	11252.99	3945.78	3094.53	111
H23C	10097.91	4124.83	2799.02	111
H24A	9252.42	777.61	−1112.47	121
H24B	8087.41	359.37	−974.3	121
H24C	9134.7	69.79	−609.83	121
H25A	11542.09	1299.89	2313.04	121
H25B	11898.5	757.9	2930.02	121
H25C	12725.49	1156.79	2472.05	121
H26A	14314.71	5359.05	6011.66	77

H26B	15443.12	5162.94	6012.48	77
H26C	14678.38	4689.68	6476.32	77
H30	4121.11	2721.04	7741.72	50
H33	3973.85	1602.7	4727.42	42
H38	6204.5	2799.77	8556.93	58
H41	8247.55	6008.21	8884.53	59
H42	6539.06	4824.3	7506.05	58
H44	7408.01	3068.32	6953.6	43
H47	6667.29	3477.08	4214.73	46
H48	5152.67	2967.41	4656.54	44
H49A	7564.47	2477.14	9545.55	123
H49B	6685.9	2791.41	9946.04	123
H49C	7885.75	2907.17	10633.2	123
H50A	9971	6650.23	9873.84	113
H50B	10617.41	7066.17	10969.68	113
H50C	9428.47	7154.87	10542.68	113
H51A	9108.98	2894.21	7367.15	93
H51B	9415.55	4049.93	7946.81	93
H51C	10411.18	3713.93	7784.58	93
H52A	8147.51	3310.97	3755.26	64
H52B	9432.61	4157.48	4168.77	64

H52C	8388.03	4465.14	4235.33	64

Sample: benzo[5,6][1,4]dioxino[2,3-b]dibenzo[b,e][1,4]dioxine-6,13-dicarbonitrile

(DCTOP, **3.39**) n19007 (LKH-4-126)

<div align="center">

X-ray Structure Report

Louise N. Dawe, PhD

Department of Chemistry and Biochemistry

Wilfrid Laurier University

Science Building

75 University Ave. W.

Waterloo, ON, ON

ldawe@wlu.ca

June 29, 2018

Introduction

</div>

Data for this structure was collected by Dr. Paul D. Boyle, Western University

All hydrogen atoms were introduced in calculated positions and refined on a riding model.

All non-hydrogen atoms were refined anisotropically.

Experimental

A single crystal of $C_{20}H_8N_2O_4$ was selected and collected on a Nonius diffractometer. The crystal was kept at 110(2) K during data collection. Using Olex2 [1], the structure was solved with the ShelXT [2] structure solution program using Intrinsic Phasing and refined with the ShelXL [3] refinement package using Least Squares minimisation.

1. Dolomanov, O.V., Bourhis, L.J., Gildea, R.J, Howard, J.A.K. & Puschmann, H. (2009), J. Appl. Cryst. 42, 339-341.

2. Sheldrick, G.M. (2015). Acta Cryst. A71, 3-8.

3. Sheldrick, G.M. (2015). Acta Cryst. C71, 3-8.

Crystal structure determination

Crystal Data for $C_{20}H_8N_2O_4$ (M =340.28 g/mol): orthorhombic, space group Pbca (no. 61), $a =$ 7.15370(10) Å, $b =$ 19.3801(3) Å, $c =$ 20.9999(4) Å, $V =$ 2911.41(8) Å^3, $Z =$ 8, $T =$ 110(2) K, μ(CuKα) = 0.925 mm^{-1}, $Dcalc$ = 1.553 g/cm^3, 52409 reflections measured (8.422° ≤ 2θ ≤ 135.15°), 2604 unique (2522 with I > 2σ(I); R_{int} = 0.0736, R_{sigma} = 0.0168) which were used in all calculations. The final R_1 was 0.0671 (I > 2σ(I)) and wR_2 was 0.1511 (all data).

Table 1 Crystal data and structure refinement

Identification code	n19007 (LKH-4-126)
Empirical formula	$C_{20}H_8N_2O_4$
Formula weight	340.28
Temperature/K	110(2)
Crystal system	orthorhombic
Space group	Pbca
a/Å	7.15370(10)
b/Å	19.3801(3)
c/Å	20.9999(4)
α/°	90
β/°	90
γ/°	90
Volume/Å^3	2911.41(8)
Z	8
ρ_{calc}g/cm^3	1.553
μ/mm^{-1}	0.925
F(000)	1392.0
Crystal size/mm^3	0.405 × 0.139 × 0.101
Radiation	CuKα (λ = 1.54184)
2Θ range for data collection/°	8.422 to 135.15

Index ranges $-6 \leq h \leq 8, -23 \leq k \leq 22, -24 \leq l \leq 24$

Reflections collected   52409

Independent reflections   2604 [2522 with $I > 2\sigma(I)$; $R_{int} = 0.0736$, $R_{sigma} = 0.0168$]

Data/restraints/parameters 2604/0/235

Goodness-of-fit on F^2 1.363

Final R indexes [I>=2σ (I)] $R_1 = 0.0671$, $wR_2 = 0.1500$

Final R indexes [all data] $R_1 = 0.0694$, $wR_2 = 0.1511$

Largest diff. peak/hole / e Å^{-3} 0.30/-0.26

Table 2 Fractional Atomic Coordinates (×10⁴) and Equivalent Isotropic Displacement Parameters (Å²×10³). U$_{eq}$ is defined as 1/3 of of the trace of the orthogonalised U$_{IJ}$ tensor.

Atom	x	y	z	U(eq)
O1	5026(3)	2343.2(9)	6620.7(8)	28.5(5)
O2	6312(3)	3261.8(9)	7594.1(8)	29.8(5)
O3	7716(3)	4936.5(9)	6034.5(8)	25.9(4)
O4	6408(3)	4027.7(9)	5060.2(8)	27.0(4)
N1	4307(3)	2407.7(11)	4994.5(11)	31.3(5)
N2	8344(4)	4887.8(11)	7666.4(10)	30.7(6)
C1	5743(4)	3197.6(12)	5857.5(12)	23.5(6)
C2	5707(4)	2988.3(12)	6491.9(12)	25.0(6)
C3	4938(4)	2170.8(13)	7263.4(12)	25.2(6)
C4	4233(4)	1529.7(13)	7420.9(13)	27.7(6)
C5	4127(4)	1340.1(13)	8056.2(13)	29.9(6)
C6	4701(4)	1790.2(13)	8530.0(13)	31.4(6)
C7	5409(4)	2431.9(13)	8365.7(13)	28.2(6)
C8	5535(4)	2616.6(13)	7738.4(13)	26.5(6)
C9	6346(4)	3427.8(12)	6962.1(12)	23.5(6)
C10	7056(4)	4074.4(12)	6794.3(12)	23.0(6)
C11	7079(4)	4285.0(12)	6160.3(12)	24.4(6)

C12	7737(4)	5124.4(13)	5396.4(12)	24.4(6)
C13	8423(4)	5768.9(13)	5245.4(12)	26.0(6)
C14	8495(4)	5970.8(13)	4611.8(13)	27.5(6)
C15	7866(4)	5532.2(13)	4135.9(13)	28.2(6)
C16	7161(4)	4880.7(13)	4291.9(12)	26.5(6)
C17	7107(4)	4685.4(13)	4917.9(12)	25.2(6)
C18	6443(4)	3847.0(13)	5689.2(12)	24.2(6)
C19	4972(4)	2754.1(13)	5374.6(12)	24.9(6)
C20	7763(4)	4528.6(12)	7279.7(12)	23.7(6)

Table 3 Anisotropic Displacement Parameters ($Å^2 \times 10^3$). The Anisotropic displacement factor exponent takes the form: $-2\pi^2[h^2a^{*2}U_{11}+2hka^*b^*U_{12}+...]$.

Atom	U_{11}	U_{22}	U_{33}	U_{23}	U_{13}	U_{12}
O1	41.7(11)	17.8(9)	26.0(10)	0.6(7)	−0.8(8)	−5.8(8)
O2	47.3(12)	18.7(9)	23.5(9)	1.6(7)	0.0(8)	−7.0(8)
O3	39.3(11)	15.0(8)	23.4(9)	0.9(7)	0.4(8)	−3.7(7)
O4	40.5(11)	18.7(9)	21.8(9)	−0.1(7)	0.5(8)	−3.1(8)
N1	39.5(14)	22.2(11)	32.3(12)	−4.2(10)	−4.7(11)	0.4(10)
N2	44.7(14)	21.7(11)	25.8(12)	0.3(9)	−2.2(10)	−2.9(10)
C1	27.0(13)	16.9(12)	26.5(13)	−4.4(10)	−0.9(11)	1.6(10)
C2	29.3(14)	15.2(12)	30.4(14)	−0.4(10)	2.8(11)	0.3(10)
C3	27.6(14)	19.9(12)	28.1(13)	3.6(10)	−0.8(11)	2.9(11)
C4	30.0(14)	19.0(12)	33.9(14)	−1.7(11)	0.5(12)	0.5(11)
C5	36.0(15)	16.8(12)	36.8(15)	4.2(11)	0.6(12)	−0.9(11)
C6	41.8(16)	23.9(13)	28.6(14)	3.4(11)	4.6(12)	2.8(12)
C7	35.6(15)	20.2(13)	28.8(14)	−0.8(10)	1.5(11)	2.0(11)
C8	30.8(14)	16.2(12)	32.4(14)	1.6(10)	1.4(11)	1.0(10)
C9	26.3(13)	19.0(12)	25.2(13)	0.0(10)	0.9(10)	2.4(10)
C10	27.7(14)	17.6(12)	23.9(13)	−0.8(10)	−0.2(11)	2.3(10)
C11	27.9(14)	16.1(12)	29.1(14)	−1.2(10)	2.4(11)	1.7(10)
C12	27.8(14)	23.2(13)	22.3(12)	−0.7(10)	2.2(11)	4.3(11)

C13	29.3(14)	18.9(12)	30.0(14)	-1.5(10)	2.0(11)	1.0(11)
C14	31.2(14)	19.9(12)	31.6(14)	5.1(11)	1.5(11)	1.7(11)
C15	33.1(15)	26.6(13)	24.8(13)	3.9(11)	2.6(11)	3.4(11)
C16	29.9(14)	22.0(13)	27.5(14)	-2.1(10)	-2.2(11)	2.1(11)
C17	26.7(14)	17.6(12)	31.1(14)	0.5(10)	1.3(11)	2.0(10)
C18	28.2(14)	19.4(12)	25.1(13)	-0.3(10)	1.5(11)	4.6(10)
C19	30.9(14)	17.6(12)	26.3(13)	2.1(10)	0.4(11)	2.9(11)
C20	30.9(14)	15.3(11)	24.9(13)	3.9(10)	-1.0(11)	-1.0(10)

Table 4 Bond Lengths.

Atom	Atom	Length/Å	Atom	Atom	Length/Å
O1	C2	1.369(3)	C3	C8	1.387(4)
O1	C3	1.392(3)	C4	C5	1.386(4)
O2	C8	1.402(3)	C5	C6	1.385(4)
O2	C9	1.366(3)	C6	C7	1.386(4)
O3	C11	1.368(3)	C7	C8	1.368(4)
O3	C12	1.389(3)	C9	C10	1.397(4)
O4	C17	1.402(3)	C10	C11	1.393(4)
O4	C18	1.367(3)	C10	C20	1.439(3)
N1	C19	1.146(3)	C11	C18	1.381(4)
N2	C20	1.147(3)	C12	C13	1.379(4)
C1	C2	1.393(4)	C12	C17	1.392(4)
C1	C18	1.400(4)	C13	C14	1.388(4)
C1	C19	1.439(4)	C14	C15	1.387(4)
C2	C9	1.382(4)	C15	C16	1.399(4)
C3	C4	1.381(4)	C16	C17	1.369(4)

Table 5 Bond Angles.

Atom	Atom	Atom	Angle/°	Atom	Atom	Atom	Angle/°
C2	O1	C3	115.3(2)	C2	C9	C10	119.5(2)
C9	O2	C8	115.3(2)	C9	C10	C20	119.9(2)
C11	O3	C12	115.60(19)	C11	C10	C9	120.5(2)
C18	O4	C17	115.6(2)	C11	C10	C20	119.6(2)
C2	C1	C18	120.7(2)	O3	C11	C10	117.3(2)
C2	C1	C19	119.5(2)	O3	C11	C18	122.6(2)
C18	C1	C19	119.7(2)	C18	C11	C10	120.1(2)
O1	C2	C1	117.5(2)	O3	C12	C17	122.2(2)
O1	C2	C9	122.6(2)	C13	C12	O3	117.6(2)
C9	C2	C1	119.9(2)	C13	C12	C17	120.2(2)
C4	C3	O1	117.7(2)	C12	C13	C14	119.3(2)
C4	C3	C8	120.0(2)	C15	C14	C13	120.4(2)
C8	C3	O1	122.3(2)	C14	C15	C16	120.1(2)
C3	C4	C5	119.3(2)	C17	C16	C15	119.0(2)
C6	C5	C4	120.5(2)	C12	C17	O4	121.2(2)
C5	C6	C7	119.6(3)	C16	C17	O4	117.8(2)
C8	C7	C6	119.9(3)	C16	C17	C12	121.0(2)
C3	C8	O2	121.5(2)	O4	C18	C1	117.9(2)
C7	C8	O2	117.9(2)	O4	C18	C11	122.8(2)

C7	C8	C3	120.6(2)	C11	C18	C1	119.3(2)
O2	C9	C2	122.9(2)	N1	C19	C1	178.0(3)
O2	C9	C10	117.6(2)	N2	C20	C10	179.3(3)

Table 6 Hydrogen Atom Coordinates (Å×10⁴) and Isotropic Displacement Parameters (Å²×10³).

Atom	x	y	z	U(eq)
H4	3824.23	1222.17	7097.26	33
H5	3656.84	897.92	8167.77	36
H6	4610.75	1659.86	8964.95	38
H7	5806.95	2742.85	8688.11	34
H13	8842.06	6071.42	5571.54	31
H14	8977.63	6412.12	4503.44	33
H15	7915.24	5674.46	3703.31	34
H16	6725.84	4578.32	3968.14	32

Sample: 2-(2-aminophenoxy)-3-fluoro-10H-phenoxazine-1,4-dicarbonitrile   (**3.22**)

(Western Univeristy Sample Code b18201)

X-ray Structure Report

Prepared by

Louise N. Dawe, PhD

Department of Chemistry and Biochemistry

Wilfrid Laurier University

Science Building

75 University Ave. W.

Waterloo, ON, ON

ldawe@wlu.ca

February 6, 2018

<u>Introduction</u>

Data for this structure was collected by Dr. Paul Boyle at Department of Chemistry X-Ray Facility, Western University.

194

N-H hydrogen atoms were introduced in difference map positions, and refined isotropically. All other H-atoms were introduced in calculated positions and refined on a riding model. Non-hydrogen atoms were refined anisotropically.

Experimental

A single crystal of $C_{20}H_{11}FN_4O_2$ was selected and collected on a Bruker APEX-II CCD diffractometer. The crystal was kept at 110(2) K during data collection. Using Olex2 [1], the structure was solved with the ShelXT [2] structure solution program using Intrinsic Phasing and refined with the ShelXL [3] refinement package using Least Squares minimisation.

1. Dolomanov, O.V., Bourhis, L.J., Gildea, R.J, Howard, J.A.K. & Puschmann, H. (2009), J. Appl. Cryst. 42, 339-341.

2. Sheldrick, G.M. (2015). Acta Cryst. A71, 3-8.

3. Sheldrick, G.M. (2015). Acta Cryst. C71, 3-8.

Crystal structure determination

Crystal Data for $C_{20}H_{11}FN_4O_2$ (M =358.33 g/mol): monoclinic, space group P2$_1$/n (no. 14), $a =$ 4.5752(12) Å, $b =$ 22.619(6) Å, $c =$ 15.627(5) Å, $\beta =$ 96.157(10)°, $V =$ 1607.9(8) Å^3, $Z =$ 4, $T =$ 110(2) K, μ(MoKα) = 0.107 mm^{-1}, $Dcalc =$ 1.480 g/cm^3, 85634 reflections measured (4.454° ≤ 2Θ ≤ 52.736°), 3293 unique (2783 with I > 2σ(I); $R_{int} =$ 0.0351, R$_{sigma}$ = 0.0126) which were used in all calculations. The final R_1 was 0.0322 (I > 2σ(I)) and wR_2 was 0.0914 (all data).

Table 1 Crystal data and structure refinement

Identification code	LKH-5-10 (Western b18201)
Empirical formula	$C_{20}H_{11}FN_4O_2$
Formula weight	358.33
Temperature/K	273.15
Crystal system	monoclinic
Space group	$P2_1/n$
a/Å	4.5752(12)
b/Å	22.619(6)
c/Å	15.627(5)
α/°	90
β/°	96.157(10)
γ/°	90
Volume/Å^3	1607.9(8)
Z	4
ρ_{calc}g/cm^3	1.480
μ/mm^{-1}	0.107
F(000)	736.0
Crystal size/mm^3	0.63 × 0.078 × 0.071
Radiation	MoKα (λ = 0.71073)
2Θ range for data collection/°	4.454 to 52.736

Index ranges $-5 \leq h \leq 5, -28 \leq k \leq 28, -19 \leq l \leq 19$

Reflections collected   85634

Independent reflections   3293 [R_{int} = 0.0351, R_{sigma} = 0.0126]

Data/restraints/parameters   3293/0/256

Goodness-of-fit on F^2 1.026

Final R indexes [I>=2σ (I)] R_1 = 0.0322, wR_2 = 0.0850

Final R indexes [all data] R_1 = 0.0409, wR_2 = 0.0914

Largest diff. peak/hole / e $Å^{-3}$ 0.22/-0.22

Table 2 Fractional Atomic Coordinates (×10⁴) and Equivalent Isotropic Displacement Parameters (Å²×10³). U_{eq} is defined as 1/3 of of the trace of the orthogonalised U_{IJ} tensor.

Atom	x	y	z	U(eq)
F2	−2779.1(16)	6469.0(3)	7707.4(4)	23.40(18)
O1	2846.1(18)	7389.9(3)	5737.0(5)	20.0(2)
O2	−1291.5(18)	5361.3(3)	7164.2(5)	20.7(2)
N1	4561(2)	6294.5(4)	5127.8(7)	20.1(2)
N3	3068(2)	4778.4(4)	5672.3(7)	23.9(2)
N4	−1904(3)	4170.2(5)	7072.0(7)	24.2(2)
N2	−1719(2)	7937.6(4)	7175.1(7)	25.4(2)
C3	62(2)	6919.8(5)	6709.8(7)	16.4(2)
C4	1926(3)	6875.2(5)	6069.4(7)	16.0(2)
C13	−894(3)	7489.0(5)	6970.9(8)	18.2(2)
C16	154(3)	4411.9(5)	7688.2(8)	19.9(3)
C2	−959(3)	6407.0(5)	7088.3(7)	18.0(2)
C5	4762(3)	7356.4(5)	5095.1(7)	17.8(2)
C15	665(3)	5019.0(5)	7723.0(7)	18.9(3)
C10	5608(3)	6814.1(5)	4783.0(7)	17.9(2)
C12	1709(3)	5818.1(5)	6168.5(8)	17.2(2)
C1	−158(3)	5860.7(5)	6831.6(8)	17.9(2)

C11	2776(3)	6318.7(5)	5775.1(7)	16.7(2)
C6	5764(3)	7882.5(5)	4794.4(8)	22.1(3)
C20	2826(3)	5271.7(5)	8287.6(8)	24.3(3)
C9	7519(3)	6805.7(5)	4147.8(8)	21.0(3)
C14	2469(3)	5240.1(5)	5895.8(8)	18.4(3)
C7	7675(3)	7869.0(6)	4158.5(8)	24.9(3)
C8	8541(3)	7332.9(6)	3839.6(8)	24.5(3)
C17	1915(3)	4063.6(6)	8274.2(9)	26.3(3)
C19	4570(3)	4914.2(6)	8854.7(9)	30.1(3)
C18	4076(3)	4310.4(6)	8845.9(9)	31.1(3)

Table 3 Anisotropic Displacement Parameters ($Å^2 \times 10^3$). The Anisotropic displacement factor exponent takes the form: $-2\pi^2[h^2a^{*2}U_{11}+2hka^*b^*U_{12}+...]$.

Atom	U_{11}	U_{22}	U_{33}	U_{23}	U_{13}	U_{12}
F2	27.6(4)	17.9(4)	27.3(4)	−2.1(3)	15.1(3)	−0.1(3)
O1	26.1(5)	11.7(4)	24.0(4)	0.8(3)	10.8(4)	0.8(3)
O2	22.1(4)	12.3(4)	28.1(5)	3.4(3)	5.2(4)	−1.7(3)
N1	26.9(6)	12.3(5)	22.7(5)	−1.3(4)	10.3(4)	3.0(4)
N3	31.6(6)	14.5(5)	27.0(6)	−0.4(4)	9.1(5)	2.8(4)
N4	29.9(6)	13.5(5)	29.7(6)	2.7(4)	5.4(5)	−3.7(5)
N2	32.1(6)	16.0(5)	29.4(6)	−3.6(4)	9.2(5)	3.2(4)
C3	18.0(6)	12.4(5)	18.7(6)	−2.1(4)	1.7(5)	1.1(4)
C4	17.9(6)	11.2(5)	18.6(6)	0.9(4)	0.8(5)	0.4(4)
C13	19.9(6)	16.1(6)	19.3(6)	0.3(5)	4.8(5)	−1.3(5)
C16	23.2(6)	16.1(5)	22.3(6)	1.4(5)	11.2(5)	0.0(5)
C2	18.4(6)	17.5(6)	19.1(6)	−1.4(4)	6.1(5)	0.4(4)
C5	17.2(6)	18.8(6)	17.7(6)	1.5(4)	3.6(5)	1.3(4)
C15	22.0(6)	15.9(6)	20.2(6)	2.1(4)	9.2(5)	1.6(4)
C10	18.2(6)	17.2(6)	17.9(6)	0.9(4)	0.9(5)	0.8(4)
C12	18.9(6)	11.9(5)	20.7(6)	−2.1(4)	2.0(5)	1.9(4)
C1	19.8(6)	12.3(5)	21.8(6)	1.2(4)	2.9(5)	−1.8(4)
C11	17.4(6)	15.7(6)	17.1(5)	−1.2(4)	2.4(4)	2.2(4)

C6	23.1(6)	17.1(6)	26.1(6)	2.1(5)	2.8(5)	0.0(5)
C20	28.8(7)	21.7(6)	23.7(6)	−1.1(5)	9.2(5)	−4.1(5)
C9	20.9(6)	23.6(6)	18.7(6)	−1.3(5)	2.6(5)	2.8(5)
C14	20.9(6)	15.3(6)	19.6(6)	2.3(4)	4.8(5)	−0.1(4)
C7	24.6(6)	24.0(6)	26.5(7)	7.3(5)	4.4(5)	−4.0(5)
C8	22.4(6)	31.4(7)	20.1(6)	3.2(5)	4.6(5)	−0.7(5)
C17	29.0(7)	20.0(6)	31.8(7)	7.6(5)	11.5(6)	3.1(5)
C19	28.3(7)	39.3(8)	22.8(6)	2.8(6)	3.2(5)	−5.5(6)
C18	28.3(7)	36.2(8)	29.6(7)	13.2(6)	6.3(6)	4.6(6)

Table 4 Bond Lengths

Atom	Atom	Length/Å	Atom	Atom	Length/Å
F2	C2	1.3497(13)	C16	C17	1.3962(18)
O1	C4	1.3598(13)	C2	C1	1.3615(16)
O1	C5	1.4031(14)	C5	C10	1.3904(16)
O2	C15	1.4126(15)	C5	C6	1.3759(16)
O2	C1	1.3686(14)	C15	C20	1.3769(18)
N1	C10	1.3988(15)	C10	C9	1.3916(17)
N1	C11	1.3675(15)	C12	C1	1.4151(17)
N3	C14	1.1436(15)	C12	C11	1.4011(16)
N4	C16	1.3851(17)	C12	C14	1.4296(15)
N2	C13	1.1401(15)	C6	C7	1.3928(18)
C3	C4	1.3865(16)	C20	C19	1.3873(19)
C3	C13	1.4330(16)	C9	C8	1.3859(18)
C3	C2	1.4047(16)	C7	C8	1.3849(18)
C4	C11	1.4091(16)	C17	C18	1.378(2)
C16	C15	1.3929(17)	C19	C18	1.384(2)

Table 5 Bond Angles

Atom	Atom	Atom	Angle/°	Atom	Atom	Atom	Angle/°
C4	O1	C5	118.00(9)	C5	C10	N1	119.09(11)
C1	O2	C15	116.51(9)	C5	C10	C9	118.84(11)
C11	N1	C10	120.52(10)	C9	C10	N1	122.06(10)
C4	C3	C13	120.07(10)	C1	C12	C14	117.77(10)
C4	C3	C2	120.13(10)	C11	C12	C1	122.16(10)
C2	C3	C13	119.78(10)	C11	C12	C14	120.07(11)
O1	C4	C3	116.93(10)	O2	C1	C12	120.33(10)
O1	C4	C11	122.19(10)	C2	C1	O2	120.81(11)
C3	C4	C11	120.88(10)	C2	C1	C12	118.71(10)
N2	C13	C3	178.44(13)	N1	C11	C4	118.99(10)
N4	C16	C15	120.98(11)	N1	C11	C12	123.78(10)
N4	C16	C17	122.32(11)	C12	C11	C4	117.23(11)
C15	C16	C17	116.62(12)	C5	C6	C7	118.85(11)
F2	C2	C3	118.33(10)	C15	C20	C19	119.46(12)
F2	C2	C1	120.79(10)	C8	C9	C10	119.81(11)
C1	C2	C3	120.88(11)	N3	C14	C12	179.54(14)
C10	C5	O1	121.15(10)	C8	C7	C6	120.10(11)
C6	C5	O1	117.00(10)	C7	C8	C9	120.56(12)
C6	C5	C10	121.85(11)	C18	C17	C16	121.34(12)

C16	C15	O2	115.08(11)	C18	C19	C20	119.12(13)
C20	C15	O2	122.17(10)	C17	C18	C19	120.75(12)
C20	C15	C16	122.69(11)				

Table 6 Hydrogen Atom Coordinates (Å×10⁴) and Isotropic Displacement Parameters (Å²×10³)

Atom	x	y	z	U(eq)
H6	5162.18	8248.59	5016.74	26
H20	3119.69	5687.49	8288.8	29
H9	8122.12	6439.54	3925.98	25
H7	8386.2	8228.17	3943.06	30
H8	9845.37	7326.5	3406	29
H17	1616.05	3648.06	8278.77	32
H19	6083.91	5081.62	9243.92	36
H18	5240.97	4063.39	9238.53	37
H4A	-2620(30)	3820(7)	7242(10)	32(4)
H4B	-3360(40)	4413(8)	6858(10)	36(4)
H1	5030(30)	5954(7)	4915(10)	32(4)

Sample: 2,3-difluoro-10H-phenoxazine-1,4-dicarbonitrile (**3.23**): (Western Univeristy Sample Code b18202)

X-ray Structure Report

Prepared by

Louise N. Dawe, PhD

Department of Chemistry and Biochemistry

Wilfrid Laurier University

Science Building

75 University Ave. W.

Waterloo, ON, ON

ldawe@wlu.ca

February 6, 2018

<u>Introduction</u>

Data for this structure was collected by Dr. Paul Boyle at Department of Chemistry X-Ray Facility, Western University.

The N-H hydrogen atom was introduced in its difference map position and refined isotropically. All other H-atoms were introduced in calculated positions and refined on a riding model. Non-hydrogen atoms were refined anisotropically.

Experimental

A single crystal of $C_{16}H_{11}F_2N_3O_2S$ was selected and collected on a Bruker APEX-II CCD diffractometer. The crystal was kept at 110(2) K during data collection. Using Olex2 [1], the structure was solved with the ShelXT [2] structure solution program using Intrinsic Phasing and refined with the ShelXL [3] refinement package using Least Squares minimisation.

4. Dolomanov, O.V., Bourhis, L.J., Gildea, R.J, Howard, J.A.K. & Puschmann, H. (2009), J. Appl. Cryst. 42, 339-341.

5. Sheldrick, G.M. (2015). Acta Cryst. A71, 3-8.

6. Sheldrick, G.M. (2015). Acta Cryst. C71, 3-8.

Crystal structure determination

Crystal Data for $C_{16}H_{11}F_2N_3O_2S$ (M =347.34 g/mol): triclinic, space group P-1 (no. 2), a = 6.840(2) Å, b = 10.791(5) Å, c = 10.962(4) Å, α = 78.435(16)°, β = 73.804(10)°, γ = 84.616(9)°, V = 760.6(5) Å^3, Z = 2, T = 109.98 K, μ(MoKα) = 0.250 mm^{-1}, $Dcalc$ = 1.517 g/cm^3, 42045 reflections measured (4.982° ≤ 2Θ ≤ 57.39°), 3935 unique (3352 with I > 2σ(I); R_{int} = 0.0462, R_{sigma} = 0.0264) which were used in all calculations. The final R_1 was 0.0336 (I > 2σ(I)) and wR_2 was 0.0905 (all data).

Table 1 Crystal data and structure refinement

Identification code	LKH-5-12 (Western b18202)
Empirical formula	$C_{16}H_{11}F_2N_3O_2S$
Formula weight	347.34
Temperature/K	109.98
Crystal system	triclinic
Space group	P-1
a/Å	6.840(2)
b/Å	10.791(5)
c/Å	10.962(4)
α/°	78.435(16)
β/°	73.804(10)
γ/°	84.616(9)
Volume/Å^3	760.6(5)
Z	2
ρ_{calc}g/cm^3	1.517
μ/mm^{-1}	0.250
F(000)	356.0
Crystal size/mm^3	0.355 × 0.122 × 0.053
Radiation	MoKα (λ = 0.71073)

2θ range for data collection/° 4.982 to 57.39

Index ranges $-9 \leq h \leq 9, -14 \leq k \leq 14, -14 \leq l \leq 14$

Reflections collected   42045

Independent reflections   3935 [R_{int} = 0.0462, R_{sigma} = 0.0264]

Data/restraints/parameters 3935/0/223

Goodness-of-fit on F^2 1.056

Final R indexes [I>=2σ (I)] R_1 = 0.0336, wR_2 = 0.0859

Final R indexes [all data] R_1 = 0.0425, wR_2 = 0.0905

Largest diff. peak/hole / e $Å^{-3}$ 0.41/-0.33

Table 2 Fractional Atomic Coordinates (×10^4) and Equivalent Isotropic Displacement Parameters (Å^2×10^3). U$_{eq}$ is defined as 1/3 of of the trace of the orthogonalised U$_{IJ}$ tensor.

Atom	x	y	z	U(eq)
F1	6979.5(12)	7702.7(7)	7932.9(7)	21.74(18)
F2	7035.2(12)	5437.2(8)	9550.6(7)	22.62(18)
O1	7553.5(15)	3266.2(8)	6130.6(9)	19.5(2)
N1	7489.6(17)	5567.1(10)	4411.6(11)	16.9(2)
N2	7245.9(19)	2233.7(11)	9408.5(11)	24.0(2)
N3	7423.2(19)	8886.8(11)	4727.4(12)	24.4(3)
C1	7100.5(18)	6619.9(12)	7490.9(12)	16.3(2)
C2	7104.3(19)	5485.7(12)	8302.8(12)	16.8(2)
C3	7232.8(18)	4357.6(12)	7829.0(12)	15.7(2)
C4	7370.1(18)	4396.0(11)	6535.8(12)	14.4(2)
C5	7668.2(18)	3283.6(11)	4833.2(11)	14.7(2)
C6	7846.5(19)	2129.4(12)	4444.6(13)	17.0(2)
C7	8008(2)	2103.3(12)	3154.0(13)	19.6(3)
C8	7974.9(19)	3227.6(13)	2283.6(13)	19.0(3)
C9	7794.5(18)	4387.1(12)	2686.5(12)	16.6(2)
C10	7646.6(18)	4423.7(11)	3972.5(12)	14.1(2)
C11	7364.9(17)	5564.4(11)	5679.5(11)	13.6(2)

C12	7244.3(18)	6676.2(11)	6180.3(12)	14.8(2)
C13	7243.3(19)	3168.0(12)	8693.0(12)	17.4(2)
C14	7321.6(19)	7899.5(12)	5365.4(12)	17.0(2)
S1	7799.4(5)	8744.4(3)	1755.2(3)	18.89(9)
O3	7375.9(18)	7374.9(9)	2332.9(10)	30.2(2)
C15	5435(2)	9604.9(13)	2174.9(14)	23.3(3)
C16	7968(2)	8855.1(13)	80.5(13)	23.7(3)

Table 3 Anisotropic Displacement Parameters (Å^2×10^3). The Anisotropic displacement factor exponent takes the form: -2π^2[h^{2}a*^{2}U$_{11}$+2hka*b*U$_{12}$+…].

Atom	U$_{11}$	U$_{22}$	U$_{33}$	U$_{23}$	U$_{13}$	U$_{12}$
F1	30.9(4)	15.1(4)	22.4(4)	-9.3(3)	-9.4(3)	3.2(3)
F2	31.5(4)	23.6(4)	14.4(4)	-4.8(3)	-8.3(3)	0.3(3)
O1	33.8(5)	10.1(4)	14.9(4)	-1.4(3)	-8.1(4)	0.1(4)
N1	27.1(6)	9.5(5)	13.6(5)	-0.5(4)	-6.0(4)	0.6(4)
N2	31.9(6)	20.1(6)	20.3(6)	-0.4(5)	-10.1(5)	-0.5(5)
N3	34.6(7)	14.9(6)	25.8(6)	-3.1(5)	-12.2(5)	0.2(5)
C1	17.5(6)	12.9(6)	20.1(6)	-7.1(5)	-5.6(5)	1.9(4)
C2	18.6(6)	19.7(6)	12.8(6)	-3.6(5)	-5.4(5)	0.3(5)
C3	16.4(6)	14.5(6)	15.4(6)	-0.2(5)	-5.2(5)	0.4(4)
C4	15.2(5)	11.2(5)	16.7(6)	-1.9(4)	-4.6(4)	-0.3(4)
C5	16.5(6)	13.8(6)	13.6(6)	-2.3(4)	-4.2(4)	-0.4(4)
C6	18.3(6)	11.6(6)	20.5(6)	-1.9(5)	-4.7(5)	-0.6(4)
C7	21.4(6)	15.2(6)	23.7(7)	-8.3(5)	-5.2(5)	-1.2(5)
C8	20.3(6)	21.2(6)	17.3(6)	-6.5(5)	-6.0(5)	0.1(5)
C9	17.4(6)	15.9(6)	16.2(6)	-2.0(5)	-5.2(5)	1.0(5)
C10	14.0(5)	11.7(5)	16.6(6)	-3.2(4)	-4.3(4)	1.0(4)
C11	13.7(5)	12.1(5)	14.3(5)	-1.4(4)	-3.4(4)	0.1(4)
C12	15.1(5)	11.8(5)	17.6(6)	-2.2(4)	-5.5(5)	0.9(4)

C13	20.5(6)	18.1(6)	14.5(6)	−3.0(5)	−6.2(5)	0.1(5)
C14	19.8(6)	13.3(6)	19.9(6)	−6.0(5)	−7.2(5)	1.5(4)
S1	28.18(17)	12.65(15)	16.34(16)	−0.47(11)	−9.41(12)	2.63(12)
O3	57.5(7)	12.0(5)	20.0(5)	1.9(4)	−13.1(5)	2.9(4)
C15	27.0(7)	19.2(6)	24.0(7)	−3.5(5)	−8.6(6)	2.0(5)
C16	34.1(7)	20.0(7)	16.6(6)	−0.5(5)	−8.8(5)	1.0(5)

Table 4 Bond Lengths

Atom	Atom	Length/Å	Atom	Atom	Length/Å
F1	C1	1.3391(15)	C4	C11	1.4131(17)
F2	C2	1.3460(15)	C5	C6	1.3795(18)
O1	C4	1.3626(16)	C5	C10	1.3939(17)
O1	C5	1.3988(15)	C6	C7	1.3937(19)
N1	C10	1.3964(17)	C7	C8	1.3876(19)
N1	C11	1.3681(17)	C8	C9	1.3921(19)
N2	C13	1.1467(18)	C9	C10	1.3932(18)
N3	C14	1.1476(17)	C11	C12	1.4028(18)
C1	C2	1.3616(18)	C12	C14	1.4343(18)
C1	C12	1.4017(18)	S1	O3	1.5071(12)
C2	C3	1.4025(18)	S1	C15	1.7787(15)
C3	C4	1.3868(18)	S1	C16	1.7873(15)
C3	C13	1.4351(18)			

Table 5 Bond Angles

Atom	Atom	Atom	Angle/°	Atom	Atom	Atom	Angle/°
C4	O1	C5	118.05(10)	C8	C7	C6	119.99(12)
C11	N1	C10	120.00(11)	C7	C8	C9	120.51(12)

F1	C1	C2	120.30(11)	C8	C9	C10	119.95(12)
F1	C1	C12	118.90(11)	C5	C10	N1	119.65(11)
C2	C1	C12	120.80(11)	C9	C10	N1	121.71(11)
F2	C2	C1	120.53(11)	C9	C10	C5	118.64(11)
F2	C2	C3	119.65(11)	N1	C11	C4	119.27(11)
C1	C2	C3	119.80(12)	N1	C11	C12	123.03(11)
C2	C3	C13	119.28(12)	C12	C11	C4	117.70(12)
C4	C3	C2	120.15(11)	C1	C12	C11	120.71(11)
C4	C3	C13	120.56(11)	C1	C12	C14	118.02(11)
O1	C4	C3	117.15(11)	C11	C12	C14	121.25(12)
O1	C4	C11	122.01(11)	N2	C13	C3	178.28(14)
C3	C4	C11	120.83(11)	N3	C14	C12	178.13(14)
C6	C5	O1	117.10(11)	O3	S1	C15	106.35(7)
C6	C5	C10	121.90(12)	O3	S1	C16	104.27(6)
C10	C5	O1	120.99(11)	C15	S1	C16	97.51(7)
C5	C6	C7	119.01(12)				

Table 6 Hydrogen Atom Coordinates (Å×10⁴) and Isotropic Displacement Parameters (Å²×10³)

Atom	x	y	z	U(eq)
H1	7540(30)	6283(18)	3841(18)	33(5)
H6	7858.81	1363.66	5047.59	20
H7	8141.55	1315.99	2870.29	23
H8	8075.97	3205.79	1406.03	23
H9	7772.29	5152.78	2084.97	20
H15A	4367.61	9171.36	2006.17	35
H15B	5550.37	10460.58	1655.99	35
H15C	5084.93	9656.8	3093.62	35
H16A	9201.75	8391.95	−324.73	36
H16B	8024.81	9746.41	−343.66	36
H16C	6768.61	8487.64	−8.24	36

Sample:	7,14-didecyl-7,14-dihydrobenzo[5,6][1,4]oxazino[2,3-b]phenoxazine-6,13-dicarbonitrile (**3.31**) n19005 (LKH-5-86)

X-ray Structure Report

Louise N. Dawe, PhD

Department of Chemistry and Biochemistry

Wilfrid Laurier University

Science Building

75 University Ave. W.

Waterloo, ON, ON

ldawe@wlu.ca

June 29, 2018

<u>Introduction</u>

Data for this structure was collected by Dr. Paul D. Boyle, Western University

All hydrogen atoms were introduced in calculated positions and refined on a riding model. All non-hydrogen atoms were refined anisotropically. The asymmetric unit contains half the molecule; the other half is generated by an inversion centre.

Experimental

A single crystal of $C_{40}H_{50}N_4O_2$ was selected and collected on a Nonius diffractometer. The crystal was kept at 110(2) K during data collection. Using Olex2 [1], the structure was solved with the ShelXT [2] structure solution program using Intrinsic Phasing and refined with the ShelXL [3] refinement package using Least Squares minimisation.

4. Dolomanov, O.V., Bourhis, L.J., Gildea, R.J, Howard, J.A.K. & Puschmann, H. (2009), J. Appl. Cryst. 42, 339-341.

5. Sheldrick, G.M. (2015). Acta Cryst. A71, 3-8.

6. Sheldrick, G.M. (2015). Acta Cryst. C71, 3-8.

Crystal structure determination

Crystal Data for $C_{40}H_{50}N_4O_2$ (M =618.84 g/mol): triclinic, space group P-1 (no. 2), a = 7.2788(2) Å, b = 8.7498(2) Å, c = 13.4900(5) Å, α = 81.525(2)°, β = 83.346(3)°, γ = 82.899(2)°, V = 839.07(4) Å^3, Z = 1, T = 110.15 K, μ(CuKα) = 0.587 mm^{-1}, $Dcalc$ = 1.225 g/cm^3, 15321 reflections measured (10.282° ≤ 2θ ≤ 134.96°), 2933 unique (2138 with I > 2σ(I); R_{int} = 0.0565, R$_{sigma}$ = 0.0307) which were used in all calculations. The final R_1 was 0.0425 (I > 2σ(I)) and wR_2 was 0.1228 (all data).

Table 1 Crystal data and structure refinement

Identification code	n19005 (LKH-5-86)
Empirical formula	$C_{40}H_{50}N_4O_2$
Formula weight	618.84
Temperature/K	110(2)
Crystal system	triclinic
Space group	P-1
a/Å	7.2788(2)
b/Å	8.7498(2)
c/Å	13.4900(5)
α/°	81.525(2)
β/°	83.346(3)
γ/°	82.899(2)
Volume/Å^3	839.07(4)
Z	1
ρ_{calc}g/cm^3	1.225
μ/mm^{-1}	0.587
F(000)	334.0
Crystal size/mm^3	0.338 × 0.193 × 0.071
Radiation	CuKα (λ = 1.54184)
2Θ range for data collection/°	10.282 to 134.96

Index ranges $-8 \leq h \leq 8, -10 \leq k \leq 7, -16 \leq l \leq 15$

Reflections collected   15321

Independent reflections   2933 [2138 with $I > 2\sigma(I)$; R_{int} = 0.0565, R_{sigma} = 0.0307]

Data/restraints/parameters   2933/0/209

Goodness-of-fit on F^2 1.055

Final R indexes [$I >= 2\sigma$ (I)] R_1 = 0.0425, wR_2 = 0.1071

Final R indexes [all data] R_1 = 0.0665, wR_2 = 0.1228

Largest diff. peak/hole / e $Å^{-3}$ 0.20/-0.23

Table 2 Fractional Atomic Coordinates (×10⁴) and Equivalent Isotropic Displacement Parameters (Å²×10³). U$_{eq}$ is defined as 1/3 of of the trace of the orthogonalised U$_{IJ}$ tensor.

Atom	x	y	z	U(eq)
O1	3422.5(15)	−1591.0(13)	9593.5(9)	27.7(3)
N1	2911.8(19)	1614.3(16)	8891.1(11)	25.3(3)
N2	1628(2)	−4398.1(18)	10958.2(13)	37.9(4)
C1	359(2)	−1564.5(18)	10332.2(13)	24.3(4)
C2	1739(2)	−730.5(19)	9765.0(13)	24.3(4)
C3	4788(2)	−893.1(19)	8935.1(13)	25.0(4)
C4	6348(2)	−1844(2)	8658.5(13)	27.0(4)
C5	7778(2)	−1220(2)	8019.5(14)	31.2(4)
C6	7612(2)	363(2)	7675.3(14)	32.7(4)
C7	6024(2)	1306(2)	7957.5(14)	29.1(4)
C8	4563(2)	698.4(19)	8589.4(13)	24.7(4)
C9	1455(2)	858.4(19)	9426.6(12)	23.6(4)
C10	1003(2)	−3156(2)	10682.7(14)	27.6(4)
C11	2988(2)	3299.7(19)	8836.2(13)	26.7(4)
C12	2571(2)	4242.9(19)	7830.4(13)	26.4(4)
C13	2746(2)	5960.1(19)	7832.6(13)	27.8(4)
C14	2423(2)	6956.1(19)	6832.6(13)	27.9(4)

C15	2721(2)	8656.5(19)	6815.2(13)	27.5(4)
C16	2286(3)	9679(2)	5840.6(14)	30.4(4)
C17	2645(3)	11360(2)	5822.3(14)	30.1(4)
C18	2271(3)	12411(2)	4847.4(14)	32.3(4)
C19	2706(3)	14059(2)	4837.8(15)	35.0(5)
C20	2440(3)	15109(2)	3848.1(16)	41.1(5)

Table 3 Anisotropic Displacement Parameters ($Å^2 \times 10^3$). The Anisotropic displacement factor exponent takes the form: $-2\pi^2[h^2a^{*2}U_{11}+2hka^*b^*U_{12}+...]$.

Atom	U_{11}	U_{22}	U_{33}	U_{23}	U_{13}	U_{12}
O1	20.2(6)	20.8(6)	38.7(7)	1.1(5)	0.7(5)	1.5(5)
N1	23.5(7)	18.5(7)	32.0(8)	0.4(6)	-0.2(6)	-1.9(6)
N2	31.3(9)	25.0(9)	51.9(11)	3.3(7)	1.8(7)	2.4(7)
C1	26.2(9)	18.1(8)	28.0(9)	-0.4(7)	-5.9(7)	-0.8(7)
C2	21.5(9)	23.5(9)	27.5(10)	-3.3(7)	-3.8(7)	0.6(7)
C3	23.0(9)	24.9(9)	26.6(9)	-0.2(7)	-3.8(7)	-3.9(7)
C4	24.8(9)	23.6(9)	32.1(10)	-2.3(7)	-6.8(7)	0.8(7)
C5	23.2(9)	31.2(10)	37.5(11)	-4.1(8)	-1.6(8)	2.2(7)
C6	24.0(9)	35.6(11)	36.2(11)	-1.1(8)	1.2(8)	-3.1(8)
C7	27.6(10)	25.6(9)	33.2(10)	0.4(8)	-3.8(8)	-3.3(7)
C8	22.5(9)	24.4(9)	27.3(9)	-2.0(7)	-4.7(7)	-1.8(7)
C9	23.9(9)	20.3(9)	25.5(9)	0.1(7)	-3.5(7)	-1.4(7)
C10	21.3(9)	25.7(10)	34.3(10)	-2.4(8)	1.2(7)	-2.3(7)
C11	25.5(9)	19.6(9)	34.1(10)	-1.4(7)	-1.3(7)	-3.9(7)
C12	25.7(9)	21.4(9)	31.2(10)	-0.7(7)	-2.1(7)	-2.6(7)
C13	30.0(9)	21.0(9)	31.6(10)	0.0(7)	-5.3(8)	-1.7(7)
C14	28.7(9)	22.9(9)	31.4(10)	-0.1(7)	-4.5(8)	-2.8(7)
C15	26.9(9)	24.4(9)	31.2(10)	-2.0(7)	-3.5(8)	-4.3(7)

C16	34.1(10)	24.4(9)	32.4(10)	-0.3(8)	-5.5(8)	-4.1(7)
C17	31.1(10)	24.9(9)	34.2(10)	1.0(8)	-4.5(8)	-6.7(7)
C18	35.8(10)	26.6(10)	34.1(11)	2.3(8)	-8.0(8)	-5.1(8)
C19	34.6(11)	28.6(10)	40.2(11)	3.3(8)	-1.3(9)	-8.0(8)
C20	40.3(12)	31.8(11)	47.0(13)	9.7(9)	-2.9(10)	-6.7(9)

Table 4 Bond Lengths

Atom	Atom	Length/Å	Atom	Atom	Length/Å
O1	C2	1.3708(19)	C5	C6	1.389(3)
O1	C3	1.391(2)	C6	C7	1.385(2)
N1	C8	1.413(2)	C7	C8	1.391(2)
N1	C9	1.392(2)	C11	C12	1.522(2)
N1	C11	1.473(2)	C12	C13	1.524(2)
N2	C10	1.151(2)	C13	C14	1.520(2)
C1	C2	1.402(2)	C14	C15	1.526(2)
C1	C9[1]	1.411(2)	C15	C16	1.520(2)
C1	C10	1.442(2)	C16	C17	1.521(2)
C2	C9	1.396(2)	C17	C18	1.521(2)
C3	C4	1.371(2)	C18	C19	1.512(2)
C3	C8	1.398(2)	C19	C20	1.523(3)
C4	C5	1.385(3)			

[1]-X,-Y,2-Z

Table 5 Bond Angles

Atom	Atom	Atom	Angle/°	Atom	Atom	Atom	Angle/°
C2	O1	C3	117.76(13)	C3	C8	N1	119.93(15)
C8	N1	C11	117.57(14)	C7	C8	N1	123.05(15)
C9	N1	C8	118.09(14)	C7	C8	C3	117.02(16)
C9	N1	C11	122.69(14)	N1	C9	C1[1]	125.39(15)
C2	C1	C9[1]	121.96(15)	N1	C9	C2	119.75(15)
C2	C1	C10	113.84(15)	C2	C9	C1[1]	114.86(15)
C9[1]	C1	C10	124.11(16)	N2	C10	C1	175.66(18)
O1	C2	C1	114.59(14)	N1	C11	C12	114.80(14)
O1	C2	C9	122.25(15)	C11	C12	C13	111.06(14)
C9	C2	C1	123.14(15)	C14	C13	C12	113.60(14)
O1	C3	C8	120.94(15)	C13	C14	C15	113.50(14)
C4	C3	O1	116.50(15)	C16	C15	C14	113.78(14)
C4	C3	C8	122.56(16)	C15	C16	C17	113.17(15)
C3	C4	C5	119.55(17)	C16	C17	C18	114.70(15)
C4	C5	C6	119.35(17)	C19	C18	C17	113.46(15)
C7	C6	C5	120.41(17)	C18	C19	C20	114.33(17)
C6	C7	C8	121.10(17)				

[1]-X,-Y,2-Z

Table 6 Hydrogen Atom Coordinates (Å×10⁴) and Isotropic Displacement Parameters (Å²×10³)

Atom	x	y	z	U(eq)
H4	6447.45	−2922.73	8903.48	32
H5	8861.91	−1868.14	7818.47	37
H6	8594.77	800.49	7243.81	39
H7	5929.55	2386.06	7715.46	35
H11A	4245.06	3475.38	8977.21	32
H11B	2086.27	3693.64	9372.1	32
H12A	1293.51	4117.32	7695.17	32
H12B	3448.01	3847.02	7285.31	32
H13A	1834.54	6353.98	8364.83	33
H13B	4005.25	6069.13	8003.48	33
H14A	1133.86	6902.95	6683.65	34
H14B	3277.52	6520.7	6293.03	34
H15A	1925.64	9071.54	7382.36	33
H15B	4033.13	8713.04	6921.62	33
H16A	963.28	9651.59	5743.98	37
H16B	3054.61	9249.05	5270.3	37
H17A	3958.52	11377.77	5940.89	36
H17B	1853.57	11790.29	6385.46	36

H18A	3028.57	11966.51	4279.19	39
H18B	944.72	12431.75	4740.39	39
H19A	4012.53	14030.01	4984.65	42
H19B	1899.24	14518.48	5384.72	42
H20A	3282.42	14696.03	3305.93	62
H20B	2717.09	16158.31	3906.59	62
H20C	1150.37	15148.93	3694.76	62

Sample: 10-ethyl-2,3-difluoro-10H-phenoxazine-1,4-dicarbonitrile (**3.32**): b19042 (LKH-6-89)

<div align="center">X-ray Structure Report</div>

<div align="center">Louise N. Dawe, PhD</div>

<div align="center">Department of Chemistry and Biochemistry</div>

<div align="center">Wilfrid Laurier University</div>

<div align="center">Science Building</div>

<div align="center">75 University Ave. W.</div>

<div align="center">Waterloo, ON, ON</div>

<div align="center">ldawe@wlu.ca</div>

<div align="center">June 29, 2018</div>

<div align="center"><u>Introduction</u></div>

Data for this structure was collected by Dr. Paul D. Boyle, Western University

All hydrogen atoms were introduced in calculated positions and refined on a riding model. All non-hydrogen atoms were refined anisotropically. The N-ethyl group was disordered with 0.891(4): 0.109(4) occupancy. N-C and C-C distances in this group were treated with a

similarity restraint (SHELX SADI) using default standard uncertainties, while the anisotropic

displacements for the carbon atoms in the ethyl group were constrained to be identical.

Experimental

A single crystal of $C_{16}H_9F_2N_3O$ was selected and collected on a Burker APEX3 diffractometer. The crystal was kept at 110(2) K during data collection. Using Olex2 [1], the structure was solved with the ShelXT [2] structure solution program using Intrinsic Phasing and refined with the ShelXL [3] refinement package using Least Squares minimisation.

7. Dolomanov, O.V., Bourhis, L.J., Gildea, R.J, Howard, J.A.K. & Puschmann, H. (2009), J. Appl. Cryst. 42, 339-341.

8. Sheldrick, G.M. (2015). Acta Cryst. A71, 3-8.

9. Sheldrick, G.M. (2015). Acta Cryst. C71, 3-8.

Crystal structure determination

Crystal Data for $C_{16}H_9F_2N_3O$ (M =297.26 g/mol): monoclinic, space group $P2_1/n$ (no. 14), $a =$ 10.5348(3) Å, $b =$ 6.6611(2) Å, $c =$ 19.1688(5) Å, $\beta =$ 98.785(3)°, $V =$ 1329.36(7) Å^3, $Z =$ 4, $T =$ 110.15 K, µ(MoKα) = 0.116 mm^{-1}, $Dcalc =$ 1.485 g/cm^3, 50162 reflections measured (6.484° ≤ 2Θ ≤ 54.2°), 2925 unique (2907 with I > 2σ(I); R_{int} = 0.0310, R_{sigma} = 0.0107) which were used in all calculations. The final R_1 was 0.0716 (I > 2σ(I)) and wR_2 was 0.1526 (all data).

Table 1 Crystal data and structure refinement

Identification code	b19042 (LKH-6-89)
Empirical formula	$C_{16}H_9F_2N_3O$
Formula weight	297.26
Temperature/K	110.15
Crystal system	monoclinic
Space group	$P2_1/n$
a/Å	10.5348(3)
b/Å	6.6611(2)
c/Å	19.1688(5)
α/°	90
β/°	98.785(3)
γ/°	90
Volume/Å^3	1329.36(7)
Z	4
ρ_{calc}g/cm^3	1.485
μ/mm^{-1}	0.116
F(000)	608.0
Crystal size/mm^3	0.280 × 0.268 × 0.080
Radiation	MoKα (λ = 0.71073)
2Θ range for data collection/°	6.484 to 54.2

Index ranges $-13 \leq h \leq 13, -8 \leq k \leq 8, -24 \leq l \leq 24$

Reflections collected 50162

Independent reflections 2925 [2907 with $I > 2\sigma(I)$; $R_{int} = 0.0310$, $R_{sigma} = 0.0107$]

Data/restraints/parameters 2925/2/208

Goodness-of-fit on F^2 1.334

Final R indexes [$I>=2\sigma$ (I)] $R_1 = 0.0716$, $wR_2 = 0.1523$

Final R indexes [all data] $R_1 = 0.0722$, $wR_2 = 0.1526$

Largest diff. peak/hole / e Å^{-3} 0.47/-0.31

Table 2 Fractional Atomic Coordinates (×10⁴) and Equivalent Isotropic Displacement Parameters (Å²×10³). U_eq is defined as 1/3 of of the trace of the orthogonalised U_IJ tensor.

Atom	x	y	z	U(eq)
F1	6348.9(14)	3234(2)	5970.5(8)	36.2(4)
F2	3983.5(15)	3156(3)	5184.2(7)	37.1(4)
O1	2069.3(14)	2603(3)	7221.5(8)	25.5(4)
N1	4442.0(16)	2563(3)	8102.7(9)	22.3(4)
N2	777(2)	2889(3)	5492.2(10)	29.7(5)
N3	7866.4(18)	3220(3)	7542.9(13)	33.7(5)
C1	3040(2)	2939(3)	6226.8(11)	19.0(4)
C2	3187.2(19)	2806(3)	6952.5(11)	16.9(4)
C3	2123.5(19)	2788(3)	7947.9(11)	17.0(4)
C4	966.5(19)	2920(3)	8191.5(12)	19.2(4)
C5	954(2)	3011(3)	8911.5(12)	24.1(5)
C6	2103(2)	2986(3)	9372.7(12)	24.2(5)
C7	3270(2)	2876(3)	9116.1(11)	20.5(4)
C8	3296.0(19)	2764(3)	8394.3(11)	16.7(4)
C9	4402.6(18)	2794(3)	7386.0(11)	16.4(4)
C10	5473.2(19)	2971(3)	7028.3(11)	18.4(4)
C11	5300(2)	3079(3)	6286.3(12)	22.8(5)

C12	4122(2)	3056(3)	5889.7(11)	23.6(5)
C13	1775(2)	2909(3)	5818.6(11)	21.3(5)
C14	6793(2)	3088(3)	7348.5(12)	21.6(5)
C15	5650(2)	2165(4)	8584.7(13)	20.7(5)
C16	6290(2)	4096(4)	8883.6(14)	27.9(6)
C15A	5625(15)	3490(30)	8572(10)	20.7(5)
C16A	6310(20)	1550(30)	8810(12)	27.9(6)

Table 3 Anisotropic Displacement Parameters ($Å^2 \times 10^3$). The Anisotropic displacement factor exponent takes the form: $-2\pi^2[h^2a^{*2}U_{11}+2hka^*b^*U_{12}+...]$.

Atom	U_{11}	U_{22}	U_{33}	U_{23}	U_{13}	U_{12}
F1	30.5(8)	50.0(10)	32.9(8)	1.3(7)	20.5(6)	1.8(7)
F2	45.1(9)	51.8(10)	15.4(7)	0.4(6)	7.4(6)	0.4(7)
O1	9.7(7)	48.6(11)	17.3(7)	-2.6(7)	-1.0(5)	-1.8(7)
N1	10.4(8)	39.5(11)	15.8(9)	-0.2(8)	-1.9(7)	1.5(7)
N2	33.0(11)	28.9(11)	22.4(10)	-1.9(8)	-11.1(8)	0.3(9)
N3	14.3(9)	37.7(12)	49.5(13)	0.8(10)	6.3(9)	-0.6(8)
C1	21.2(10)	17.4(10)	17.0(10)	-1.6(8)	-2.1(8)	2.6(8)
C2	13.0(9)	19.3(10)	18.2(10)	-1.7(8)	1.9(7)	0.4(8)
C3	15.1(9)	19.6(10)	15.9(9)	1.3(8)	0.9(7)	-0.2(8)
C4	12.2(9)	16.6(10)	28.5(11)	0.5(8)	2.7(8)	-0.3(8)
C5	22.4(11)	21.1(11)	32.2(12)	0.0(9)	15.1(9)	-2.8(9)
C6	31.2(12)	25.5(11)	18.0(10)	1.1(9)	10.2(9)	-3.3(9)
C7	22.9(11)	18.9(10)	19.1(10)	1.0(8)	0.9(8)	-1.1(8)
C8	12.3(9)	18.6(10)	18.8(10)	1.7(8)	1.2(7)	0.0(8)
C9	11.9(9)	19.3(10)	18.0(10)	-1.4(8)	1.8(7)	1.0(8)
C10	13.4(9)	17.5(10)	24.6(11)	-2.3(8)	3.5(8)	0.6(8)
C11	20.3(11)	25.2(11)	25.6(11)	0.0(9)	11.6(9)	1.2(9)
C12	32.9(12)	24.7(11)	14.2(10)	-0.4(8)	6.5(8)	2.3(9)

C13	27.8(12)	18.9(10)	15.1(9)	−1.0(8)	−3.9(8)	0.6(9)
C14	15.1(10)	20.6(11)	30.8(12)	−1.4(9)	8.5(8)	0.6(8)
C15	11.9(11)	26.7(13)	21.5(11)	4.7(10)	−3.7(9)	0.8(10)
C16	19.6(12)	38.3(15)	23.7(13)	−2.9(11)	−3.3(10)	−6.0(11)
C15A	11.9(11)	26.7(13)	21.5(11)	4.7(10)	−3.7(9)	0.8(10)
C16A	19.6(12)	38.3(15)	23.7(13)	−2.9(11)	−3.3(10)	−6.0(11)

Table 4 Bond Lengths

Atom	Atom	Length/Å	Atom	Atom	Length/Å
F1	C11	1.342(2)	C2	C9	1.416(3)
F2	C12	1.339(2)	C3	C4	1.373(3)
O1	C2	1.363(2)	C3	C8	1.391(3)
O1	C3	1.390(2)	C4	C5	1.384(3)
N1	C8	1.412(3)	C5	C6	1.386(3)
N1	C9	1.377(3)	C6	C7	1.394(3)
N1	C15	1.478(3)	C7	C8	1.390(3)
N1	C15A	1.550(15)	C9	C10	1.411(3)
N2	C13	1.139(3)	C10	C11	1.408(3)
N3	C14	1.139(3)	C10	C14	1.433(3)
C1	C2	1.379(3)	C11	C12	1.353(3)
C1	C12	1.397(3)	C15	C16	1.523(4)
C1	C13	1.438(3)	C15A	C16A	1.518(18)

Table 5 Bond Angles

Atom	Atom	Atom	Angle/°	Atom	Atom	Atom	Angle/°
C2	O1	C3	117.68(16)	C3	C8	N1	119.35(18)
C8	N1	C15	118.42(18)	C7	C8	N1	123.17(18)
C8	N1	C15A	113.1(8)	C7	C8	C3	117.45(19)
C9	N1	C8	119.15(17)	N1	C9	C2	118.23(18)
C9	N1	C15	122.41(18)	N1	C9	C10	126.12(18)
C9	N1	C15A	115.7(8)	C10	C9	C2	115.62(18)
C2	C1	C12	119.75(19)	C9	C10	C14	126.2(2)
C2	C1	C13	120.03(19)	C11	C10	C9	120.35(19)
C12	C1	C13	120.21(19)	C11	C10	C14	113.41(19)
O1	C2	C1	114.67(18)	F1	C11	C10	118.10(19)
O1	C2	C9	122.25(18)	F1	C11	C12	119.7(2)
C1	C2	C9	123.03(19)	C12	C11	C10	122.23(19)
O1	C3	C8	120.78(18)	F2	C12	C1	119.9(2)
C4	C3	O1	116.33(18)	F2	C12	C11	121.1(2)
C4	C3	C8	122.85(19)	C11	C12	C1	118.98(19)
C3	C4	C5	119.1(2)	N2	C13	C1	179.6(3)
C4	C5	C6	119.7(2)	N3	C14	C10	173.7(2)
C5	C6	C7	120.5(2)	N1	C15	C16	111.9(2)
C8	C7	C6	120.4(2)	C16A	C15A	N1	98.0(13)

243

Table 6 Hydrogen Atom Coordinates (Å×10⁴) and Isotropic Displacement Parameters (Å²×10³)

Atom	*x*	*y*	*z*	U(eq)
H4	185.16	2949.1	7870.1	23
H5	161.65	3090.46	9088.94	29
H6	2095.73	3044.23	9867.26	29
H7	4052.63	2876.87	9436.59	25
H15A	6247.66	1425.18	8326.35	25
H15B	5464.6	1304.45	8978.22	25
H16A	6389.9	5011.73	8495.77	42
H16B	7135.58	3784.85	9150.99	42
H16C	5754.81	4732.86	9196.54	42
H15C	6137.93	4347.47	8298.32	25
H15D	5381.9	4263.31	8972.87	25
H16D	6371.68	704.5	8398.24	42
H16E	5828.48	836.15	9132.3	42
H16F	7176.25	1852.67	9054.71	42

Table 7 Atomic Occupancy

Atom	*Occupancy*	Atom	*Occupancy*	Atom	*Occupancy*

C15	0.891(4)	H15A	0.891(4)	H15B	0.891(4)
C16	0.891(4)	H16A	0.891(4)	H16B	0.891(4)
H16C	0.891(4)	C15A	0.109(4)	H15C	0.109(4)
H15D	0.109(4)	C16A	0.109(4)	H16D	0.109(4)
H16E	0.109(4)	H16F	0.109(4)		

Sample: 10-benzyl-2,3-difluoro-10H-phenoxazine-1,4-dicarbonitrile (**3.38**)

X-ray Structure Report

Louise N. Dawe, PhD

Department of Chemistry and Biochemistry

Wilfrid Laurier University

Science Building

75 University Ave. W.

Waterloo, ON, ON

ldawe@wlu.ca

July 1, 2018

Introduction

Data for this structure was collected by Dr. Paul D. Boyle, Western University

All hydrogen atoms were introduced in calculated positions and refined on a riding model.

All non-hydrogen atoms were refined anisotropically.

Experimental

A single crystal of $C_{21}H_{11}N_3OF_2$ was selected and collected on a Nonius diffractometer. The crystal was kept at 110(2) K during data collection. Using Olex2 [1], the structure was solved with the ShelXT [2] structure solution program using Intrinsic Phasing and refined with the ShelXL [3] refinement package using Least Squares minimisation.

10. Dolomanov, O.V., Bourhis, L.J., Gildea, R.J, Howard, J.A.K. & Puschmann, H. (2009), J. Appl. Cryst. 42, 339-341.

11. Sheldrick, G.M. (2015). Acta Cryst. A71, 3-8.

12. Sheldrick, G.M. (2015). Acta Cryst. C71, 3-8.

Crystal structure determination

Crystal Data for $C_{21}H_{11}N_3OF_2$ (M =359.33 g/mol): monoclinic, space group $P2_1/c$ (no. 14), $a =$ 10.5788(2) Å, $b =$ 7.2672(2) Å, $c =$ 21.1444(6) Å, $\beta =$ 96.154(2)°, $V =$ 1616.18(7) Å^3, $Z =$ 4, $T =$ 110(2) K, μ(CuKα) = 0.919 mm^{-1}, $Dcalc =$ 1.477 g/cm^3, 13578 reflections measured (8.406° $\leq 2\theta \leq$ 132.832°), 2780 unique (2312 with I > 2σ(I); $R_{int} =$ 0.0394, $R_{sigma} =$ 0.0202) which were used in all calculations. The final R_1 was 0.0587 (I > 2σ(I)) and wR_2 was 0.1719 (all data).

Table 1 Crystal data and structure refinement

Identification code	n18049 (LKH-5-64)
Empirical formula	$C_{21}H_{11}N_3OF_2$
Formula weight	359.33
Temperature/K	110(2)
Crystal system	monoclinic
Space group	$P2_1/c$
a/Å	10.5788(2)
b/Å	7.2672(2)
c/Å	21.1444(6)
α/°	90
β/°	96.154(2)
γ/°	90
Volume/Å^3	1616.18(7)
Z	4
ρ_{calc}g/cm^3	1.477
μ/mm^{-1}	0.919
F(000)	736.0
Crystal size/mm^3	0.782 × 0.280 × 0.142
Radiation	CuKα (λ = 1.54184)
2Θ range for data collection/°	8.406 to 132.832

Index ranges $-12 \leq h \leq 12, -8 \leq k \leq 5, -24 \leq l \leq 25$

Reflections collected   13578

Independent reflections   2780 [2312 with $I > 2\sigma(I)$; $R_{int} = 0.0394$, $R_{sigma} = 0.0202$]

Data/restraints/parameters   2780/0/244

Goodness-of-fit on F^2 1.063

Final R indexes [$I>=2\sigma (I)$] $R_1 = 0.0587$, $wR_2 = 0.1563$

Final R indexes [all data] $R_1 = 0.0701$, $wR_2 = 0.1719$

Largest diff. peak/hole / e $Å^{-3}$ 0.49/-0.35

Table 2 Fractional Atomic Coordinates (×10⁴) and Equivalent Isotropic Displacement Parameters (Å²×10³). U_{eq} is defined as 1/3 of of the trace of the orthogonalised U_{IJ} tensor.

Atom	x	y	z	U(eq)
F1	8551.1(12)	7166(2)	5791.9(7)	39.5(4)
F2	6249.0(14)	7180(2)	5117.4(7)	44.5(4)
O1	4274.0(14)	6048(2)	6963.9(8)	36.2(4)
N1	6608.7(17)	5986(3)	7720.7(9)	33.1(5)
N2	3070(2)	6976(4)	5409.7(11)	53.2(7)
N3	9948(2)	7048(3)	7274.6(11)	45.4(6)
C1	5274(2)	6620(3)	6054.0(12)	34.3(5)
C2	5382(2)	6326(3)	6703.0(12)	32.5(5)
C3	4308(2)	6215(3)	7623.0(11)	32.7(5)
C4	3168(2)	6353(3)	7872.0(12)	35.5(6)
C5	3147(2)	6502(3)	8520.9(13)	38.7(6)
C6	4292(2)	6478(4)	8913.7(12)	39.7(6)
C7	5438(2)	6312(3)	8658.0(12)	36.8(6)
C8	5470(2)	6179(3)	8004.9(11)	32.3(5)

C9	6578(2)	6279(3)	7072.9(11)	31.4(5)
C10	7646(2)	6594(3)	6748.7(12)	33.1(5)
C11	7521(2)	6832(3)	6089.0(12)	34.4(5)
C12	6353(2)	6859(3)	5743.5(12)	36.2(6)
C13	4036(2)	6773(4)	5699.2(12)	40.4(6)
C14	8920(2)	6801(4)	7062.3(12)	37.3(6)
C15	7685(2)	5067(3)	8089.9(11)	35.0(6)
C16	8510(2)	6274(3)	8546.9(10)	31.3(5)
C17	8403(2)	8169(4)	8570.6(12)	37.1(6)
C18	9223(2)	9179(4)	8990.6(12)	39.6(6)
C19	10161(2)	8310(4)	9389.5(11)	37.7(6)
C20	10265(2)	6423(4)	9373.6(11)	37.3(6)
C21	9437(2)	5401(4)	8957.2(11)	35.2(5)

Table 3 Anisotropic Displacement Parameters ($Å^2 \times 10^3$). The Anisotropic displacement factor exponent takes the form: $-2\pi^2[h^2a^{*2}U_{11}+2hka^*b^*U_{12}+...]$.

Atom	U_{11}	U_{22}	U_{33}	U_{23}	U_{13}	U_{12}
F1	23.8(7)	55.3(9)	39.6(8)	1.0(6)	4.6(6)	−1.6(6)
F2	33.3(8)	67.3(10)	32.1(8)	5.3(7)	−0.7(6)	1.4(7)
O1	20.9(8)	52.3(10)	34.8(9)	−0.3(7)	−0.8(6)	−2.3(7)
N1	20.8(9)	43.7(11)	33.7(11)	0.0(9)	−2.5(8)	1.1(8)
N2	31.1(12)	82.3(18)	43.8(14)	5.2(12)	−7.5(10)	−1.6(11)
N3	23.3(11)	68.1(15)	43.4(13)	1.0(11)	−1.9(9)	−3.5(10)
C1	25.9(12)	39.4(13)	36.1(13)	−1.3(10)	−4.6(9)	0.2(10)
C2	22.9(11)	36.0(12)	37.7(13)	−2.7(10)	−1.0(9)	0.4(9)
C3	27.4(11)	34.7(12)	35.2(13)	−0.6(9)	−0.7(9)	−0.6(9)
C4	22.6(11)	38.0(13)	45.1(14)	3.1(10)	−0.3(9)	0.4(9)
C5	27.9(12)	43.0(14)	46.2(15)	0.4(11)	8.6(10)	−0.5(10)
C6	37.4(13)	45.0(14)	36.9(13)	−0.9(11)	4.7(10)	−3.7(11)
C7	26.6(12)	45.2(14)	37.3(13)	0.4(10)	−2.1(10)	−2.0(10)
C8	23.3(11)	35.6(12)	37.3(13)	−0.2(10)	0.7(9)	0.7(9)
C9	24.1(11)	34.5(12)	34.7(12)	−2.1(9)	−1.8(9)	−0.1(9)
C10	22.8(11)	36.5(12)	39.3(13)	−3.0(10)	−0.5(9)	2.0(9)
C11	24.8(11)	38.1(12)	40.1(13)	−1.4(10)	3.0(10)	−0.4(9)
C12	32.2(13)	43.0(14)	32.9(13)	0.3(10)	0.6(10)	1.7(10)

253

C13	29.5(13)	56.4(16)	34.4(13)	1.5(11)	−0.8(10)	−0.8(11)
C14	27.2(13)	47.9(14)	36.7(13)	0.0(11)	2.9(10)	−0.3(10)
C15	25.9(11)	40.4(13)	37.3(13)	2.1(10)	−4.0(9)	2.6(10)
C16	20.7(11)	42.4(13)	30.4(12)	2.0(10)	0.1(9)	−1.9(9)
C17	24.6(11)	47.9(14)	37.4(14)	2.7(11)	−3.5(10)	4.5(10)
C18	32.0(12)	40.9(14)	45.0(14)	−5.4(11)	−0.2(10)	−3.1(10)
C19	24.2(11)	55.8(16)	32.2(13)	−5.6(11)	−1.1(9)	−5.9(10)
C20	23.5(11)	54.2(16)	33.3(13)	3.3(11)	−1.7(9)	0.9(10)
C21	28.8(12)	41.9(13)	33.6(12)	1.9(10)	−1.8(9)	0.1(10)

Table 4 Bond Lengths.

Atom	Atom	Length/Å	Atom	Atom	Length/Å
F1	C11	1.337(3)	C4	C5	1.379(4)
F2	C12	1.337(3)	C5	C6	1.393(4)
O1	C2	1.363(3)	C6	C7	1.384(3)
O1	C3	1.396(3)	C7	C8	1.388(3)
N1	C8	1.409(3)	C9	C10	1.401(3)
N1	C9	1.383(3)	C10	C11	1.398(4)
N1	C15	1.470(3)	C10	C14	1.446(3)
N2	C13	1.143(3)	C11	C12	1.367(3)
N3	C14	1.145(3)	C15	C16	1.511(3)
C1	C2	1.381(3)	C16	C17	1.383(4)
C1	C12	1.387(3)	C16	C21	1.391(3)
C1	C13	1.442(3)	C17	C18	1.384(3)
C2	C9	1.415(3)	C18	C19	1.384(4)
C3	C4	1.370(3)	C19	C20	1.377(4)
C3	C8	1.397(3)	C20	C21	1.389(3)

Table 5 Bond Angles.

Atom	Atom	Atom	Angle/°	Atom	Atom	Atom	Angle/°
C2	O1	C3	117.42(17)	C10	C9	C2	116.5(2)
C8	N1	C15	117.87(19)	C9	C10	C14	123.6(2)
C9	N1	C8	118.46(18)	C11	C10	C9	120.9(2)
C9	N1	C15	122.02(19)	C11	C10	C14	115.3(2)
C2	C1	C12	120.3(2)	F1	C11	C10	119.8(2)
C2	C1	C13	120.2(2)	F1	C11	C12	118.8(2)
C12	C1	C13	119.4(2)	C12	C11	C10	121.2(2)
O1	C2	C1	116.2(2)	F2	C12	C1	120.4(2)
O1	C2	C9	122.0(2)	F2	C12	C11	120.3(2)
C1	C2	C9	121.8(2)	C11	C12	C1	119.2(2)
O1	C3	C8	120.1(2)	N2	C13	C1	176.8(3)
C4	C3	O1	117.5(2)	N3	C14	C10	175.0(3)
C4	C3	C8	122.4(2)	N1	C15	C16	115.9(2)
C3	C4	C5	119.8(2)	C17	C16	C15	123.9(2)
C4	C5	C6	119.1(2)	C17	C16	C21	119.1(2)
C7	C6	C5	120.7(2)	C21	C16	C15	117.0(2)
C6	C7	C8	120.7(2)	C16	C17	C18	120.2(2)
C3	C8	N1	119.7(2)	C17	C18	C19	120.6(2)
C7	C8	N1	123.0(2)	C20	C19	C18	119.5(2)

C7	C8	C3	117.3(2)	C19	C20	C21	120.1(2)
N1	C9	C2	118.4(2)	C20	C21	C16	120.4(2)
N1	C9	C10	125.1(2)				

Table 6 Hydrogen Atom Coordinates (Å×10⁴) and Isotropic Displacement Parameters (Å²×10³)

Atom	x	y	z	U(eq)
H4	2394.87	6346.45	7598.47	43
H5	2362.6	6619.89	8697.82	46
H6	4286.54	6575.75	9361.42	48
H7	6210.12	6289.81	8932.27	44
H15A	8228.8	4510.12	7788.23	42
H15B	7347.61	4051.61	8334.8	42
H17	7765.24	8779.4	8297.54	45
H18	9141.82	10479.28	9005.2	48
H19	10729.88	9011.8	9672.43	45
H20	10903.6	5818.07	9648	45
H21	9504.28	4097.52	8952.41	42

2,3,5,6-Tetrafluoroterephthalonitrile (2.4):
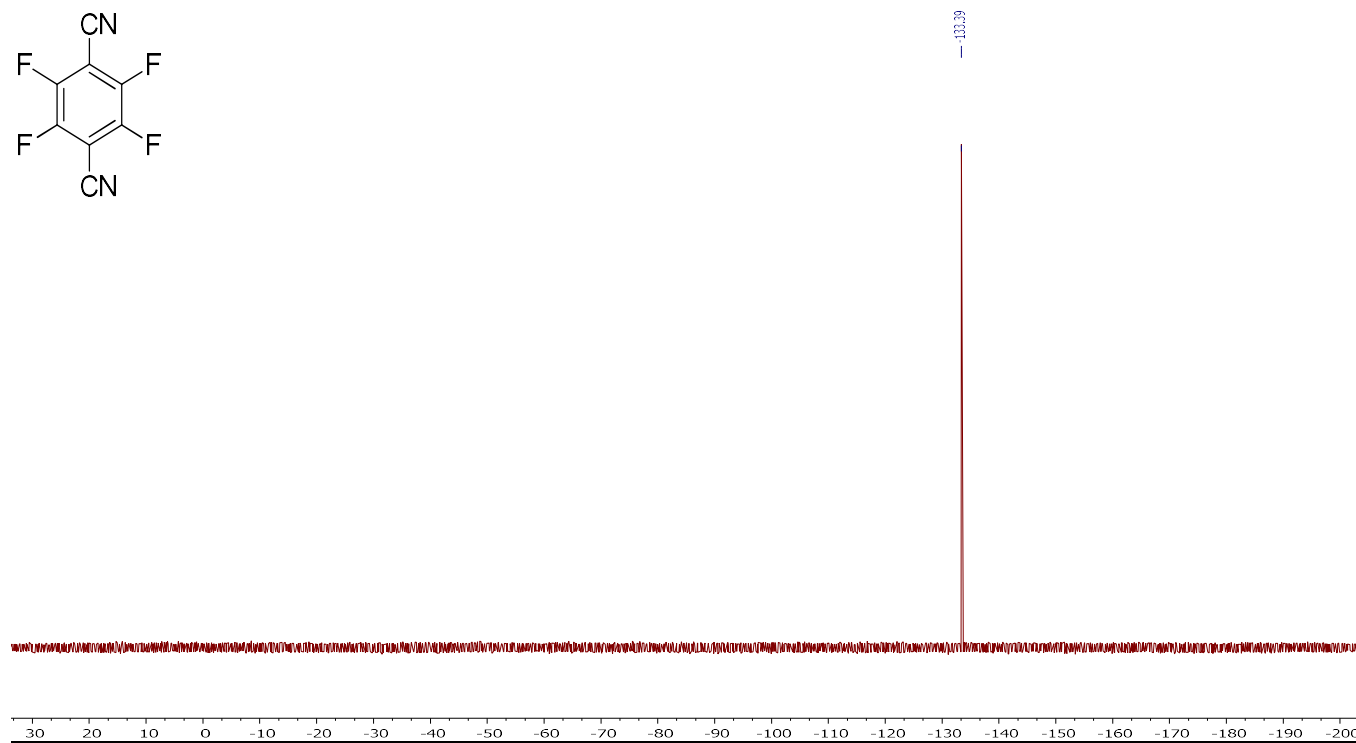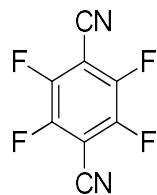
1,2-dibromo-4,5-bis(methoxymethoxy)benzene (2.12)
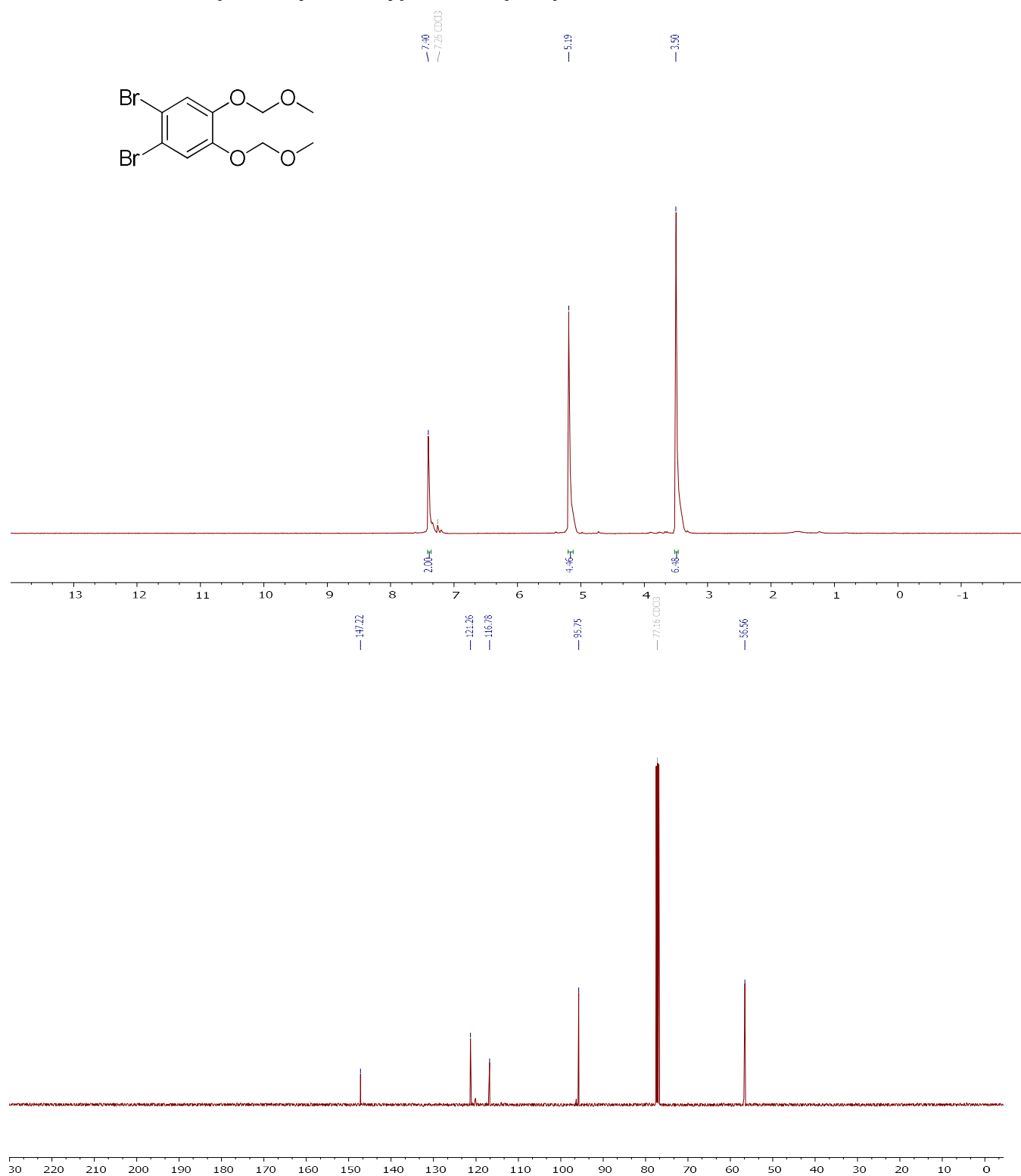
3,3'',4,4''-tetramethoxy-4',5'-bis(methoxymethoxy)-1,1':2',1''-terphenyl (2.13)
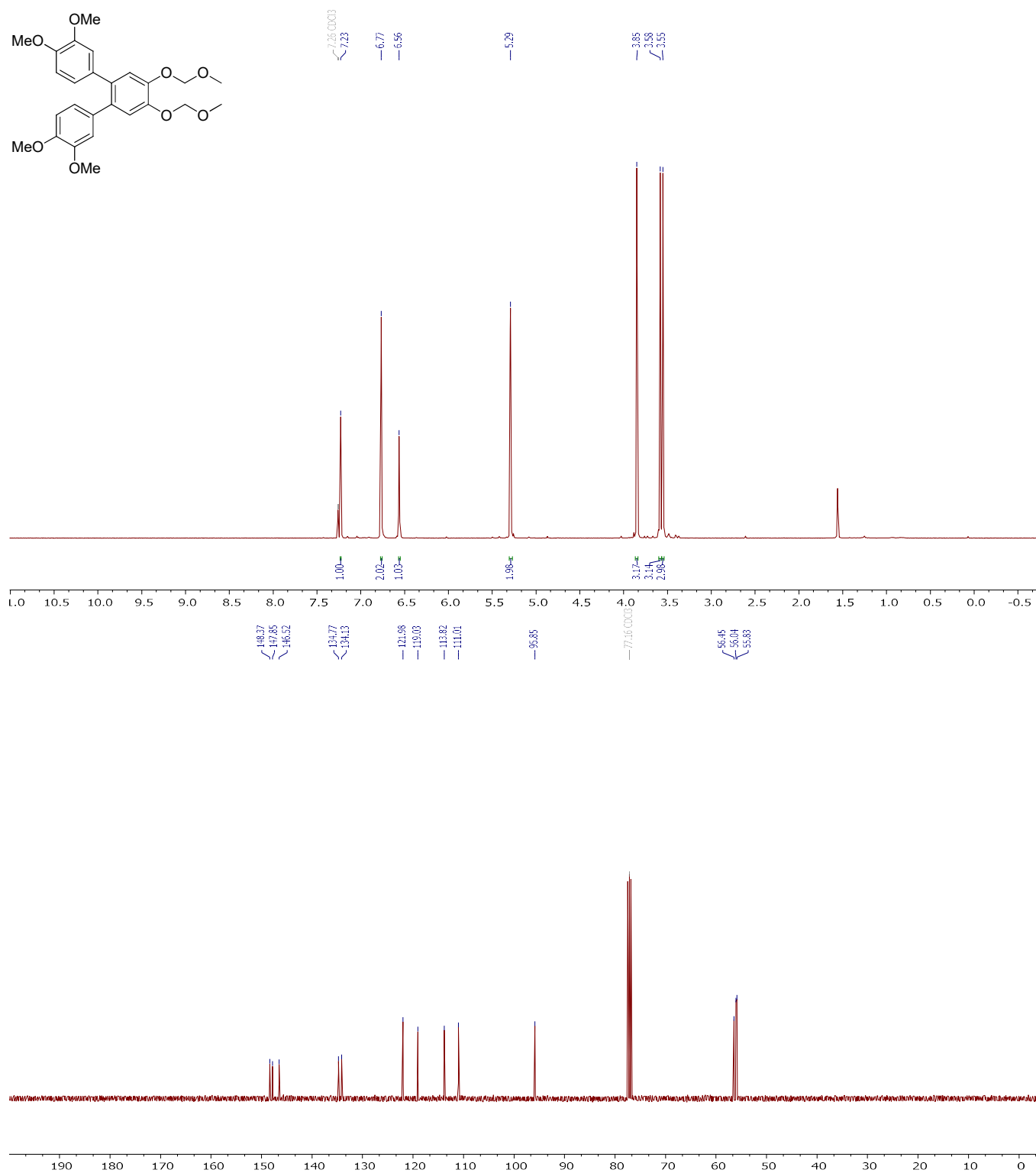
3,3'',4,4''-tetrakis(hexyloxy)-4',5'-bis(methoxymethoxy)-1,1':2',1''-terphenyl (2.16b)
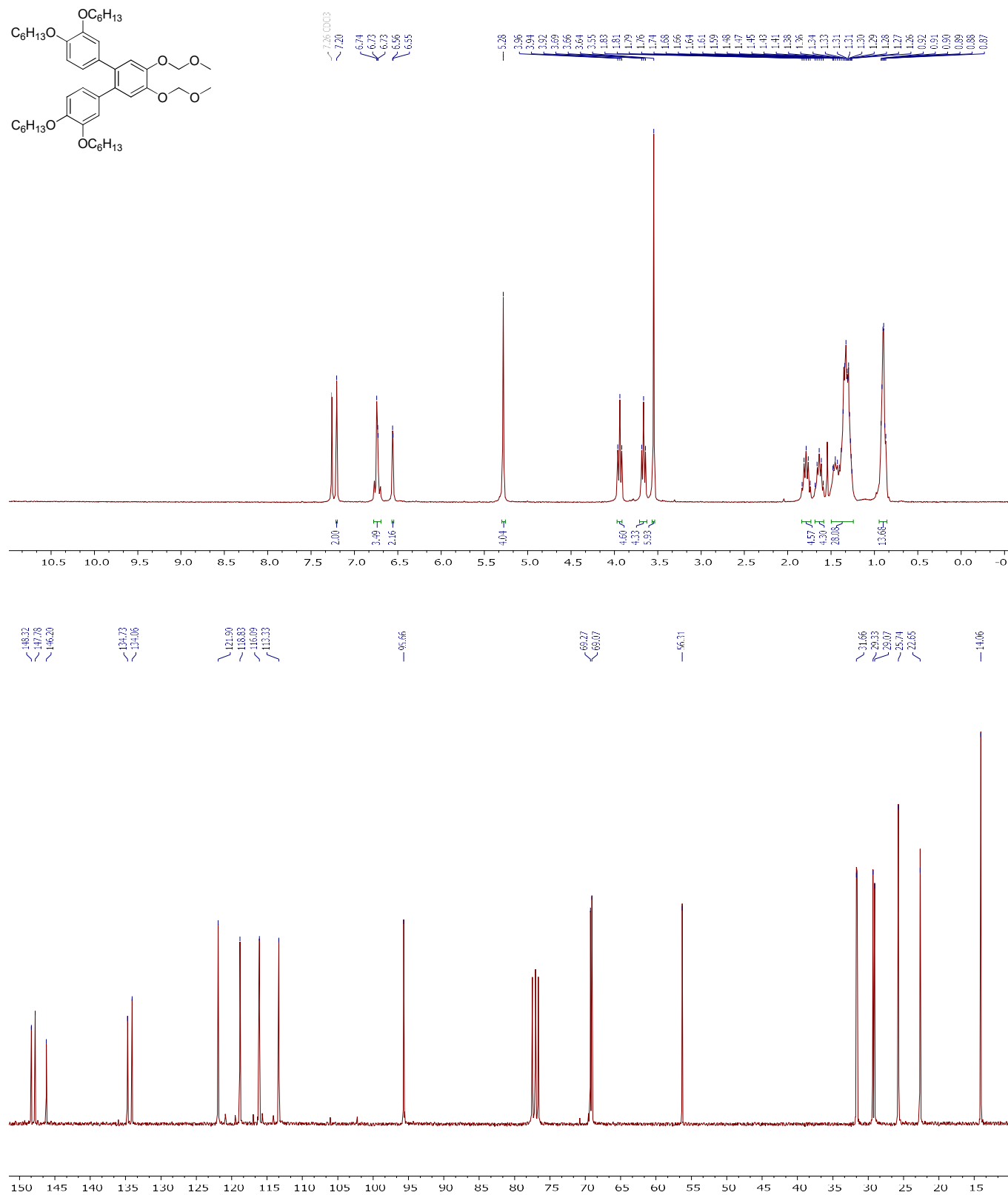
3,3'',4,4''-tetrakis(decyloxy)-4',5'-bis(methoxymethoxy)-1,1':2',1''-terphenyl (2.16a)
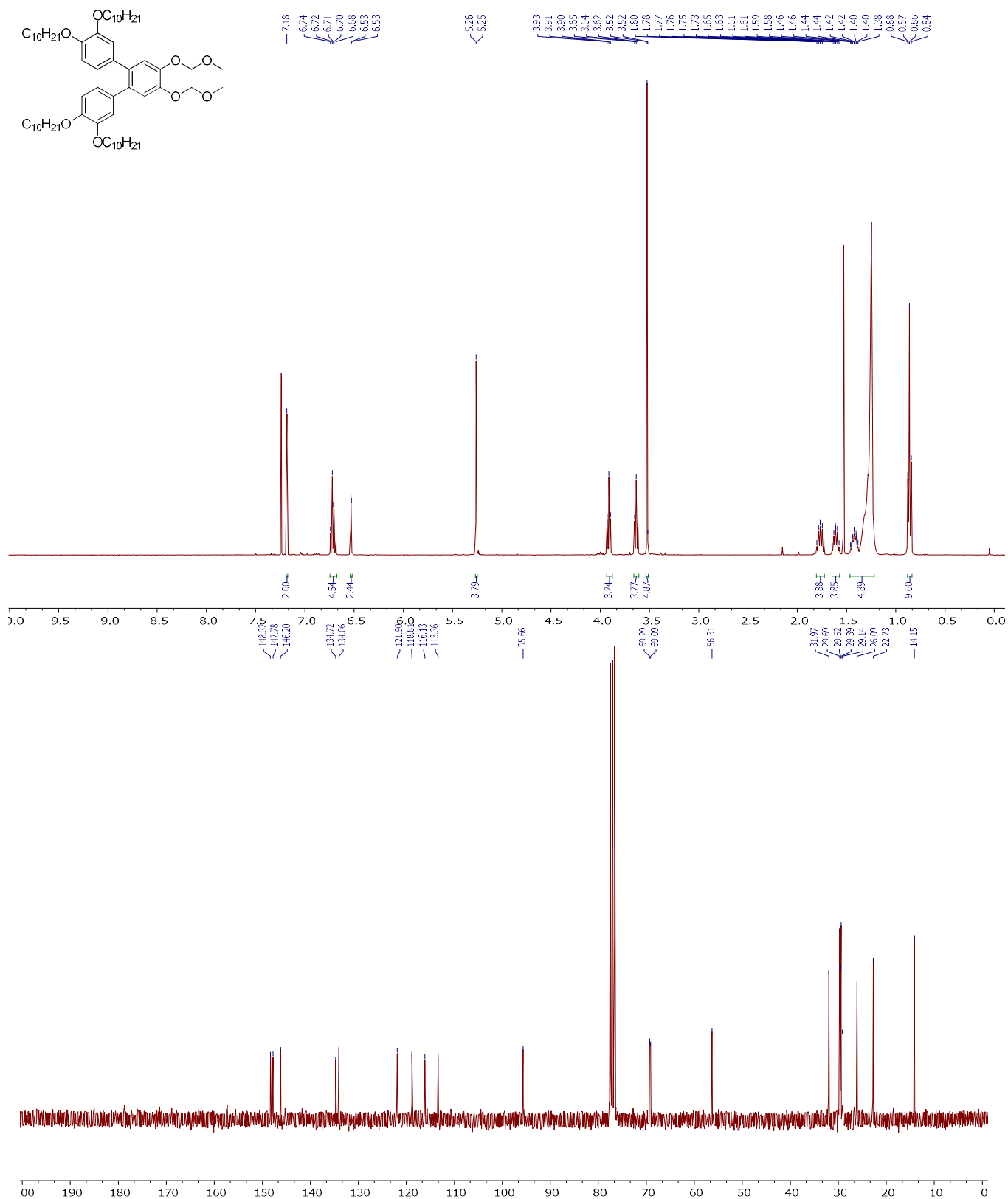
3,3'',4,4''-tetramethoxy-[1,1':2',1''-terphenyl]-4',5'-diol (2.14)
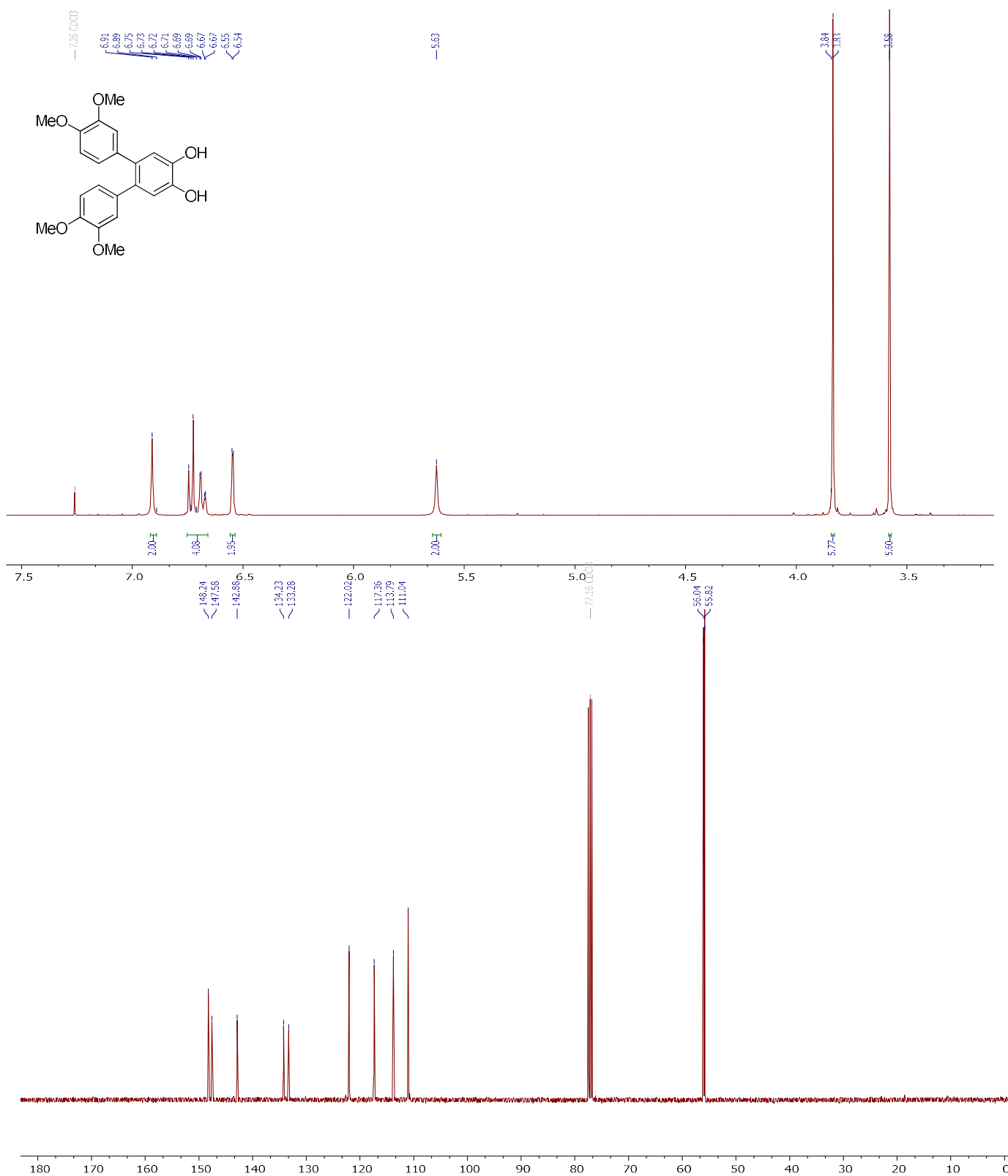
3,3'',4,4''-tetrakis(hexyloxy)-[1,1':2',1''-terphenyl]-4',5'-diol (2.17b)

3,3'',4,4''-tetrakis(decyloxy)-[1,1':2',1''-terphenyl]-4',5'-diol (2.17a)
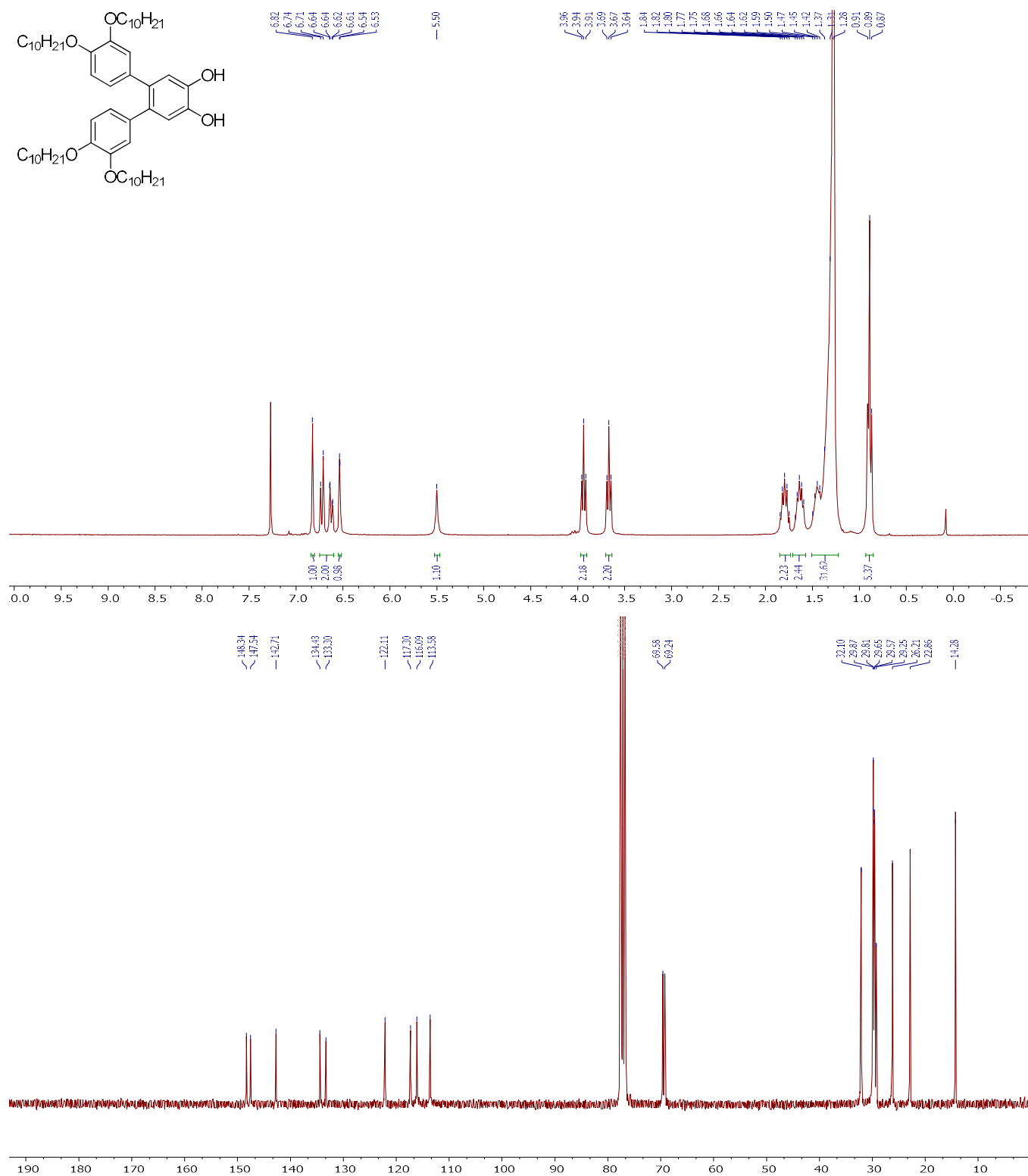
2,3,9,10-tetrakis(3,4-dimethoxyphenyl)benzo[5,6][1,4]dioxino[2,3-b]dibenzo[b,e][1,4]dioxine-6,13-dicarbonitrile (2.1c)
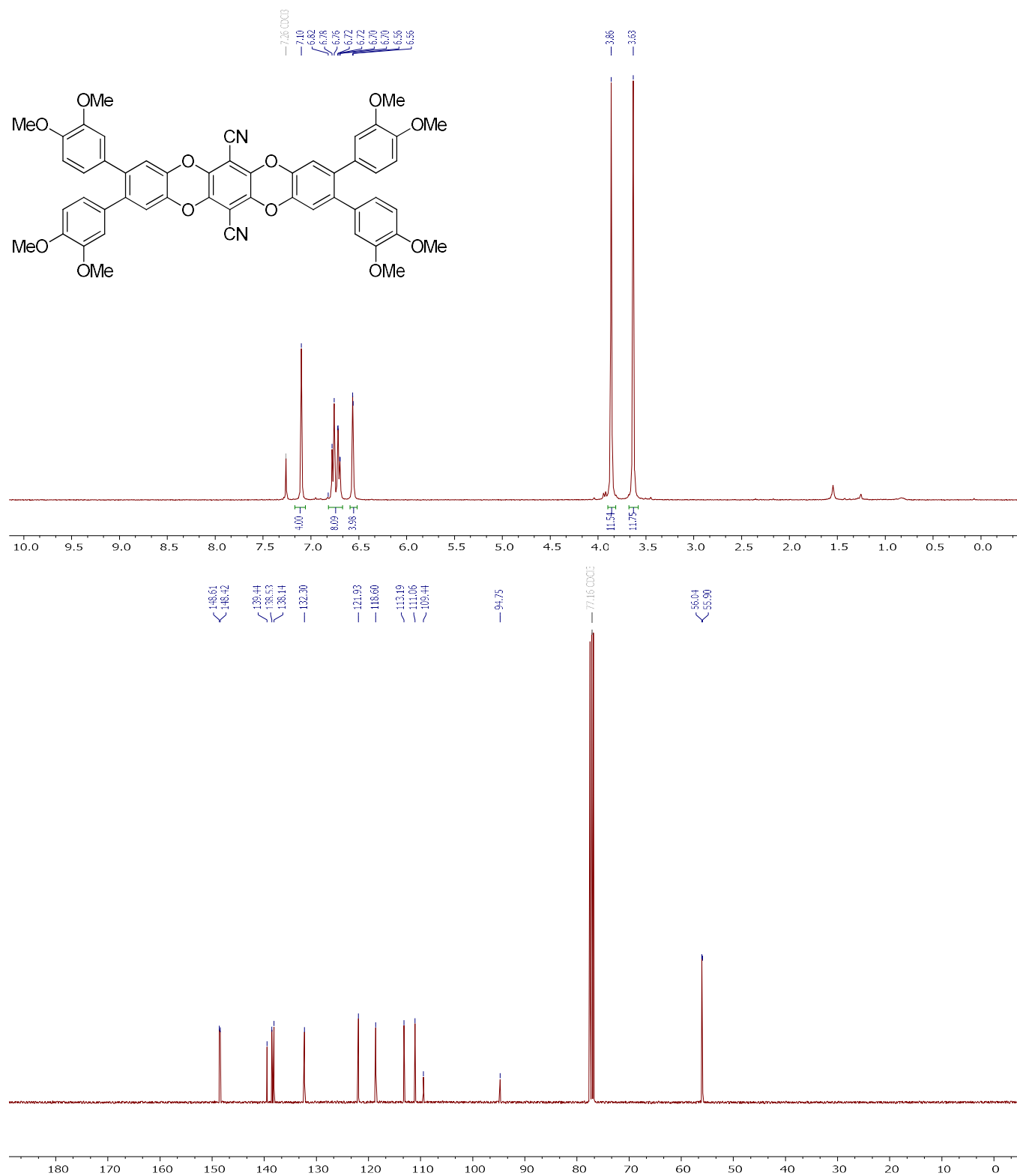
2,3,9,10-tetrakis(3,4-bis(hexyloxy)phenyl)benzo[5,6][1,4]dioxino[2,3-b]dibenzo[b,e][1,4]dioxine-6,13-dicarbonitrile (2.1b)
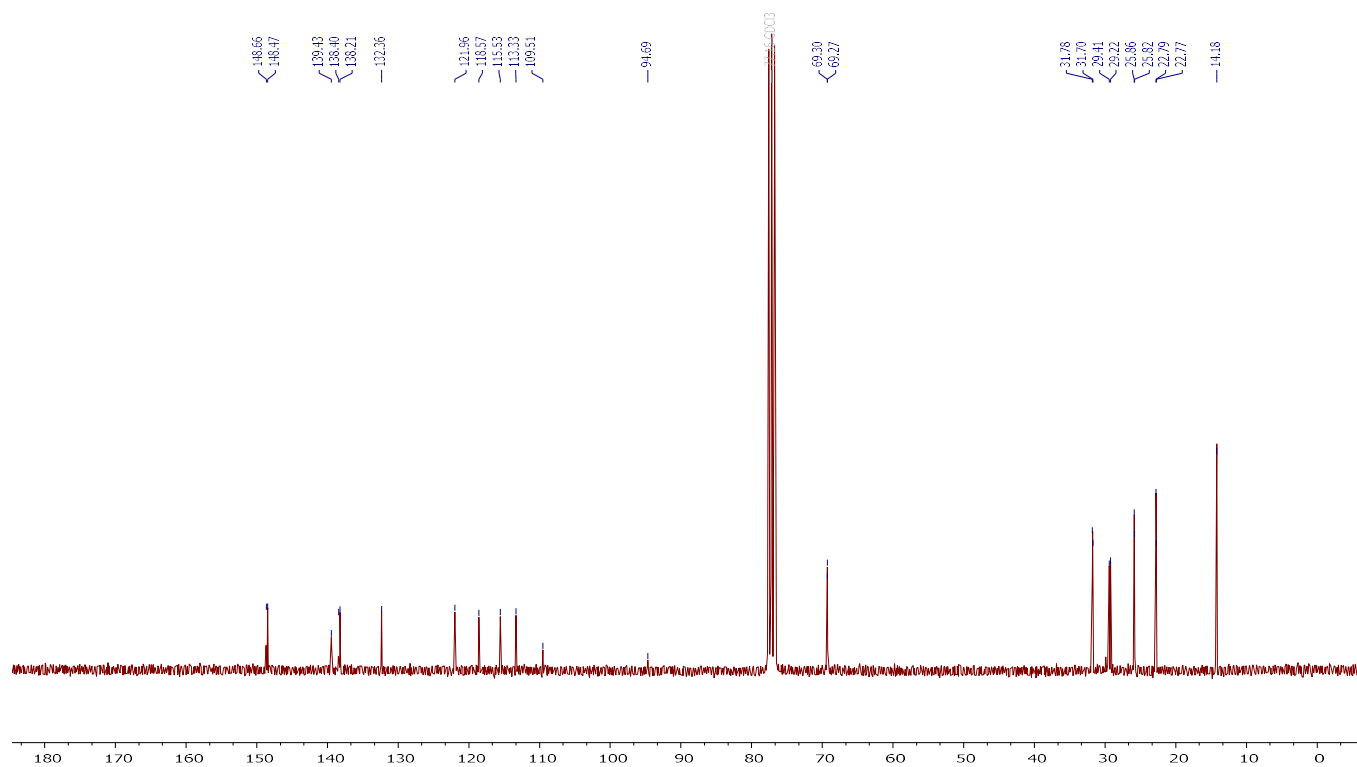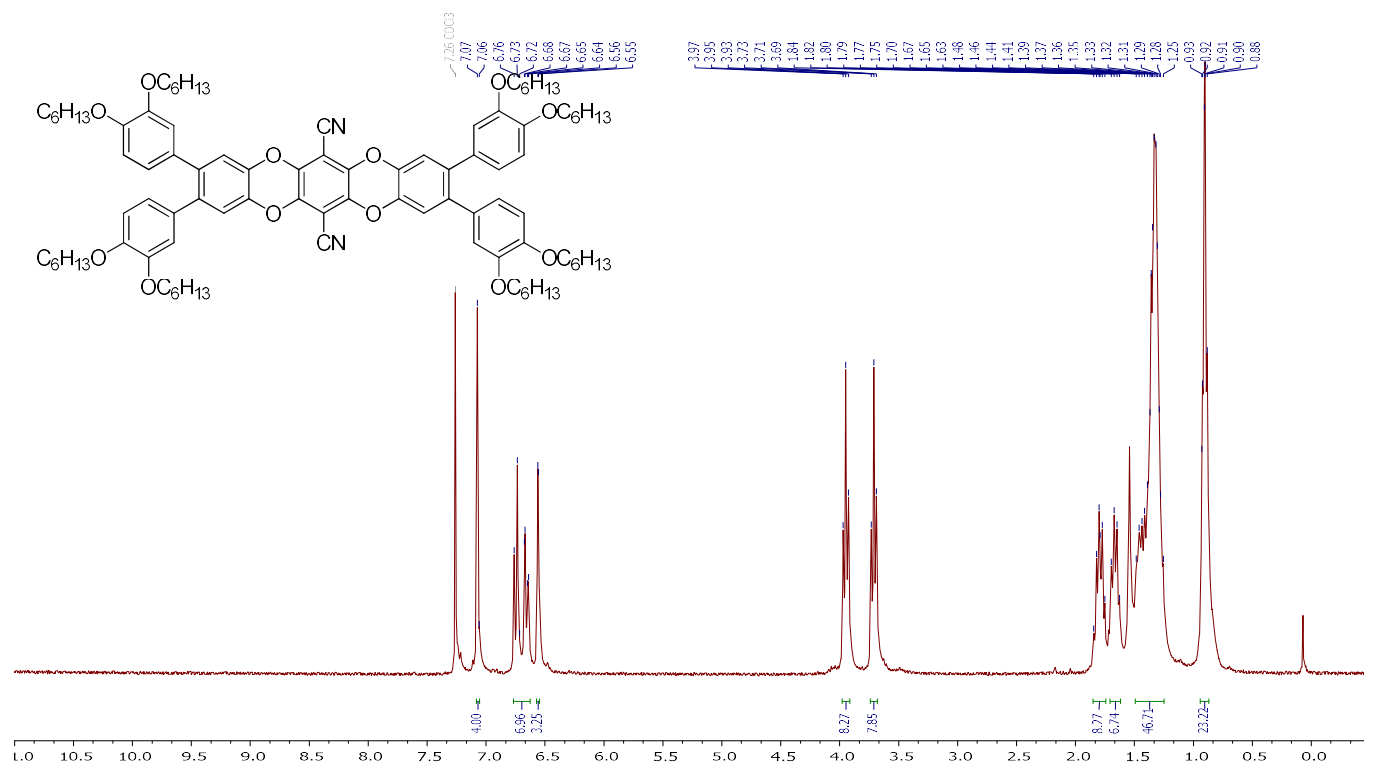
2,3,9,10-tetrakis(3,4-bis(decyloxy)phenyl)benzo[5,6][1,4]dioxino[2,3-b]dibenzo[b,e][1,4]dioxine-6,13-dicarbonitrile (2.1a)

7,8-bis(3,4-dimethoxyphenyl)-2,3-difluorodibenzo[b,e][1,4]dioxine-1,4-   dicarbonitrile
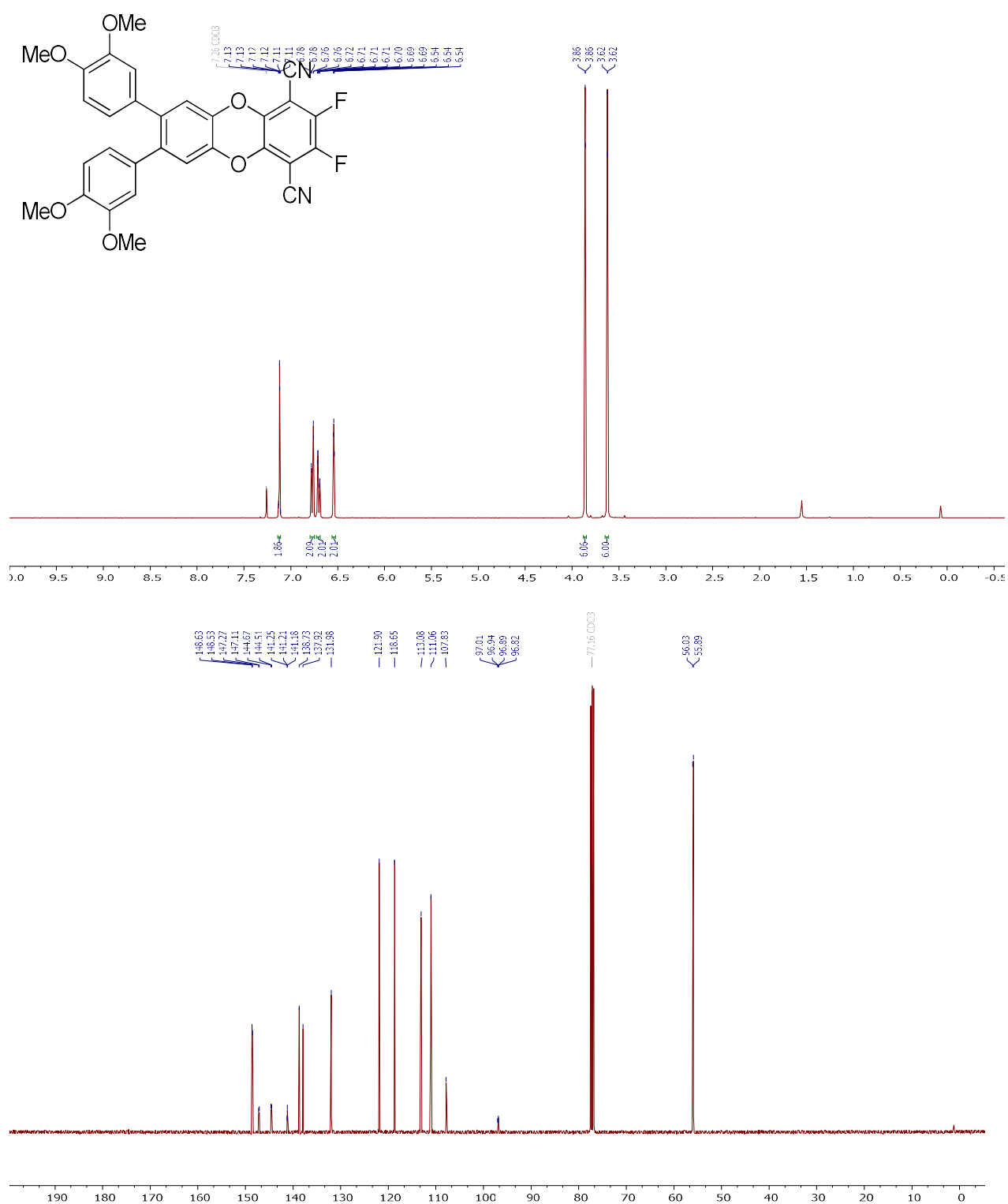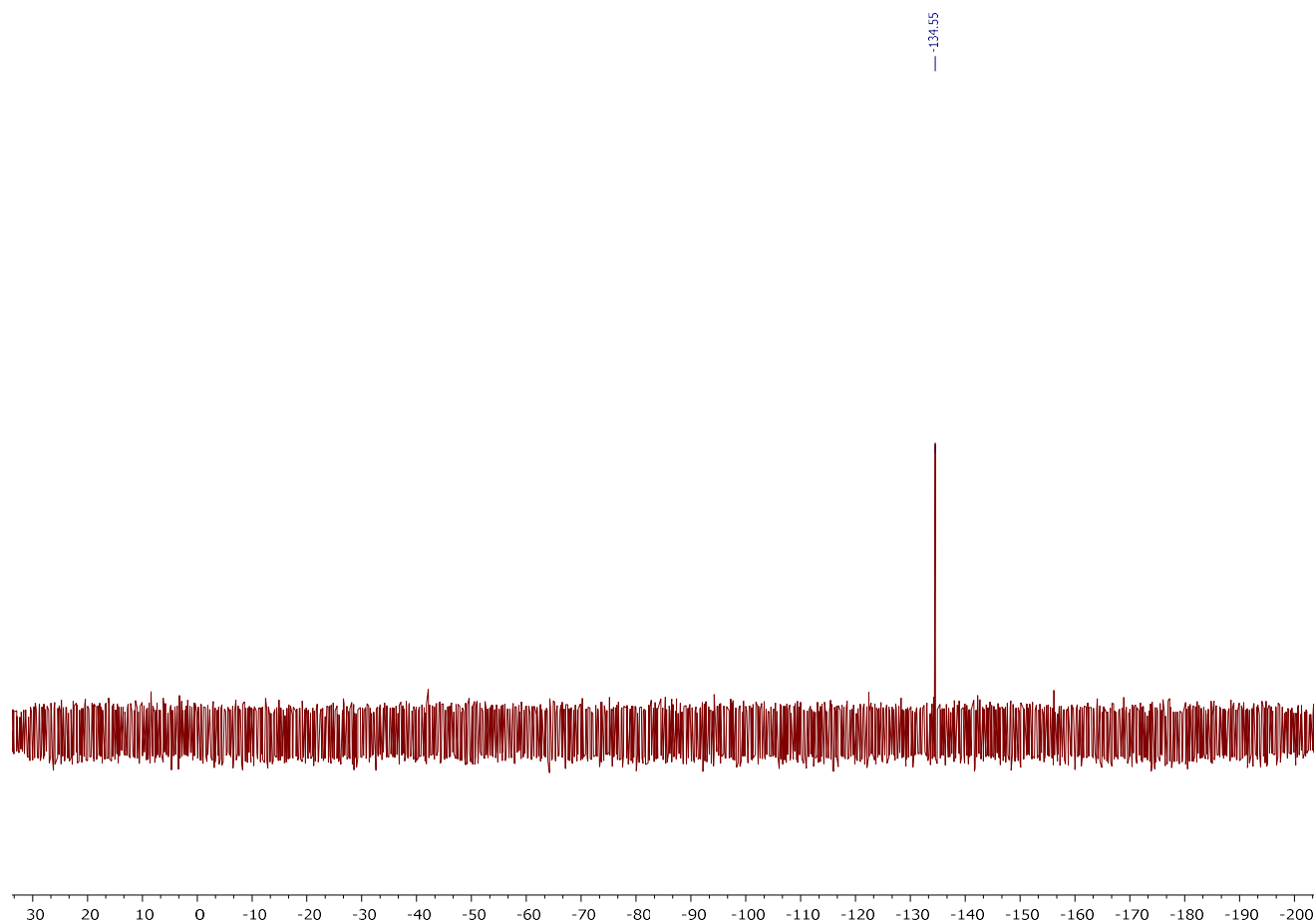
(2.18)

—134.55

30 20 10 0 -10 -20 -30 -40 -50 -60 -70 -80 -90 -100 -110 -120 -130 -140 -150 -160 -170 -180 -190 -200

271

2,3-bis(3,4-dimethoxyphenyl)benzo[5,6][1,4]dioxino[2,3-]dibenzo[b,e][1,4]dioxine-6,13-dicarbonitrile (2.19):

2,3-difluoro-10H-phenoxazine-1,4-dicarbonitrile (3.23):

* = DMF

* = DMF
** = CHCl3

142.29
142.36
148.14
148.21

B (d)
-148.17
J(19.81)

A (d)
-142.32
J(19.61)

-141 -143 -145 -147 -149 -151

30 20 10 0 -10 -20 -30 -40 -50 -60 -70 -80 -90 -100 -110 -120 -130 -140 -150 -160 -170 -180 -190 -2
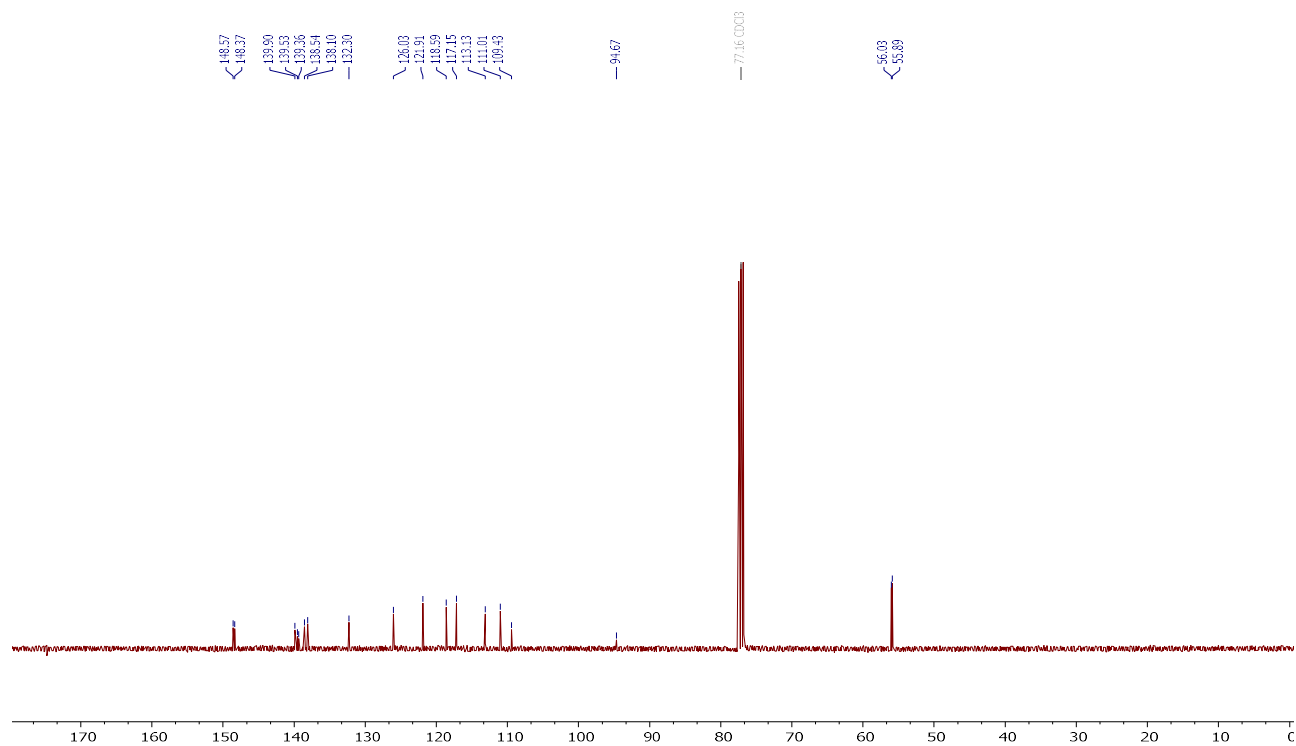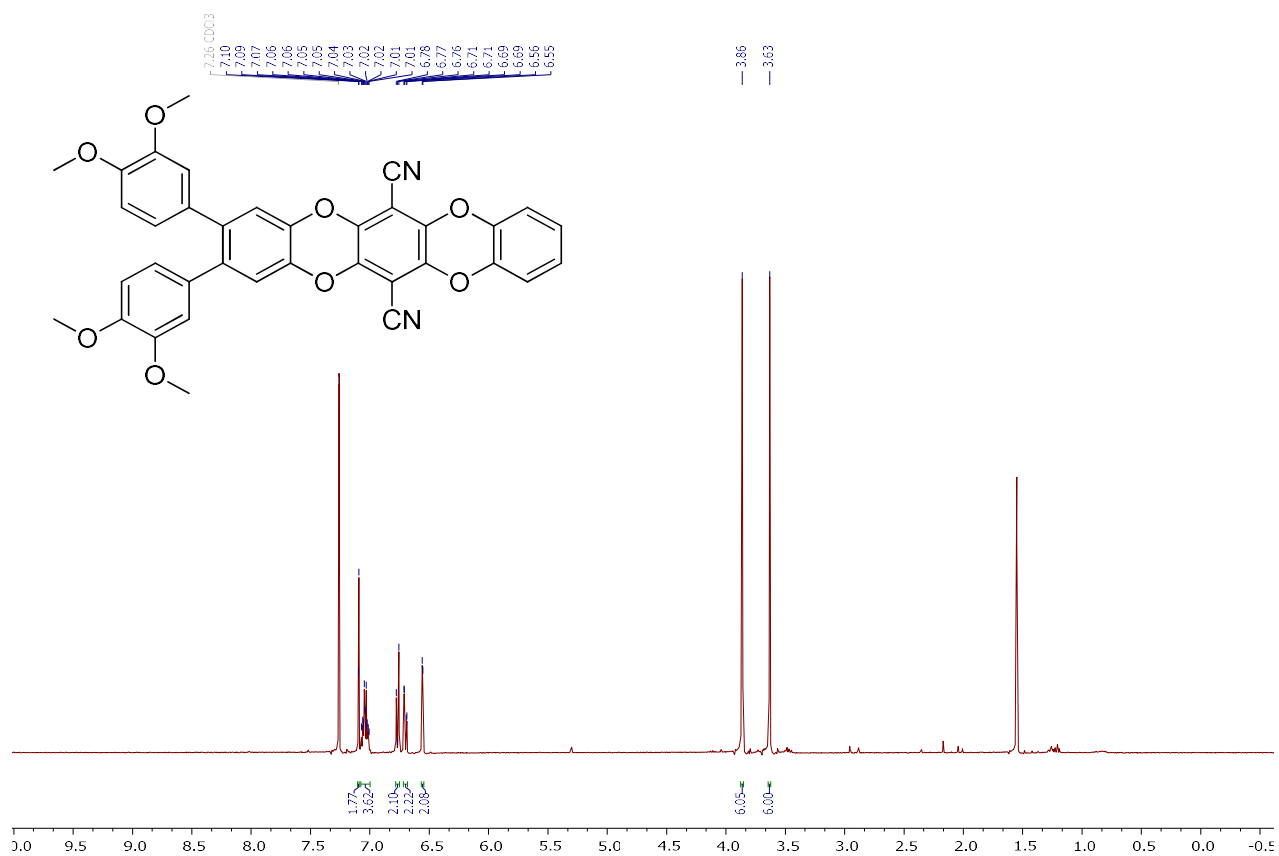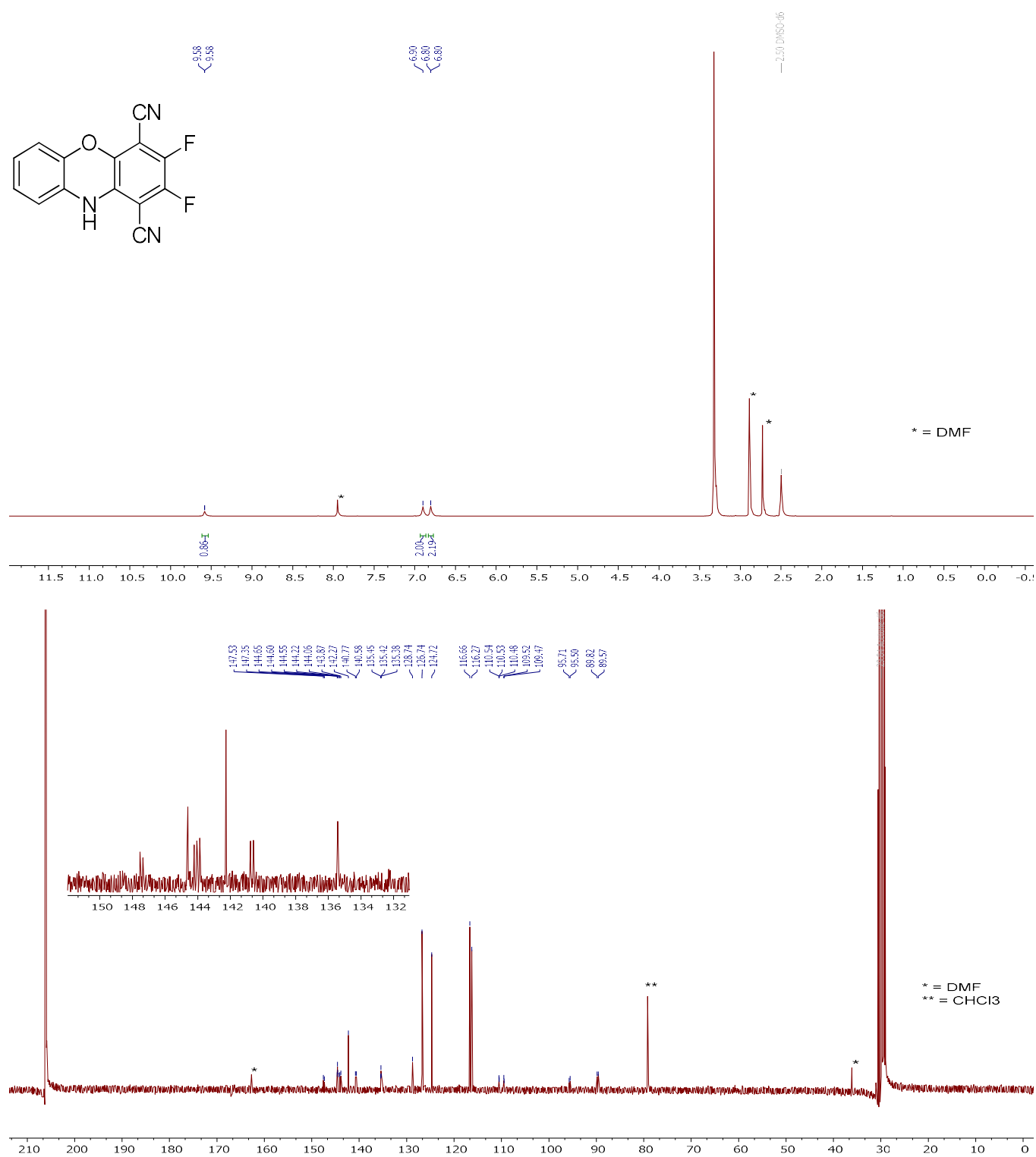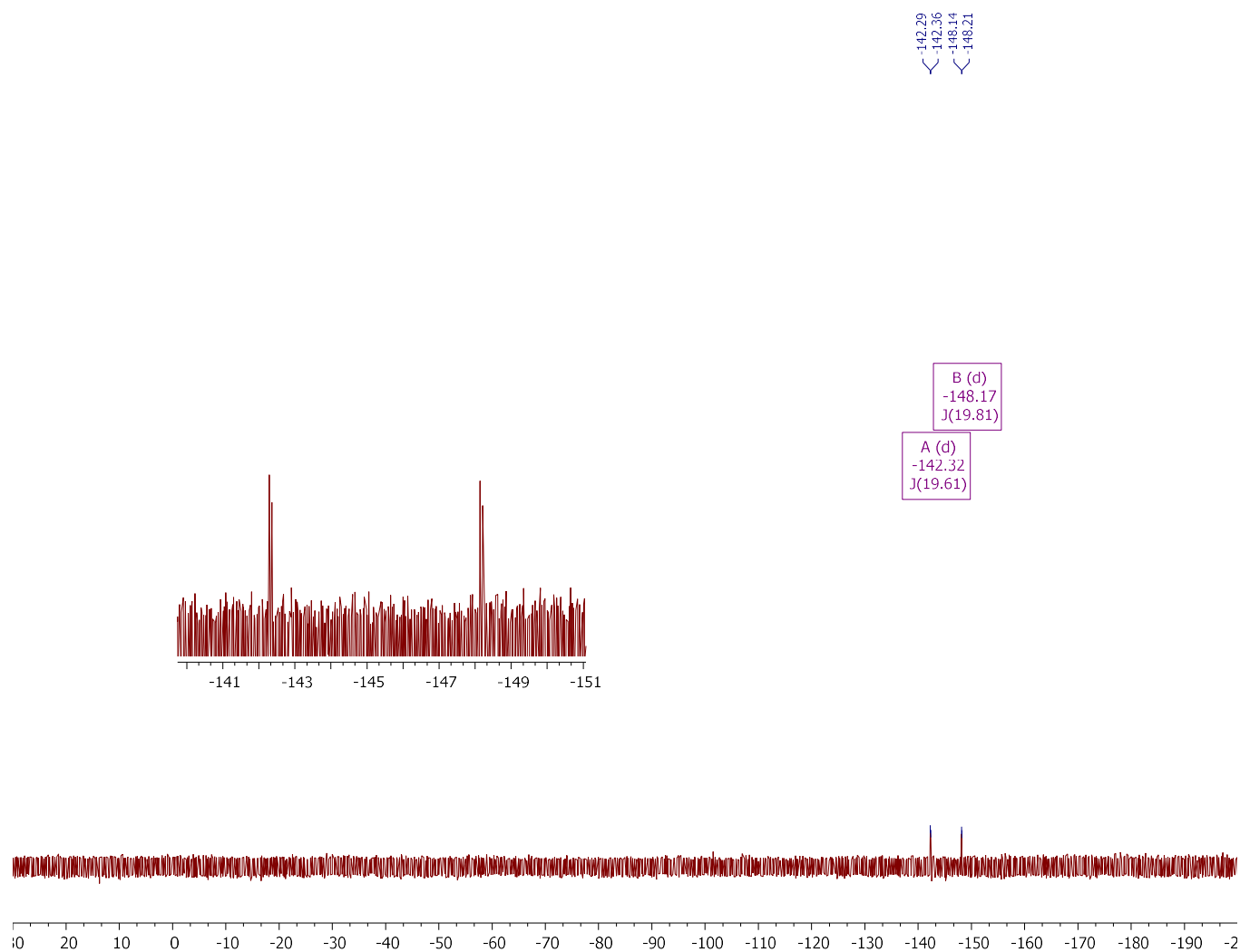
N-(2-hydroxyphenyl)acetamide (3.26):
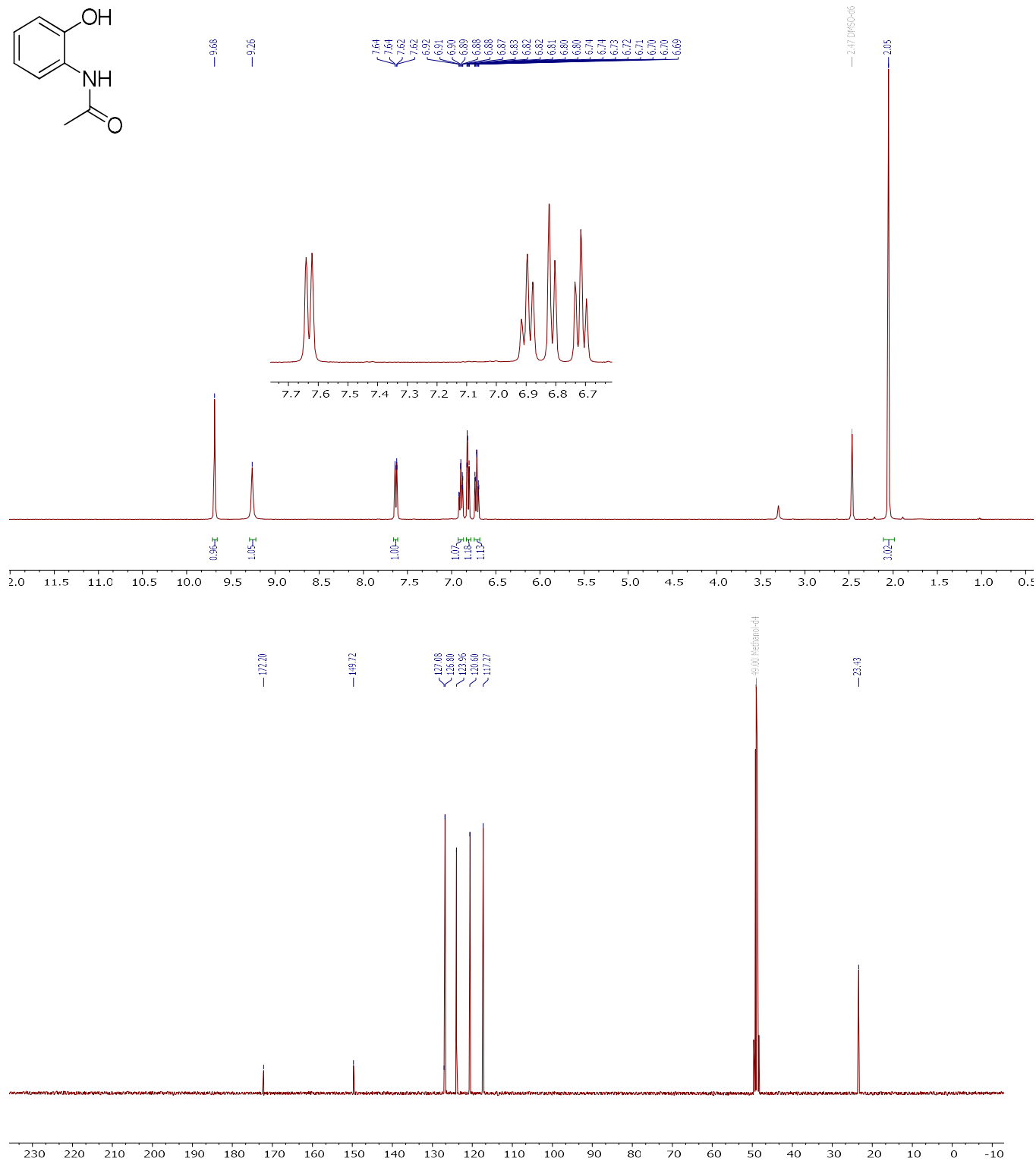
2-(N-ethylamino)phenol   (3.27):
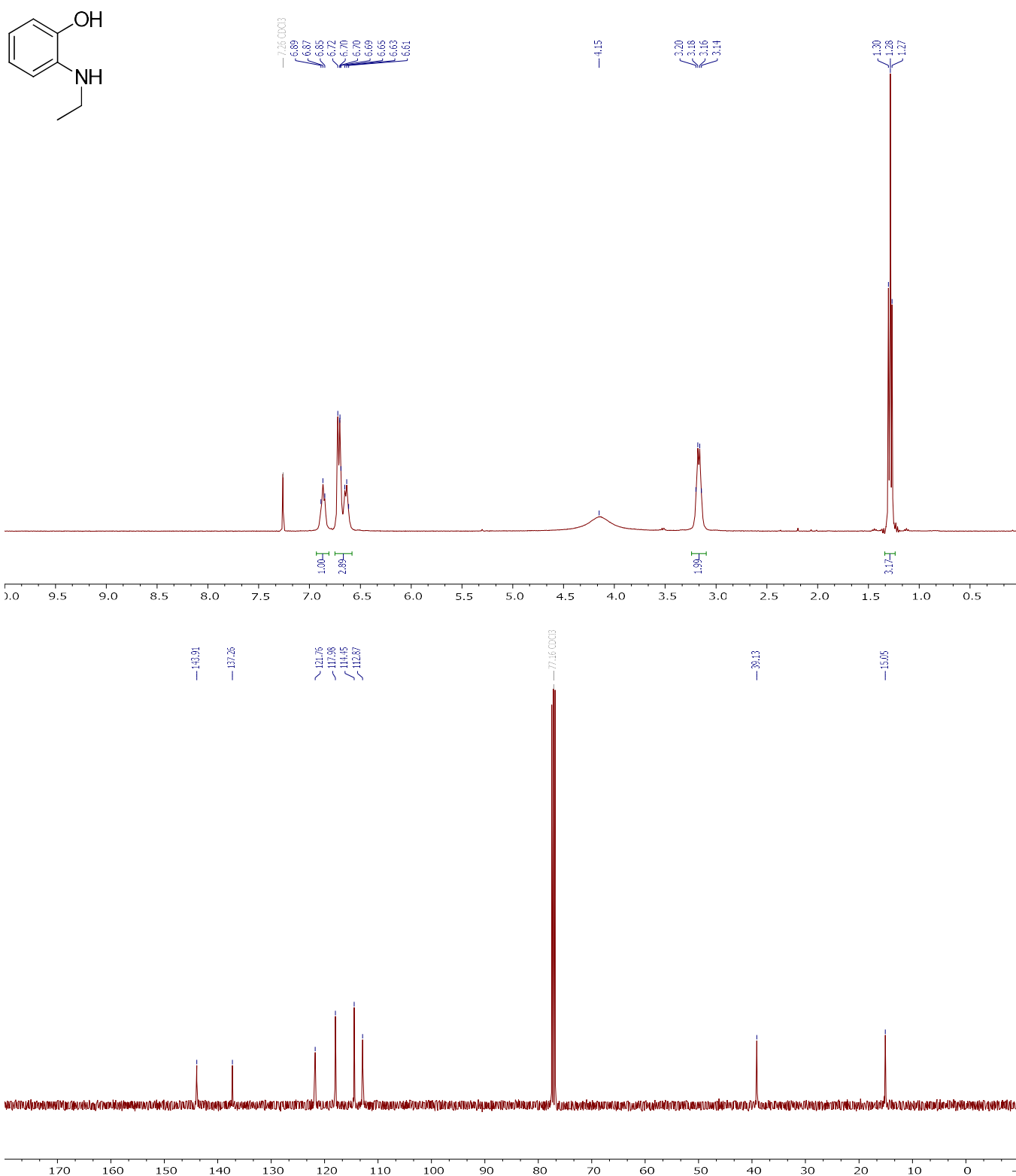
7,14-diethyl-7,14-dihydrobenzo[5,6][1,4]oxazino[2,3-b]phenoxazine-6,13-dicarbonitrile (3.28):
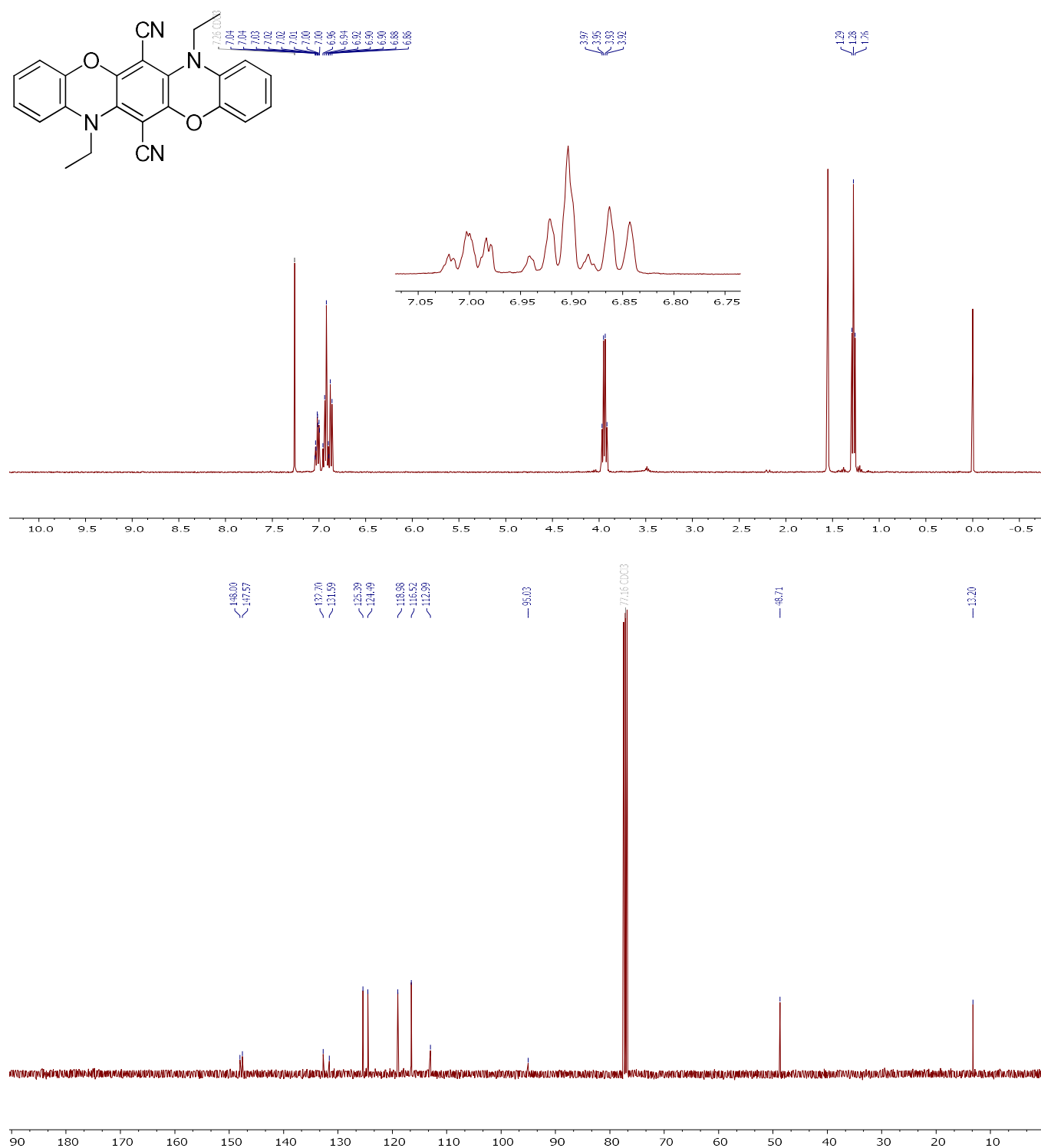
N-(2-hydroxyphenyl)decanamide (3.29):
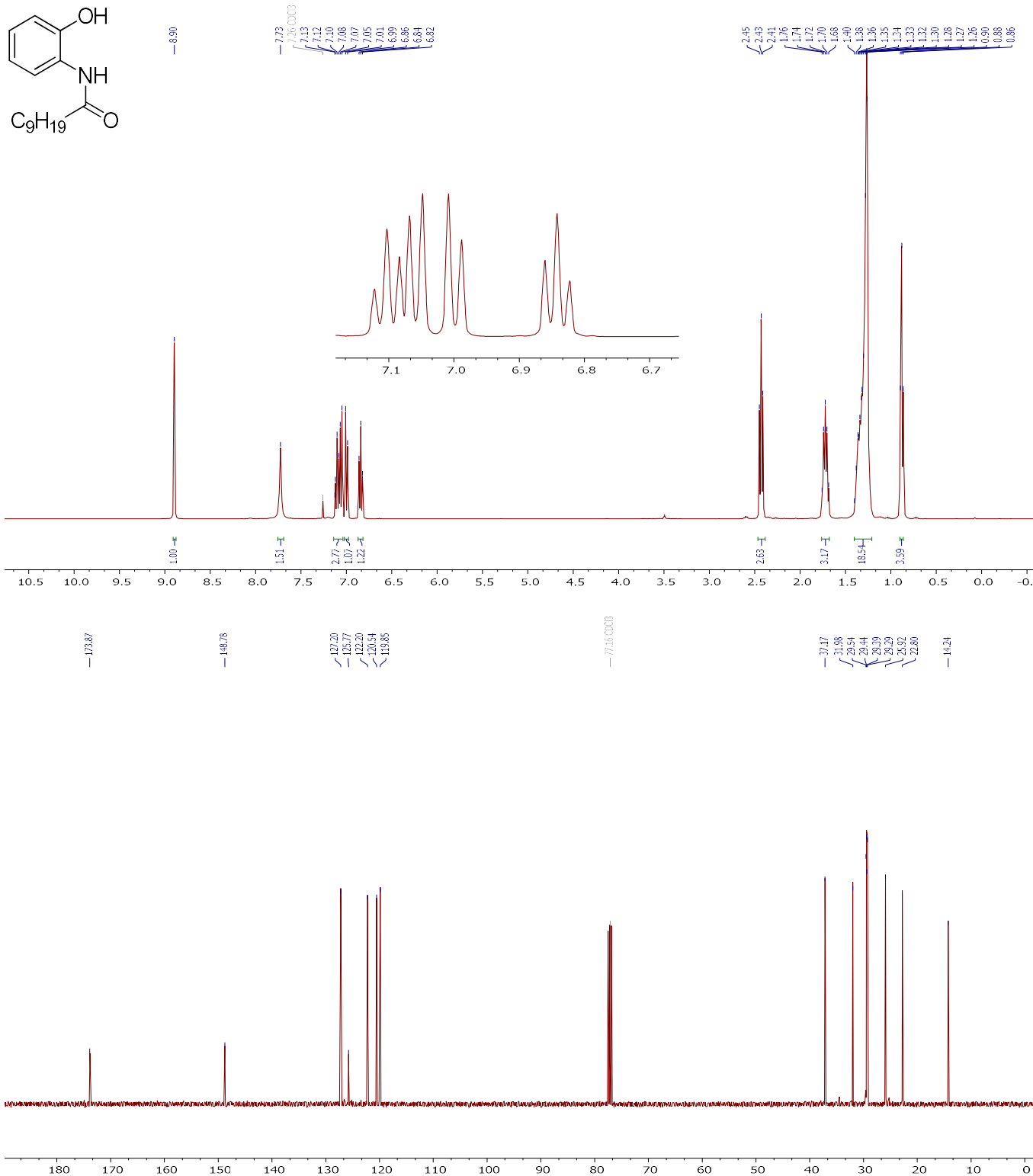
2-(N-decylamino)phenol (3.30):
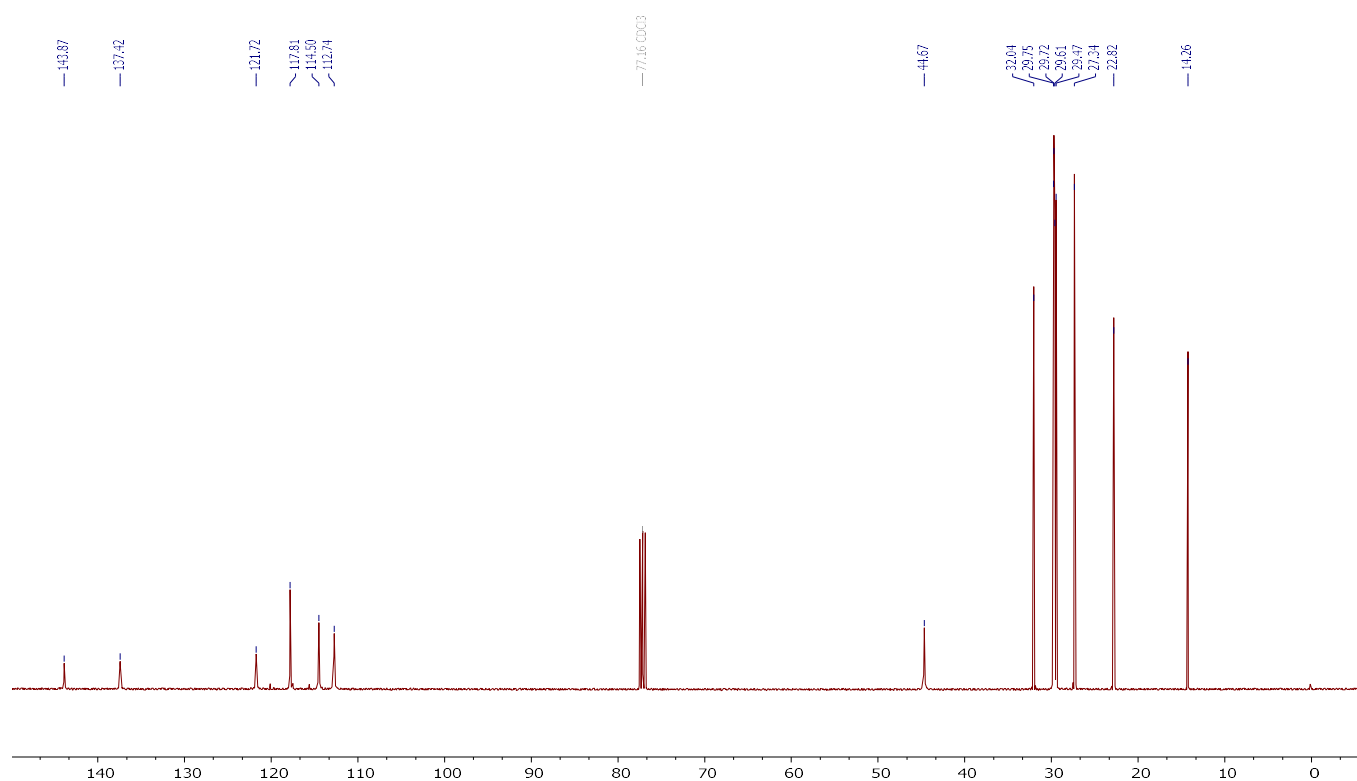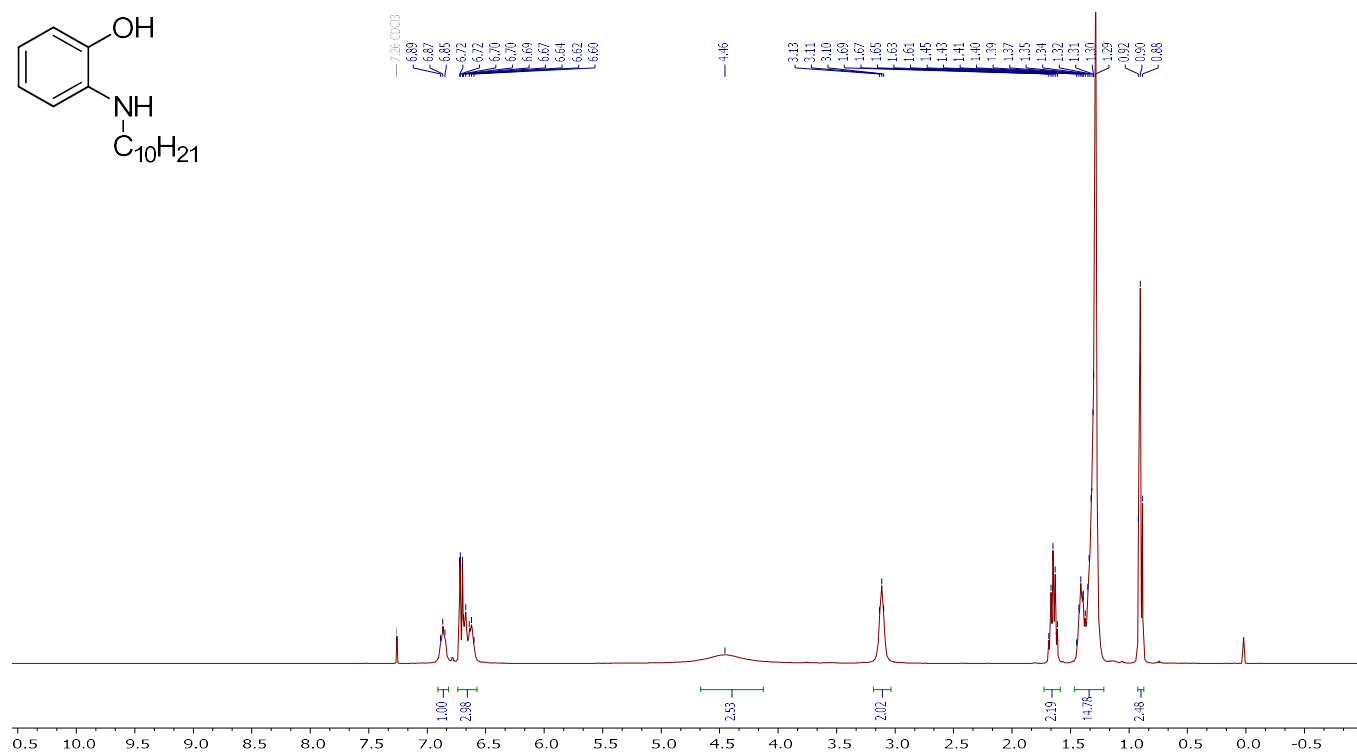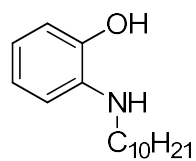
7,14-didecyl-7,14-dihydrobenzo[5,6][1,4]oxazino[2,3-b]phenoxazine-6,13-dicarbonitrile (3.31):

10-ethyl-2,3-difluoro-10H-phenoxazine-1,4-dicarbonitrile (3.32):

283

10-benzyl-2,3-difluoro-10H-phenoxazine-1,4-dicarbonitrile (3.38):

B (d)
-139.16
J(20.46)

A (d)
-143.93
J(20.71)

-139.13
-139.18
-143.90
-143.95

| 30 | 20 | 10 | 0 | -10 | -20 | -30 | -40 | -50 | -60 | -70 | -80 | -90 | -100 | -110 | -120 | -130 | -140 | -150 | -160 | -170 | -180 | -190 | -200 |

2,3-difluorodibenzo[b,e][1,4]dioxine-1,4-dicarbonitrile (3.16):

—134.75

14-ethyl-14H-benzo[5,6][1,4]dioxino[2,3-b]phenoxazine-6,13-dicarbonitrile (3.51):

9,10-bis(3,4-dimethoxyphenyl)-14-ethyl-14H-benzo[5,6][1,4]dioxino[2,3-b]phenoxazine-6,13-dicarbonitrile (5.53):

N,N'-(1,2-phenylene)diacetamide (3.61):

N1,N2-diethyl-1,2-benzenediamine (3.62):
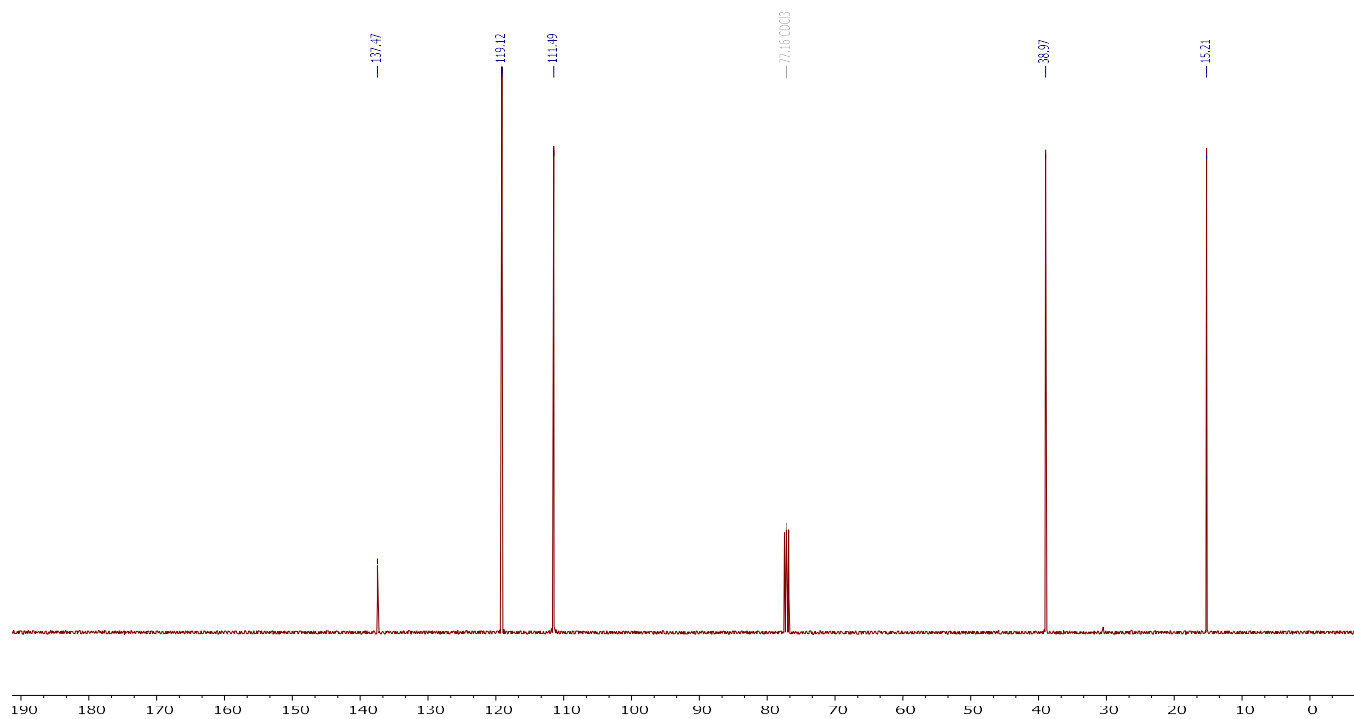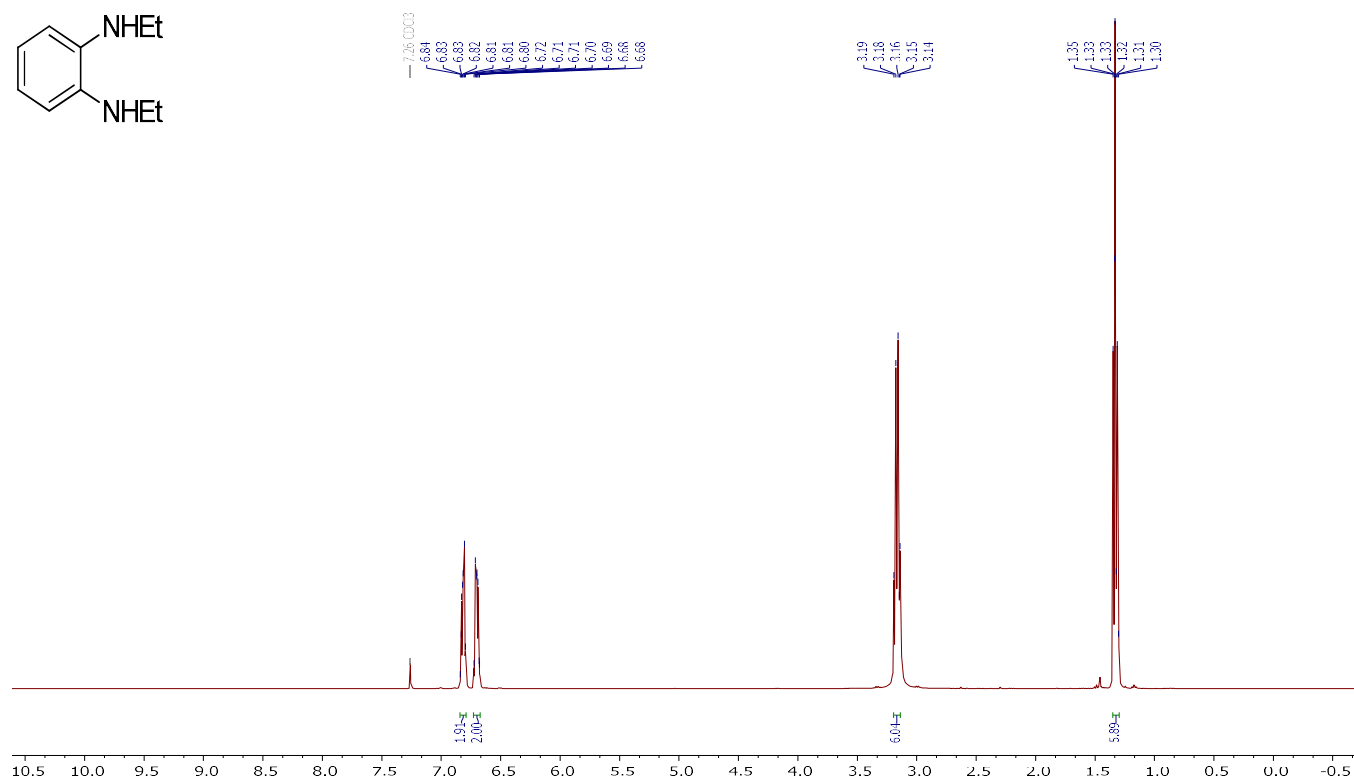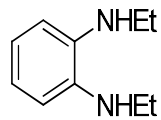
5,10-diethyl-2,3-difluoro-5,10-dihydrophenazine-1,4-dicarbonitrile **(3.69):**
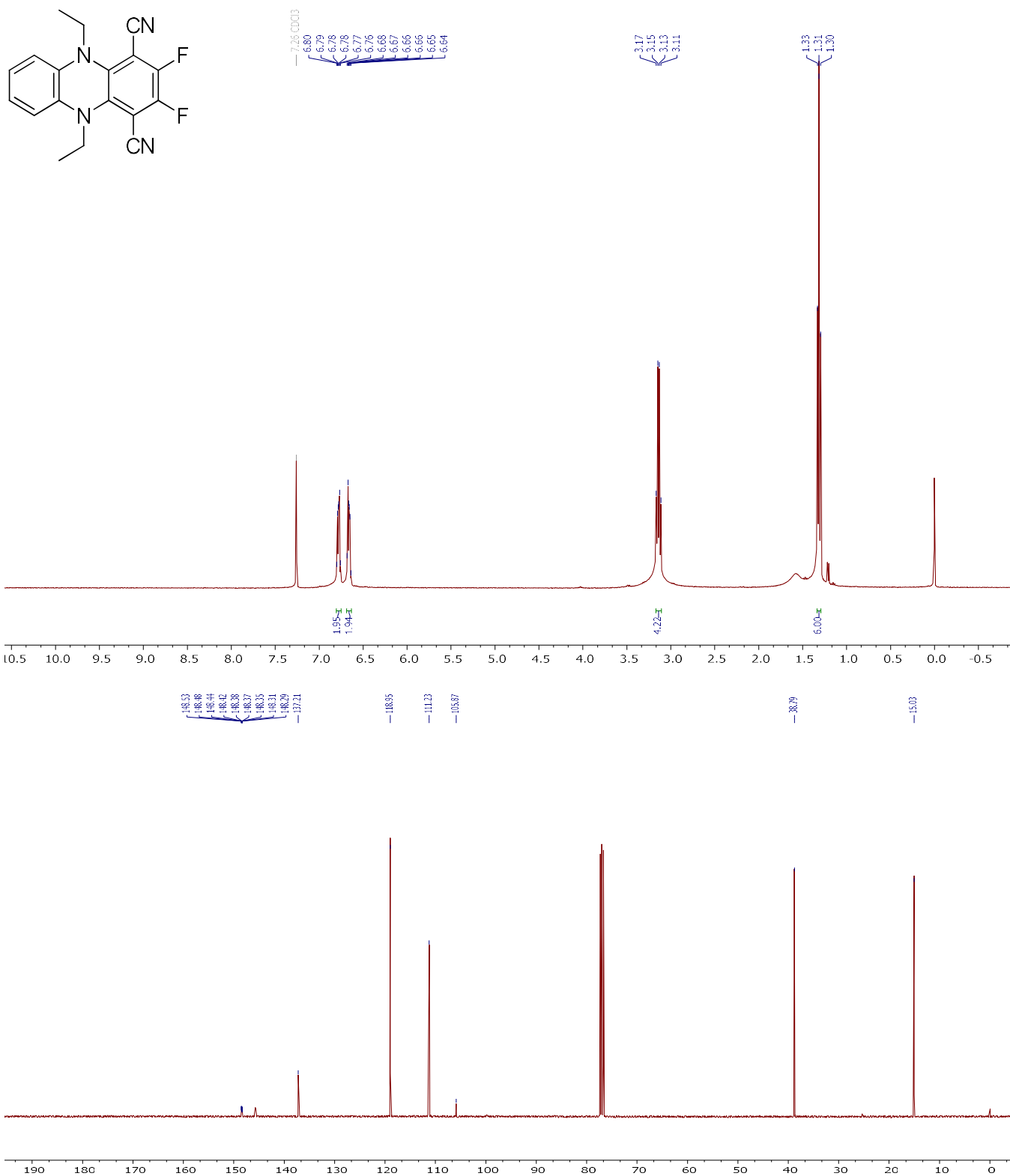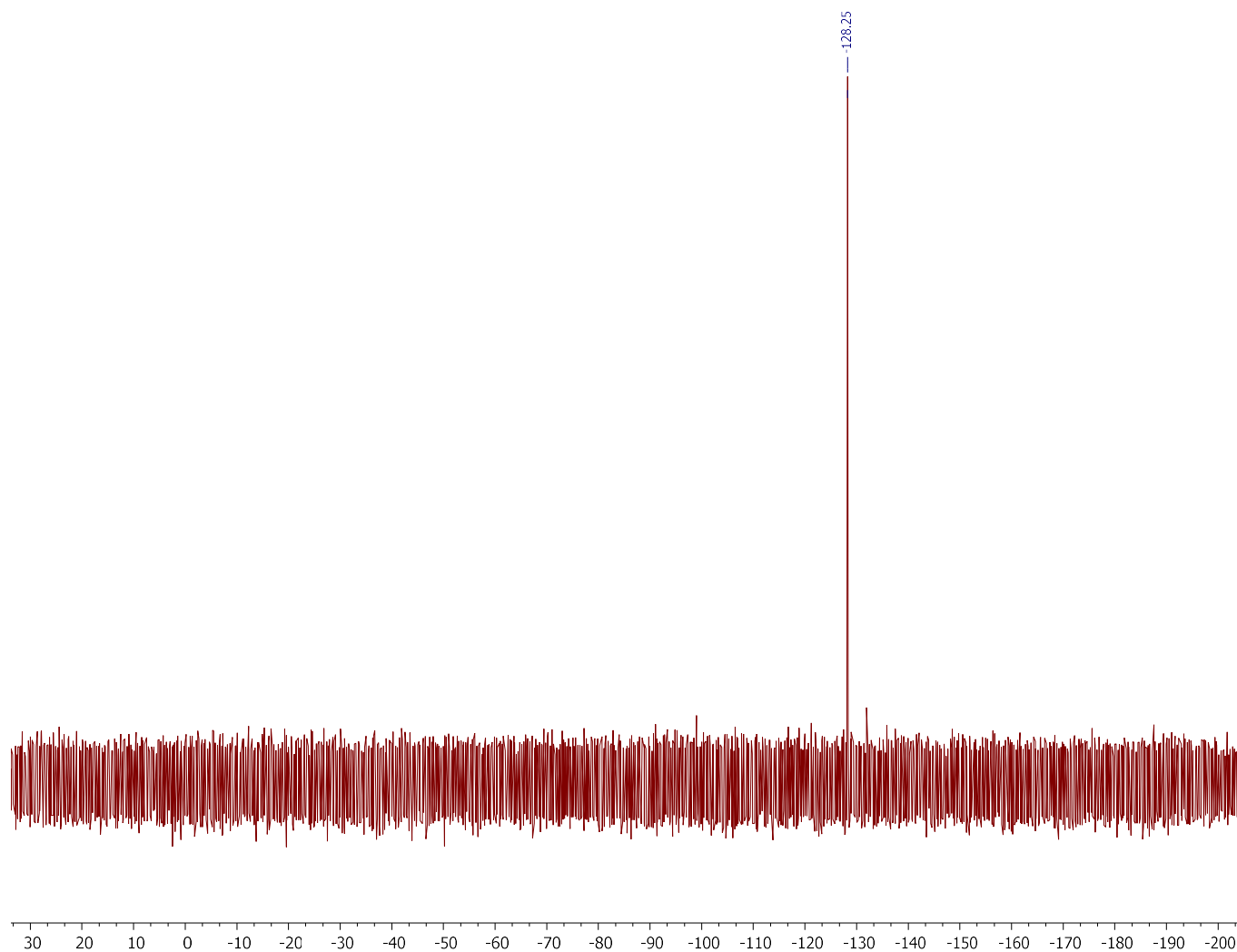
—-128.25

293

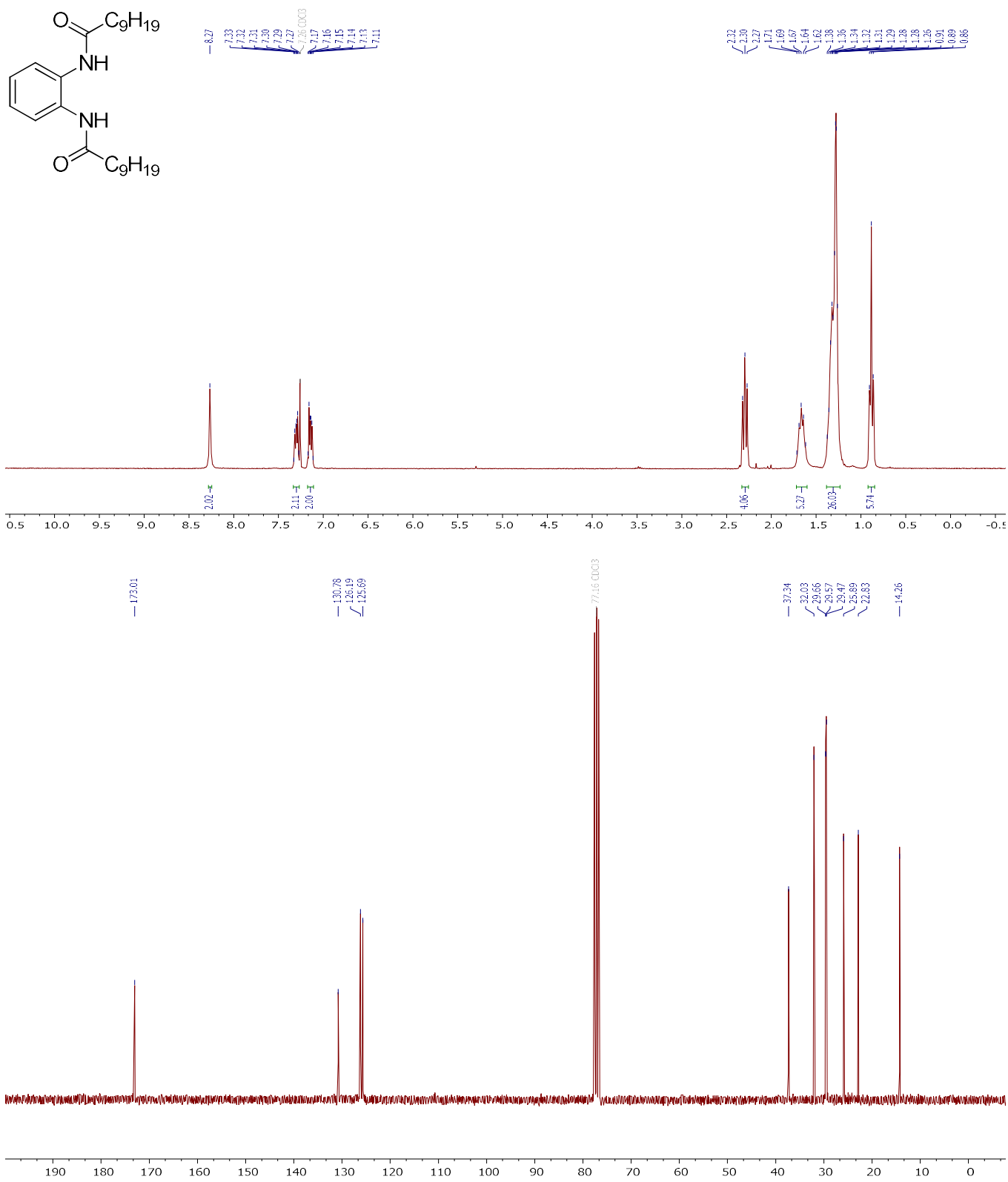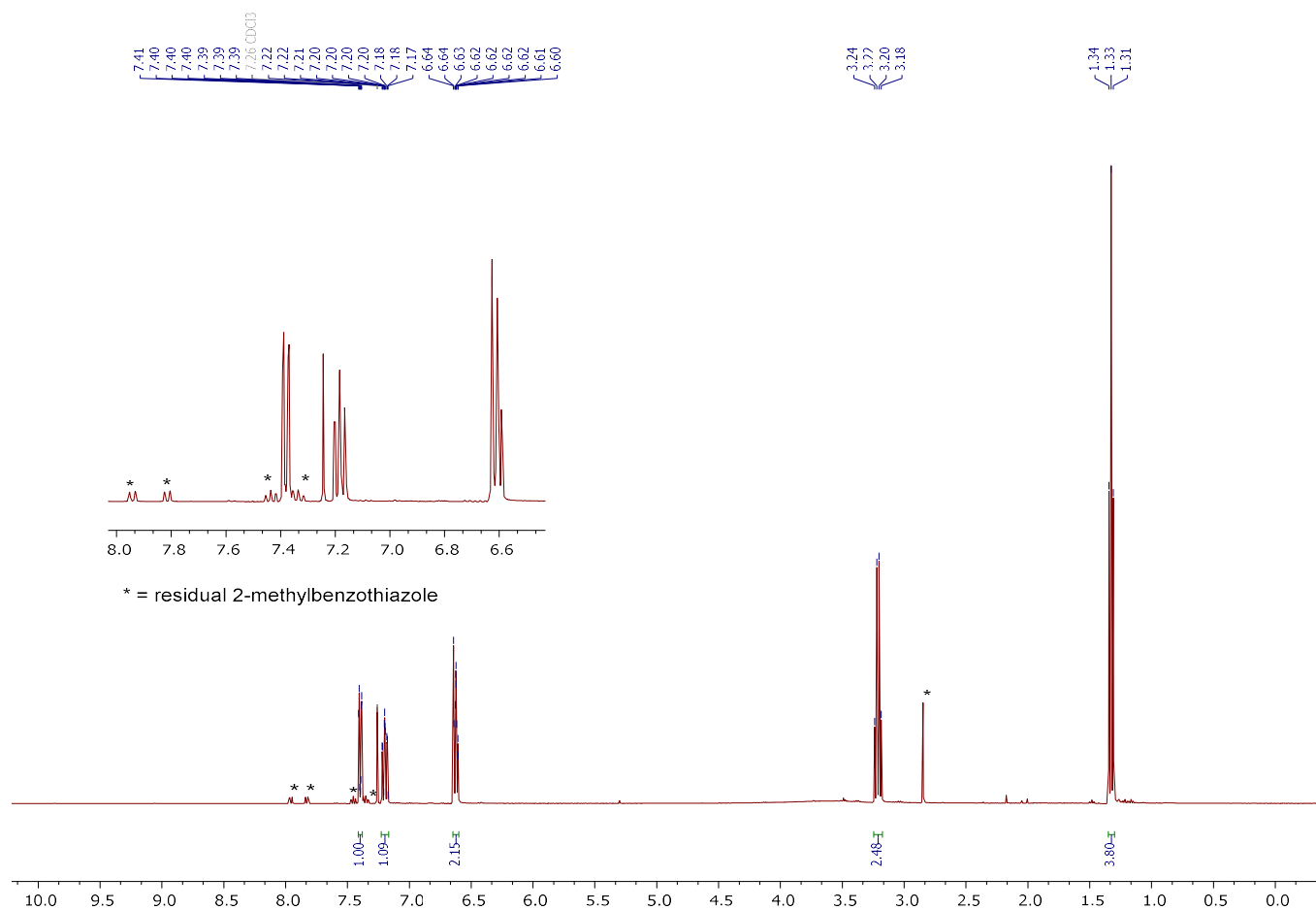## 2,3-difluoro-5,10-dihydrophenazine-1,4-dicarbonitrile (3.17):

—150.93

30   20   10   0   -10   -20   -30   -40   -50   -60   -70   -80   -90   -100   -110   -120   -130   -140   -150   -160   -170   -180   -190   -200

295
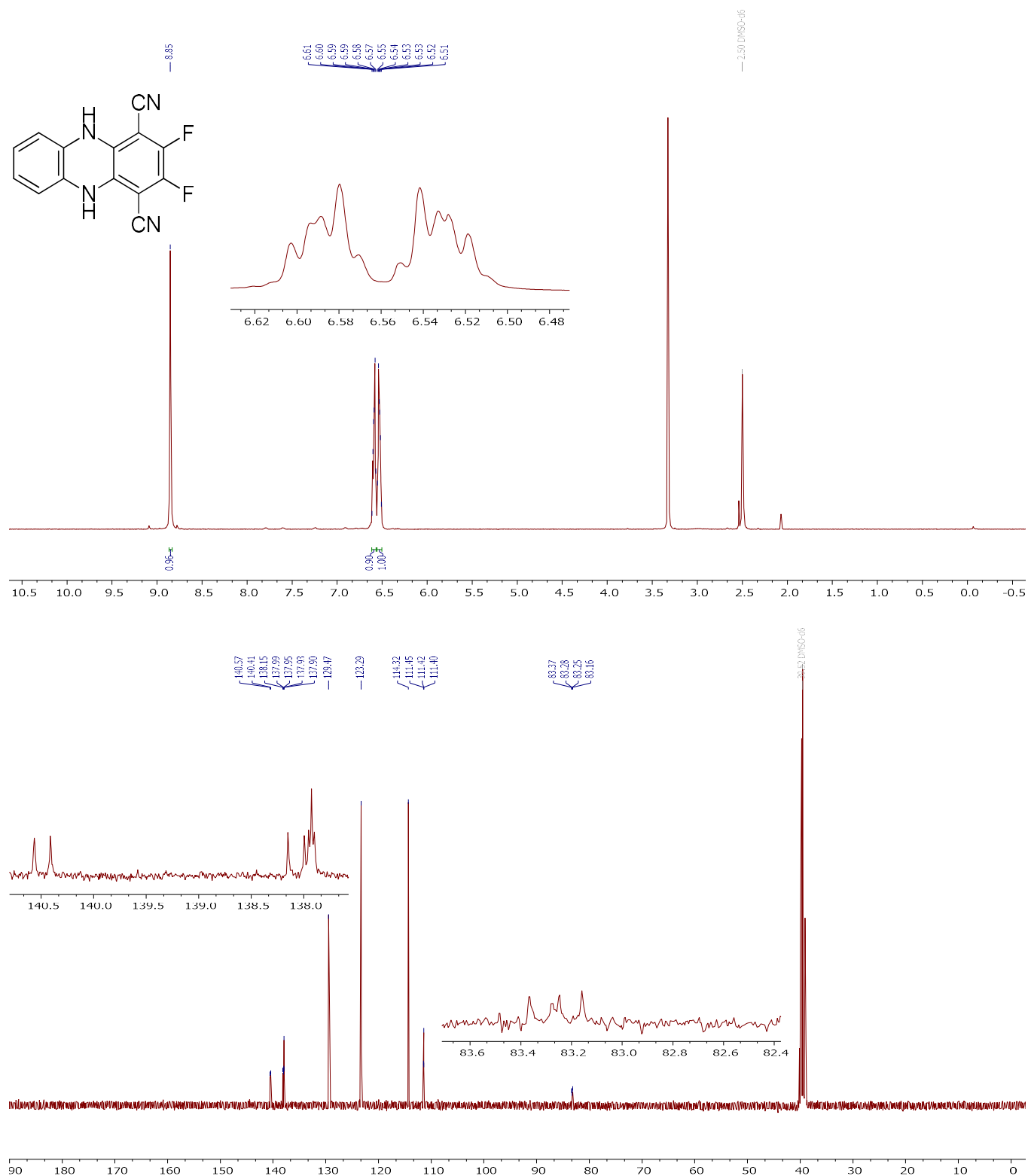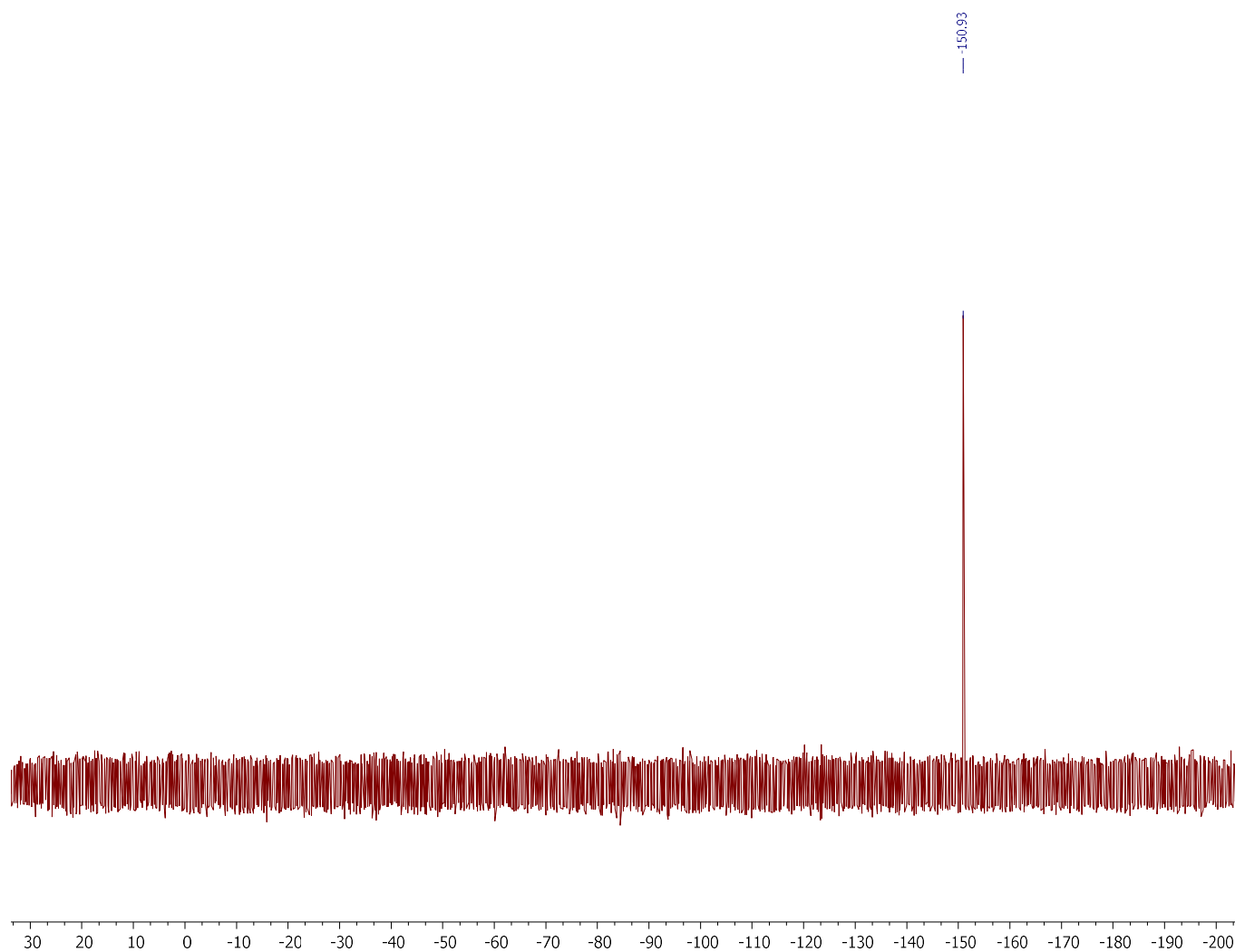
_N,N'_-(1,2-phenylene)bis(decanamide) (3.65):

2-(N-ethylamino)thiophenol (3.77):

* = residual 2-methylbenzothiazole

7,14-diethyl-7,14-dihydrobenzo[5,6][1,4]thiazino[2,3-b]phenothiazine-6,13-dicarbonitrile (3.80):

12-ethyl-12H-benzo[5,6][1,4]dioxino[2,3-b]phenothiazine-6,13-dicarbonitrile

(3.84):